DEVELOPMENT AND ANALYSIS OF A NOVEL ISOSCELES TRAPEZOIDAL DIELECTRIC RESONATOR ANTENNA FOR WIRELESS COMMUNICATION

A thesis submitted by

GOPAKUMAR C.

in partial fulfillment of the requirements for the degree of

DOCTOR OF PHILOSOPHY

Under the guidance of

Dr. K. T. MATHEW

DEPARTMENT OF ELECTRONICS
FACULTY OF TECHNOLOGY
COCHIN UNIVERSTIY OF SCIENCE AND TECHNOLOGY
COCHIN-22, INDIA

January 2011

Dedicated to my father…

who made me what I am…

DEPARTMENT OF ELECTRONICS

COCHIN UNIVERSITY OF SCIENCE AND TECHNOLOGY,

KOCHI – 682 022

Dr. K. T. Mathew
(Supervising Guide)
Professor
Department of Electronics
Cochin University of Science and Technology

Certificate

This is to certify that this thesis entitled "**DEVELOPMENT AND ANALYSIS OF A NOVEL ISOSCELES TRAPEZOIDAL DIELECTRIC RESONATOR ANTENNA FOR WIRELESS COMMUNICATION"** is a bonafide record of the research work carried out by Mr. Gopakumar C. under my supervision in the Department of Electronics, Cochin University of Science and Technology. The results embodied in this thesis or parts of it have not been presented for any other degree.

Cochin-22   **Dr. K. T. Mathew**
14th January 2011

iv

DECLARATION

I hereby declare that the work presented in this thesis entitled "**DEVELOPMENT AND ANALYSIS OF A NOVEL ISOSCELES TRAPEZOIDAL DIELECTRIC RESONATOR ANTENNA FOR WIRELESS COMMUNICATION**" is a bonafide record of the research work done by me under the supervision of Dr. K. T. Mathew, Professor, Department of Electronics, Cochin University of Science and Technology, India and that no part thereof has been presented for the award of any other degree.

Cochin-22
14th January 2011

Gopakumar C.
Research Scholar
Department of Electronics
Cochin University of Science and Technology

ABSTRACT

This thesis describes the development and analysis of an Isosceles Trapezoidal Dielectric Resonator Antenna (ITDRA) by realizing different DR orientations with suitable feed configurations enabling it to be used as *multiband*, *dual band dual polarized* and *wideband* applications.

The motivation for this work has been inspired by the need for compact, high efficient, low cost antenna suitable for multi band application, dual band dual polarized operation and broadband operation with the possibility of using with MICs, and to ensure less expensive, more efficient and quality wireless communication systems. To satisfy these challenging demands a novel shaped Dielectric Resonator (DR) is fabricated and investigated for the possibility of above required properties by trying out different orientations of the DR on a simple microstrip feed and with slotted ground plane as well.

The thesis initially discusses and evaluates recent and past developments taken place within the microwave industry on this topic through a concise review of literature. Then the theoretical aspects of DRA and different feeding techniques are described. Following this, fabrication and characterization of DRA is explained.

To achieve the desired requirements as above both simulations and experimental measurements were undertaken. A 3-D finite element method (FEM) electromagnetic simulation tool, HFSS^{TM} by Agilent, is used to determine the optimum geometry of the dielectric resonator. It was found to be useful in producing approximate results although it had some limitations. A numerical analysis technique, finite difference time domain (FDTD) is used for validating the results of wide band design at the end. MATLAB is used for modeling the ITDR and implementing FDTD analysis.

In conclusion this work offers a new, efficient and relatively simple alternative for antennas to be used for multiple requirements in the wireless communication system.

AKNOWLEDGEMENT

me in innumerable ways. My parents were a constant source of inspiration and moral support. Special thanks to my wife for her support, encouragement and prayers throughout all the uncertain times. Her sacrifices helped me a lot to complete this work. Also thanks to my father-in-law and mother-in-law, for giving me constant support and encouragement.

I would like to express my thanks and appreciation to the Director, IHRD and Dr. V.P. Devassia, Principal, College of Engineering, Chengannur who permitted me to undertake the research. Last but not least, I would like to thank all the colleagues at College of Engineering, Chengannur for their continuous encouragement and support.

Above all there is that supreme power whose blessings and kindness helped me a lot to sail through…

Gopakumar C

CONTENTS

CHAPTER 1   **INTRODUCTION**

CHAPTER 2   **REVIEW OF LITERATURE**

CHAPTER 3   DIELECTRIC RESONATOR ANTENNA – THEORY AND FABRICATION

CHAPTER 4   **EXPERIMENTAL AND SIMULATED STUDY OF ISOSCELES TRAPEZOIDAL DIELECTRIC RESONATOR ANTENNA**

CHAPTER 5   **FINITE DFFERENCE TIME DOMAIN METHOD**
                      -A NUMERICAL ANALYSIS TECHNIQUE

CHAPTER 6   **CONCLUSION AND FUTURE SCOPE**

APPENDIX –A

AN INVESTIGATION OF WIDEBAND CIRCULAR CYLIDRICAL SECTOR DIELECTRIC RESONATOR ANTENNA WITH MICROSTRIPLINE FEED

APPENDIX –B

A NOVEL TECHNIQUE FOR REDUCING THE IMAGING DOMAIN IN MICROWAVE IMAGING OF TWO DIMENSIONAL CIRCULARLY SYMMETRIC SCATTERERS

List of figures

List of tables

CHAPTER 1   **INTRODUCTION**

1.1 OVERVIEW OF WIRELESS COMMUNICATION

Wireless is the fastest growing sector of communication industry. Now a days the media's attention and the public's imagination are being influenced by this sector. The exponential growth of cellular system shows that currently two billion users are there in worldwide. In fact, it becomes part of everyday life and a critical business tool in most developed and developing countries. Besides, wireless local area networks (WLAN) presently replace wireless network in many homes, business and campuses. Various new applications, including wireless sensor networks, automated highways and factories, remote telemedicine, smart homes and appliances, are emerging from research ideas to real systems. The boom in the growth of wireless systems coupled with the development of laptop and palmtop computers along with the evolution of new microwave devices and components show a brilliant future for wireless networks, both as individual systems and as part of the larger networking infrastructure. However many technical challenges remain in designing robust wireless networks that deliver the performance necessary to support emerging applications.

1.2 HISTORY OF MICROWAVE COMMUNICATION

The history of microwave communication over the past several decades comprises some of the major advances and applications of science and technology. Microwaves are electromagnetic waves. Hence the history of microwaves is embodied in the evolution of electromagnetic waves.

James Clerk Maxwell (1831-1879) unified all previous known results, experimental and theoretical, on electromagnetic waves in four equations and predicted the existence of electromagnetic waves. Heinrich Rudolf Hertz (1857-1937) experimentally confirmed Maxwell's prediction. Guglielmo Marconi (1874-1937) transmitted information on an experimental basis at microwave frequencies. George C. Southworth (1930) really carried out Marconi's experiments on a commercial basis. During World war- II (1945) based on the previous developments; radar was invented and was exploited for military applications.

The people then were trying to investigate how devices could operate in the UHF/microwave bands with larger powers. The conventional vacuum tube was the best set, but then it had several hitches at these frequencies like inter-electrode capacitances (IEC) between elements within the vacuum tube and a longer electron transit time. The IEC effectively shorting at higher frequencies and the longer transit time causing them to be used only at lower operating frequencies.

(i) Early History of communication

1844- The first demonstration of electrical communication over a substantial distance was by Samuel F. B. Morse with a dot-dash message over a single wire between Baltimore and Washington.

1858- First transatlantic telegraph cable was installed.

1876- Alexander Graham Bell demonstrated that the human voice could be electrically, transmitted over wire and -was granted a patent [1], [2] for the telephone.

1878- Bell started the first telephone company in New Haven, CT. The expansion of this small system to the giant ATT was a remarkable achievement with no parallel in history.

1864- Englishman James Clark Maxwell's theoretical work hypothesized that light was an electromagnetic (EM) phenomena, and that EM energy propagated as waves in space.

1888- In Germany, Heinrich Hertz experimentally proved Maxwell's theories and consequently established the basis for wireless communication.

1894- The Englishman, Oliver Lodge, improved the sensitivity of Hertz's loop detector [1], [3] by coupling the spark gap loop to a "Coherer," invented in 1892, by another Englishman, Edward Branly.

1898- Lodge also patented the concept of a tuned transmitter and receiver, one of the most famous and important patents in radio history.

(ii) Development of Radio

1894- Guglielmo Marconi [1], [4], at the young age of 20, first read about Hertz's experiments and started work to develop wireless communications.

1897- Marconi moved to England and established the British Marconi Company and an American subsidiary two years later.

1901- Marconi demonstrated transatlantic transmission of telegraphy over a 1700-mi path from England to Newfoundland.

1900- An understanding of the physics of propagation in the atmosphere was gained through the work of the Englishman, Heaviside, and others. Their major discoveries were the effects of ionized layers on propagation of EM waves.

1906- Fessenden was successful [1], [5] with an 80-KHz alternator built by the General Electric Company. Several years later Ernest Alexanderson of GE built alternators capable of transatlantic transmission.

1883- Thomas Edison, first noted the emission of electrons from heated filaments.

1904- J. Ambrose Fleming used this effect in his diode detector and patented.

1907- Lee De Forest invented the triode vacuum tube for the control of a flow of electrons.

1914- ATT constructed a 170-KHz transmitter using parallel banks of tubes, each capable of producing several watts of undistorted power [1], [6].

1914- Experiments to apply the same type of transmitters to transoceanic distance were also conducted by ATT.

1933- A 20-ft-long waveguide was built and used to demonstrate transmission of telegraph signals.

(iii)   Radio with High Frequency

Wavelengths of 200 to 10000 m seemed adequate for the initial radio work. However, some effort was directed towards higher frequencies again, since the hope of communication with highly directive antennas was very attractive.

1917- The General Electric Company produced a 250-W air-cooled triode called a Pilotron.

1920s- Marconi returned to experimentation with higher frequency radio [1], [7]. The band between 3 and 20 MHz was explored on 100-300-mi paths between Holland and England.

1931- Marconi conducted radio tests of the system in Italy, and was able to establish good quality speech over an 18-mi path between Santa Margherita and Levante.

(iv) The First Microwave Radios

1932- Vatican authorities [1], [8] approached Marconi to install a 57-cm microwave link between Vatican City and the summer residence of the Pope at Castel Gandolfo, a path of 15 mi. The installation was completed, and service was inaugurated by Pope Pius XI in February of 1933.

1935- A very important breakthrough in the technology of microwave tubes occurred in Germany when Heil and Heil published their historic paper [1], [9] in which they discussed the velocity modulation of electrons in a short gap, and the consequent bunching as the electrons traverse a drift tube.

1939- A. L. Samuel [1], [10] and his BTL (Bell Laboratories) team built a klystron suited for waveguide use and achieved 15-dB gain over a 5-MHz bandwidth at 3 GHz, with an output power of 1 w.

(v) World War II and Microwave Communication

Enormous strides in the development of microwave technology were made during World War II, with the bulk of the effort aimed at radar systems

- The first prototypes of the U.S. Army radio, the AN/TRC-6, were completed at the end of 1943, and production started shortly after.

- The AN/TRC-6 [1], [11] was a pulse-position modulation system that provided eight duplex voice channels through, time division multiplexing and operated at 4.5 GHz. This radio, which was radically different than any previous microwave radio, was one of the first to have multichannel capability.

(vi) Early Post War Microwave Radio

1943- A bold proposal was made to ATT management [1], [12] to set up a large microwave radio relay demonstration from New York City to Boston. The system was formally opened in 1947. Following the successful implementation of the New York-Boston system, work was started at ATT on a 4-GHz transcontinental network, the TD-2 system [1], [13]. The TD-2 system was designed with a capability of expansion to a 4000-mi overall path length with 125 repeaters spaced 25-30 mi apart.

1951- By the end of 1951, over 20000 radio channel-miles of microwave were in operation for the Bell System. Two-thirds of the capacity was used for television transmission and one-third for over 600000 telephone voice circuit-miles.

(vii)   Modern Microwave Radio

Microwave radio systems have undergone very significant improvements and changes during the 30-year period following the introduction of the radios described in the previous section.

1970s- GaAs FET's were applied in receivers to achieve extremely low-noise front ends and also for transmitter power amplifiers in the 4- and 6-GHz bands.

- Waveguide circuits were replaced by microwave integrated circuits using microstrip or other circuit forms on teflon-based, or ceramic, substrates.

- Dielectric resonators were used as high-Q resonators for oscillators and filters.

- Space and frequency diversity, and multiline switching systems, were introduced to provide very reliable operation with protection against equipment failure and path fades.

- The increase of the capacity of microwave radios made possible by the above technologies. The MAR-6C [1], [14], manufactured by Collins Transmission Systems Division of Rockwell International, uses a 5-W, 37-dB gain GRAS FET power amplifier, a GaAs low-noise 6-GHz receiver preamplifier, fundamental sources using a 6-GHz silicon bipolar transistor, and a directly modulated source for terminal applications.

(viii)   The Wave Guide Communication System

The waveguide transmission work started by Southworth, and described earlier, was given emphasis at Bell Labs during the post-war years.

1970s- millimeter-wave IMPATT diodes were developed and practical implementation of the millimeter wave system was conceived.

- Methods of mode control in the waveguide itself had to be developed to prevent conversion from the low-loss TE_{01} mode to the higher loss TM_{11} mode, which is degenerate with the TE_{01} mode.

- An ambitious program [1], [15] to develop a digital system that had a capacity of 230,000 duplex voice circuits over the band from 40–110 GHz in a single waveguide was undertaken

- During this time, development of fiber-optics systems was started.

(ix)   Satellite Communication Systems

Satellite communication systems are an outstanding successful example of the application of microwave technology.

1946- The first proposal for the use of synchronous satellite repeaters was by Arthur C. Clarke in an article in *Wireless World* entitled "Extraterrestrial relays".

   - One of the earliest steps towards satellite communications was an experiment conducted by the U.S. Army Signal Corps when radio signals were bounced off the moon and were successfully detected on earth.

1954- Experiments on the moon bounce continued and the first voice message path established by the US Navy

1956- A permanent relay service established between Washington, D. C., and Hawaii.

1954- J. R. Pierce [1], [16] of Bell Labs proposed the concept of communication satellites for telephony in a talk to the Princeton Section of the IRE. He considered active and passive repeaters and orbiting as well as synchronous satellites.

1960- Progress in the development of rocketry and space vehicles enabled the test of a passive repeater in space, the ECHO satellite (a plastic, metal-covered balloon) at an altitude of 1500 KM, for communications between transmitting and receiving stations in New Jersey and California at frequencies of 0.96 GHz and 2.3 GHz. A severe problem with passive repeaters was that, in systems such as the ECHO relay, only one part in 10^{18} of the transmitted power is returned to earth.

1958- The first active U.S. communication satellite, a broadcast system called SCORE, was launched, and transmitted President Eisenhower's Christmas message to the world with a satellite power of 8 W at 122 MHz

1962- The Telstar active satellite built by ATT was launched. This orbiting satellite which used a 6-GHz up-link and 4-GHz down-link was used for television

transmission, and for demonstrations of telephony between American and European cities.

1964- The first successful synchronous active satellite, Syncom 111, built by Hughes Aircraft, was placed in orbit.

1965- The first commercial communication satellite, Early Bird built by Hughes Aircraft Company, was placed in orbit, and provided 240 telephone circuits and television transmission between the U.S. and Europe.

1973- More than eight synchronous satellites stationed over the Atlantic, Pacific, and Indian Oceans beamed telephone, television, telegraph, and facsimile signals to ground stations in 39 countries.

The capacities of satellites by 1980s, such as INTELSAL IV, had increased to about 6000 telephone circuits or 12 color-TV channels. The satellite systems increased the number of transoceanic voice circuits from 1000 in 1957 to more than 25,000 in 1973.

(x) Mobile communication

1980s- First generation (1G) mobile Communication- only voice service- analog technology is used.

1990s- Second Generation (2G) digital cellular deployed throughout the world. Mostly for voice service- Data delivery possible. Digital Technology-TDMA, CDMA used.

2000s- Third Generation (3G) digital systems standardized at the network level to allow worldwide roaming.- Mainly for Data service- Voice service also possible. (Wideband CDMA technology is used)

The advances in satellite communications were made possible by greatly improved technology for space vehicles and significant advances in microwave components for satellite and earth station applications.

1.3 INTRODUCTION TO ANTENNAS

An antenna is usually defined as the structure associated with region of transition between a guided wave and a free-space wave, or vice versa [17]. On transmission, an antenna accepts electromagnetic energy from a transmission line (coaxial cable or waveguide) and radiates it into space, and on reception, an antenna collects the electromagnetic energy from an incident wave and sends it through the transmission line.

In ideal conditions it is desirable that the energy generated by the source is totally transferred to the antenna. However in practice this total transfer of energy is not possible due to conduction-dielectric losses and lossy nature of the transmission line and the antenna. Also if the transmission line is not properly matched to the antenna there will be reflection losses at their interface. Therefore it is very important that the characteristic impedance of the antenna is matched to the impedance of the antenna.

In wireless communication systems the antenna is one of the most critical components. A good design of antenna can improve overall system performance and reduce system requirements. In order to meet the system requirements of today's mobile and wireless communication systems and the increasing demand on their performances, much advancement in the field of antenna engineering have occurred in the last few decades.

1.3.1 TYPES OF ANTENNAS

Many types of antennas have been developed to date that are used in radio and television broadcast, cellular and wireless phone communications, marine and satellite communications and many other applications. In this section only few common forms and various types of antennas will be briefly described.

1.3.1.1 WIRE ANTENNAS

Wire antennas are seen in everyday life situations- on cars, buildings, ships, aircrafts and so on. Wire antennas come in various shapes such as straight wire (dipole), loop, and helix all of which are shown in Figure 1.4.1.1.1. Loop antennas may take the form of a rectangle, square, ellipse or any other configuration.

(a) Dipole   (b) Circular (square) loop
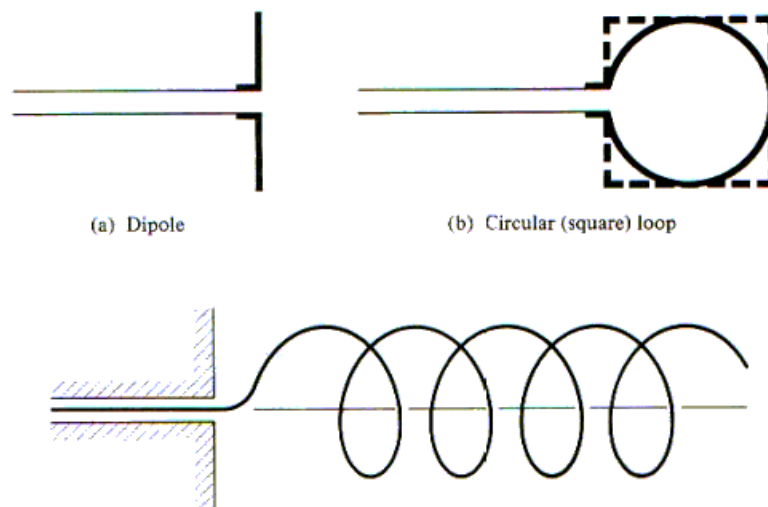
Figure 1.3.1.1.1: Wire antenna configurations [18].

1.3.1.2 APERTURE ANTENNAS

Due to the increasing demand for more sophisticated forms of antennas and utilization of higher frequencies the aperture antenna is more common today. Some forms of aperture antennas are shown in Figure 1.4.1.2.1. They are used for aircraft and

spacecraft applications because they can be easily flush-mounted on the skin of the aircraft or spacecraft. Additionally they can be covered with suitable dielectric materials to protect them from hazardous conditions of the environment in which aircrafts and spacecrafts usually operate.

(a) Pyramidal horn

(b) Conical horn

(c) Rectangular waveguide
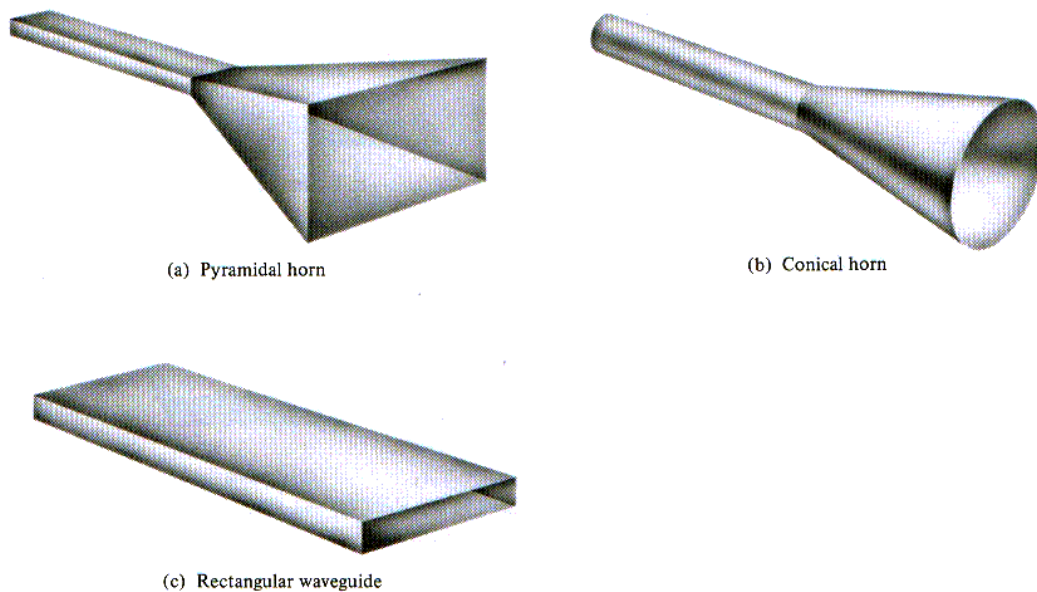
Figure 1.3.1.2.1: Aperture antenna configurations [18].

1.3.1.3 MICROSTRIP ANTENNAS

Microstrip antennas became very popular in the 1970s primarily for space borne applications. Today they can be found in many other government and commercial applications. They usually consist of a metallic patch on a grounded substrate and can take many different configurations. Rectangular and circular patches, shown in Figure 1.4.1.3.1, are the most popular because of the ease of analysis and fabrication and attractive radiation characteristics. Microstrip antennas are low-profile, conformable to

planar and non planar surfaces, simple and inexpensive to fabricate using modern printed circuit technology. They can be mounted on surface of high-performance aircraft, spacecraft, satellites, missiles, cars and even mobile phones.
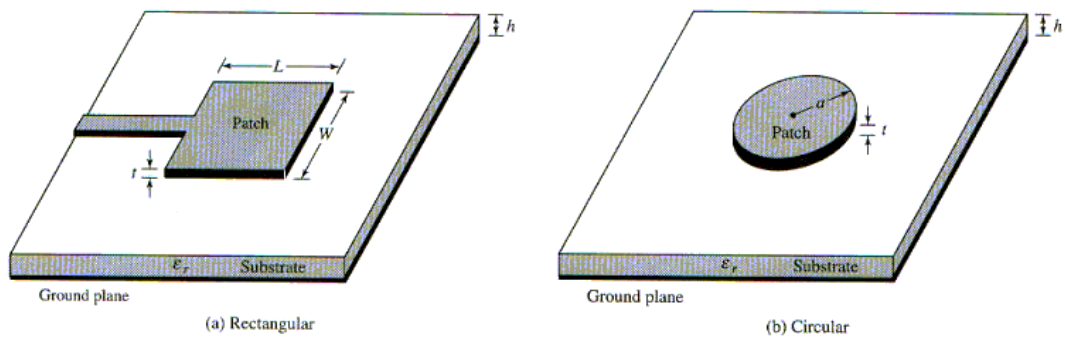
Figure 1.3.1.3.1: Rectangular and circular microstrip patch antennas [18].

1.3.1.4 ARRAY ANTENNAS

Many applications require radiation characteristics that can only be achieved if a number of radiating elements are arranged in a geometrical or an electrical manner that will result in the desired radiation pattern. The arrangement of such element is called an array and is used primarily to achieve a radiation pattern in a particular direction or directions. As will be discussed later, antenna arrays are used in cellular base stations to create directional patterns covering only desired area. These antennas, which are usually made up of an array of 4 to 12 elements, are referred to in cellular systems as sectored or directional antennas and take form of a panel array. Typical examples of arrays are shown in Figure 1.4.1.4.1.

(a) Yagi-Uda array

(b) Aperture array

(c) Microstrip patch array

(d) Slotted-waveguide array
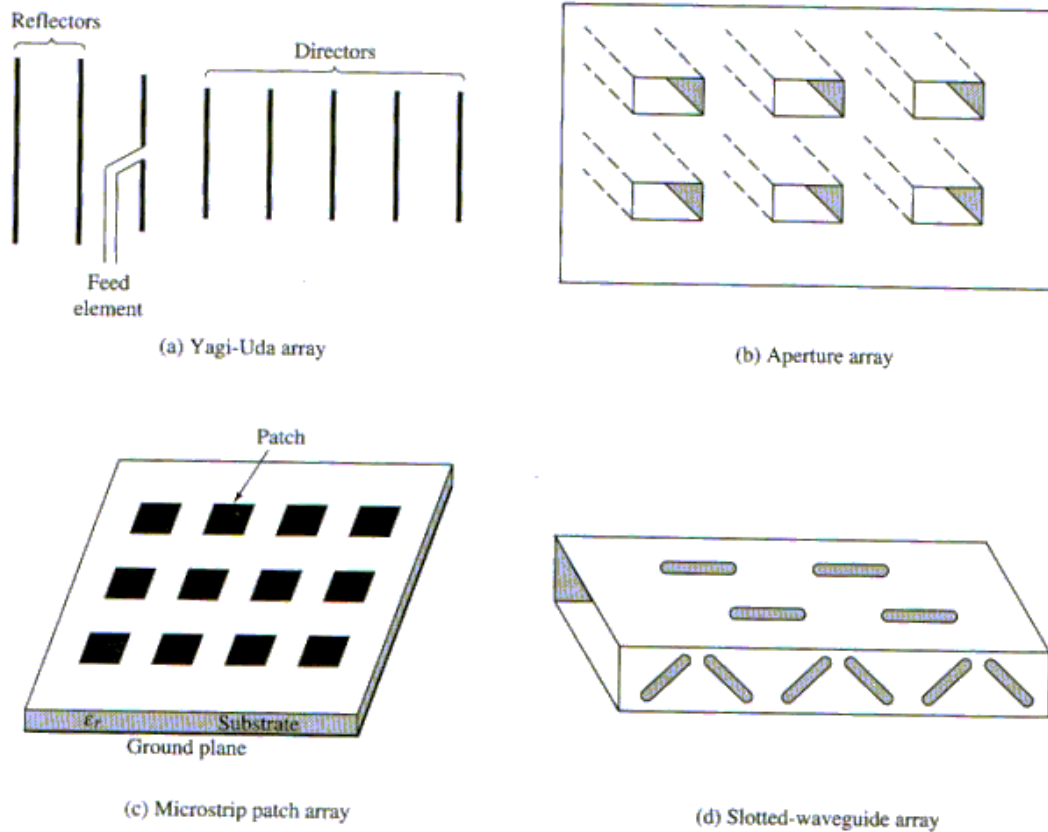
Figure 1.3.1.4.1: Typical wire, aperture and microstrip array configurations [18].

1.3.1.5 LATEST TREND

The antenna community had to wait until the early 1980s for a competitor to the microstrip patch antenna (MPA) – the dielectric resonator antenna (DRA). A DRA contains a known volume of dielectric material or puck, called the dielectric resonator (DR), of appropriate characteristics especially a high dielectric constant and low loss. Like the MPA, the DRA also offers the advantages of low-profile, light-weight and flexible excitation schemes. Both antennas are candidates for numerous applications, either as individual elements or as array elements. But the lack of metallic losses in DRAs assures higher radiation efficiency than MPAs, especially in the millimeter wave applications. Also the possibility of exciting low Q-radiating modes offers a higher

operating bandwidth to them than the MPAs. A comparative study between the DRA and MPA shows that the former is a real competitor to MPAs in terms of performance.

1.4 COMPUTATIONAL ELECTROMAGNETICS

1.4.1 BACKGROUND

Several problems in Electromagnetics are not analytically computable (for example: radiation, scattering, waveguiding etc.) especially for the irregular geometries found in actual devices. To overcome the inability to derive closed form solutions of Maxwell's equations, under boundary conditions and various constitutive relations of media, computational numerical techniques can be used. So it is important to use the computational electromagnetic (CEM) to the design and modeling of antenna, radar, satellite and other communication systems.

Generally CEM solves the problem of computing the E (Electric) and H (Magnetic) fields across the problem domain. For example, if we required computing the radiation patterns of an arbitrary shaped antenna structure we can use any of the methods in CEM.

By means of CEM, in time domain, transient response and impulse field effects are more accurately modeled by the method of Finite Difference Time Domain (FDTD). Objects with curved geometrical shapes are treated more accurately as finite elements by Finite Element Modeling (FEM), or non-orthogonal grids. . In electromagnetic field analysis, MoM solution directly provides the surface current on a conductor or the polarization current in a dielectric. Similar to FDTD, complex, nonlinear materials are readily modeled in TLM and also impulse responses and the time-domain behavior of systems are determined explicitly.

Method of moments [19], Finite element method [20], Finite difference time domain method [21] and Transmission line matrix method [22] are the most commonly used numerical techniques.

1.4.2 OVERVIEW OF METHODS

Discretizing the computational domain in terms of grids (both orthogonal, and non-orthogonal) and solving Maxwell's equations at each point in the grid is the usual approach. Discretization requires much amount of computer memory, and solution of the differential equations takes significant time. So CEM problems in large scale face memory and CPU limitations. When modeled by finite element methods (FEM), general formulations involve either time-stepping through the equations over the whole domain for each time instant; or through banded matrix inversion to calculate the weights of basis functions. When transfer matrix methods are used, matrix products are utilized. For method of moments (MoM), calculations of integrals are involved. The computation by split-step method or BPM, is based on the fast fourier transforms, and time iterations. For this reason, normally, CEM problems require supercomputers, high performance clusters, vector processors and/or parallel computer.

1.4.2.1 METHOD OF MOMENTS (MoM)

The method of moments is a computational electromagnetic technique for solving linear operator equations [23]. It is essentially the method of weighted residuals hence applicable for solving both differential and integral equations. The Method of Moments in Computational Electromagnetics is initially used by Harrington [24]. Its origin and progress are fully documented by Harrington [25, 26]. MoM has become more popular since the 1980s. A wide variety of EM problems of practical interest has been using this

method successfully. They include radiation due to thin wire elements and arrays, scattering problems, analysis of microstrip and lossy structures, propagation over an inhomogeneous earth, and antenna beam pattern etc. MoM is a method of solving a differential equation or an integral equation numerically by transforming the equation into simultaneous equations. Because it requires calculating only boundary values, rather than values throughout the space, it is significantly more efficient in terms of computational resources for problems with a small surface/volume ratio. Conceptually, it works by constructing a "mesh" over the modeled surface.

1.4.2.2 FINITE ELEMENT METHOD (FEM)

This is a method of solution of a wide class of partial differential or integral equations. In the mid-1970's Mei, Morgan and Chang introduced the finite-element approach for the Helmholtz equation [23]. Finite element techniques require the entire volume of the configuration to be meshed as opposed to surface integral techniques, which require only the surfaces to be meshed.

Initial step in finite element analysis is to divide the configuration into a number of small homogeneous elements or pieces. The model contains information about the device geometry, material constants, excitations, and boundary constraints. The corners of the elements are called nodes. Second step is to assignment of nodes to each element and then choosing an interpolation function (polynomials) to represent the variation of the field variable over the element. The degree of the polynomial chosen depends on the number of nodes assigned to the element, the nature and number of unknowns at each node, and certain continuity requirements imposed at the nodes and along the element boundaries. The magnitudes of the field variable and their derivatives may be the

unknowns at the nodes. Finite element model is now established. Next step is to determine the matrix equations expressing the properties of the individual elements and hence to form the matrix equations expressing the behavior of the entire system. Appropriate boundary conditions are then applied, to give a set of simultaneous equations. Now these are to be solved to obtain the unknown nodal values of the problem.

It is possible to model complicated geometrical configurations and many arbitrarily shaped dielectric regions using FEM method, as the major advantage of this technique is the easiness of defining electrical and geometric properties of each element independently.

1.4.2.3 FINITE-DIFFERENCE TIME-DOMAIN (FDTD)

Finite-difference time-domain (FDTD) is a popular CEM technique. It is easy to understand and easy to implement in software. One of its plus point is that, as it is a time-domain method, solutions can cover a wide frequency range with a single simulation run.

It includes in the class of grid-based differential time-domain numerical modeling methods. In this method, using central-difference approximations, the time-dependent Maxwell's equations (in partial differential form) are discretized to the space and time partial derivatives. Then the resulting finite-difference equations are solved in either hardware or software system in a leapfrog approach. That is the E field vector components in the given volume of space are solved at a given instant in time; then the magnetic field vector components in the same spatial volume are solved at the next

instant in time. The process is repeated over and over again until the desired transient or steady-state electromagnetic field behavior is completely evolved.

The basic FDTD space grid and time-stepping algorithm trace back to a seminal 1966 paper by Kane Yee in IEEE Transactions on Antennas and Propagation [27]. The descriptor "Finite-difference time-domain" and its corresponding "FDTD" acronym were originated by Allen Taflove in a 1980 paper in IEEE Transactions on Electromagnetic Compatibility.[28]

Initially a computational domain must be established for the use of FDTD. The computational domain is simply the region over which the simulation is going to be performed. The Electric (E) and Magnetic (H) fields are determined at every point in space within that computational domain. The material of all the cells within the computational domain must be specified. Any material can be used as long as the permittivity, permeability and conductivity are specified.

1.4.2.4 TRANSMISSION LINE MATRIX (TLM)

This method (TLM) can be formulated in several means as a direct set of lumped elements solvable directly by a circuit solver (ala SPICE, HSPICE, et al.), as a custom network of elements or via a scattering matrix approach. TLM is similar to FDTD when the flexibility of analysis strategy is concerned.

It is used for solving field problems using circuit equivalents and is based on the equivalence between Maxwell's equations and the equations for voltages and currents on a mesh of continuous two-wire transmission Lines. It can be programmed for a wide range of applications. The main feature of the method is the simplicity of formulation. Unlike other methods such as finite difference and finite element methods, which are

mathematical discretization approaches, the TLM is a physical discretization approach. The nodes of the grids are interconnected by virtual transmission line. The excitation at the source node propagates to the adjacent nodes through these virtual transmission lines. Analysis is performed in time domain.

The major advantage of the TLM method, as compared with other numerical techniques, is the ease with which even the most complicated structures can be analyzed. The great flexibility and versatility of the method reside in the fact that the TLM mesh incorporates the properties of EM fields and their interaction with the boundaries and material media. Hence, the EM problem need not be formulated for every new structure. Another advantage of using the TLM method is that certain stability properties can be deduced by inspection of the circuit. There are no problems with convergence, stability or spurious solutions.

1.5 MOTIVATION OF THE RESEARCH WORK

Dielectric Resonator Antenna designers are faced with the problem of widening bandwidth, in addition to miniaturization and optimization of properties like multiband operation, dual band dual polarization operation etc. Now a days, bandwidth requirements are very high for modern communications and DRA technology needs to keep up with them. Combination of multiple resonators, use of additional impedance matching techniques, reducing radiation Q factor are some of the techniques that can be followed for achieving the wide band response.

Another trend is to miniaturize the antenna. DRA size can be made smaller, through the use of high permittivity materials, since the guided wavelength is inversely proportional to the permittivity of the dielectric material $\left(\lambda_d = \lambda_0 / \sqrt{\varepsilon_d} \right)$. But high

permittivity material results in increased Q factor at a rate of $\varepsilon_r^{3/2}$ and leads to a narrow bandwidth.

With the development of wireless communication systems, dual or multi-frequency antennas are highly desirable. Recently, many investigations have been reported on dielectric resonator antennas (DRAs) with dual-frequency or wideband operation using various approaches, such as exciting two modes, or stacking two DRAs. But stacking two DRAs increases the size and the weight of DRA and can lead to a complex fabrication process.

Antennas with dual band dual polarization operation have been in demand for many applications, particularly for wireless communication. Polarization-diversity antennas are needed because they can better handle information than singly polarized antennas in certain situations; for example, they can reduce multi-path effects.

The latest advances in the DRA technology is paying attention on novel DRA elements to meet the above cited continually increasing challenges posed by emerging communication systems. The flexibility and advantages of DRAs offer excellent performance to more traditional antennas. As DRA technology grows-up, however it should prove a viable alternative to the more-established antenna candidates, offering the engineer more options to solve potentially challenging problems.

The motivation for this work has been inspired by the need for compact, high efficient, low cost antenna suitable for using as multi band operation, dual band dual polarized operation and broadband operation with the possibility of using with MICs, and to ensure less expensive, more efficient and quality wireless communication systems. To

satisfy these challenging demands a novel shaped DR is fabricated and investigated for the possibility of above required properties.

In this work, the properties of the microstrip-fed Isosceles Trapezoidal Dielectric Resonator Antenna (ITDRA) are investigated. The Isosceles trapezoidal shape can be treated as a geometrical extension of the dielectric rectangular parallelepiped. Rectangular DRA's offer practical advantages over cylindrical and spherical shape. For example, the mode degeneracy can be avoided in the case of rectangular DRA's by properly choosing the three dimensions of the resonator. It may be noted that mode degeneracy always exists in the case of a spherical DRA and in the case of hybrid modes of a cylindrical DRA. The mode degeneracy can enhance the cross-polar levels of an antenna, thus limiting its performance. Further, for a given resonant frequency, two aspect ratios of a rectangular DRA (height/length and width/length) can be chosen independently. Since the bandwidth of a DRA also depends on its aspect ratio(s), a rectangular-shaped DRA provides more flexibility in terms of bandwidth control. In addition, the fundamental TE_{111} mode of the rectangular DRA has a low Q-factor and therefore high radiation efficiency. Moreover, the horizontal magnetic dipole-like radiation of the TE_{111} mode results in broadside patterns and very high polarization purity. Since the ITDR can be considered as the geometrical extension of the rectangular DR, as mentioned above, the advantages as mentioned here for a rectangular DR may be applicable to the trapezoidal DR also to certain extend.

The characteristics of the antenna when excited with microstrip feed is described for different orientations by showing the reflection and radiation properties like return loss, input impedance, gain, 2D radiation pattern, half power beam width (HPBW), cross

polar levels, field distributions, 3D gain pattern etc. Wideband operation is achieved with the slotted ground plane structure along with parasitic conducting strips. Ground-plane-slots are also shown to be a technique for enhancing the miniaturization of DR. The antenna performance is optimized for the feed location, dimensions of the slots in ground plane, and that of slanted and parasitic strips as well. The high frequency structure simulation software (HFSS^{TM}), based on Finite Element Modeling (FEM), is used to ease the design procedure. A numerical analysis technique, finite difference time domain (FDTD) is used for validating the results of wide band design at the end. MATLAB is used for modeling the ITDR and implementing FDTD analysis.

1.6 OUTLINE OF THESIS

The thesis is organized into 6 chapters, the present one being ***Chapter 1***.

Chapter 2 deals with the review of the evolution of dielectric resonator antenna (DRA) technology and the major progress in its research over the past 3 decades.

Chapter 3 covers the theoretical aspects of DRA, different feeding techniques usually adopted, the fabrication technique used and the characterization techniques followed in this work.

Chapter 4 discusses the details of measured and simulated results of the different designs. The modes of resonances of the DR in different configurations are also identified. Influence of different physical parameters of the antenna on its performances are also discussed.

Chapter 5 describes the numerical analysis method FDTD and the modeling of the wide band design using this. The measured results are compared with the computed results.

Chapter 6 gives the conclusion drawn from the work and the scope for future work.

Two appendices A and B are also included at the end which deals with the works done by the author in the field of DRA and microwave imaging.

REFERENCES

[1] Sobol, H., "Microwave Communications--An Historical Perspective", *IEEE Transactions on Microwave Theory and Techniques,* Vol. 32, No. 9, pp. 1170 – 1181, 1984.

[2] C. Meynart, "Landmarks in the history of telecommunications", *Telecommunications J.*, vol. 32, pp. 503-515, Dec. 1965.

[3] MacLaurin, W. Rupert, *Invention and Innovation in the Radio Industry*, New York: Macmillan, pp. 18-20, 1949.

[4] MacLaurin, W. Rupert, *Invention and Innovation in the Radio Industry*, New York: Macmillan, pp. 31-32, 1949.

[5] MacLaurin, W. Rupert, *Invention and Innovation in the Radio Industry*, New York: Macmillan, pp. 59-60, 1949.

[6] G. C. Southworth, *Forty Years of Radio Research*. New York: Gordon and Breach, pp. 23-25, 1962.

[7] G. A. Isted, " The Later experimental work of Guglielmo Marconi", The Marconi Review, pp. 3-17, First Quarter 1974.

[8] ____, "The later work of Guglielmo Marconi", The Marconi review, pp. 3-17, First Quarter 1974.

[9] A. A. Heil and O. Heil, "A new method of generating short undamped electromagnetic waves of high intensity," *Zeit fur Phys*., vol. 95, pp. 752–773, July 1935.

[10] G. C. Southworth, *Forty Years of Radio Research*, New York: Gordon and Breach, p. 238, 1962.

[11] H. S. Black, J. W. Beyer, T. J. Gneser and F. A. Polkinghom, "A multi-channel microwave radio relay system", *AIEE Trans. Electrical Engineering*. Vol. 65, pp. 798-805. Dec. 1946.

[12] MacLaurin, W. Rupert, *Invention and Innovation in the Radio Industry*, New York: Macmillan, pp. 43-48, 1949.

[13] A. A. Roetken, K. D. Smith and R. W. Friis, "The TD-2 microwave radio relay system," *Bell Syst. Tech. J*., vol. 30, no. 4, pp. 1041–1077, Oct. 1951.

[14] M. P. Salas, "A new high capacity analog radio," *Nat. Telecommunications Conf. Rec*., Vol. 1, p. A5.3, 1981.

[15] T. A. Abele, D. A. Alsberg, and P. Hutchinson, "A high-capacity digital communication system utilizing TE_{01} transmission in circular waveguide," *IEEE ,TRANS on Microwave Theory Tech*., Vol. MTT- 23, pp. 326-333, Apr. 1975.

[16] J.R. Pierce, "Orbital radio relays", *Jet Propulsion*, vol. 25, pp. 153-157, Apr. 1955.

[17] R.C. Johnson, "Antenna Engineering Handbook", 3rd edition, McGraw-Hill Inc, New York, 1993.

[18] C.A. Balanis, "*Antenna Theory*: Analysis and Design", 2nd Edition, John Wiley & Sons, New York, 1997.

[19] M. M. Ney, "Method of Moments applied as Applied to Electromagnetic Problems", *IEEE Trans. Microwave Theory Tech.*, Vol. 33, pp 972-980, October 1985.

[20] J. Cousty, S. Verdeyme, M. Aubourg and P. Guillon, "Finite Elements for Microwave Device Simulation: Application to Microwave Dielectric Resonator Filters", *IEEE Trans. Microwave Theory. Tech*, Vol. 40, pp. 925-932, May 1992.

[21] K. S. Yee, "Numerical Solution of Initial Boundary Value Problems Involving Maxwell's Equations in Isotropic Media", *IEEE Tran. Antennas Propagat.*, Vol. 14, 302–307, May 1966

[22] P. B. Johns and R. L. Beurle, "Numerical Solution of Two-Dimensional Scattering Problems Using a Transmission-Line Matrix", *Proc. IEEE,* Vol. 118, pp. 1203-1209, 1971.

[23] Karoda Umashankar and Allan Taflov, "Computational Electromagnetics," *Artech House*, Norwood, MA, 1993.

[24] R.F. Harrington, "Field Computation by Moment Methods", Malabar, FL: Krieger, 1968.

[25] B.J. Strait, "Applications of the Method of Moments to Electromagnetics*", St. Cloud, FL: SCEEE Press*, 1980.

[26] R.F. Harrington, "Origin and development of the method moments for field computation," in E.K. Miller et al., *Computational Electromagnetics.,* New York: IEEE Press, 1992, pp. 43–47.

[27] Kane Yee "Numerical solution of initial boundary value problems involving Maxwell's equations in isotropic media", *IEEE Transactions on Antennas and Propagation*, Vol. 14, Issue: 3, pg 302–307., May 1966.

[28] A. Taflove "Application of the finite-difference time-domain method to sinusoidal steady state electromagnetic penetration problems". *IEEE Transactions on Electromagnetic Compatibility*, Vol. EMC-22, Issue: 3, pp. 191–202., Aug. 1980.

[29] W.J.R. Hoefer, "The transmission-line matrix method—theory and applications," *IEEE Trans. Microwave Theory Tech.,* vol. MTT-33, No. 10, Oct. 1985, pp. 882–893.

[30] C. Christopoulos, "The Transmission-Line Modeling Method (TLM)", New York: IEEE Press, 1995.

CHAPTER 2   **REVIEW OF LITERATURE**

This chapter deals with the review of the evolution of dielectric resonator antenna (DRA) technology over the past 3 decades. A report of the existing design aspects for multi-band operation, dual band dual polarization operation, broad band operation, circular polarization, different coupling schemes and different DR geometries is presented. A review on numerical analysis techniques especially FDTD analysis applicable to the analysis of antennas is also done at the end.

2.1 ESTABLISHING DR AS AN ANTENNA

The dielectric resonator is usually made of high permittivity lossless dielectric material normally with a dielectric constant greater than 20 with an unloaded Q factor usually ranging from 50 to 500. As they have been primarily used in microwave circuits such as in oscillators and filters for many years [1], DR was usually treated as energy storage device rather than radiators. But radiation from open DRs was realized by Richtmyer in 1939 [2]. The idea of using DR as antenna was initially accepted only when the first original paper on Cylindrical DRA [3] was published in 1983. The open dielectric resonators (DR's) are potentially useful antenna elements [4]. They offer several attractive features such as small size, high radiation efficiency [5], compatibility with MIC's, intrinsic mechanical simplicity, and the ability to obtain different radiation patterns using different modes. When the frequency range of interest for much system had commonly progressed upwards to the millimeter and near millimeter range (100-300 GHz) the conductor loss of metallic antennas became severe and the efficiency of the

28

antennas was reduced significantly. As the only loss for a DRA is that due to the imperfect dielectric material, which can be very small in practice, it can be used as a suitable alternative for the above range of frequencies. In addition, DRAs exhibit a relatively large bandwidth (~ 10% for ε_r ~ 10), whereas in their basic form patch antennas have a typical bandwidth of only 1%–3%. Systematic experimental investigations on dielectric resonator antennas (DRA's) were first carried out by Long *et al*. [6]–[8]. Since then, theoretical and experimental investigations have been reported by many investigators on DRA's of various shapes such as spherical, cylindrical (or cylindrical ring), rectangular, etc. (e.g., [9]–[16]).

2.2 MULTIBAND OPERATION

With the development of wireless communication systems, the compact, high frequency and dual or multi-frequency antennas are highly desirable. But in compact systems, microstrip antennas are widely used, and have been extensively investigated with reference to dual-frequency applications [17]. Recently, many investigations have been reported on dielectric resonator antennas (DRAs) with dual-frequency or wideband operation using various approaches, such as exciting two modes, or stacking two DRAs [18]-[19]. However, dual-mode excitation is hardly designed because the different modes in a DRA are sensitive to the antenna configuration. And stacking two DRAs increases the size and the weight of DRA and can lead to a complex fabrication process. In [20], a slot coupled dielectric resonator antenna with wide bandwidth was studied, in which, the slot performed a dual-function of a radiator and a feeding mechanism for the DR at the same time, the slot resonance and the DR resonance were slightly offset in order to obtain

a wider impedance bandwidth also. However, in [20], the slot etched on the ground plane of a microstrip line, the dielectric loss and surface wave loss will increase when used at higher frequency. A new configuration, in which, the DRA is excited by a slot etched on the top metallic surface of the substrate integrated waveguide (SIW) is proposed in [21]. SIW is synthesized in a planar substrate with two rows of metallic vias using standard printed circuit board fabrication process.

A novel and simple design method using a cylindrical DRA to achieve single microstripline feed dual-band CP operation is proposed in [22]. The proposed DRA can easily be implemented by embedding a pair of C-shaped slots in the ground plane. In [23], the zonal slot antenna is combined with the dielectric resonator antenna (DRA) to give a dual band antenna. The zonal slot is cut onto the cavity. An L-probe is used to excite the slot antenna directly and to excite the DRA indirectly through the aperture-coupled source. In [24], a simple design method using a cylindrical DRA to achieve single microstrip line feed dual-band circular polarized operation. The proposed DRA is implemented by embedding a pair of C-shaped slots in the ground plane. In [25], a slot-coupled rectangular DRA, for dual band operation is explained. In this, the distance between the slot and the center of DR can be tuned to excite two modes, and through a suitable arrangement, impedance in dual band is matched well. Additionally, a broadside radiation pattern and equivalent to a horizontal magnetic dipole is achieved in lower band, and in upper band, directional electric monopole-like patterns are excited. In [26], a hybrid dielectric resonator antenna with radiating slot for dual-frequency operation is described. For this, the main goal is to design a new hybrid structure antenna that can operate at two different frequencies with a large beam width. The paper [27] describes techniques to enhance the response provided by the natural resonance frequencies of (DRA), by adding

parasitically coupled conducting strips, to enable multi-band operation. In [28], a multi-eccentric ring slot feed structure is presented, which neither increases the antenna volume nor changes dielectric shapes and materials, to realize multi-frequency operations. In [29], Yoonjae Lee et. al. discuss a stacked DRA with a circular microstrip antenna for dual frequency operation, which is designed to produce circular polarization (CP), frequently required in many satellite communication applications.

2.3 DUAL BAND DUAL POLARIZATION OPERATION

Antennas with dual polarization operation have been in demand for many applications, particularly for wireless communication. Polarization-diversity antennas are needed because they can better handle information than singly polarized antennas in certain situations; for example, they can reduce multi-path effects. Much work has been reported on dual polarized microstrip patch antennas [30-32]. However, metallic losses of patch antennas become significant in the X-band. Dielectric resonator antennas (DRAs) are good substitutes at these high frequencies since the resonators do not have metallic loss.

Although extensive researches have been performed on the wideband linearly polarized DRAs, few studies were devoted to dual polarized applications. A dual polarized DRA was reported but with narrow bandwidth [33]. In [33], a cylindrical disk was excited by two orthogonal ports, which gave about 10% bandwidth. Dually polarized DRA are very challenging at high frequencies because the DRA and the excitation for two ports becomes difficult to have without direct coupling between the feeding microstrip lines and achieve high isolation. In [34] a wideband dual polarized DRA is designed. A two steps stair shaped DRA is excited through a cross-shaped slot by two

orthogonal ports. Microstrip lines are terminated with U-shaped tuning stub to optimize the matching. Both ports are able to give more than 20% bandwidth. Recently dual-band and dual polarized antenna arrays have been widely studied for satellite and wireless communication applications, particularly for synthetic aperture radar (SAR) applications [35-38]. In [39] of dual-band dual-polarized antenna array, for the X-band, the hybrid feeding structure in the dielectric resonator antenna element design adopts an H-shaped slot coupling for the horizontal polarization and two U-shaped slot coupling feeds with 180° out of phase for the vertical polarization. For S-band, the two stacked dipoles with different polarization are located orthogonally in different layers. A dual-band dual-polarized antenna array design for WLAN applications is presented in [40]. A phased array by interleaving two types of dual-polarization elements to achieve dual-linear or dual-circular polarizations is presented in [41]. Two high input-isolation dual-polarized dielectric resonator (DR) antennas are presented in [42]. First, a slot-coupled feed technique with two narrow slots forming a "T" configuration is employed to design a dual-polarized DR antenna. Input isolation exceeding 35 dB has been obtained in the band for this design. Secondly, a hybrid feed mechanism with a coplanar waveguide (CPW) feed and a slot feed is used to achieve a dual-polarized DR antenna. In [43], a dual-band dual-polarization stacked microstrip-dielectric antenna is analyzed and designed. It transmits left-hand circularly polarized (LHCP) signals in L band and receives right-hand circularly polarized (RHCP) signals in S band. The antenna has been realized by two stacked square patches which are fed by four quadrature pins placed symmetrically on the two main axis. A dually polarized DRA was reported with using two rectangular slots or hybrid feed in [44].

2.4 WIDE BAND OPERATION

When a single shaped DRA operates in a fundamental mode, its bandwidth is typically below 10%. The research of the wide-band DRA was first experimentally carried out in 1989 by Kishk *et al.* [45], who stacked two different DRAs on the top of one another to obtain a dual-resonance operation. Since then other wide-band DRAs using stacking methods have been reported [46]–[49]. Alternatively, coplanar parasitic DR elements were placed beside the DRA to increase the impedance bandwidth [50, 51]. Moreover, some methods that need only a single DRA to achieve wide-band operation were reported [52]–[59]. Recently, various bandwidth enhancement techniques have been developed for DRAs, such as co-planar parasitic DRAs [60], stacked DRAs [61, 62], and deformed DRAs [63]. More recently, Ong *et al.* proposed a disc-ring DRA by combining one smaller cylindrical DR and one larger annular-ring DR concentrically together to achieve a 45% impedance bandwidth [64]. In the above mentioned wide-band techniques, most cases are devoted to producing broadside radiation patterns.

In [65], a novel stacked double annular-ring DRA is proposed to achieve wide-band operation. At either layer, a larger annular- ring DR is placed concentrically outside a smaller annular-ring one to form a double annular-ring DRA. The antenna is operating in the end-fire mode. Many feeding techniques have been proposed to widen the bandwidth of the DRA's; a parasitic slot in the ground plane was used in [66] to enhance the bandwidth of the hemispherical DRA as the maximum obtained bandwidth was 21%. A modified microstrip line was used to widen the bandwidth from 12 to 26 % for the cylindrical DRA [67].

In [68], a half-cylindrical DRA on the ground plane is used for size reduction. The feeding network is composed of an aperture coupling slot surrounded by a parasitic U-shaped slot. A miniaturized antenna to be used for wireless LAN in the frequency band (5.2/5.8 GHz) is described in [69]. In [70], broadband DRAs using narrow slot aperture coupled to a microstrip line feed are presented. Two different shapes of dielectric resonators tapered in a stair-like structure have been designed for wideband applications. The design of a broadband Dielectric Resonator Antenna (DRA) tailored and modified appropriately for implementation as a textile wearable antenna in Body Area Networks (BAN) is discussed in [71].

2.5 CIRCULARLY POLARIZED DRA

For many years, significant research effort has been devoted to the study of the circularly polarized (CP) antenna. This is because, when compared with the linearly polarized (LP) system, the CP system allows a more flexible orientation between the transmitting and receiving antennas. In addition, CP fields are less sensitive to the propagation effect than LP fields. As a result, the CP system is widely used in satellite communications. CP antenna design using DRAs started with [72] that propose a rectangular DR with two diagonally opposite corners truncated similar to the design implemented with rectangular patch antennas to produce CP. Later, Mongia *et al.* [73] produced CP by exciting the two orthogonal $HE_{11\delta}$ modes of a cylindrical ring DRA using a 3dB quadrature coupler. In [74] the orthogonal $HE_{11\delta}$ modes of a cylindrical dielectric resonator are excited by two probes fed in phase quadrature by a microstrip line. In [75] a slot-coupled rectangular DRA is used where the DRA position is adjusted 45° with respect to the slot to produce CP from a cylindrical DRA over a bandwidth of

3.4 % and beam width of 110°. A cross-slot of unequal slot lengths in the ground plane of a microstrip line has been used **[76]** to produce CP from a cylindrical DRA over 3.91 % of bandwidth. A design with dual conformal strip feed **[77]** can also produce CP but over a wide bandwidth of 20 %. A cylindrical DRA is fed by a perturbed annular ring slot **[78]** to achieve an axial ratio bandwidth of 3.4 %. In this design, a backing cavity of hemispherical shape was used to block the back lobe radiation. Effect of parasitic conducting strip loading on the impedance characteristics of a cylindrical DRA has been studied **[79]** where CP is achieved by varying the angular position of the parasitic strip relative to the conformal feed.

In the last decade, excitation of CP fields has been a popular topic in the research of dielectric resonator antennas (DRAs) [80]–[85]. In [86], *M.B. Oliver et. al* report the development of a new rectangular CP DRA with a single slot or probe feed. The circular polarization is obtained by the excitation of two nearly degenerate orthogonal magnetic dipole modes. In [87], *A. Elboushi et. al.* presented a novel DRA/Microstrip hybrid high gain and circularly polarized antenna for MMW applications. It consists of a printed rectangular patch with a shaped corners and a hollow rectangular DR radiator works together as a single antenna element fed by a rectangular aperture in the ground plane.

2.6 DIFFERENT DR GEOMETRIES

Subsequent to the cylindrical DRA, Long and his colleagues investigated the rectangular [88] and hemispherical [89] DRAs. This work created the foundation for future investigations of the DRA. Kishk et al. studied the radiation characteristics of cylindrical DRA with new applications [90]. Many other shapes such as triangular [91], spherical-cap [92], cylindrical ring [93-94], conical [95], and tetrahedron [96] were also

35

studied. Section-spherical [97], flipped staired pyramid [98], stepped [99], stacked double annular ring [100], Elliptical [101], two layer hemispherical [102], and Sierpinski carpet fractal patterned cylindrical [103] were also used recently for the enhancement of various antenna properties. The basic principle and mode nomenclatures of the DRA were discussed in the review paper [104].

2.7 DIFFERENT COUPLING SCHEMES

Different methods are used for exciting the antenna, which are coaxial probe [105-107], aperture coupling with a microstrip feedline [108,109], aperture coupling with coaxial feed line [110, 111], direct microstrip feed line [112, 113], coplanar feed [114], soldered through probe [115], slot line [116], strip line [117], conformal strip [118-120], dielectric image guide [121] and waveguide probe [122].

2.8 NUMERICAL ANALYSIS TECHNIQUE- FDTD METHOD

Various numerical techniques have been used in the analysis of the DRA. The spherical mode expansion was used to analyze a hemispherical DRA [123]. The Surface Integral Equation with the Method of Moments (SIE/MoM) has been used to analyze a rotationally symmetric DRA [124]. The modal expansion method with some approximation was used in [125] to analyze the rectangular DRA, and the Finite Difference Time Domain(FDTD) method has been used to analyze a rectangular DRA and cylindrical DRA with a staircased cell approximation [126,127].

Modeling of DR based structures using the FDTD method has been a major research area during the past few years. In 1991, Navarro *et al.* **[128]** theoretically obtained the resonant frequencies of a cylindrical DR enclosed in a metallic cavity, using

FDTD combined with discrete Fourier transform (DFT). Kaneda *et al*. presented a modified contour-path integral FDTD [129] to analyze a shielded cylindrical DR, while maintaining the rectangular cells. In [130] Dey *et al*. discuss a conformal FDTD approach for cylindrical DR modeling based on weighted volume effective dielectric constant. An alternate and easier method was proposed [131] by Yu *et al*. that was based on a linear average effective dielectric constant concept. A fast and more accurate computation of resonant properties of axisymmetric DRs using FDTD was presented by Shi *et al*., by using the Pade´-DFT technique.

Much works on the modeling and analysis of DRAs using FDTD are not available in the literature. In 1994, Shum *et al*. studied the effect of an air gap between the DRA and the ground plane on the resonant frequency of a coaxial fed cylindrical ring DRA using FDTD [132]. The FDTD coordinate system used was cylindrical (r, Φ and z) because of the axial symmetry of the structure. An absorbing boundary condition (ABC) based on a parabolic interpolation was used to terminate the boundary and was placed at distances three times the dimensions of the DRA. A Gaussian-modulated sinusoidal pulse was used for excitation. The same team also calculated the resonant frequency of an aperture coupled rectangular DRA using FDTD [133]. Later, Esselle [134] obtained the radiation patterns of an aperture coupled low-profile rectangular DRA using FDTD. Mur's ABC was used to terminate the volume. The patterns were obtained by using the equivalence principle over a fictitious surface enclosing the DRA.

2.9 CONCLUSION

This chapter contains the review of past work done in the field of Dielectric Resonator Antenna. A brief description of the research works done in the field of multi band operation, dual band dual polarization operation, broadband operation, circular polarization, different DR geometries and FDTD method are presented here. In view of these ideas a novel, isosceles trapezoidal shaped DRA for few of the above mentioned applications is developed and investigated its properties in the forth coming chapters.

REFERENCES

[1] D.Kajfez and P. Guillon, Eds., "Dielectric Resonators", Norwood, MA: Artech house, 1986.

[2] R. D. Richtmyer, "Dielectric Resonators", *J. Appl. Phys,* Vol. 10, pp. 391-398, June 1939

[3] S.A Long and M.W McAllister and L.C. Shen, "The resonant cylindrical dielectric cavity antenna", *IEEE Trans. Antennas Propagat.*, vol. 31, pp. 406-412, May 1983.

[4] R. K. Mongia and P. Bhartia, "Dielectric resonator antennas—A review and general design relations for resonant frequency and bandwidth," *Int.J. Microwave Millimeter-Wave Eng.*, vol. 4, pp. 230–247, July 1994.

[5] R. K. Mongia, A. Ittipiboon, and M. Cuhaci, "Measurement of radiation efficiency of dielectric resonator antennas," *IEEE Microwave Guided Wave Lett.*, vol. 4, pp. 80–82, Mar. 1994.

[6] S. A. Long, M. McAllister, and L. C. Shen, "The resonant cylindrical cavity antenna," *IEEE Trans. Antennas Propagat.*, vol. AP-31, pp. 406–412, May 1983.

[7] M. McAllister, S. A. Long, and G. L. Conway, "Rectangular dielectric resonator antenna," *Electron. Lett.*, vol. 19, pp. 219–220, Mar. 1983.

[8] M. McAllister and S. A. Long, "Resonant hemspherical dielectric antenna," *Electron. Lett.*, vol. 20, pp. 657–659, Aug. 1984.

[9] M. Haneishi and H. Takazawa, "Broadband circularly polarized planar array composed of a pair of dielectric resonator antennas," *Electron.Lett.*, vol. 21, pp. 437–438, 1985.

[10] A. A. Kishk, H. A. Auda, and B. C. Ahn "Radiation characteristics of cylindrical resonant antennas with new applications," *IEEE Antennas Propagat. Soc. Newslett.*, vol. 31, pp. 7–16, Feb. 1989.

[11] R. K. Mongia, "Half-split dielectric resonator placed on a metallic plane for antenna applications," *Electron. Lett.*, vol. 25, pp. 462–464, Mar. 1989.

[12] K. W. Leung, K. M. Luk, K. Y. A. Lai, and D. Lin, "Theory and experiment of a coaxial probe fed hemspherical dielectric resonator antenna," *IEEE Trans. Antennas Propagat.*, vol. 41, pp. 1390–1398, Oct. 1993.

[13] R. K. Mongia, A. Ittipiboon, Y. M. M. Antar, P. Bhartia, and M. Cuhaci, "A half-split dielectric resonator antenna using slot coupling," *IEEE Microwave Guided Wave Lett.*, vol. 3, pp. 38–39, Feb. 1993.

[14] R. K. Mongia, A. Ittipiboon, P. Bhartia, and M. Cuhaci, "Electric monopole antenna using a dielectric ring resonator," *Electron. Lett.*, vol. 29, pp. 1530–1531, Aug. 1993.

[15] A. Ittipiboon, R. K. Mongia, Y. M. M. Antar, P. Bhartia, and M. Cuhaci, "Aperture fed rectangular and triangular dielectric resonators for use as magnetic dipole antennas," *Electron. Lett.*, vol. 29, pp. 2001–2002, 1993.

[16] Y. M. M. Antar and Z. Fan, "Characteristics of aperture coupled rectangular dielectric resonator antenna," *Electron. Lett.*, vol. 31, pp. 1209–1210, July 1995.

[17] J.Y.Jan, "Single-layer single-feed dual- frequency circular microstrip antenna with an offset open-ring slot," *IEEE Trans. Antennas propagate.*, Vol.51, pp.3010-3012, Oct, 2003.

[18] R. Chair, A. A. Kishk, K. F. Lee, "Wideband Simple Cylindrical Dielectric Resonator Antennas," *IEEE Microwave and Wireless Components Letters*, Vol.15, No.4, pp.241-243, April, 2005.

[19] A. A. Kishk, X. Zhang, A.W.Glisson, and D.Kajfez, "Numerical analysis of stacked dielectric resonantor antennas excited by a coaxial probe for wideband applications," *IEEE Trans. Antennas Propag.*, Vol.51, NO.8, pp.1996-2006, Aug.2003.

[20] G. Almpanis, C.Fumeaux and R. Vahldieck, "Dual Mode Slot Coupled Cylindrical Dielectric Resonator Antenna," *IEEE Antennas and Propagation Society International Symposium*, pp.2511-2514, 2006.

[21] Tan Ke-jun, Luan Xiu-zhen, Safavi-Naeini S., "A Dual-Frequency DRA Based on Substrate Integrated Waveguide", *International Symposium on Microwave, Antenna, Propagation and EMC Technologies for Wireless Communications*, pp. 508 – 511, 2007.

[22] Ching-Wei Ling and Chih-Yu Huang, "Dual-band Circularly Polarized Dielectric Resonator Antenna", *Antennas and Propagation Society International Symposium*, IEEE, vol.3, pp. 496 – 499, 2003.

[23] Ding Y., Leung K.W., Or Y.C.,"Dualband DRA-slot hybrid slot antenna", *Antennas and Propagation Society International Symposium, IEEE,* pp. *976 – 979, 2007.*

[24] Ching-Wei Ling, Chih-Yu Huang, "Dual-band circularly polarized dielectric resonator antenna", *Antennas and Propagation Society International Symposium*, IEEE, vol.3, pp. 496 - 499, 2003.

[25] Sheng-Ming Deng, Cho-Kang Hsu, Ching-Long Tsai, "A slot-coupled rectangular dielectric resonator antenna for dual-band operations", *Antennas and Propagation Society International Symposium, IEEE*, Vol. 2A, pp. 188 – 191, 2005.

[26] Denidni T.A., Qinjiang Rao, "Hybrid dielectric resonator antennas with radiating slot for dual-frequency operation", *Antennas and Wireless Propagation Letters, IEEE,* Vol. 3, pp. 321 – 323, 2004.

[27] Bit-Babik,G., Di Nallo C., Faraone A., "Multimode dielectric resonator antenna of very high permittivity", *Antennas and Propagation Society International Symposium*, IEEE, Vol. 2 , pp. 1383 – 1386, 2004.

[28] Denidni T.A., Qinjiang Rao, Sebak A.R.,"Multi-eccentric ring slot-fed dielectric resonator antennas for multi-frequency operations", *Antennas and Propagation Society International Symposium, IEEE*, Vol. 2, pp. 1379 – 1382, 2004.

[29] Yoonjae Lee, Junho Yeo, Mittra, R., "A dual frequency circularly polarized antenna design using a combination of DRA and microstrip patch", *Antennas and Propagation Society International Symposium, IEEE*, Vol. 4, pp. 1379 – 1382, 2003.

[30] S. C. Gao, L. W. Li, M. S. Leong and T. S. Yeo, "Dual-polarized slot coupled planar antenna with wide bandwidth," *IEEE Trans. Antennas and Propagat.,* vol. 51, no. 3, pp. 441-448, March 2003.

[31] K. Ghorbani and R. B. Waterhouse, "Dual polarized wide-band aperture stacked patch antennas," *IEEE Trans. Antennas and Propagat.*, vol. 52, no. 8, pp. 2171-2174, August 2004.

[32] H. Wong, K. L. Lau and K. M. Luk, "Design of dual-polarized L-porbe patch antenna arrays with high isolation," *IEEE Trans. Antennas and Propagat.,* vol. 52, no. 1, pp. 45-52, January 2004.

[33] Y. X. Guo and K. M. Luk, "Dual-polarized dielectric resonator antennas", *IEEE Trans. Antennas and Propagat.,* vol. 51, no. 5, pp. 1120 - 1123, May 2003.

[34] Chair R., Kishk A.A. and Lee K.F., "Wideband dual polarized dielectric resonator antennas at X-band", *Antennas and Propagation Society International Symposium, IEEE*, Vol. 4B, pp. 214 – 217, 2005.

[35] Pozar D. M. and S. D. Targonski, "A shared-aperture dual-band dual-polarized microstrip array," *IEEE Trans. Antennas and Propag.*, Vol. 49, No. 2, 150-157, 2001.

[36] Pokuls R., J. Uher, and D. M. Pozar, "Dual-frequency and dual-polarized microstrip antenna for SAR application," *IEEE Trans. Antennas and Propag.*, Vol. 46, No. 9, 1289-1296, 1998.

[37] Vetharatnam G., C. Kuan and C. H. Teik, "Combined feed network for a shared-aperture dual-band dual-polarized array," *IEEE Antennas and Wireless Propag. Lett.*, Vol. 4, 297-299, 2005.

[38] Shafai L. L., W. A. Chamma M. Barakat, P. C. Strickland and G. Seguin, "Dual-band dual- polarized perforated microstrip antennas for SAR application," *IEEE Trans. Antennas and Propag.*, Vol. 48, No. 1, 58-66, 2000.

[39] L. N. Zhang1, S. S. Zhong1 and X. L. Liang, "Dual-band Dual-polarized Hybrid Antenna Array", *PIERS Proceedings*, *Xi'an, China*, March 22-26, 2010.

[40] J. M. Steyn, J. W. Odendaal and J. Joubert, "Dual band dual polarized arrays for WLAN   application", *Progress In Electromagnetics Research C,* Vol. 10, pp. 151-161, 2009.

[41] Kuan Min Lee, Wang A.T.S., and Ruey Shi Chu, "Dual-band, dual-polarization, interleaved cross-dipole and cavity-backed disc elements phased array antenna", *Antennas and Propagation Society International Symposium,* IEEE, 1997 Digest, Vol. 2, pp. 694 – 697, 1997.

[42] Yong-Xin Guo and Kwai-Man Luk, "Dual-polarized dielectric resonator antennas", IEEE *Transactions on Antennas and Propagation,* Vol. 51, No. 5, pp. 1120 – 1124, 2003.

[43] Bin Huang, Yuan Yao and Zhenghe Feng, "A Novel Wide Beam Dual-band Dual-Polarization Stacked Microstrip - Dielectric Antenna", *International Conference on Microwave and Millimeter Wave Technology, ICMMT '07,* pp. 1 – 4, 2007.

[44] Y. X. Guo and K. M. Luk, "Dual polarized dielectric resonator antennas", *IEEE Trans. Antennas and Propagat.,* vol. 51, no. 5, pp. 1120-1123, May 2003.

[45] A. A. Kishk, B. Ahn and D. Kajfez, "Broadband stacked dielectric resonator antennas," *Electron. Lett.*, vol. 25, pp. 1232–1233, Aug. 1989.

[46] S. M. Shum and K. M. Luk, "Stacked annular-ring dielectric resonator antenna excited by axi-symmetric coaxial probe," *IEEE Trans. Antennas Propag.*, vol. 43, no. 8, pp. 889–892, Aug. 1995.

[47] K. W. Leung, K. M. Luk, K. Y. Chow and E. K. N. Yung, "Bandwidth enhancement of dielectric resonator antenna by loading a low-profile dielectric disk of very high permittivity," *Electron. Lett.*, vol. 33, pp. 725–726, Apr. 1997.

[48] A. Sangiovanni, J. Y. Dauvignac and C. Pichot, "Stacked dielectric resonator antenna for multifrequency operation," *Microw. Opt. Technol. Lett.*, vol. 18, pp. 303–306, Jul. 1998.

[49] A. A. Kishk, X. Zhang, A.W. Glisson and D. Kajfez, "Numerical analysis of stacked dielectric resonator antennas excited by a coaxial probe for wide-band applications," *IEEE Trans. Antennas Propag.*, vol. 51, no. 8, pp. 1996–2006, Aug. 2003.

[50] R. N. Simons and R. Q. Lee, "Effect of parasitic dielectric resonators on CPW/aperture-coupled dielectric resonator antennas," *Proc. Inst. Elect. Eng.* , pt. H, vol. 140, pp. 336–338, Oct. 1993.

[51] Z. Fan, Y. M. M. Antar, A. Ittipiboon and A. Petosa, "Parasitic coplanar three-element dielectric resonator antenna subarray," *Electron Lett.*, vol. 32, pp. 789–790, Apr. 1996.

[52] K. L. Wong, N. C. Chen and H. T. Chen, "Analysis of a hemisphere dielectric resonator antenna with an air gap," *IEEE Microw. Guided Wave Lett.*, vol. 3, pp. 355–357, Oct. 1993.

[53] K. M. Luk, M. T. Lee, K. W. Leung and E. K. N. Yung, "Technique for improving coupling between microstrip line and dielectric resonator antenna," *Electron. Lett.*, vol. 35, no. 5, pp. 357–358, Mar. 1999.

[54] Y. X. Guo and K. M. Luk, "On improving coupling between a coplanar waveguide and a dielectric resonator antenna," *IEEE Trans. Antennas Propag.*, vol. 51, no. 8, pp. 2144–2146, Aug. 2003.

[55] H. K. Ngand and K. W. Leung, "Conformal-strip-excited dielectric resonator antenna with a parasitic strip," in *Proc. IEEE Antennas and Propagation Soc. Int. Symp. Dig.*, vol. 4, Salt Lake City, UT, Jul. 2000, pp. 2080–2083.

[56] R. T. Long, R. J. Dorris, S. A. Long, M. A. Khayat, and J. T. Williams, "Use of parasitic strip to produce circular polarization and increased bandwidth for cylindrical dielectric resonator antenna," *Electron. Lett.*, vol. 37, no. 7, pp. 406–408, Mar. 2001.

[57] A. Laisne, R. Gillard and G. Piton, "Robust slot-fed dielectric resonator antenna using an intermediate substrate," *Electron Lett.*, vol. 37, no. 25, pp. 1497–1498, Dec. 2001.

[58] K. P. Esselle, "A dielectric-resonator-on patch (DROP) antenna for broadband wireless applications: Concept and results," in *Proc. IEEE Antennas and Propagation Soc. Int. Symp. Dig.*, vol. 1, Boston, MA, pp. 22–25, Jul. 2001.

[59] A. A. Kishk, Y. Yin and A. W. Glisson, "Conical dielectric resonator antenna for wide-band applications," *IEEE Trans Antennas Propag.*, vol. 50, no. 4, pp. 469–474, Apr. 2002.

[60] Z. Fan andY. M. M. Antar, "Slot-coupledDRantenna for dual-frequency operation," *IEEE Trans Antennas Propag.*, vol. 45, no. 2, pp. 306–308, Feb. 1997.

[61] Z. Fan andY. M. M. Antar, "Slot-coupledDRantenna for dual-frequency operation," *IEEE Trans Antennas Propag.*, vol. 45, no. 2, pp. 306–308, Feb. 1997.

[62] M. H. Al Sharkawy, A. Z. Elsherbeni, and C. E. Smith, "Stacked elliptical dielectric resonator antennas for wideband," in *IEEE Antennas Propagation Soc. Int. Symp. Dig.*, vol. 2, Jun. 2004, pp. 1371–1374.

[63] A. A. Kishk, "Wide-band truncated tetrahedron dielectric resonator antenna excited by a coaxial probe," *IEEE Trans. Antennas Propag.*, vol. 51, no. 10, pp. 2913–2917, Oct. 2003.

[64] S. H. Ong, A. A. Kishk, and A. W. Glisson, "Wide-band disc-ring dielectric resonator antenna," *Microw. Opt. Technol. Lett.*, vol. 35, no. 6, Dec. 2002.

[65] Yong-Xin Guo, Yu-Feng Ruan and Xiang-Quan Shi, "Wide-band stacked double annular-ring dielectric resonator antenna at the end-fire mode operation", *IEEE Transactions on Antennas and Propagation,* Vol. 53, No. 10, pp. 3394 – 3397, 2005.

[66] A. Petosa, "Dielectric Resonator Antenna Handbook", Norwood, MA: Artech house, Inc., 2007.

[67] P. V. Bijumon, S. K. Menon, M. N. Suma, M. T. Sebastian, and P. Mohanan, "Broadband cylindrical dielectric resonator antenna excited by modified microstrip line," Electron lett, Vol 41, No.7, March 2005.

[68] Abumazwed A., Ahmed O., Sebak A.R., "Broadband half-cylindrical DRA for future WLAN applications", *3rd European Conference on Antennas and Propagation, EuCAP 2009.*, pp. 389 – 392, 2009.

[69] Abumazwed A.A., Sebak A., "Compact DRA for broadband wireless applications", IEEE *Antennas and Propagation Society International Symposium,* APSURSI '09, pp. 1-4, 2009.

[70] Chair R., Kishk A.A., Lee K.F., Smith C.E., "Broadband aperture coupled flipped staired pyramid and conical dielectric resonator antennas", *IEEE, Antennas and Propagation Society International Symposium,* Vol. 2, pp. 1375 – 1378, 2004.

[71] Mashhadi S. H. H., Wu Z., Thamae L. Z., "Investigation of a wearable broadband textile Dielectric Resonator Antenna", *Antennas and Propagation Conference (LAPC), Loughborough,* pp. 349 – 352, 2010.

[72] M. Haneishi and H. Takazawa, Broadband Circularly Polarized Planar Array Composed of a Pair of Dielectric Resonator Antennas, Electron. Lett., Vol. 21, pp. 437-438, May 1985.

[73] R. K. Mongia, A. Ittipiboon, M. Cuhaci and D. Roscoe, Circularly Polarized Dielectric Resonator Antenna, Electron. Lett., Vol. 30, pp. 1361-1362, August 1994

[74] G. Drossos, Z. Wu and L. E. Davis, Circular Polarized Cylindrical Dielectric Resonator Antenna, Electron. Lett, Vol. 32, pp. 281-283, February 1996

[75] K. P. Esselle, Circularly Polarized Higher-order Rectangular Dielectric-Resonator Antenna, Electron. Lett, Vol. 32, pp. 150-151, February 1996

[76] Chih-Yu Huang, Jian-Yi Wu and Kin-Lu Wong, Cross-slot Coupled Microstrip Antenna and Dielectric Resonator Antenna for Circular Polarization, IEEE Trans. on Antennas Propag., Vol. 47, pp. 605-609, April 1999

[77] K. W. Leung, W. C. Wong, K. M. Luk and E. K. N. Yung, Circularly Polarized Dielectric Resonator Antenna excited by Dual Conformal Strips, Electron. Lett,Vol. 36, pp. 484-486, March 2000

[78] K. W. Leung and S. K. Mok, Circularly Polarized Dielectric Resonator Antenna Excited by Perturbed Annular Slot with Backing Cavity, Electron. Lett, Vol. 37, pp. 934-936, July 2001

[79] R. T. Long, R. J. Dorris, S. A. Long, M. A. Khayat and J. T. Williams, Use of Parasitic Strip to Produce Circular Polarization and Increased Bandwidth for Cylindrical Dielectric Resonator Antenna, Electron. Lett, Vol. 37, pp. 406-408, March 2001

[80] R. K. Mongia, A. Ittipiboon, M. Cuhaci, and D. Roscoe, "Circular polarized dielectric resonator antenna," *Electron. Lett.*, vol. 30, pp. 1361–1362, Aug. 1994.

[81] G. Drossos, Z. Wu, and L. E. Davis, "Circular polarized cylindrical dielectric resonator antenna," *Electron. Lett.*, vol. 32, pp. 281–283, Feb. 1996.

[82] K. W. Leung, W. C. Wong, K. M. Luk, and E. K. N. Yung, "Circularpolarized dielectric resonator antenna excited by dual conformal strips," *Electron. Lett.*, vol. 36, no. 6, pp. 484–486, Mar. 2000.

[83] A. Petosa, A. Ittipiboon, and M. Cuhaci, "Array of circular-polarized cross dielectric resonator antenna," *Electron. Lett.*, vol. 32, pp. 1742–1743, Sep. 1996.

[84] K. W. Leung and H. K. Ng, "Theory and experiment of circularly polarized dielectric resonator antenna with a parasitic patch," *IEEE Trans. Antennas Propag.*, vol. 51, no. 3, pp. 405–412, Mar. 2003.

[85] R. T. Long, R. J. Dorris, S. A. Long, M. A. Khayat, and J. T. Williams, "Use of parasitic strip to produce circular polarization and increased bandwidth for cylindrical dielectric resonator antenna," *Electron. Lett.*, vol. 37, pp. 406–408, Mar. 2001.

[86] Oliver M.B., Mongia R.K., Antar Y.M.M., "A new broadband circularly polarized dielectric resonator antenna", *Antennas and Propagation Society International Symposium, AP-S. Digest*, Vol. 1, pp. 738 – 741, 1995.

[87] Elboushi A., Haraz O.M., Sebak A., Denidni T., "A new circularly polarized high gain DRA millimeter-wave antenna", *IEEE, Antennas and Propagation Society International Symposium (APSURSI)*, pp. 1 – 4, 2010.

[88] M.W McAllister, S.A Long and G.L Convey, Rectangular dielectric resonator antenna, Electron. Lett., vol. 19, pp.218-219, March 1983.

[89] M.W McAllister and S.A Long, Resonant hemispherical dielectric antenna, Electron. Lett., vol. 20, pp.657-659, Aug. 1984.

[90] A.A.Kishk, H.A. Auda and B.C. Ahn, Radiation characteristics of cylindrical dielectric resonator antennas with new applications, IEEE Antennas Propagat. Soc. Newsletter, vol. 31, pp. 587-589, 1989.

[91] A. Ittipiboon, R.K. Mongia, Y.M.M. Antar, P. Bhartia and M. Cuhaci, Aperture fed rectangular and triangular dielectric resonators for use as magnetic dipole antennas, Electron. Lett., vol. 29, pp.2001-2002, Nov. 1993.

[92] K.W. Leung, K.M. Luk and E.K.N Yung, Spherical cap dielectric resonator antenna using aperture coupling, Electron. Lett., vol. 30, pp.1366-1367, Aug. 1994.

[93] R.K. Mongia, A. Ittipiboon, P. Bhartia and M. Cuhaci, Electric monopole antenna using dielectric ring resonator, Electron. Lett., vol. 29, pp.1530-1531, Aug. 1993.

[94] K.W. Leung, K.Y. Chow, K.M. Luk and E.K.N Yung, Excitation of dielectric resonator antenna using a soldered through probe, Electron. Lett., vol. 33, pp.349-350, Feb.1997.

[95] A.A. Kishk, Yan Yin and A.W. Glisson, Conical dielectric resonator antenna for wideband applications, IEEE Trans. Antennas Propagat., vol. 50, pp. 469-474, April 2002.

[96] A.A. Kishk, Wideband truncated tetrahedron dielectric resonator antenna excited by a coaxial probe, IEEE Trans. Antennas Propagat., vol. 51, pp.2913-2917, Oct. 2003.

[97] Hong-Twu Chen, Yuan-Tung Cheng, Shyh-Yeoung Ke, "Probe-fed section-spherical dielectric resonator antennas", *Microwave Conference, 1999 Asia Pacific*, Vol. 2, pp. 359 – 362, 1999.

[98] Chair R., Kishk A.A., Lee K.F., Smith C.E., "Wideband flipped staired pyramid dielectric resonator antennas", *Electronics Letters,* Vol. 40, No. 10, pp. 581 – 582, 2004.

[99] Pliakostathis K., Mirshekar-Syahkal D., "Stepped dielectric resonator antennas for wideband applications", *IEEE, Antennas and Propagation Society International Symposium,* Vol. 2, pp. 1367 – 1370, 2004.

[100] Yong-Xin Guo, Yu-Feng Ruan, Xiang-Quan Shi, "Wide-band stacked double annular-ring dielectric resonator antenna at the end-fire mode operation", *IEEE*

Transactions on Antennas and Propagation, Vol. 53, No. 10, pp. 3394 – 3397, 2005.

[101] Shing-lung Steven Yang, Ricky Chair, Ahmed A. Kishk, Kai-Fong Lee, Kwai-Man Luk, "Study on Sequential Feeding Networks for Subarrays of Circularly Polarized Elliptical Dielectric Resonator Antenna", *IEEE Transactions on Antennas and Propagation,* Vol. 55, No. 2, pp. 321 – 333, 2007.

[102] Leung K.W., So K.K., "Theory and Experiment of the Wideband Two-Layer Hemispherical Dielectric Resonator Antenna", *IEEE Transactions on Antennas and Propagation*, Vol. 57, No. 4, part 2, pp. 1280 – 1284, 2009.

[103] Karmakar D.P., Soren D., Ghatak R., Poddar D.R., Mishra R.K., "A wideband Sierpinski carpet fractal cylindrical dielectric resonator antenna for X-Band application", *Applied Electromagnetics Conference (AEMC),* pp. 1 – 3, 2009.

[104] R.K. Mongia, and P. Bhartia, Dielectric resonator antennas – A review and general design relations for resonant frequency and bandwidth, International journal of Microwave and Millimeter wave computer aided engg., vol. 4, pp.230-247, 1994.

[105] S.A Long and M.W McAllister and L.C. Shen, "The resonant cylindrical dielectric cavity antenna", *IEEE Trans. Antennas Propagat.*, vol. 31, pp. 406-412, May 1983.

[106] M.W McAllister, S.A Long and G.L Convey, "Rectangular dielectric resonator antenna", *Electron. Lett.*, vol. 19, pp.218-219, March 1983.

[107] M.W McAllister and S.A Long, "Resonant hemispherical dielectric antenna", *Electron. Lett.*, vol. 20, pp.657-659, Aug. 1984

[108]   A. Ittipiboon, R.K. Mongia, Y.M.M. Antar, P. Bhartia and M. Cuhaci, "Aperture fed rectangular and triangular dielectric resonators for use as magnetic dipole antennas", *Electron. Lett.*, vol. 29, pp.2001-2002, Nov. 1993.

[109]   K.W. Leung, K.M. Luk and E.K.N Yung, "Spherical cap dielectric resonator antenna using aperture coupling", *Electron. Lett.*, vol. 30, pp.1366-1367, Aug. 1994.

[110]   K.Y. Chow and K.W. Leung, "Theory and experiment of the cavity backed slot excited dielectric resonator antenna", *IEEE Trans. Electromagnetic Compatibility*, vol. 42, pp. 290-297, Aug. 2000.

[111]   K.Y.Chow, K.W. Leung, K.M. Luk and E.K.N. Yung, "Input impedance of the slot fed dielectric resonator natenna with/without a backed cavity", *IEEE Trans. Antennas Propagat.*, vol. 49, pp.307-309, Feb. 2001.

[112] R.A. Karaneburg and S.A.Long, "microstrip transmission line excitation of dielectric resonator antenna", *Electron. Lett.*, vol. 24, pp. 1156-1157, Sept. 1988.

[113] K.W. Leung, K.Y. Chow, K.M. Luk, and E.K.N. Yung, "Low profile circular disk DR antenna of very high permittivity excited by a microstrip line", *Electron. Lett.*, Vol. 33, pp.1004-1005, June. 1997.

[114] R.A. Karaneburg, S.A.Long and J.T.Williams, "coplanar waveguide excitation of dielectric resonator antenna", *IEEE Trans. Antennas Propagat.*, vol. 39, pp. 119-122, Sept. 1991.

[115] K.W. Leung, K.Y. Chow, K.M. Luk and E.K.N Yung, "Excitation of dielectric resonator antenna using a soldered through probe", *Electron. Lett.,* vol. 33, pp.349-350, Feb.1997.

[116] H.Y.Lo, K.W. Leung and K.M. Luk, "slot line excited equilateral triangular dielectric resonator antenna of very high permittivity", *Microw. And Opt. Techn. Lett.*, vol. 29, pp. 230-231,Apr. 2001.

[117] K.W. Leung, M.L. Poon, W.C. Wong, K.M. Luk, and E.K.N. Yung, "Aperture coupled dielectric r esonator antenna using a stripline feed", *Microw. and Opt. Techn. Lett.*, vol. 24, pp.120-121, Jan. 2000

[118] K.W. Leung, "Conformal strip excitation of dielectric resonator antenna", *IEEE Trans. Antennas Propagat.* vol. 48, pp. 961-967, June. 2000.

[119] K.W. Leung, "Simple result for a conformal strip excited hemispherical dielectric resonator antenna", *Electron. Lett.* vol. 36, pp. 933-935, May. 2000.

[120] H.Y. Lo and K.W. Leung, "Excitation of low profile equilateral triangular dielectric resonator antenna using a conducting conformal strip", *Microw. And Opt. Lett.*, Vol. 29, pp. 317-319, June 2001.

[121] M.T. Birand and R.V. Gelsthorpe, "Experimental millimetric array using dielectric radiators fed by means of dielectric waveguide", *Electron. Lett.*, vol. 17, pp. 633-635, Sept. 1981.

[122] Islam A. Eshrah, Ahmed A. Kishk, Alexander B. Yakovlev, and Allen W. Glisson, "Equivalent Circuit Model for a Waveguide Probe With Application to DRA Excitation", *IEEE transactions on antennas and propagation*, vol. 54, no. 5, pp. 1433-1441, 2006.

[123] Kishk A. A. and G. Zhou, and A.W. Glisson, "Analysis of dielectric resonator antennas with emphasis on hemispherical structures," IEEE Antennas Pmpagat. Magazine, vol. 36, no. 2, pp. 20-31, April 1994

[124] G.P. Junker, A.A. Kishk, A.W. Glisson, "Input impedance of aperture coupled dielectric resonator antenna," *IEEE Trans. Antenna prpagat.,* vol. 44, no. 5, pp. 600-607, May 1996.

[125] Y.M.M. Antar and Z.Fan, " Theoritical investigation of aperture coupled rectangular dielectric resonator antenna," *IEE Proc..-Microw. Antennas Propagt.,* Vol. 143, Apr. 1996.

[126] S. M. Shum and K. M. Luk, "Analysis of aperture coupled rectangular dielectric resonator antenna," *Electronics Lett.,* vol. 30, pp. 1726-1727, 1994.

[127] S. M. Shum and K. M. Luk, "FDTD analysis *of* probe fed cylindrical dielectric resonator antenna," *IEEE Trans., Antennas propagate*., vol. 46, no. 3, pp. 325-333, Mar. 1998.

[128] A. Navarro, M. J. Nunez and E. Martin, "Study of TE_0 and TM_0 Modes In Dielectric Resonators by a Finite Difference Time Domain Coupled with the Discrete Fourier Transform", *IEEE Trans. Microwave Theory Tech.,* Vol. 39, pp. 14–17, January 1991

[129] N. Kaneda, B. Houshm, and T. Itoh, "FDTD Analysis of Dielectric Resonators with Curved Surfaces", *IEEE Trans. Microwave Theory Tech.*, vol. 45, pp. 1645–1649, September 1997

[130] S. Dey and Raj Mittra, "A Conformal Finite-Difference Time-Domain Technique for Modeling Cylindrical Dielectric Resonators", *IEEE Trans. Microwave Theory Tech.*, Vol. 47, pp. 1737-1739, September 1999

[131] W. Yu, and Raj Mittra, "A Conformal Finite Difference Time Domain Technique for Modeling Curved Dielectric Surfaces", *IEEE Microwave Wireless Comp. Lett,* Vol. 11, pp. 25-27, January 2001

[132] S. M. Shum and K. M. Luk, "Characteristics of Dielectric Ring Resonator Antenna with   an Air Gap", *Electro. Lett.*, Vol.30, pp. 277-278, February 1994

[133] S. M. Shum and K. M. Luk, "Analysis of Aperture Coupled Rectangular Dielectric Resonator Antenna", *Electro. Lett.*, Vol.30, pp. 1726-1727, October 1994

[134] S. M. Shum and K. M. Luk, "FDTD Analysis of a Probe Fed Cylindrical Dielectric Resonator Antenna Operating in the Fundamental Broadside Mode", *Electro. Lett.,* Vol.31, pp. 1210-1212, July 1995

CHAPTER 3
DIELECTRIC RESONATOR ANTENNA
- THEORY AND FABRICATION

This chapter describes the fundamental concepts and theory of the dielectric resonator antenna. The methodology for fabricating DRA and that for the experimental measurements of various parameters of the antenna such as return loss, gain, radiation patterns etc. are also explained. The method of characterization of the DR and the basic facilities used for the measurement of antenna parameters are also highlighted.

3.1 DIELECTRIC RESONATOR ANTENNAS

The DRA is an open resonating structure, fabricated from a low loss microwave dielectric material. Dielectric resonators (DR's) have proved themselves to be ideal candidates for antenna applications by virtue of their high radiation efficiency, flexible feed arrangement, simple geometry, small size and the ability to produce different radiation pattern using different modes[1]. Feeding techniques like probe feed, aperture slot, microstrip line and coplanar line can be used with the DRAs, which enables them for integration with microwave printed technology.

Additionally, DRA's avoid some limitations of the patch antenna including the high conductor losses at millimeter-wave frequencies, sensitivity to tolerances, and narrow bandwidth. DRA's of cylindrical, hemispherical and rectangular shapes are most widely used and investigated. The rectangular shape is much easier to fabricate and one or more dimensional parameters are available as additional degrees of freedom for the design [2]. Impedance bandwidth varies over a wide range with resonator parameters. It

can be as small as a few percent with high ε_r material or over 20 % with small ε_r in conjunction with certain geometries and resonant modes. Different far field radiation patterns are supported. For a given DRA geometry, the radiation pattern can be made to change by exciting different modes.

Systematic experimental investigations on dielectric resonator antennas (DRA's) were first carried out by Long *et al*. [3],[4]–[6]. Since then, theoretical and experimental investigations have been reported by many investigators on DRA's of various shapes such as spherical, cylindrical (or cylindrical ring), rectangular, etc. (e.g., [3],[7]–[12]). DRAs with various other shapes are also reported in different literature.

3.2 ADVANTAGES OF DRAs

DRAs offer a high degree of flexibility and versatility over a wide frequency range, allowing for designers to suit many requirements. DRAs offer the following advantages:

➢ DRAs come in simple geometries like circular cylinder, hemisphere, rectangular etc. are readily available and can be easily fabricated.

➢ The DRA size is proportional to $\dfrac{\lambda_0}{\sqrt{\varepsilon_r}}$, where λ_0 is the wavelength at resonant frequency and ε_r is the dielectric constant of the DR. Thus for the same frequency there is a natural reduction in size, compared with their conventional counterparts like microstrip antennas. Also, different values of ε_r (ranging from 4 to 100) can be used, thus allowing the designer the flexibility in controlling the size and bandwidth.

➢ Depending on the resonator shape, various modes can be excited within the DRA element. These modes can produce different radiation patterns for various coverage requirements. Also, the Q-factor of some of these modes will depend on the aspect ratio of the DRA, thus allowing one more degree of flexibility in the design.

➢ Many of the existing feeding schemes can be used (slots, probes, microstrip, coplanar waveguides, dielectric image guide, etc.). This makes them easy to integrate with existing technologies.

➢ Compared with the microstrip antenna, DRA has a much wider impedance bandwidth. This is because the microstrip antenna radiates only through two narrow radiation slots, whereas the DRA radiates through the whole antenna surface except the grounded part. Moreover the operating bandwidth of a DRA can be varied by suitably choosing the dielectric constant of the resonator material and its dimensions.

➢ DRAs have been designed to operate over a wide frequency range (1 GHz to 44 GHz) compared with other antennas existing in the literature.

➢ DRAs have a high dielectric strength and hence higher power handling capacity. Moreover the temperature-stable ceramics enable the antenna to operate in a wide temperature range.

➢ There is no inherent conductor loss for a DRA. High radiation efficiency is thus possible in case of DR antennas. It is especially attractive for high frequency millimeter wave applications, where the loss from metallic antennas can be high.

3.3 RECTANGULAR DRA

Rectangular DRAs offer practical advantages over cylindrical and spherical shape. For example, the mode degeneracy can be avoided in the case of rectangular DRA's by properly choosing the three dimensions of the resonator. It may be noted that mode degeneracy always exists in the case of a spherical DRA [13] and in the case of hybrid modes of a cylindrical DRA [14]. The mode degeneracy can enhance the cross-polar levels of an antenna, thus limiting its performance. Further, for a given resonant frequency, two aspect ratios of a rectangular DRA (height/length and width/length) can be chosen independently. Since the bandwidth of a DRA also depends on its aspect ratio(s), a rectangular-shaped DRA provides more flexibility in terms of bandwidth control [3].

A rectangular DRA support two type modes, TM and TE, but TM modes have never been observed experimentally [3]. Therefore the existence of TM modes appears to be doubtful. Figure 3.3.1 shows a rectangular DRA with the corresponding coordinate system. The resonant modes can be TE to either dimension, denoted as TE^x, TE^y, or TE^z. A rectangular DR has three independent dimensions. The modes of a DR can therefore, be TE to any of three dimensions.

Referring to the DR and co-ordinates system shown in figure 3.3.1, the modes with lowest order indexes are TE^z_{111}, TE^y_{111} and TE^x_{111} [15]. If the dimensions of the DR are such that $a > b > d$, the modes in the order of increasing resonant frequency are TE_{111}, TE^y_{101} and TE^x_{011}. The analysis of all the modes is similar. For example, for TE mode,

the analysis for the field components inside the resonator can be done from the directed

magnetic potential ϕ^h [3],[16].
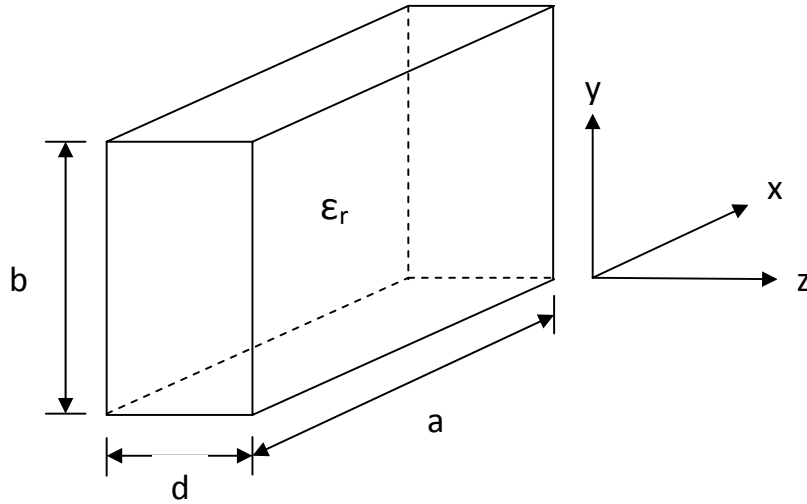
Figure 3.3.1: Isolated rectangular DRA.

$$H_z = \frac{\left(k_x^2 + k_y^2\right)}{j\omega\mu_0} A\cos(k_x x)\cos(k_y y)\cos(k_z z) \quad \cdots\cdots\cdots\cdots\cdots (1)$$

$$H_x = \frac{\left(k_x k_z\right)}{j\omega\mu_0} A\sin(k_x x)\cos(k_y y)\sin(k_z z) \quad \cdots\cdots\cdots\cdots\cdots\cdots (2)$$

$$H_y = \frac{\left(k_y k_z\right)}{j\omega\mu_0} A\cos(k_x x)\sin(k_y y)\sin(k_z z) \quad \cdots\cdots\cdots\cdots\cdots\cdots (3)$$

$$E_x = Ak_y \cos(k_x x)\sin(k_y y)\cos(k_z z) \quad \cdots\cdots\cdots\cdots\cdots\cdots\cdots (4)$$

$$E_y = -Ak_x \sin(k_x x)\cos(k_y y)\cos(k_z z) \quad \cdots\cdots\cdots\cdots\cdots\cdots (5)$$

where A is an arbitrary constant and k_x, k_y, and k_z denote the wavenumbers along the x, y, and z directions, respectively, inside the DR.

$$k_x{}^2 + k_y{}^2 + k_z{}^2 = \varepsilon_r k_0{}^2 \qquad \dots\dots\dots\dots\dots\dots\dots (6)$$

$$k_z \tan\left(\frac{k_z d}{2}\right) \sqrt{\left((\varepsilon_r - 1)k_0{}^2 - k_z{}^2\right)} \qquad \dots\dots\dots\dots\dots\dots\dots (7)$$

The dimensions of the radiating portion of the DR were determined using the equation (7) developed for the dielectric waveguide model (DWM) [15] for a rectangular resonator in free-space [3].

where

$$Q = \frac{2\omega W_e}{P_{rad}} \qquad (8)$$

$$k_x = \frac{\Pi}{a}; k_y = \frac{\Pi}{b}; k_o = \frac{2\Pi f_o}{C}; C = 3 \times 10^8 m/S \qquad (9)$$

Figure shows the rectangular resonator with length a, breadth b and height d. Resonances can occur at the following frequencies

$$f_{mnp} = \frac{1}{2\sqrt{\varepsilon\mu}} \sqrt{\left(\frac{m}{a}\right)^2 + \left(\frac{n}{b}\right)^2 + \left(\frac{p}{d}\right)^2} \qquad (10)$$

where ϵ is the permittivity, μ is the material permeability, and m, n and p are integers. In this configuration, $TE^x{}_{011}$ mode is the dominant mode, because it occurs at the lowest frequency at which a cavity resonance can exist. From equation (10) it can be seen that the frequency at which this dominant resonant mode can exists (the cutoff frequency) is inversely proportional to the square root of the product of material parameters, ϵ and μ.

3.4 DIFFERENT FEED TECHNIQUES FOR DR

Electromagnetic power can be coupled to the DR in several ways. These coupling mechanisms can have a significant impact on the resonant frequency and Q-factor. Numerous feeding techniques are available in the literature. Some of the commonly used techniques are,

3.4.1 SLOT/APERTURE COUPLING

Figure below depicts a DRA fed by an aperture. The aperture behaves like a magnetic current running parallel to the length of the slot, which excites the magnetic fields in the DRA. The aperture consists of a slot cut in a ground plane and fed by a microstrip line beneath the ground plane. This coupling mechanism has the advantage of having the feed network located below the ground plane, thus avoiding spurious radiation [17]. The microstrip stub can be designed to cancel out the reactive component of the slot, thus allowing for an impedance match to the DRA. Moreover, slot coupling is an attractive method for integrating DRAs with printed feed structures .The coupling level can be adjusted by moving the DRA with respect to the slot.
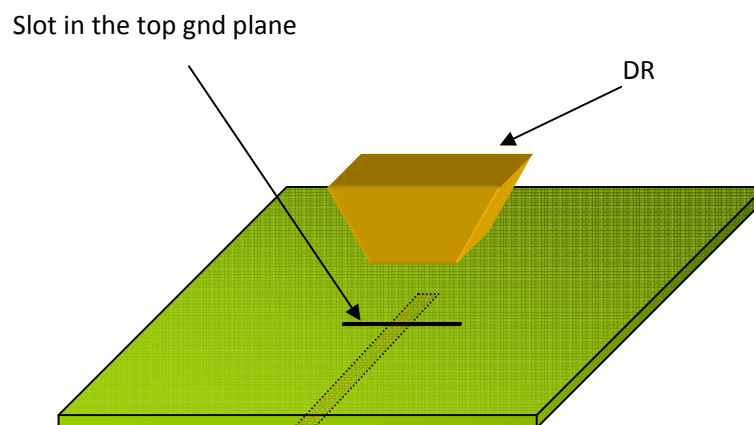
Figure 3.4.1.1: Slot fed DRA

3.4.2 COAXIAL PROBE COUPLING

The coaxial probe can either be located adjacent to the DRA or can be embedded within it. The amount of coupling can be optimized by adjusting the probe height and the DRA location. Also, depending on the location of the probe, various modes can be excited. For the probe located adjacent to the DRA, the magnetic fields of the $TE_{11\delta}$ mode of the rectangular DRA are excited (which radiate like a horizontal magnetic dipole). For a probe located in the centre of a cylindrical DRA, the TE_{011} mode is excited (radiating like a vertical dipole) [17]. Another advantage of using probe coupling is that one can couple directly into a 50Ω system, without the need for a matching network. Probes are useful at lower frequencies where aperture coupling may not be practical due to the large size of the slot requited [18-21].
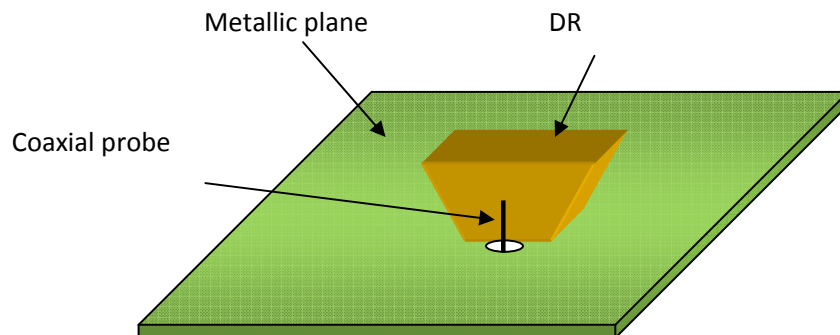
Figure 3.4.2.1: Coaxial probe fed DRA

3.4.3 MICROSTRIP TRANSMISSION LINE / PROXIMITY COUPLING

Another common method for coupling to dielectric resonators in microwave circuits is by proximity coupling to microstrip lines. This approach is equally applicable

to DRAs as shown in figure. Mictrostrip coupling will excite the magnetic fields in the DRA to produce the short horizontal magnetic dipole mode. A metallic strip of definite width is etched on one side of a low loss dielectric substrate of known permittivity and thickness, the other side of which is metalized and grounded. An advantage of microstrip feed is that it is easier to fabricate, match and model. The feed is shown in Figure 3.4.3.1.

Coupling of EM energy and the input impedance are set by adjusting the lateral position of the DR with respect to the strip line [22, 23]. It is more convenient for the DRA arrays as well [24]. One disadvantage of this feed is that at higher frequency, surface wave modes are also excited in the substrate which affects the radiation pattern and efficiency of the DRA [25]. For lower permittivity values (necessary for DRAs requiring wide bandwidth), the amount of coupling is generally quite small.
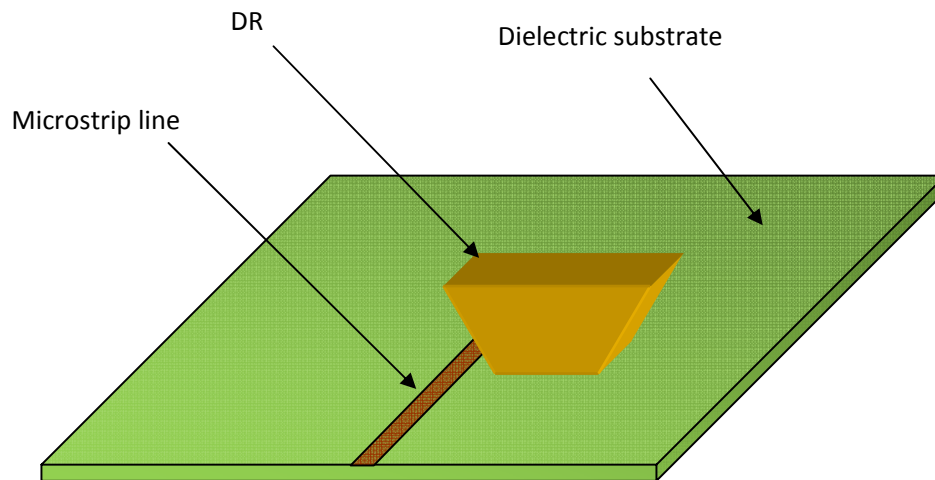
Figure 3.4.3.1: Microstrip line fed DRA

3.4.4 COPLANAR SLOT FEEDS

Coupling to DRAs can also be achieved using co-planar feeds. Figure shows a ITDRA coupled to a co-planar loop. The coupling level can be adjusted by positioning

the DRA over the loop. The coupling behavior of the co-planar loop is similar to that of

the coaxial probe, but the loop offers the advantage of being non obtrusive. By moving

the loop from the edge of the DRA to the centre, one can couple into either the $HE_{11\delta}$

mode or the TE_{011} mode of the cylindrical DRA [17, 26]. A coplanar slot can also be used

to feed the DRA as shown in figure.
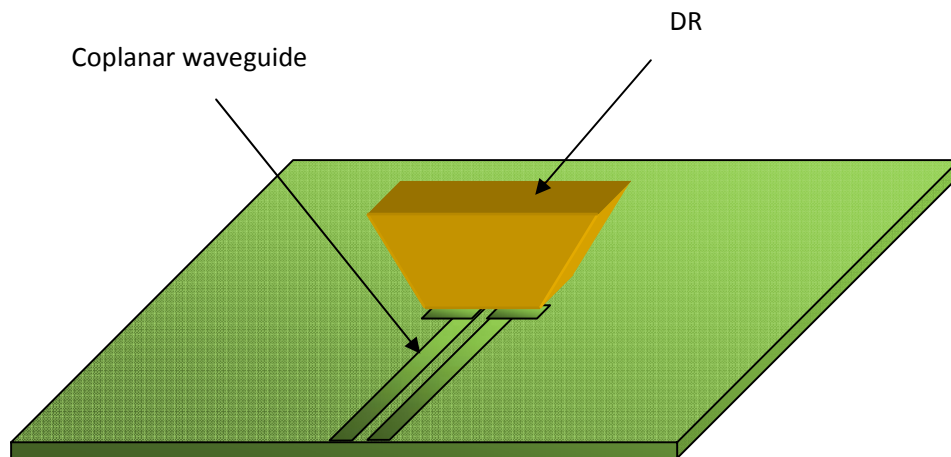
Figure 3.4.4.1: Co-planar slot feed DRA

3.4.5 WAVE GUIDE FEED

The primary advantage of a waveguide is that it is extremely less lossy in the

millimeter wave band. Since the wave is completely guided within the metallic structure,

there is no threat of radiation loss when used as a feed line. As both the waveguide and

DR are very low-loss, they form an excellent combination for low-loss millimeter-wave

communication systems [27, 28]. Coupling to the DR can be achieved through a probe

[29] or a slot [30]. A waveguide probe fed DRA is shown in Figure 3.4.5.1.

Rectangular waveguide
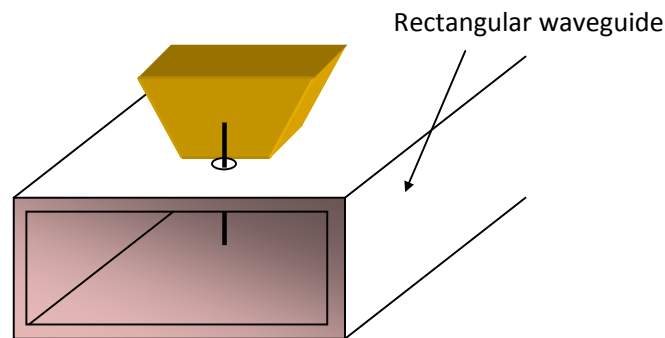
Figure 3.4.5.1: Waveguide probe fed DRA

3.5   DIFFERENT DR GEOMETRIES

One of the attractive features of a DRA is that it can assume a number of shapes. Moreover the mode of operation and performance of a DRA can be varied by selecting a DR with desired structure [31]. Hence a number of DRA geometries have already been tried experimentally. The first systematic, theoretical, and experimental study was made on cylindrical disk DRA geometry. Later geometries such as split cylinder, sectored cylinder, cylindrical rings, metallized DRAs, triangular, rectangular, notched rectangular DRA, chamfered DRA, conical, elliptical, spherical, hemispherical, spherical cap, tetrahedral, perforated DRA, stepped DRAs, and hybrid DRAs, have been reported. It was found that DRAs operating at their fundamental modes radiate like an electric or magnetic dipole, which depends on the mode of excitation and geometry of the bulk dielectric material. Geometries like conical [32], stair [33], stacked triangular [34] etc emerged for dualband or wideband applications while those like cross [35], elliptical [36], hexagonal [37], cylindrical-comb [38] etc emerged for circular

polarization applications. Figure 3.5.1 shows the DR geometries, explained so far. Though several geometries have been introduced, the most studied and common structures are still the cylindrical and rectangular DRAs because of the simplicity in their design, fabrication, and analysis.

Figure 3.5.1: Different DR geometries used

3.6 CHARACTERISTICS OF A DIELECTRIC RESONATOR

3.6.1 DIELECTRIC CONSTANT

The dielectric constant of a material under given conditions reflects the extent to which it concentrates electrostatic lines of flux. In other words, it is the ratio of the amount of electrical energy stored in a material by an applied voltage, relative to that stored in a vacuum. An important property of a dielectric material is its ability to support

an electric field while dissipating minimal energy in the form of heat. The lower the dielectric loss, the more effective a dielectric material is.

The net flux density D can be expressed as

$$D = \varepsilon_o E + P \qquad \text{.......(11)}$$

where E is the electric field intensity and P is the net polarization given by

$$P = \varepsilon_o \chi E \qquad \text{........} \qquad (12)$$

Where χ is the electric susceptibility. Now Eq. (11) becomes

$$D = \varepsilon_o (1 + \chi) E \qquad \text{…..…..…} \quad (13)$$
$$= \varepsilon_o \varepsilon_r E$$

Now we define the relative permittivity as,

$$\varepsilon_r = 1 + \chi \qquad \text{… ………} \quad (14)$$

in the complex form,

$$\varepsilon_r = \varepsilon_r{}' - j\varepsilon_r{}'' \qquad \text{………….} \quad (15)$$

In Eq. (15), the real part is called the dielectric constant and the ratio $\dfrac{\varepsilon_r{}''}{\varepsilon_r{}'} = \tan\delta$ is called the dissipation or loss tangent of the dielectric.

Hence it is clear that the dielectric properties of a DR are resulted from the phenomenon called dielectric polarization that occurs when electromagnetic fields pass through them. A DR at rest contains randomly oriented permanent electric dipoles. When an external field is applied, the dipoles align themselves in the direction of the field and the material is said to be polarized. For most materials P vanishes as E vanishes.

68

3.6.2 QUALITY FACTOR

The radiation Q-factor of the DRA is determined using [3]:

$$Q = \frac{2\omega W_e}{P_{rad}}$$

(16)

where *We* and *P$_{rad}$* are the stored energy and radiated power, respectively. These quantities are given by:

$$W_e = \frac{\varepsilon_o \varepsilon_r abd}{32}\left(1 + \frac{\sin(k_z d)}{k_z d}\right)\left(k_x^2 + k_y^2\right)$$

(17)

$$P_{rad} = 10 k_o^4 |\boldsymbol{p_m}|^2$$

(18)

where $\boldsymbol{p_m}$ is the magnetic dipole moment of the DRA:

$$\boldsymbol{p_m} = \frac{-j\omega 8\varepsilon_o(\varepsilon_r - 1)}{k_x k_y k_z}\sin(k_z d/2)\hat{\boldsymbol{z}}$$

(19)

The impedance bandwidth (BW) of the DRA can be estimated from the radiation Q-factor using:

$$BW = \frac{S-1}{Q\sqrt{S}}$$

(20)

where *S* is the maximum acceptable voltage standing-wave ratio (VSWR). The above equations can be used to generate the graphs which plot the normalized Q-factor (*Q$_e$*) as a function of the DRA dimensions *d/b* for various values of dielectric constant and various values of *a/b*. The normalized Q-factor is defined as:

$$Q_e = \frac{Q}{\varepsilon_r^{3/2}}$$
(21)

Thus these curves can be used to estimate the Q-factor of a DRA without having to rely on the preceding equations.

3.7   FABRICATION OF THE DIELECTRIC RESONATOR

The DR is fabricated through the mixed oxide or solid state route which is a time consuming process, involving many steps [39] such as Mixing and Grinding, Calcination process, Pellet shaping, Sintering process and Surface finishing. During these processes we can minimize the free energy of the material and redistribute the atoms. The minimization involves the reduction of internal surface area and an increase in the grain size.

3.7.1   MIXING AND GRINDING

Here, the preparation of DR sample from $ZnTiO_3$ material is explained as an example as it is used for the work in this thesis. Titanates (TiO_2) have many uses in electronic and material industry due to its piezoelectric, ferroelectrics and other properties.

We start with the chemical equation of the compound **$ZnTiO_3$** which is

$ZnO + TiO_2 \rightarrow ZnTiO_3$ or in terms of atomic weight,
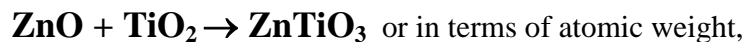
(65.39 (Zn)+15.999(O)) gms of ZnO + (47.67(Ti)+2*15.999(O)) gms of $TiO_2 \rightarrow$

(65.39(Zn)+47.67(Ti)+3*15.999) gms of $ZnTiO_3$

or

70

81.389 gms of ZnO + 79.668 gms of $TiO_2 \rightarrow$ 161.057 gms of $ZnTiO_3$

This gives the fact that 1 gm of $ZnTiO_3$ requires 0.5053 gm of ZnO and 0.4947 gm of TiO_2. Thus the stochiometric quantities of ZnO and TiO_2 required for forming *N* gms of $ZnTiO_3$ as the final product can be calculated easily. The next step is mixing for eliminating aggregates and/or reducing the particle size. The weighed powders of ZnO and TiO_2 are mixed well with 100−200 % of distilled water for about 12 hrs in a ball-mill, which is a motor-driven barrel that rotates on its axis. The barrel is filled with the ceramic beads made of alumina or silicon carbide that act as the grinding medium for the powder. The creamy mixer is then dried in an oven at a 100°C.

3.7.2   CALCINATION PROCESS

In this process the endothermic decomposition reaction is taken place. Any salt such as carbonate or hydroxide, decomposes, leaving an oxide as a solid product by liberating a gas. This process causes the interaction of the constituents by the interdiffusion of their ions and so reduces the extent of the diffusion that must occur during sintering in order to obtain a homogeneous body. The calcinations conditions are important factors determining the shrinkage of the pellet during the sintering. The thermal conductivity of powdered materials is always low, so that a sufficiently uniform temperature can only be obtained through a depth of a few centimeters when the period at maximum temperature is 1 or 2 hours in most cases. If compound formation is to occur during calcinating or firing, the matter of neighboring particles must inter-diffuse and the time taken to complete the process is proportional to the square of the particle size. Here

the well mixed powder is taken in an alumina crucible and calcinated at a temperature of 1000°C in an electric muffle furnace, for 2 hrs.

3.7.3   PELLET SHAPING

After the calcination process, the powder is crushed well in an agate mortar to form finer powder and then, mixed well with 4 % of Poly Vinyl Alcohol (PVA), an organic binder. Mixing with the binder provides sufficient strength to resist the disintegrating effect of small stress on the shaped pellets prior to sintering. Dry pressing is carried out in dye with movable top and bottom punches, made of hardened steel as shown in figure 3.7.3.1.

Figure 3.7.3.1: Photograph of Dyes used for ITDR and Cylindrical DR

The die used in this work is hexagonal in shape that can be used for fabricating hexagonal DR as well. After fixing the dye cavity on the bottom punch, one of the top

punches is placed inside the cavity. To fabricate ITDR, the remaining void space in the cavity is filled with an adequate amount of free-flowing powder (already prepared) and the top punch is descended to compress the powder to a predetermined volume, to a set pressure (75−300 MPa). Highly polished dye and punch surfaces ensure reduced wall friction. Shapes with a uniform section in the pressing direction are the easiest to produce by dry pressing. The time taken on an automatic pressing machine varies from 0.2 second for pieces of diameter around 1 mm to 5 seconds for large complex shapes.

(a) Dye Cavity

(b) Top Punches

(c) Bottom Punch

(d) Fabricated ITDR
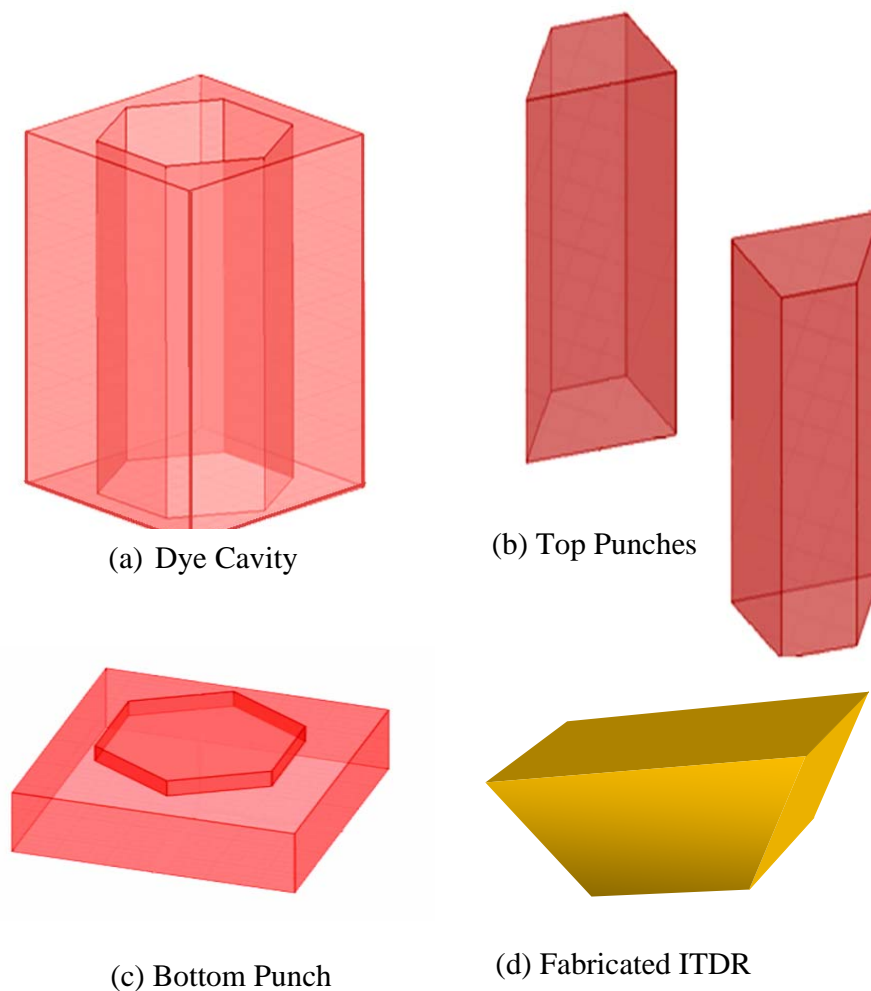
Figure 3.7.3.2: Schematic Sketches of the Dye and ITDR pellet

73

3.7.4 SINTERING PROCESS

Sintering converts the compacted powder in to a denser structure of crystallites jointed to one another by grain boundaries, at elevated temperatures below the melting point of the material. The energetic basis for sintering lies in the reduction of surface energy by transferring matter from the interior of grains along the grain boundaries to adjacent pores, which are eventually filled. Usually the powder compact is heated at fixed sintering temperature, held at this temperature for the required time and finally cooled at the room temperature. This is referred to as isothermal sintering. The organic binder is burnt out at the lower sintering temperatures. In the present case, isothermal sintering of the pellets, placed on an alumina slab at 1150°C for 5 hours is carried out after which it is cooled to the room temperature.

3.7.5 SURFACE FINISHING

Tool wear during the pellet shaping and variations in shrinkage during sintering and drying contribute to 1−2 % variation in the dimensions of the sintered pellets. For experimental studies, especially in the case of material characterisation, the surfaces of the pellets need to be as smooth as possible. Usually it is done by grinding and lapping the dense sample with tools consisting of silicon carbide, diamond powder etc. Here we use a silicon carbide water roof paper for finishing the pellets. A photograph of the final DR samples is shown in Figure 3.7.5.1.

Figure 3.7.5.1: Photograph of the fabricated DRs

3.8 MICROWAVE SUBSTRATES

Selection of substrates in microwave circuits is very important. Low loss substrates are very important at microwave bands. As frequency of operation increases, the loss tangent of the material used for substrates slightly increases, which in turn adversely affect the efficiency of the antenna. The power handling capability of the antenna depends on the substrate materials also. At high power certain substrate materials cannot withstand. A variety of substrate materials are available in the market. Flexible substrate materials are also available, so that the antenna can be mounted on curved surfaces. The selection of dielectric constant of the substrate depends on the application of the antenna and the radiation characteristics specifications. It is worth noting that surface waves will be excited in high dielectric constant substrates. This will generate spurious radiations in unwanted directions from the antenna. In this thesis importance is

given to compactness of the antenna structure. Prototype of antennas was fabricated on FR4 substrate which has a dielectric constant = 4.4, tan δ = 0.02 and thickness = 1.6 mm.

3.9   CHARACTERIZATION METHODES OF DR

Dielectric constant and quality factor of the fabricated DRs are measured using the well-known cavity methods as described below.

3.9.1   Measuring Dielectric Constant using Hakki - Coleman Method

Depending on the operating principle, methods for measuring the complex permittivity of materials at microwave frequencies can be classified as (1) methods that depend on the standing wave field within the dielectric (2) methods that depend on transmitted waves or waves reflected from the dielectric and (3) resonance methods. When the material is available only in small volume, cavity perturbation techniques [40, 41] are suitable, but the measurement accuracy is limited to dielectric constants less than 10. Hakki and Coleman method [42] is most suited when the ceramic samples have higher dielectric constant, and the method uses a dielectric post resonator for this purpose.

The measurement setup consists of a cylindrical DR puck sandwiched between two conducting plates (of infinite extent theoretically) to form a parallel-plate DR. This method restricts most of the stored energy to the dielectric and allows the experimental configuration to closely approximate the analytical model. If the distance between the two parallel plates is smaller than one-half wavelength, then the excited TE_{011} mode will not radiate [43] and the sides of the resonator can be left open for providing the coaxial

coupling probes. The maximum dimensions of the specimen are set by the diameter of the shorting plates while the minimum dimensions by the diameter of the coupling probes. The setup is shown in Figure 3.9.1.1.
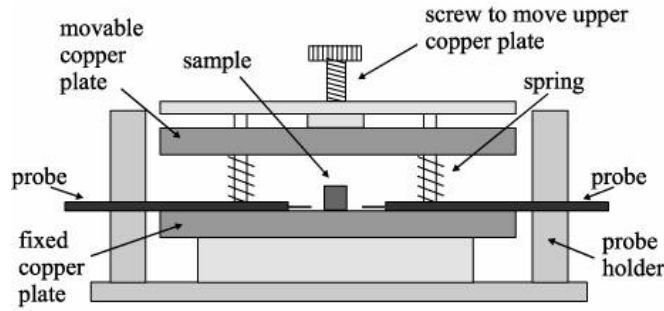
Figure 3.9.1.1: Hakki-Coleman setup for measuring dielectric constant

Consider a cylindrical DR of length L and radius a placed in the above setup. Then the characteristic equation for the TE_{0nl} mode of operation is given by

$$\alpha \frac{J_0(\alpha)}{J_1(\alpha)} = -\beta \frac{K_0(\beta)}{K_1(\beta)} \tag{22}$$

where $J_0(\alpha)$ and $J_1(\alpha)$ are the Bessel functions of the first kind of orders zero and one respectively, while $K_0(\beta)$ and $K_1(\beta)$ are the modified Bessel functions of the second kind of orders zero and one respectively. Also

$$\alpha_n = \frac{2\pi a}{\lambda_0} \sqrt{\varepsilon_r - \left(\frac{l\lambda_0}{2L}\right)^2} \tag{23}$$

$$\beta_l = \frac{2\pi a}{\lambda_0} \sqrt{\left(\frac{l\lambda_0}{2L}\right)^2 - 1}, \tag{24}$$

where l is the axial wave number. Thus the dielectric constant can be obtained from (23) and (24) as

$$\varepsilon_r = 1.0 + \left(\frac{c}{\pi D f_1}\right)^2 \left(\alpha_1^{\,2} + \beta_1^{\,2}\right) \qquad (25)$$

where $c = 3 \times 10^8$ m/s, α_1 and β_1 are the first roots of the characteristics equation with $n = l = 1$ corresponding to the TE_{011} mode.

3.9.2 Measurement of Quality factor using Cavity Method

Q-measurement methods are mainly of two types – time domain and frequency domain. Time domain methods mainly depend on measuring the decay time constant τ of the stored energy in the cavity at frequency f_o, and by using the following relation [44].

$$Q_L = 2\pi f_o \tau \qquad (26)$$

Three useful frequency domain techniques are the reflection method, the reactance method and the transmission method. Transmission method is the simplest and requires a transmission type cavity as shown in Figure 3.9.2.1.

As shown in the figure, a microstrip transmission line is fabricated on a dielectric substrate. The DR is coupled magnetically to the transmission line by placing it nearby it on the substrate. The lateral distance d between the strip and the centre of the DR determines the coupling coefficient between them. By properly adjusting d, the $TE_{01\delta}$ mode can be excited in the DR. In order to suppress the radiation losses, the entire structure is covered with a metallic cavity of dimensions at least 3 times the size of the

DR, with a top plate that can be moved up and down using a screw. The shielding conditions affect the resonant frequency and the Q of the DR.

Metallic cavity

Dielectric substrate

Microstrip line

Input port

d

Output port

DR sample
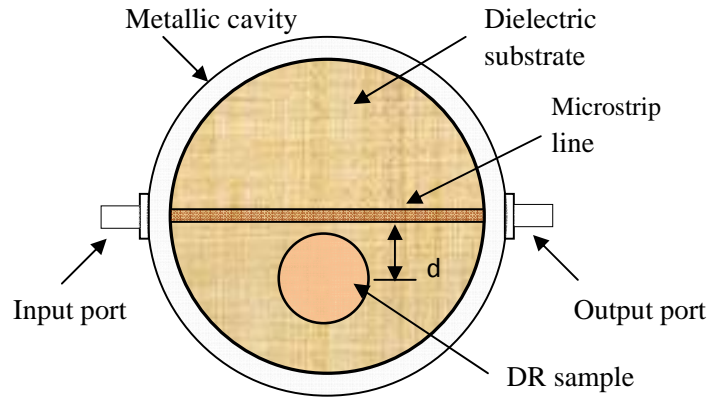
Figure 3.9.2.1: Top view of the transmission type cavity setup for Q-factor measurement

The degree of coupling is adjusted such that the transmission loss is of the order of −40 dB. By bringing the top metal plate close to the DR, the $TE_{01\delta}$ resonant frequency can be observed increasing, indicating that the stored energy in the cavity is predominantly magnetic. If the stored energy is electric, then a decrease in the resonant peak is expected. From the transmission coefficient ($|S_{21}|$) plot around the resonant frequency, the loaded and unloaded Q-factors-Q_L and Q_u respectively can be calculated as illustrated in Figure 3.9.2.2.

Here the parameter x is given by **[10]**

$$x = 3 - 10 . log \left(1 + 10^{-0.1|S_{21}|_{dB}} \right) \qquad (27)$$

Now the Q-factor is given by the well-known equation, $Q = \dfrac{f_0}{\Delta f}$
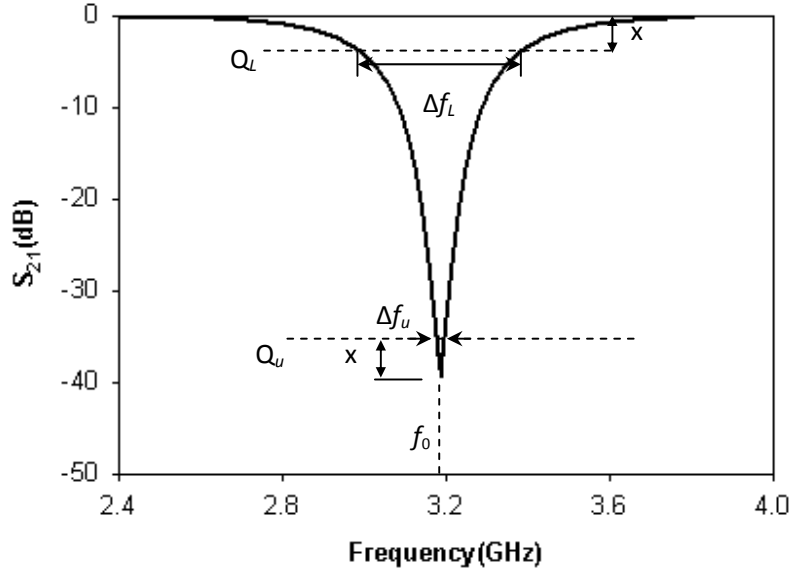
Figure 3.9.2.2: Measurement of Q-factor from the S_{21} curve

For the measurement of the temperature coefficient of resonant frequency (τ_f), the Hakki-Coleman transmission cavity is placed in a temperature stable furnace with outlets for signal coupling. The temperature is varied over a desired range in discrete steps and the shift in the TE_{011} frequency is noted. Now τ_f can be calculated as given by Eq. (28). Here 'f_0' is the TE_{011} resonant frequency at room temperature and 'Δf_0' is the frequency shift for a temperature gradient of 'ΔT'. The τ_f can be either positive or negative depending on whether the frequency is increasing or decreasing respectively with the rise in temperature.

$$\tau_f = \frac{1}{f_0} \cdot \frac{\Delta f_0}{\Delta T} \quad \text{parts per million or ppm} /^{\text{o}} \text{C} \qquad (28)$$

3.10   EXPERIMENTAL CHARACTERIZATION SETUP

Antenna characteristics such as return loss, radiation pattern and gain are measured using the HP8510C and associated setup. The indegeneously developed CREMA SOFT is used for the automatic measurement of the radiation properties using HP 8510C Network analyzer. The important systems used for the antenna characterization are Vector network Analyzer, Anechoic Chamber, Automated turn table etc.

3.10.1 HP 8510C VECTOR NETWORK ANALYZER

This is a sophisticated Vector Network Analyzer (VNA) from Hewlett Packard with time domain and frequency domain operation capability [45]. The NWA can measure the magnitude and phase of the S parameters. The microprocessor based system can measure two port network parameters such as s_{11}, s_{12}, s_{21} and s_{22} very accurately. The in built signal processing algorithms of the network analyzer process the transmit and receive data and finally displays the measured values in many plot formats. The schematic of the VNA is shown in Fig. 3.10.1.1.

The network analyzer consists of a microwave generator, S parameter test set, signal processor and the display unit as illustrated in Fig. 3.2. The synthesized sweep generator HP 83651B uses an open loop YIG tuned element to generate the RF stimulus. It can synthesize frequencies from 10 MHz to 50 GHz. The frequencies can be set in step mode or ramp mode depending on the required measurement accuracy.
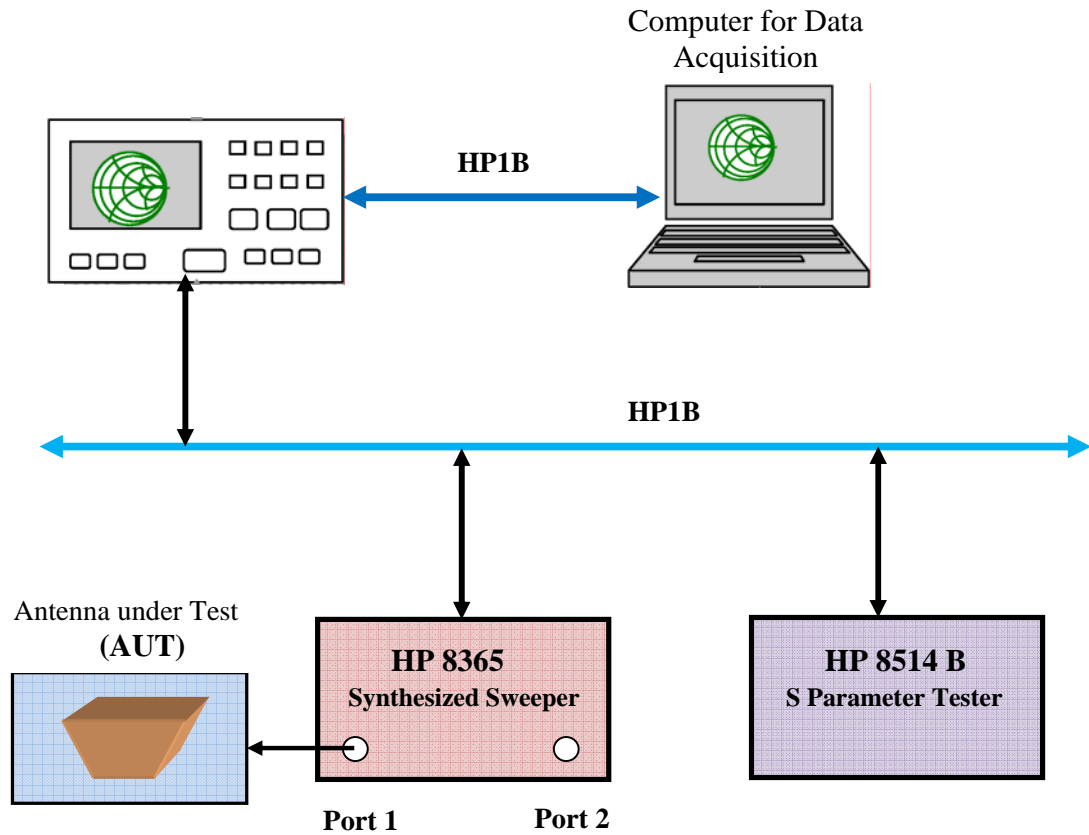
Figure 3.10.1.1: Schematic diagram of HP 8510C vector network analyzer set up used for the characterization of the antennas

The antenna under test (AUT) is connected to the port of the S-parameter test set HP8514B and the forward and reflected power at the measurement point is separated and down converted to 20MHz using frequency down converter. It is again down converted to lower frequency and processed in the HP8510C processing unit. All the systems discussed above are interconnected using HPIB bus. A computer interfaced to the system is used for coordinating the whole operation remotely. Measurement data can be saved on a storage medium using it.

3.10.2 ANECHOIC CHAMBER

The anechoic chamber provides a quiet zone needed to simulate space environment required in pattern measurements. The absorbers used for building the chamber are made from high quality, low-density form impregnated with dielectrically/ magnetically lossy medium. The wall of the chamber (24' X 12' X 10') used for the measurements is properly shaped (tapered chamber) and covered with carbon black impregnated poly urethene (PU) foam based pyramidal, wedge, or flat absorbers of appropriate sizes. The PU foam structure gives the geometrical impedance matching while the dispersed carbon gives the required attenuation (up to –40 dB) for a wide frequency (500 MHz to 18 GHz) range. The chamber is made free of EMI by surrounding with thin aluminium sheet.

3.10.3 TURN TABLE ASSEMBLY FOR FAR FIELD RADIATION PATTERN MEASUREMENT

The turn table assembly consists of a stepper motor driven rotating platform for mounting the Antenna Under Test (AUT). The in-house developed microcontroller based antenna positioner STIC 310C is used for radiation pattern measurement. The main lobe tracking for gain measurement and radiation pattern measurement is done using this setup. A standard wideband horn (1-18GHz) is used as receiving antenna for radiation pattern measurements. The in-housed developed automation software '*Crema Soft*' coordinates all the measurements.

3.10.4 MEASUREMENT PROCEDURE

The experimental procedures followed to determine the antenna characteristics are discussed below. The network analyzer in real practice is connected to

large cables and connectors. The connectors and cables will have its losses associated at higher microwave bands. Thus the instrument should be calibrated with known standards of open, short and matched loads to get accurate scattering parameters. There are many calibration procedures available in the network analyzer. Single port, full two port and TRL calibration methods are usually used. The two port passive or active device scattering parameters can be accurately measured using TRL calibration method. Return loss, VSWR and input impedance can be characterized using single port calibration method.

3.10.4.1 RETURN LOSS, RESONANT FREQUENCY AND BANDWIDTH

The return loss characteristic of the antenna is obtained by connecting the antenna to any one of the network analyzer port and operating the VNA in s_{11}/s_{22} mode. The calibration of the port is done for the frequency range of interest using the standard open, short and matched load. The calibrated instrument including the port cable is now connected to the device under test. The frequency vs reflection parameter (s_{11}/s_{22}) values is then stored on a computer using the 'Crema Soft' automation software.

The frequency for which the return loss value is minimum is taken as resonant frequency of the antenna. The range of frequencies for which the return loss value is with in the -10dB points is usually treated as the bandwidth of the antenna. The antenna bandwidth is usually expressed as percentage of bandwidth, which is defined as

$$\% \, Bandwidth = \frac{bandwidth}{centre frequency} * 100$$

At -10dB points the VSWR is ~2. This implies that at resonance the VSWR value approaches unity. The above bandwidth is sometimes referred to as 2:1 VSWR bandwidth.

3.10.4.2 FAR FIELD RADIATION PATTERN

The measurement of far field radiation pattern is conducted in an anechoic chamber. The AUT is placed in the quite zone of the chamber on a turn table and connected to one port of the network analyzer. A wideband horn is used as a transmitter and connected to the other port of the network analyzer. The turn table is controlled by a STIC positioner controller. The automated radiation pattern measurement process is coordinated by the '*Crema Soft'* software in the remote computer.

In order to measure the radiation pattern, the network analyzer is kept in S_{21}/S_{12} mode with the frequency range within the -10dB return loss bandwidth. The number of frequency points are set according to the convenience. The start angle, stop angle and step angle of the motor is also configured in the '*Crema Soft'*. The antenna positioner is boresighted manually. Now the THRU calibration is performed for the frequency band specified and saved in the CAL set. Suitable gate parameters are provided in the time domain to avoid spurious radiations if any. The *Crema Soft* will automatically perform the radiation pattern measurement and store it as a text file.

3.10.4.3 ANTENNA GAIN

The gain of the antenna under test is measured in the bore sight direction. The gain transfer method using a standard gain antenna is employed to determine the absolute

gain of the AUT [46-47]. The experimental setup is similar to the radiation pattern measurement setup. An antenna with known gain is first placed in the antenna positioner and the THRU calibration is done for the frequency range of interest. Standard antenna is then replaced by the AUT and the change in S_{21} is noted. Note that the AUT should be aligned so that the gain in the main beam direction is measured. This is the relative gain of the antenna with respect to the reference antenna. The absolute gain of the antenna is obtained by adding this relative gain to the original gain of the standard antenna.

3.10.4.4 RADIATION EFFICIENCY OF DRA

The radiation efficiency η_{rad} describes the losses within the antenna structure. It is defined by the ratio of the radiated power P_{rad} over the power P_{in} going into the antenna terminal.

$$\text{Radiation Efficiency, } \eta = \frac{P_{rad}}{P_{in}} = \frac{P_{rad}}{P_{rad} + P_{loss}} = \frac{R_{rad}}{R_{rad} + R_{loss}} \qquad (3.27)$$

Where P_{rad} = power radiated

P_{in} = power fed to antenna (W)

P_{loss} = power lost by the antenna (W)

R_{rad} = radiation resistance of the antenna (Ω)

R_{loss} = loss resistance of the antenna (Ω)

For physically small antennas, the Wheeler cap method **[48]** is highly preferred for measuring the radiation efficiency. According to this method, if a radiation shield is placed around the antenna so as to enclose the near fields of the antenna, the radiation resistance of the antenna is reduced to zero while the loss resistance and the stored energy

remain the same as for the unshielded antenna [49]. When covering the antenna with a metal cap, the radiation is suppressed and the input power (proportional to the input resistance) is equal to the power loss (proportional to the loss resistance). Without the cap, the input power is equal to the radiated power plus the power loss (input resistance + loss resistance). The radiation efficiency of the antenna can be obtained from these two parameters.

3.11 ANTENNA UNDER TEST

The antenna under test (AUT) is the DRA designed using the fabricated ITDRs. Mainly three feeding methods are used. One with microstrip line feed alone and the other two are microstrip line feed with slotted ground plane. The slots provided in the ground plane are slightly different in shape for the use in Design 5-1 and Design 5-2 as would be seen in section 4.5.1 and 4.5.2 in chapter 4. The feed with substrate is shown in the figure.
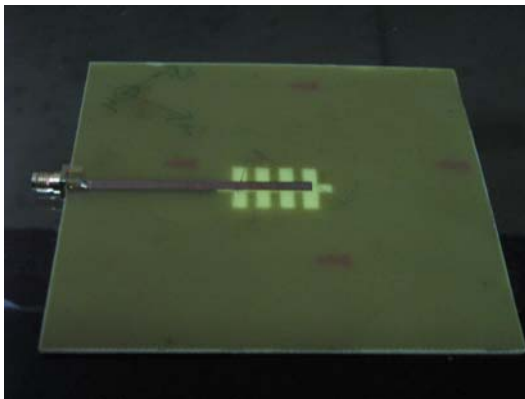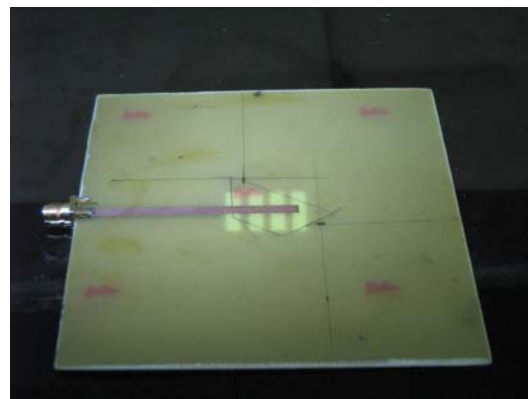
(a)   **(b)**
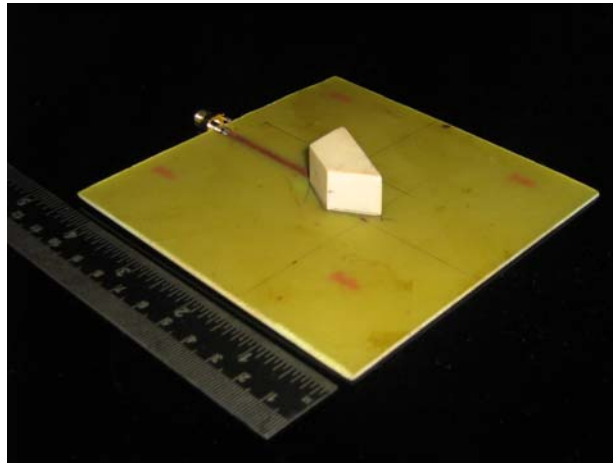
(c)

Figure 3.11.1: Photographs of the **(a)** feed used in Design 5-1 **(b)** feed used in -

Design 5-2 and **(b)** the antenna configuration with microstrip feed alone.

REFERENCES:

[1] A petosa, A. Ittipiboon, Y.M. M. Antar, D. Rossoe and M. Cuhaci, "Recent advances
in dielectric resonator antenna technology," *IEEE Antennas Propagat. Mag*., Vol.40
pp 35-48 June 1998.

[2] Y. M. M. Antar and Z. Fan, "Theoretical investigations of aperture coupled
rectangular dielectric resonator antenna," *Proc.Inst. Elect. Eng., Part H*, Vol 143,
no.2, pp 113-118, April 1996.

[3] R. K. Mongia and A. Ittipiboon, "Theoretical and experimental investigations on
rectangular dielectric resonator antennas" *IEEE Trans. Antennas Propagat*., 1997,
Vol.AP-45, no.9, pp 1348-1356.

[4] S. A. Long, M. McAllister, and L. C. Shen, "The resonant cylindrical cavity antenna," *IEEE Trans. Antennas Propagat.*, vol. AP-31, pp. 406–412, May 1983.

[5] M. McAllister, S. A. Long and G. L. Conway, "Rectangular dielectric resonator antenna," *Electron. Lett.*, vol. 19, pp. 219–220, Mar. 1983.

[6] M. McAllister and S. A. Long, "Resonant hemispherical dielectric antenna," *Electron. Lett.*, vol. 20, pp. 657–659, Aug. 1984.

[7] A. A. Kishk, H. A. Auda, and B. C. Ahn, "Radiation characteristics of cylindrical resonant antennas with new applications," *IEEE Antennas Propagat. Soc. Newslett.*, vol. 31, pp. 7–16, Feb. 1989.

[8] R. K. Mongia, "Half-split dielectric resonator placed on a metallic plane for antenna applications," *Electron. Lett.*, vol. 25, pp. 462–464, Mar. 1989.

[9] K. W. Leung, K. M. Luk, K. Y. A. Lai and D. Lin, "Theory and experiment of a coaxial probe fed hemispherical dielectric resonator antenna," *IEEE Trans. Antennas Propagat.*, vol. 41, pp. 1390–1398, Oct. 1993.

[10] R. K. Mongia, A. Ittipiboon, P. Bhartia, and M. Cuhaci, "Electric monopole antenna using a dielectric ring resonator," *Electron. Lett.*, vol. 29, pp. 1530–1531, Aug. 1993.

[11] A. Ittipiboon, R. K. Mongia, Y. M. M. Antar, P. Bhartia and M. Cuhaci, "Aperture fed rectangular and triangular dielectric resonators for use as magnetic dipole antennas," *Electron. Lett.*, vol. 29, pp. 2001–2002, 1993.

[12] R. K. Mongia, A. Ittipiboon, M. Cuhaci, and D. Roscoe, "Radiation Q-factor of rectangular dielectric resonator antennas—Theory and experiment," in *Int. IEEE AP-S Symp.*, Seattle, WA, June 1994, pp. 764–767.

[13] M. Gastine, L. Courtois and J. J. Dormann, "Electromagnetic resonances of free dielectric spheres," *IEEE Trans. Microwave Theory Tech.*, vol. MTT-15, pp. 694–700, Dec. 1967.

[14] D. Kajfez and P. Guillon, Eds., *Dielectric Resonators*. Norwood, MA: Artech, 1986.

[15] R. K. Mongia, "Theoretical and experimental resonant frequencies of rectangular dielectric resonators," *Proc. Inst. Elect. Eng.*, vol. 139, pt. H, pp. 98–104, Feb. 1992.

[16] R. F. Harrington, *Time Harmonic Electromagnetic Fields*. New York: McGraw-Hill, 1961.

[17] A. Petosa, A. Ittipiboon, and Y. M. M. Antar, Rectangular dielectric Resonator Antennas, chapter 2 - *Dielectric Resonator Antennas*, Edited by K.M. Luk, K. W. Leung, Research Studies Press Ltd., 2003.

[18] G. Zhou, A.A. Kishk, A.W. Glisson, "Input Impedance of a Hemispherical Dielectric Resonator Antenna Excited by a Coaxial Probe," *IEEE Antennas and Propagation Symposium*, Ann Arbour Michigan, June 1993, pp. 1038-1041.

[19] G.P. Junker, A.A. Kishk, A.W. Glisson, D. Kajfez, "Effect of an Air Gap Around the Coaxial Probe Exciting a Cylindrical Dielectric Resonator Antenna," *IEE Electronics Letters*, Vol. 30, No. 3, Feb. 1994, pp. 177-178.

[20] G.P. Junker, A.A. Kishk, and A.W. Glisson, "Input Impedance of Dielectric Resonator Antennas Excited by a Coaxial Probe," *IEEE Trans. Antennas and Propagation*, Vol. 42, No. 7, July 1994, pp. 960-966.

[21] M. Cooper, A. Petosa, A. Ittipiboon, J.S. Wight, "Investigation of Dielectric Resonator Antennas for L-Band Communications," *Antenna Technology and Applied Electromagnetics Symp ANTEM '96*, Ottawa, Canada, Aug. 1996, pp. 167-170.

[22] R. A. Kranenburg and S. A. Long, "Microstrip Transmission Line Excitation of Dielectric Resonator Antennas", Electro. Lett., Vol. 24, pp. 1156-1157, January 1988

[23] Leung K. W., K. Y. Chow, K. M. Luk and E. K. N. Yung, "Low-profile Circular Disk DR antenna of very high permittivity excited by a Microstrip line", *Electron. Lett*. ,Vol. 33,pp. 1004-1005, June 1997

[24] A. Petosa, R. K. Mongia, A. Ittipiboon, and J. S. Wight, "Design of Microstrip-fed Series Array of Dielectric Resonator Antennas", Electron. Lett., vol. 31, pp. 1306–1307, August 1995

[25] R. K Mongia and P. Bhartia, "Dielectric Resonator Antennas-A Review and General Design Relations for Resonant Frequency and Bandwidth", *Inter. Journal of Microwave and Millimeter-Wave Computer- aided Engineering*, Vol.4, pp. 230-247 , July 1994.

[26] R. Kranenberg, S.A. Long, J.T. Williams, "Coplanar Waveguide Excitation of Dielectric-Resonator Antennas," *IEEE Transactions on Antennas and Propagation*, Vol. 39, Jan. 1991, pp. 119-122.

[27] K. W. Leung, H. Y. Lo, K. K. So and K. M. Luk, "High-permittivity Dielectric Resonator Antenna Excited by a Rectangular Waveguide", *Micro. Optical Tech. Lett.*, Vol. 34, pp. 157–158, August 2002

[28] K. W. Leung and K. K. So, "Rectangular Waveguide Excitation of Dielectric Resonator Antennas", *IEEE Trans. on Antennas Propag.*, Vol.51, pp. 2477-2481, September 2003.

[29] I. A. Eshrah, A. A. Kishk, A. B. Yakovlev, and A. W. Glisson, "Excitation of Dielectric Resonator Antennas by a Waveguide Probe: Modeling Technique and Wide-Band Design", *IEEE Trans. on Antennas Propag.*, Vol. 53, pp. 1028-1037, March 2005

[30] I. A. Eshrah, A. A. Kishk, A. B. Yakovlev and A. W. Glisson, "Theory and Implementation of Dielectric Resonator Antenna Excited by a Waveguide Slot", *IEEE Trans. on Antennas Propag.*, Vol. 53, pp. 483-494, January 2005

[31] R. K. Mongia and A. Ittipiboon, "Theoretical and Experimental Investigations on Rectangular Dielectric Resonator Antennas", *IEEE Trans. on Antenn. Propagat.*, ,Vol. 45, pp.1348-1356, September 1997

[32] A. A. Kishk, Yan Yin, and A. W. Glisson, "Conical Dielectric Resonator Antennas for Wide-Band Applications", *IEEE Trans. on Antenn. Propagat* Vol. 50, pp. 469-474, April 2002

[33] R. Chair, A. A. Kishk, K. F. Lee and C. E. Smith, "Wideband Flipped Staired Pyramid Dielectric Resonator Antennas", *Electron. Lett.*, Vol. 40, pp. 581- 582, May 2004

[34] Q. Rao, T. A. Denidni, and A. R. Sebak, "Broadband Compact Stacked T-Shaped DRA with Equilateral-triangle Cross Sections", *IEEE Micro. Wireless Comp. Lett,* Vol. 16, pp. 7-9, January 2006

[35] A. Petosa, A. Ittipiboon, Y. M. M Antar, D. Roscoe and M. Cuhaci, "Recent Advances in Dielectric Resonator Antenna Technology", *IEEE Antennas Propag. Magazine*, Vol. 40, pp. 35-48, June 1998.

[36] V. Hamsakutty, A.V. P. Kumar, J. Yohannan, K. T. Mathew, "Coaxial Fed Hexagonal Dielectric Resonator Antenna for Circular Polarization", *Micro. and Opt. Tech. Letters*., Vol. 48, pp. 581- 582, March 2006.

[37] L. C. Y. Chu, D. Guha and Y. M. M. Antar, "Comb-shaped Circularly Polarized Dielectric Resonator Antenna", *Electron. Lett.* Vol. 42, pp. 785-787, July 2006.

[38] A. A. Kishk, M. R. Zunoubi and D. Kajfez, "A Numerical Study of a Dielectric Disk Antenna above a Grounded Dielectric Substrate", *IEEE Trans. on Antennas Propag*., Vol.41, pp. 813-821, June 1993.

[39] A. J. Moulson and J. M. Herbert, Chapter 3 – Processing of Ceramics in Electroceramics: *Materials, Properties, Applications*, 2nd edition, Wiley.

[40] W. E. Courtney, "Analysis And Evaluation of a Method of Measuring the Complex Permittivity and Permeability of Microwave Insulators", *IEEE Trans. Microwave Theory Tech*., Vol.18 ,pp. 476-485, August1970

[41] K. T. Mathew, "Perturbation Theory, Encyclopedia of RF and Microwave Engineering", *Wiley-VCH Publications*,Vol.4, pp. 3725-3735, 2005

[42] B. W. Hakki and P. D. Coleman, "A Dielectric Resonator Method of Measuring Inductive Capacities in the Millimeter Range", IRE Tran. Microwave Theory Tech., Vol. 8, pp. 402-410, July 1960.

[43] H. A. Auda and D. Kajfez, Chapter 3- Dielectric Rod Waveguides in *Dielectric resonators*, Edited by D. Kajfez and Pierre Guillon, Artech House, 1986.

[44] D. F. Hanson, Chapter 2- Microwave resonators in *Dielectric resonators*, Edited by D. Kajfez and Pierre Guillon, Artech House, 1986.

[45] HP 8510C   Network Analyzer operating and programming manual, *Hewlett Packard*, 1988.

[46] C. A. Balanis, "Antenna Theory: Analysis and Design", Second Edition, *John Wiley & Sons Inc*. 1982.

[47] John D. Kraus, "Antennas" *Mc. Graw Hill International*, second edition, 1988.

[48] D. M. Pozar and B. Kaufman, "Comparison of Three Methods for the Measurement of Printed antenna Efficiency", *IEEE Trans. on Antennas Propag.,* Vol. 36, pp. 136-139, January 1988.

[49] R. K. Mongia, A. Ittipiboon and M. Cuhaci, "Measurement of Radiation Efficiency of Dielectric Resonator Antennas", *IEEE Microwave and Guided wave Letters*, Vol. 4, pp. 80-82, March 1994.

CHAPTER 4   **EXPERIMENTAL AND SIMULATED STUDY OF ISOSCELES TRAPEZOIDAL DIELECTRIC RESONATOR ANTENNA**

The aim of the work was to fabricate and develop a broadband antenna using a novel geometry to be used in some practical application band. Almost all geometry except a few like Isosceles Trapezoidal shape was already developed and reported in literature by others and hence it was decided to develop Isosceles Trapezoidal DRA for the purpose. On the way to the broadband design, it was identified that the proposed DR with simple microstrip feed can be used for Multiband operation and Dual band dual polarization operation as well.

This chapter discusses the antenna design using the fabricated Isosceles Trapezoidal Dielectric Resonator (ITDR), with the support of measured and simulated results. Starting with different orientations of the DRA on a microstrip line feed for the fundamental broadside operation, a step-by-step development of the proposed antenna for Multiband operation, Dual band dual polarization operation and Wide band operation is presented. The antenna properties such as return loss, input impedance, radiation pattern, gain and radiation efficiency are measured using HP 8510C vector network analyzer. Simulations with Ansoft HFSS™ [1] are used for explaining the mode of excitation of the DR and the radiation properties and are given at the end of each section.

The Isosceles Trapezoidal DR (DR1) used is of dielectric constant $\varepsilon_r = 24$, unloaded quality factor, $Q_u = 6154$ at 2.43 GHz, bases b1 = 16.5 mm (0.12 λ_o), b2 = 33 mm (0.24 λ_o), height h = 14.3 mm (0.10 λ_o) and thickness h1 = 13.8 mm (0.101 λ_o), λ_o

being the free space wave length corresponding to the lowest mode frequency f = 2.2 GHz of the DRA. The broad band designs (Designs 5-1 and 5-2) are optimized with more compact DR, i.e. (DR2) also, with slightly varying dimensions, viz. ε_r = 20.8, unloaded quality factor, Q_u = 6273 at 2.84 GHz, bases b1 = 15.4 mm (0.11 λ_o), b2 = 30.8 mm (0.23 λ_o), height h = 13.3 mm (0.10 λ_o) and thickness h1 = 13 mm (0.10 λ_o), λ_o being the free space wave length corresponding to the lowest mode frequency of the DRA.

The designs corresponding to different orientations to be discussed are intended for:

1. Lower band operations.

2. Higher band operation.

3. Multi band operation.

4. Dual band Dual Polarization operation.

5. Wideband operation.

4.1 LOWER BAND OPERATIONS

4.1.1 DESIGN 1-1 ($TE^x_{1\delta0}$ MODE)

In this design, ITDRA is operating at the fundamental $TE^x_{1\delta0}$ mode suitable for WLAN application is presented and the characteristics are studied. The DRA is fed at its smaller rectangular base, which is the plane of symmetry of the DR which causes radiation from its slanted and flat surfaces. It is observed that the DRA exhibits a 2:1 VSWR bandwidth of ~11.6 %, a gain of as high as 7.22 dBi and broad radiation patterns with good cross-polar levels that are consistent over the operating band. The antenna covers important application band of ISM: Bluetooth/ WLAN 2.4/ Wibree (802.11 b/g/n

)/ ZigBee. As it is operating in the ISM band, it can as well be used in medical tomographic set up described in Appendix-B. Details of the design along with experimental and simulation results are presented and discussed.

4.1.1.1 ANTENNA CONFIGURATION

Antenna structure is shown in figure 4.1.1.1.1(a). An isosceles trapezoidal DRA of permittivity ε_{r1} = 24, bases b1 = 16.5 mm, b2 = 33 mm, height h = 14.3 mm and thickness h1 = 13.8 mm is fed by a 50Ω transmission line of 77 mm (length) X 3mm (width) fabricated on a microwave substrate of permittivity ε_{r2}= 4.2 with size 115mm (length) X 115mm (breadth) X 1.6mm (thickness). The condition that ε_{r1} ›› ε_{r2} for efficient coupling between the strip-line and the DR is satisfied here. Offset Length (L) of the feed is optimized as 9mm for getting the desired response as the maximum energy is coupled magnetically when the DR is located at the point of maximum electric field on the feed. The reflection (S11), impedance (Z), far field radiation characteristics and gain of the DRA are measured and discussed in the following section.

Figure 4.1.1.1.1 (a): Geometry of the Isosceles Trapezoidal DRA.
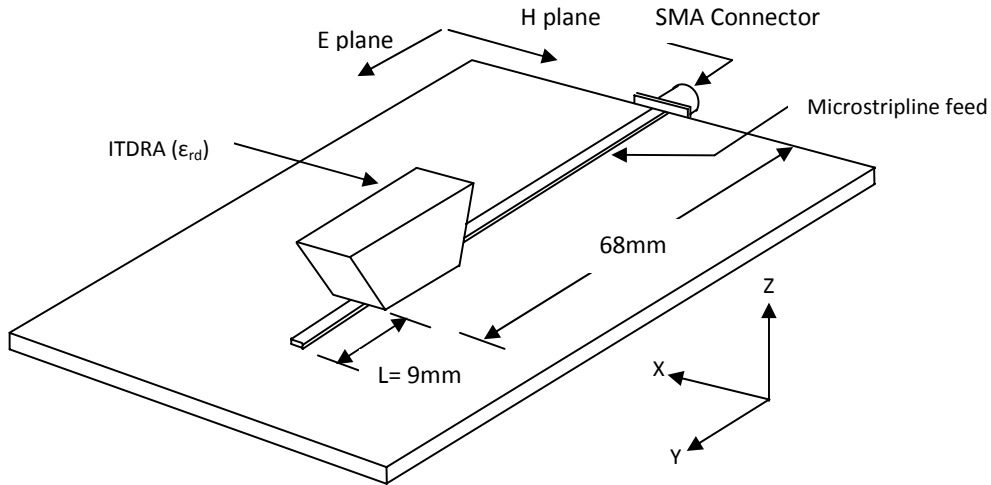
Figure 4.1.1.1.1 (b): Excitation of ITDRA by microstrip line in Design1-1.

4.1.1.2 EFFECT OF MICROSTRIP FEED POSITION OF ITDRA

The schematic diagram of a microstrip fed ITDRA is given in figure 4.1.1.1.1 (b). For optimizing the feed the DRA position is varied along x and y direction, where x and y are defined respectively as the distances from the strip line end to the centre of DR in x and y directions as shown in figure 4.1.1.2.1.
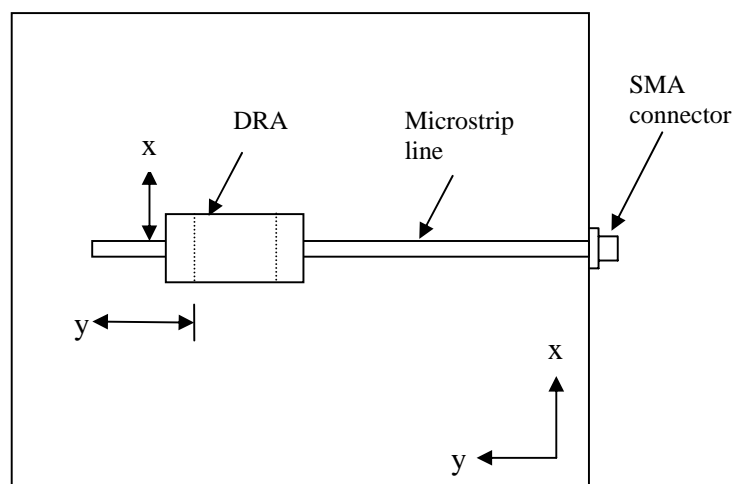
Figure 4.1.1.2.1: Sketch of top view of the antenna.

4.1.1.3 RESULTS AND DISCUSSIONS

(i) Optimization of feed position

To get a symmetrical radiation pattern, x is kept at zero while y is varied. The variation of return loss $|S_{11}|$ with position x = 0 and y varied is plotted in figure 4.1.1.3.1. It is observed that when the position of DRA along the strip line 'y' is varied the resonance frequency is also varied. It is verified that the optimum position is that which corresponding to the offset length y = 9mm for a useful band of operation and bandwidth.
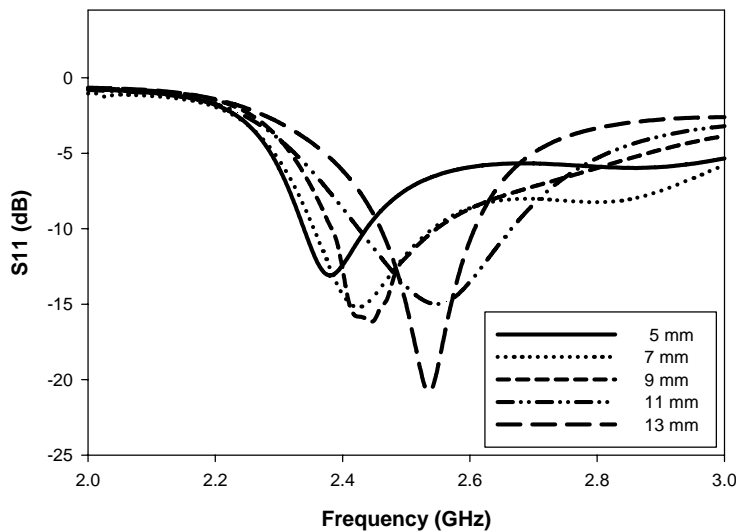
Figure 4.1.1.3.1: Simulated Return loss characteristics for different 'y' values
for x = 0mm

(ii) Reflection characteristics

The reflection and transmission characteristics of the antenna are studied. Measured and simulated plot of return loss ($|S11|$), of the DRA are compared in figure 4.1.1.3.2 and shown that they are in good agreement. The antenna has a 2:1 SWR

bandwidth ranging from 2.38 GHz to 2.54 GHz with a percentage bandwidth of 11.6 % that includes the 2.4 GHz WLAN band (2.4 to 2.485 GHz).
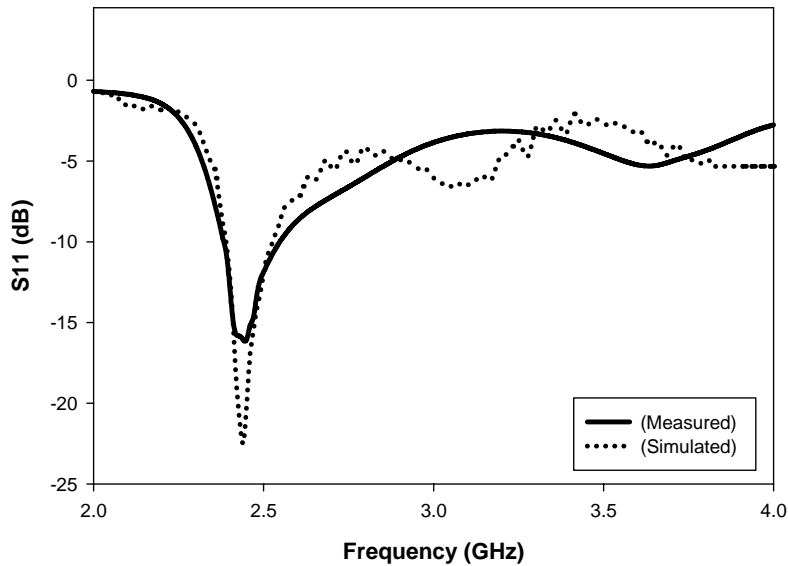
Figure 4.1.1.3.2 : Measured and simulated Return Loss of the DRA

Antenna Position		Resonant frequency (GHz)		Bandwidth (GHz)		% Error	
X	Y	Experime ntal	**Simulated**	Experime ntal	**Simulated**	Resonant frequency	Bandwidth
0 mm	**9 mm**	**2.439**	**2.443**	**0.13**	**0.17**	**0.16%**	**30.7%**

Table 4.1.1.3.1: Resonant frequency and Bandwidth of Measured and

Simulated results

(iii)   Gain of the antenna

The measured gain of the antenna in the bore sight direction is shown in figure 4.1.1.3.3. The antenna has a peak gain of 7.22 dBi at 2.48 GHz and a least of 3.54 dBi at 2.36 GHz with an average value of 5.38 dBi. Gain at the resonance frequency is 6.56.
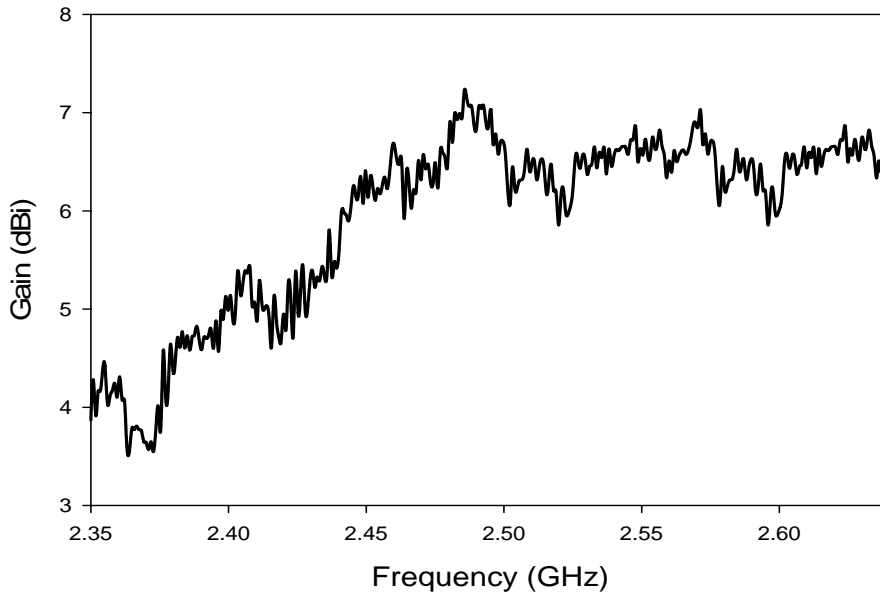
Figure 4.1.1.3.3: Gain vs Frequency

Range of Frequencies (GHz)	Centre frequency(f_0) (GHz)	Percentage Impedance Band width	Gain in the band (dBi)			
			Maximum	Minimum	Average	At f_0
2.38 - 2.54	**2.46**	**11.6%**	**7.22** (at 2.48 GHz)	**3.54** (at 2.36 GHz)	**5.38**	**6.56**

Table 4.1.1.3.2: Reflection characteristics and Gain of the antenna

(iv) **Radiation patterns**

The polarization of the antenna is also verified. The low cross-polarization levels confirm that the antenna is linearly polarized over the entire impedance band. The normalized XZ and YZ plane radiation patterns of the antenna in the resonance band are measured and are shown in figure 4.1.1.3.4. The front-to-back ratio for XZ and YZ plane

101

are 20dB and 26dB respectively. The half power beam widths are 91° and 107° in the elevation planes of XZ and YZ respectively.
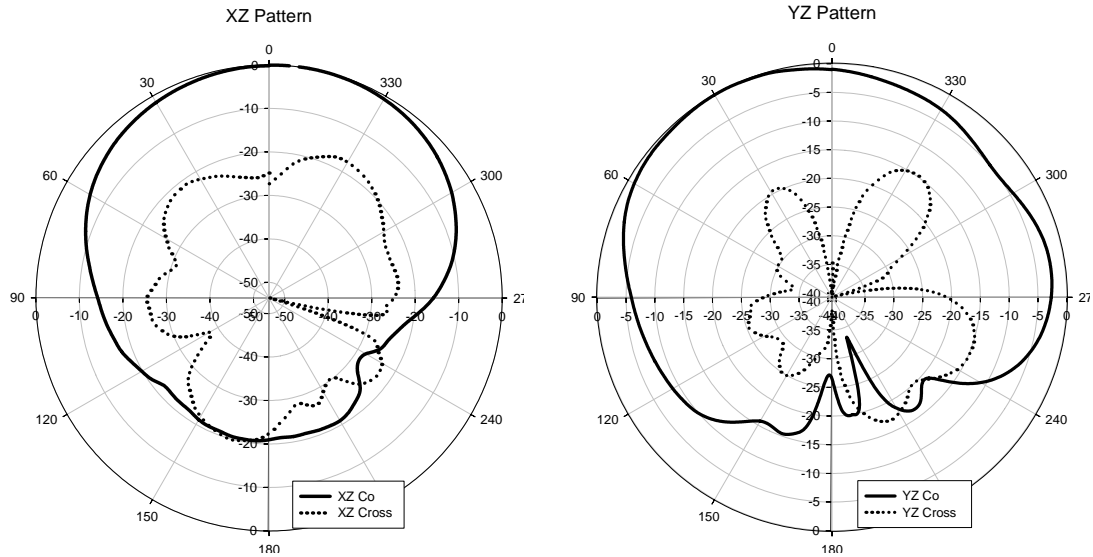
Figure 4.1.1.3.4: Measured Radiation Patterns at 2.46 GHz.
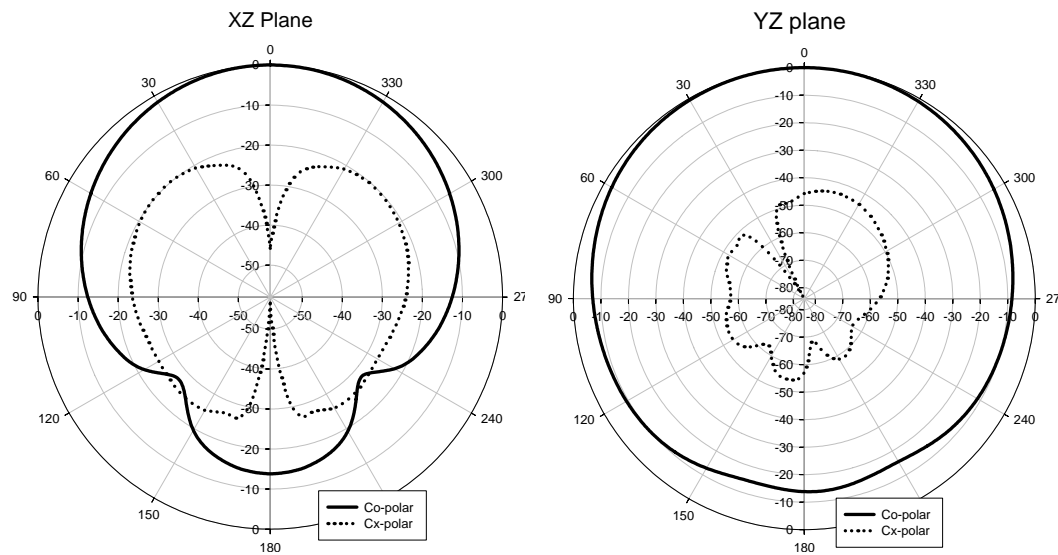
Figure 4.1.1.3.5: Simulated Radiation Patterns at 2.46 GHz.

The simulated 2D radiation pattern is shown in figure 4.1.1.3.5. A good agreement can be observed between the simulated and measured results.

(v) Input Impedance

Plot of input impedance against frequency which is shown in figure 4.1.1.3.6 confirms that a good and steady impedance matching is occurred between the feed and antenna at frequency corresponding to the resonant mode. The input impedance at the resonance frequency is shown as $57 + j10$ ohms.
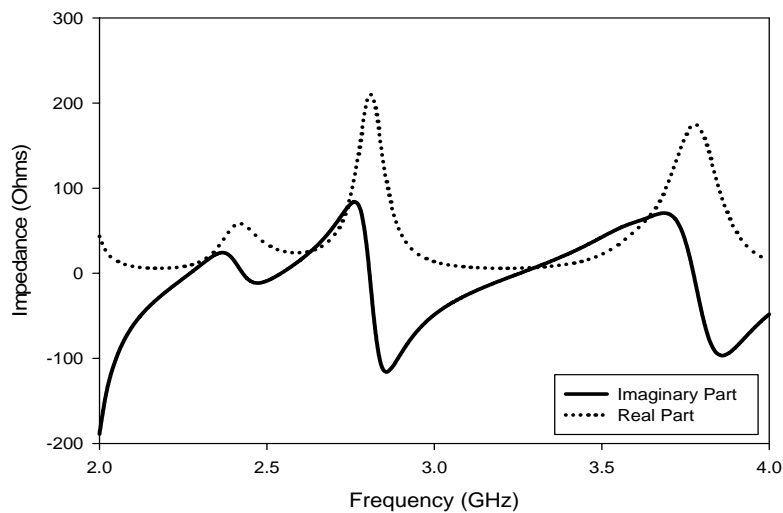
Figure 4.1.1.3.6: Measured Input Impedance of the antenna

Polarization	Half Power Beam width		Boresight Cx-polar level (dB)		Peak radiation direction (θ_p, Deg.)		Cx-polar level in θ_p direction (dB)		Front to Back Ratio (dB)	
	(XZ plane)	(YZ plane)	(XZ plane)	(YZ plane)	(XZ plane)	(YZ plane)	(XZ plane)	(YZ plane)	(XZ plane)	(YZ plane)
Linear	**92°**	**106°**	**-25**	**-35**	**-4°**	**30°**	**-25**	**-19**	**20**	**26**

Table 4.1.1.3.3: Radiation characteristics of the antenna.

(vi)   3D Radiation Pattern

The 3D radiation pattern drawn using Ansoft HFSS at the optimum feed position (x_0=13mm and y_0=9mm) for frequencies 2.46 GHz is shown in figure 4.1.1.3.7. It shows a broadside radiation pattern and is in agreement with experimental results.
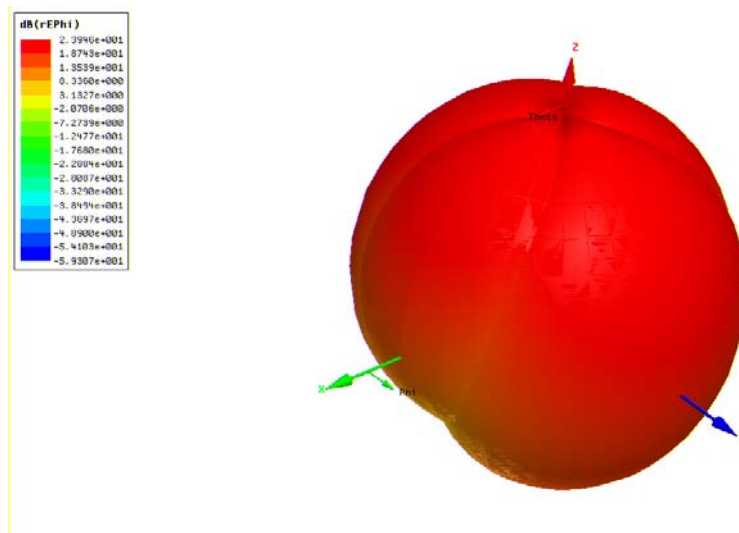
Figure 4.1.1.3.7: 3D Radiation Pattern at 2.46 GHz

(vii)   Mode analysis using HFSS Simulation

The magnitude of electric field distribution for the resonant frequency is simulated using HFSS and is shown in figure 4.1.1.3.8 (a). The number of half wave variation along the three dimensions shows that the DR is in $\mathrm{TE}^{z}_{1\delta0}$ mode. The Electric vector distribution within the DR is also shown in figure 4.1.1.3.8 (b).
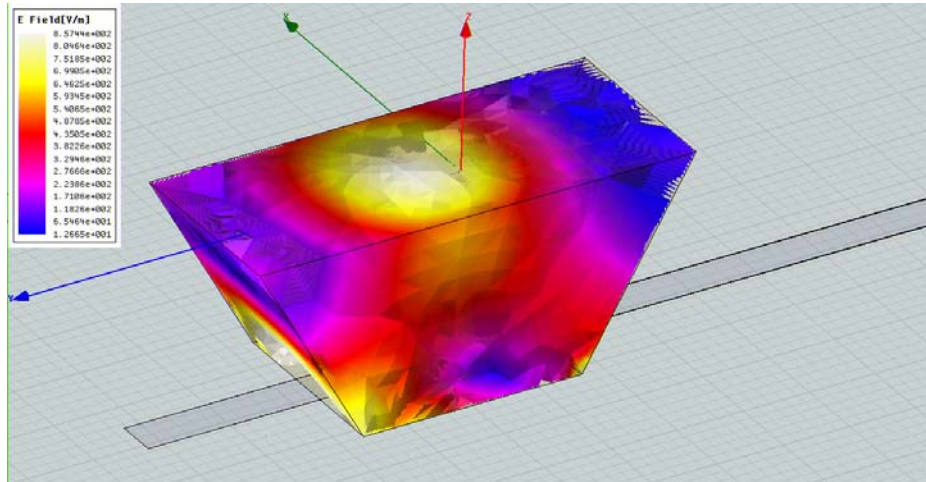
(a)
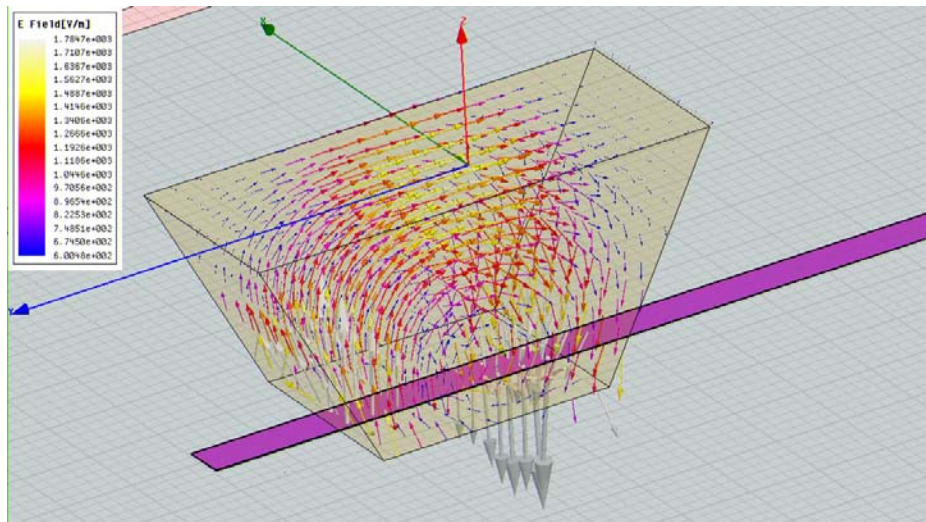
(b)

Figure 4.1.1.3.8: **(a)** E field and **(b)** E Vector distribution within ITDRA

The E field vector distribution within DR shows that the electric field is transverse to the *X* axis and hence the mode is TE^{x}. Number of half wave variations along

each dimension of the DR b1, h and h1, as shown in figure 4.1.1.3.8 (a) implies that the mode of resonance is $TE^x_{1\delta0}$.

4.1.2 DESIGN 1-2 ($TE^y_{1\delta1}$ MODE)

In this design, ITDRA operating at the resonance mode $TE^y_{1\delta1}$ is presented and the characteristics are studied. The ITDRA is placed in the orientation as shown in figure 4.1.2.1.1 fed at its smaller rectangular face.

4.1.2.1. ANTENNA CONFIGURATION

Antenna structure is shown in figure 4.1.2.1.1. An isosceles trapezoidal DRA of permittivity $\varepsilon_{r1} = 24$, bases b1 = 16.5 mm, b2 = 33 mm, height h = 14.3 mm and thickness h1 = 13.8 mm is fed by a 50Ω transmission line of 77 mm (length) X 3mm (width) fabricated on a microwave substrate of permittivity ε_{r2}= 4.2 with size 115mm (length) X 115mm (breadth) X 1.6mm (thickness). The condition that ε_{r1} ›› ε_{r2} for efficient coupling between the strip-line and the DR is satisfied here. Offset Length (L) of the feed is optimized as 19mm for getting the desired response as the maximum energy is coupled magnetically when the DR is located at the point of maximum electric field on the feed. The reflection (S11), impedance (Z), far field radiation characteristics and gain of the DRA are measured and discussed in the following section.

Figure 4.1.2.1.1: Excitation of ITDRA in Design 1.2

4.1.2.2. EFFECT OF MICROSTRIP FEED POSITION OF ITDRA
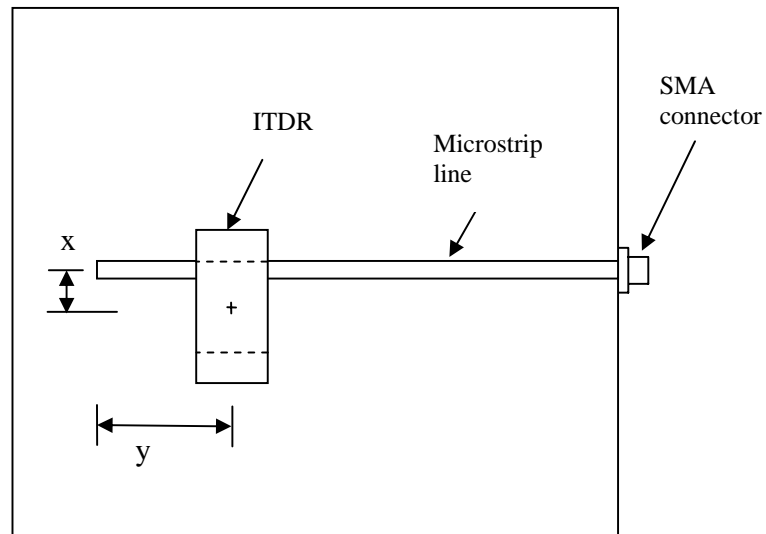
Figure 4.1.2.2.1: Sketch of top view of the antenna.

The schematic diagram of the top view of the microstrip fed ITDRA is shown in figure 4.1.2.2.1. For optimizing the feed the DRA position is varied along x and y direction, where x and y are defined respectively as the distances from the strip line end to the centre of DR in x and y directions as shown in figure 4.1.2.2.1. Reflection characteristics

107

corresponding to the displacement of the DR along 'y' and 'x' direction is shown in figure 4.1.2.3.1 and 4.1.2.3.2 respectively.

4.1.2.3. RESULTS AND DISCUSSIONS

(i) Optimization of feed position
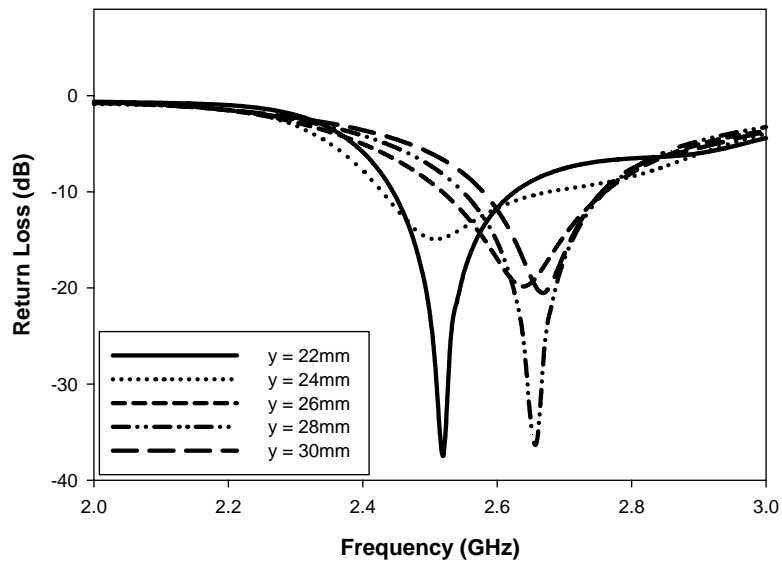
Figure 4.1.2.3.1: Simulated Return loss characteristics for different 'y' values
for x = 6.75mm

Figure 4.1.2.3.1 shows the effect of displacement of the ITDRA along the y-direction on the return loss of the antenna for x = 6.75 mm. It can be seen that the resonant frequency increases progressively with increased values of offset distance from the centre of the DR to the microstrip feed end. Here y = 26mm is chosen as the optimum as it gives a maximum bandwidth.
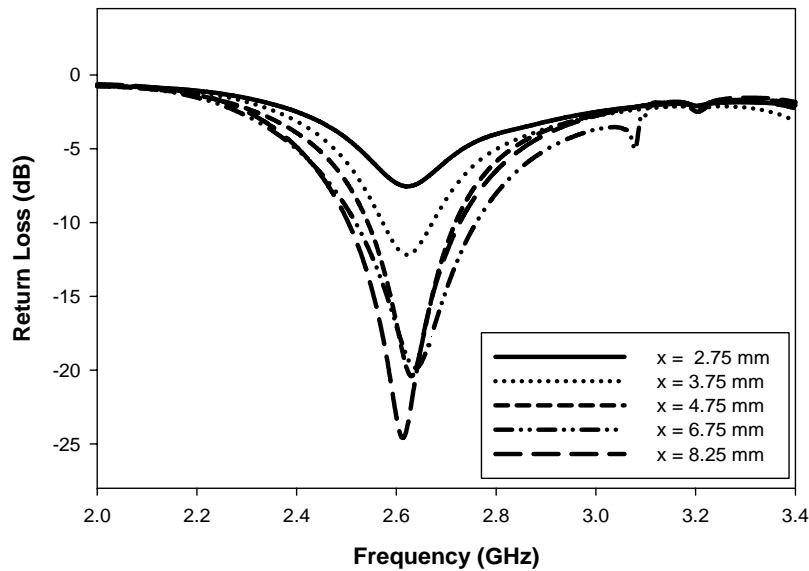
Figure 4.1.2.3.2: Simulated Return loss characteristics for different 'x' values for y = 26 mm

Variation of the return loss corresponding to the displacement of the DR along x-direction is also shown in figure 4.1.2.3.2 As it is seen in the figure, the resonance frequency does not vary corresponding to the displacement. But the return loss decreases as the x value increases. An optimum value is chosen as the one with maximum impedance bandwidth is obtained.

(ii) Reflection Characteristics

The measured and simulated return los of the antenna are shown in figure 4.1.2.3.3. As seen in the figure, a strong resonance is occurred at 2.64 GHz which comprises of a frequency range from 2.5 GHz to 2.76 GHz with a -10 dB impedance bandwidth of 9.89 %.
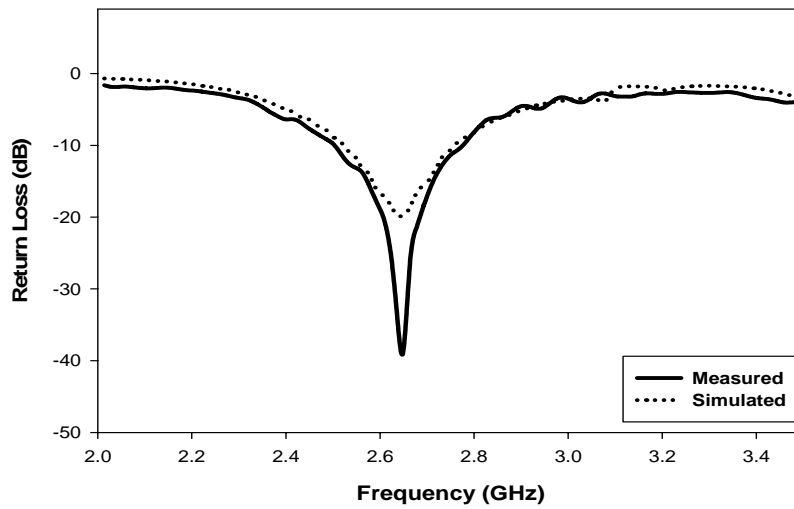
Figure 4.1.2.3.3: Measured and Simulated Return loss of the antenna

(iii) Gain of the Antenna
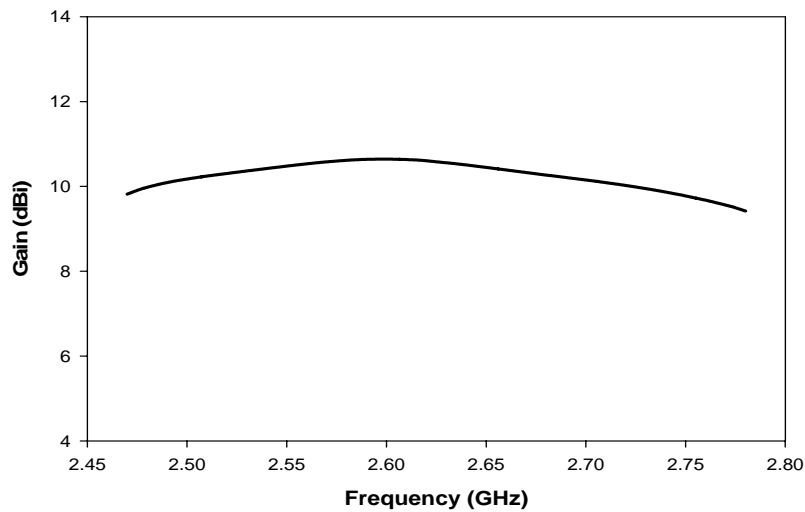
Figure 4.1.2.3.4: Gain of the proposed antenna

The gain of the antenna measured at the useful band of frequencies is plotted and shown in figure 4.1.2.3.4. A maximum of 10.66 dB is obtained at 2.59 GHz and a

minimum of 9.67 dB at 2.76 GHz with an average value of 10.16 dB. At the resonance

frequency 2.64 GHz, the gain obtained is 10.51 dB.

Range of Frequencies (GHz)	Centre frequency(f_0) (GHz0	Percentage Impedance Band width	Gain in the band (dBi)			
			Maximum	Minimum	Average	At f_0
2.50 - 2.76	**2.64**	**9.89%**	**10.66 (at 2.59 GHz)**	**9.67 (at 2.76 GHz)**	**10.16**	**10.51**

Table 4.1.2.3.1: Reflection characteristics and Gain of the antenna

(iv) Radiation Pattern
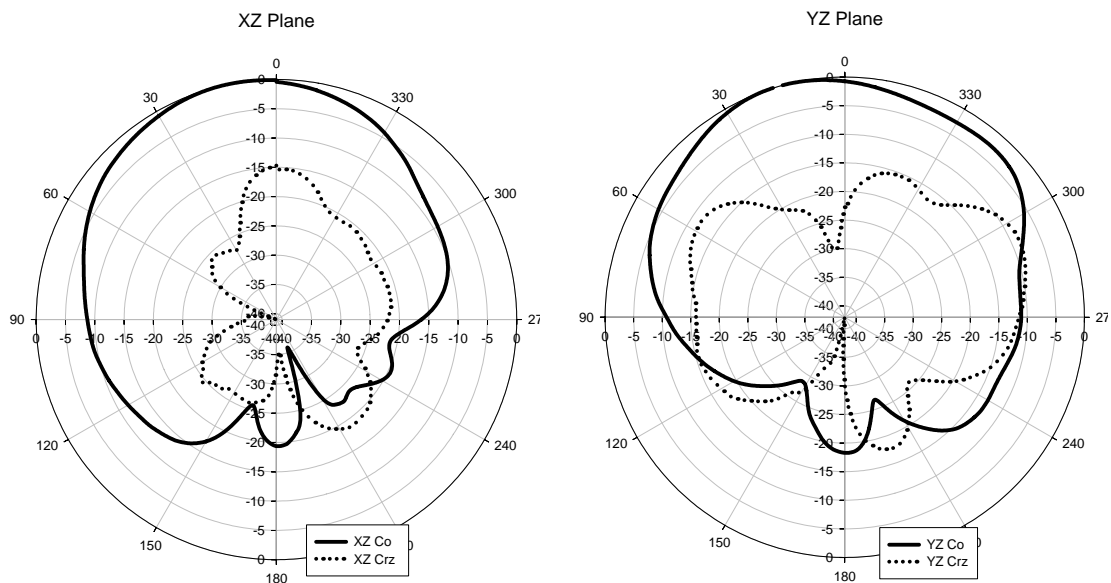
Figure 4.1.2.3.5: Measured 2D Radiation pattern of the antenna at 2.64 GHz

Polarization	Half Power Beam width		Boresight Cx-polar level (dB)		Peak radiation direction (θ_p, Deg.)		Cx-polar level in θ_p direction (dB)		Front to Back Ratio (dB)	
	(XZ plane)	(YZ plane)	(XZ plane)	(YZ plane)	(XZ plane)	(YZ plane)	(XZ plane)	(YZ plane)	(XZ plane)	(YZ plane)
Linear	78.5°	95.3°	-14.69	-22.66	13.8°	15.2°	-18.48	-25.0	32.5	29.25

Table 4.1.2.3.2: Radiation characteristics of the antenna
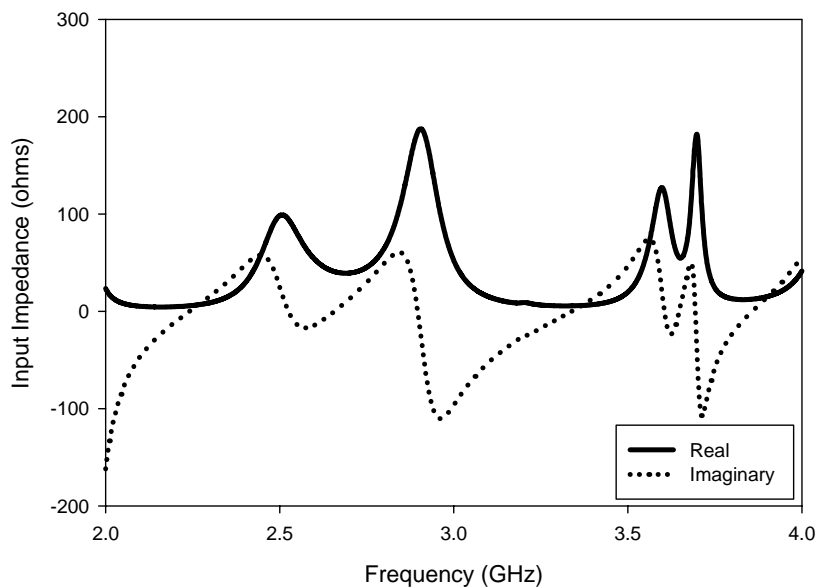
Figure 4.1.2.3.6: Input Impedance of the antenna

In put impedance of the antenna plotted against the frequency is shown in figure 4.1.2.3.6 which verifies that the resonance occurs only corresponding to the frequency where real and imaginary part of the impedance are near to 50 Ω and 0 Ω respectively.

112

(v) Simulated Results
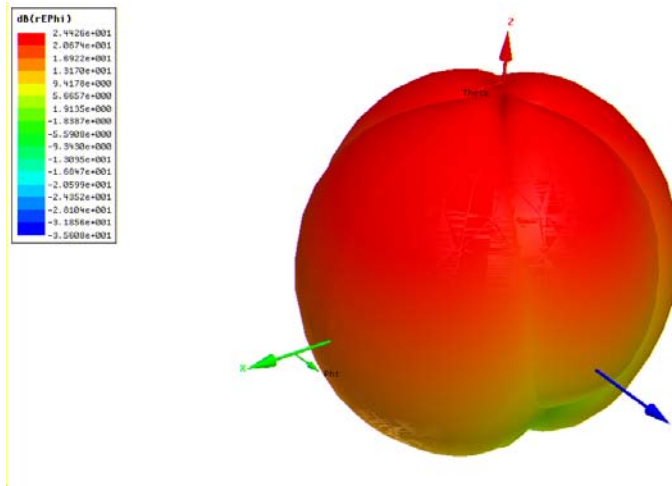
Figure 4.1.2.3.7: 3D Radiation Pattern at 2.64 GHz

The 3D radiation pattern simulated by HFSS (figure 4.1.2.3.7) shows that the antenna gives a broad side radiation pattern with sufficient beam width.

The E field vector distribution within DR shows that the electric field is transverse to the Y axis and hence the mode is TE^y.
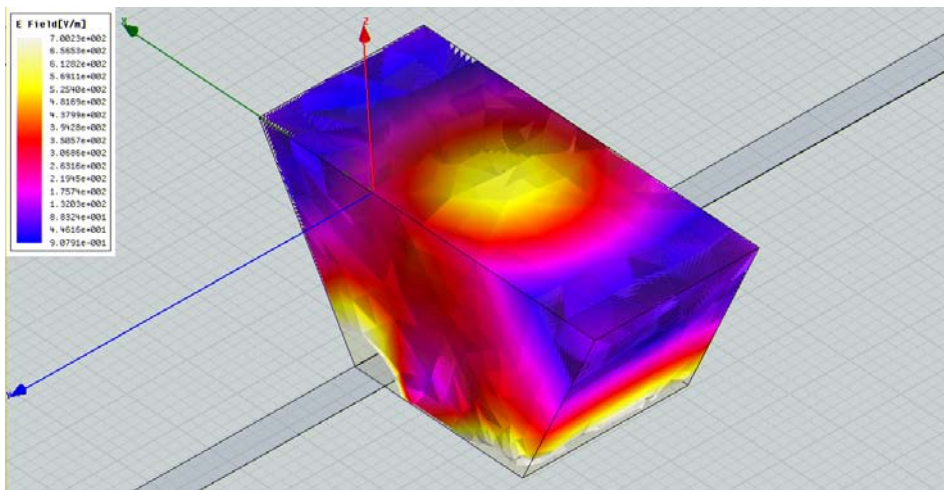
(a)
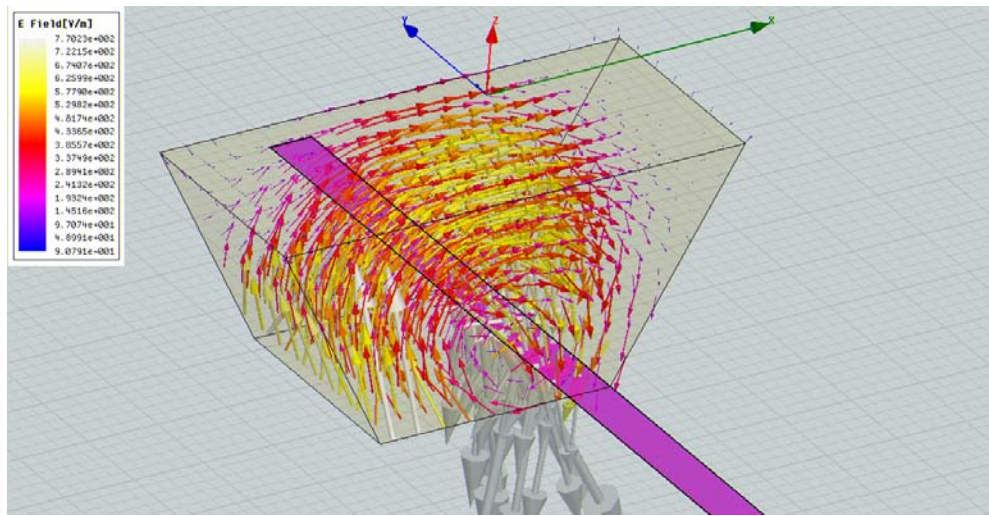
(b)

Figure 4.1.2.3.8: (a) E field and **(b)** E field vector distribution within DRA

Number of half wave variations along each dimensions b2, h and h1 of the DR as shown in figure 4.1.2.3.8 (a) implies that the mode of resonance is $TE^y_{1\delta 1}$.

4.1.3 DESIGN 1-3   (TE^Y_{110} MODE)

In this design, ITDRA operating at the resonance mode TE^y_{110} is presented and the characteristics are studied. The ITDRA is placed in the orientation as shown in figure 4.1.3.1.1 and fed at its larger rectangular base.

4.1.3.1. ANTENNA CONFIGURATION

An isosceles trapezoidal DRA of permittivity $\varepsilon_{r1} = 24$, bases b1 = 16.5 mm, b2 = 33 mm, height h = 14.3 mm and thickness h1 = 13.8 mm is fed by a 50Ω transmission line of 77 mm (length) Χ 3mm (width) fabricated on a microwave substrate of permittivity ε_{r2}= 4.2 with size 115mm (length) Χ 115mm (breadth) Χ 1.6mm (thickness).

The condition that $\varepsilon_{r1} \gg \varepsilon_{r2}$ for efficient coupling between the strip-line and the DR is satisfied here. Offset Length (L) of the feed is optimized as 24mm for getting the desired response as the maximum energy is coupled magnetically when the DR is located at the point of maximum electric field on the feed. The reflection (S11), impedance (Z), far field radiation characteristics and gain of the DRA are measured and discussed in the following section.
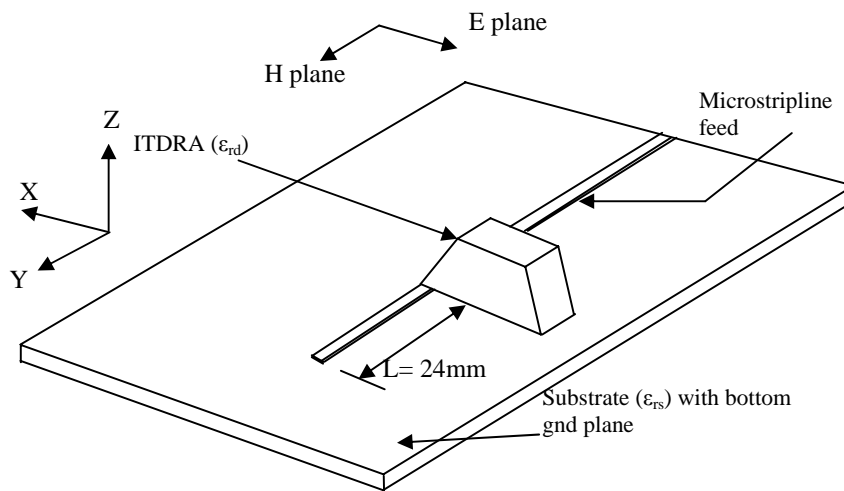
Figure 4.1.3.1.1: Excitation of ITDRA in Design 1.3

4.1.3.2. EFFECT OF MICROSTRIP FEED POSITION OF ITDRA

The schematic diagram of the top view of the microstrip fed ITDRA is shown in figure 4.1.3.2.1. For optimizing the feed the DRA position is varied along x and y direction, where x and y are defined respectively as the distances from the strip line end to the centre of DR in x and y directions as shown in figure 4.1.3.2.1. Reflection characteristics

corresponding to the displacement of the DR along 'y' and 'x' direction is shown in figure 4.1.3.3.1 and 4.1.3.3.2 respectively.
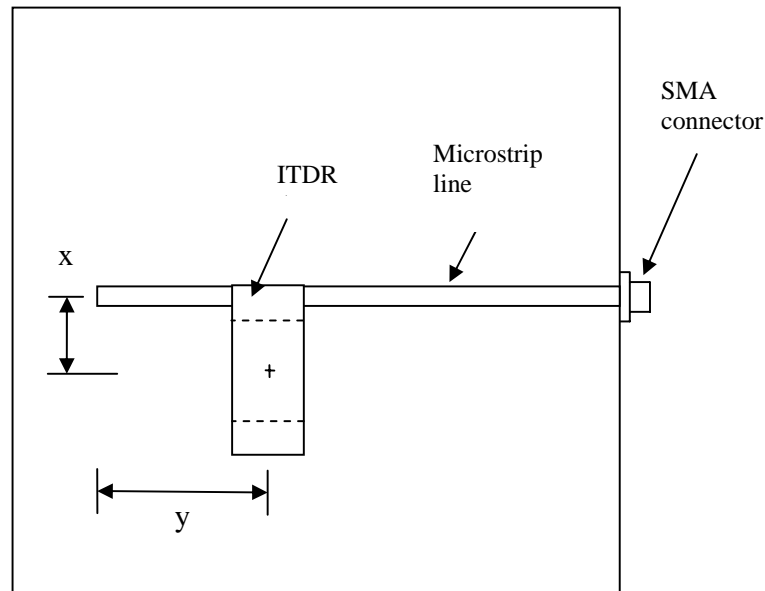
Figure 4.1.3.2.1: Sketch of top view of the antenna.

4.1.3.3. RESULTS AND DISCUSSIONS

(i) Optimization of feed position

Figure 4.1.3.3.1 shows the effect of displacement of the ITDRA along the y-direction, on the return loss of the antenna for x = 15 mm. It can be seen that a distance y = 31mm is optimum in the sense that it gives a minimum return loss in the resonant frequency as well as a maximum band width.
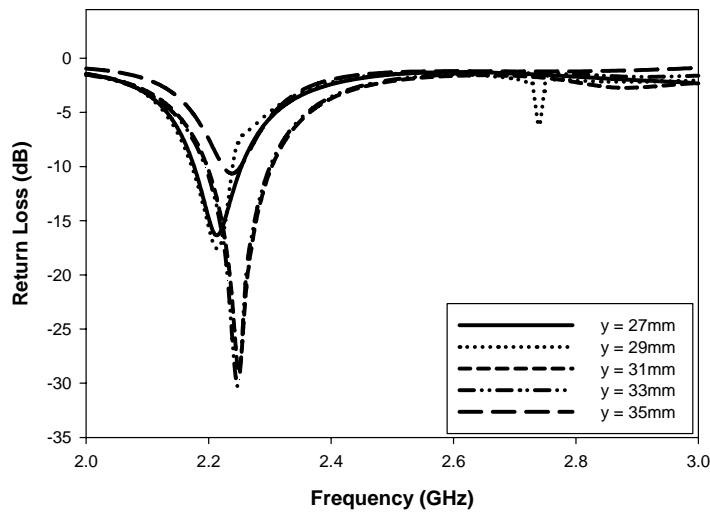
Figure 4.1.3.3.1: Simulated Return loss characteristics for different 'y' values
for x = 15mm
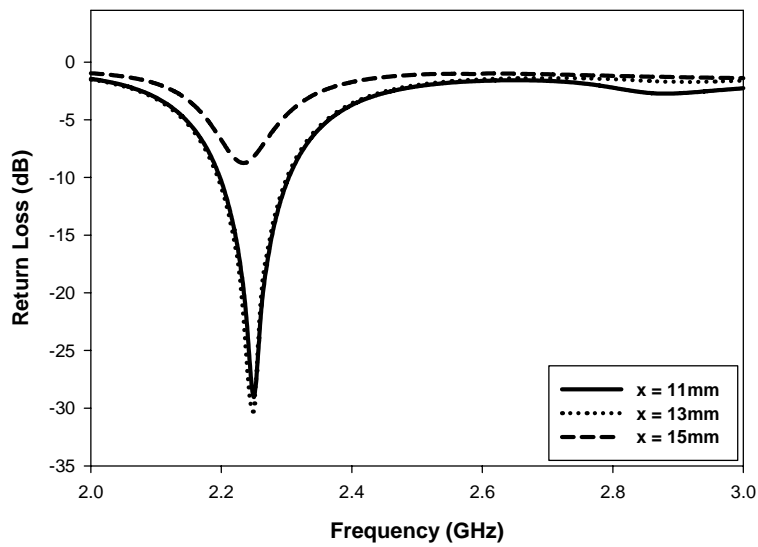
Figure 4.1.3.3.2: Simulated Return loss characteristics for different 'x' values
for y = 31 mm

Variation of the return loss corresponding to the displacement of the DR along x-direction is also shown in figure 4.1.3.3.2. As it is seen in the figure, the resonance

117

frequency does not vary corresponding to the displacement. But the return loss decreases as the x value increases initially and then it becomes almost constant. An optimum value (y = 31mm and x = 11mm) is chosen as the one with minimum return loss and maximum impedance bandwidth is obtained.
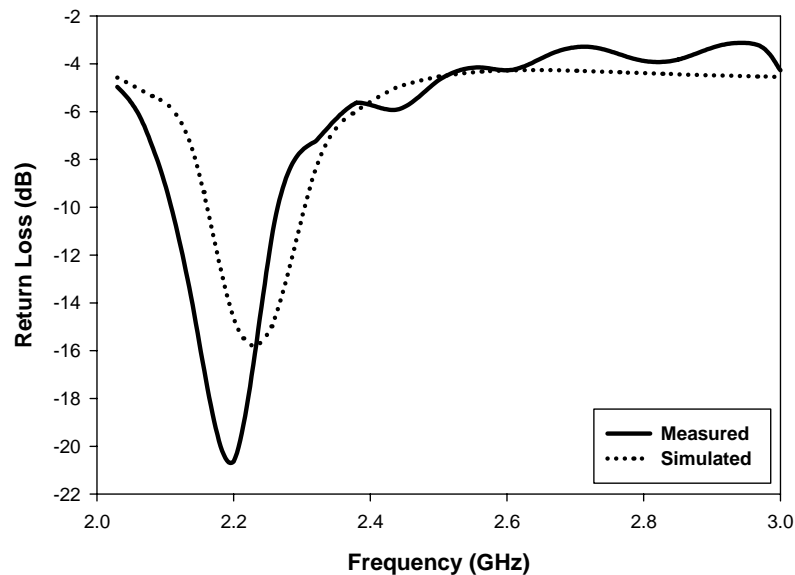
(ii) Reflection Characteristics

Figure 4.1.3.3.3: Measured and Simulated Return Loss of the Antenna

The reflection and transmission characteristics of the antenna are studied. Measured and simulated plot of return loss (|S11|), of the DRA are compared in figure 4.1.3.3.3 and shown that they are in good agreement. The antenna has a 2:1 SWR bandwidth ranging from 2.12 GHz to 2.28 GHz with a percentage bandwidth of 7.27 %.

(i) Gain of the Antenna
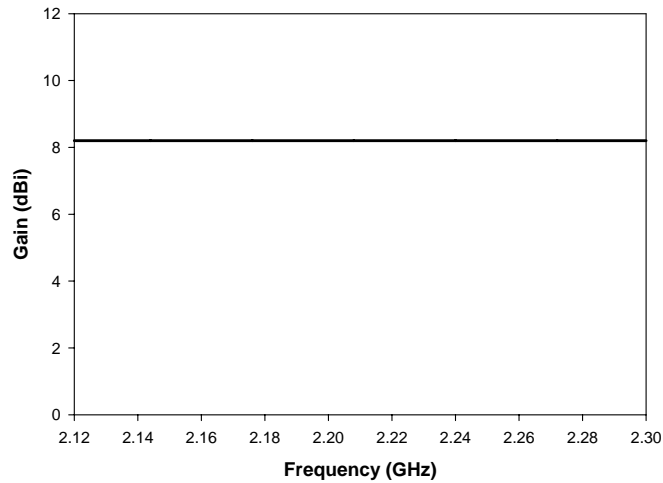
Figure 4.1.3.3.4: Gain of the proposed antenna

The gain of the antenna measured at the useful band of frequencies is plotted and shown in figure 4.1.3.2.4. The gain is seen to be constant throughout the band with a gain of 8.23. The reflection characteristics and Gain are tabulated in the table 4.1.3.3.4.

Range of Frequencies (GHz)	Centre frequency(f_0) (GHz)	Percentage Impedance Band width	Gain in the band (dBi)			
			Maximum	Minimum	Average	At f_0
2.12 - 2.28	2.20	7.27%	8.23 (at all frequencies in the band)	8.23	8.23	8.23

Table 4.1.3.3.1: Reflection characteristics and Gain of the antenna

119

(ii) Radiation Pattern
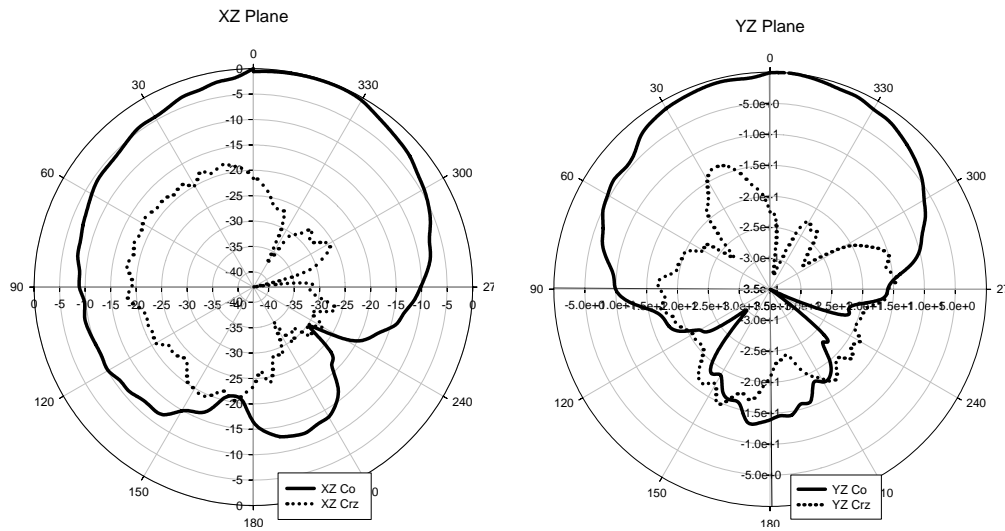
Figure 4.1.3.3.5: 2D Radiation pattern of the antenna at 2.24 GHz

The 2 D radiation patterns of the antenna in XZ and YZ plane are given in figure 4.1.3.3.5. It shows that a half power beam width of 72.1° and 86.9° are obtained in the XZ and YZ plane respectively. The polarization levels are sufficiently low for a linearly polarized antenna. Peak radiation directions are -14.8° and -6.0° respectively in the XZ and YZ planes. Cross polarization levels in the peak radiation directions are also given as **-26.5** and -26.70 respectively in two planes. A front to back ratio of 22.9 and 20.79 is also obtained. The radiation characteristics of the antenna are tabulated in the table 4.1.3.3.2.

Polarization	Half Power Beam width		Boresight Cx-polar level (dB)		Peak radiation direction (θ_p, Deg.)		Cx-polar level in θ_p direction (dB)		Front to Back Ratio (dB)	
	(XZ plane)	(YZ plane)	(XZ plane)	(YZ plane)	(XZ plane)	(YZ plane)	(XZ plane)	(YZ plane)	(XZ plane)	(YZ plane)
Linear	**72.1°**	**86.9°**	**-21.39**	**-22.4**	**-14.8°**	**-6.0°**	**-26.5**	**-26.7**	**22.9**	**20.79**

Table 4.1.3.3.2: Radiation characteristics of the antenna
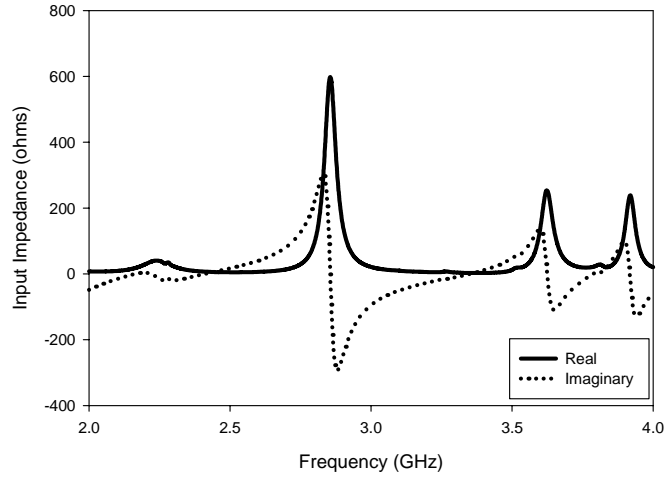
Figure 4.1.3.3.6: Input Impedance of the antenna

In put impedance of the antenna plotted against the frequency is shown in figure 4.1.3.3.6 which verifies that the resonance occurs only corresponding to the frequency where real and imaginary part of the impedance are near to 50 Ω and 0 Ω respectively.

(iii) Simulated Results
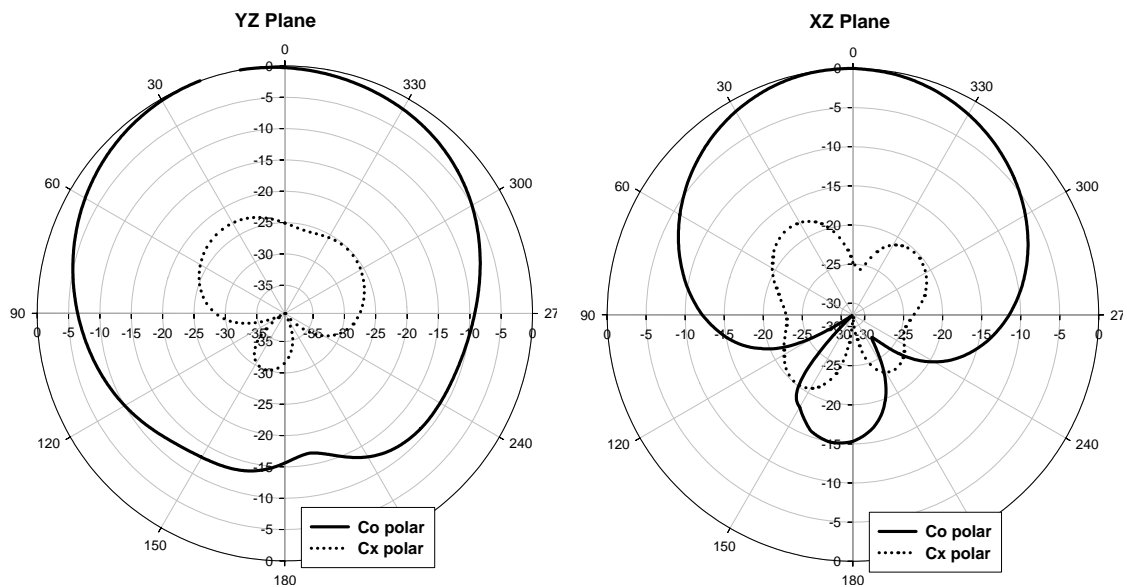
Figure 4.1.3.3.7: Simulated 2D radiation pattern of the antenna

121

As it is seen in figure 4.1.3.3.7., simulated and measured radiation patterns are agreed.
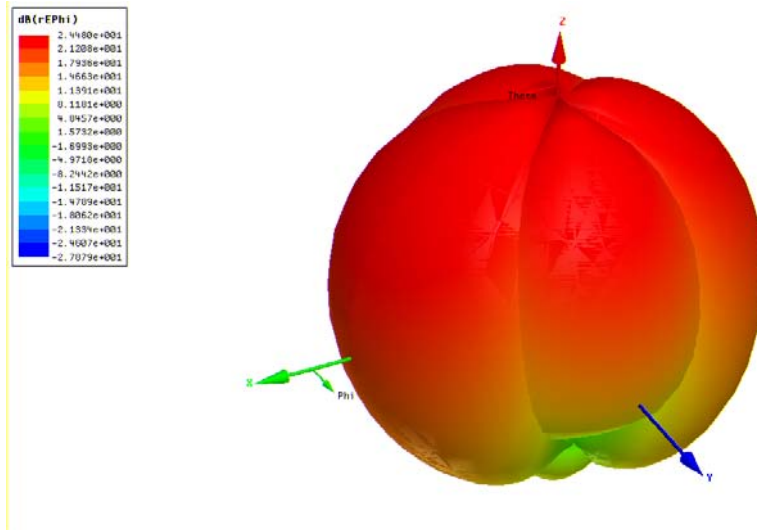
Figure 4.1.3.3.8: 3D Radiation Pattern at 2.24 GHz

The 3D radiation pattern simulated by HFSS (figure 4.1.3.3.8) shows that the antenna gives a broad side radiation pattern with sufficient beam width.

The E field vector distribution within DR shows that the electric field is transverse to the Y axis and hence the mode is TE^y.

(a)

122
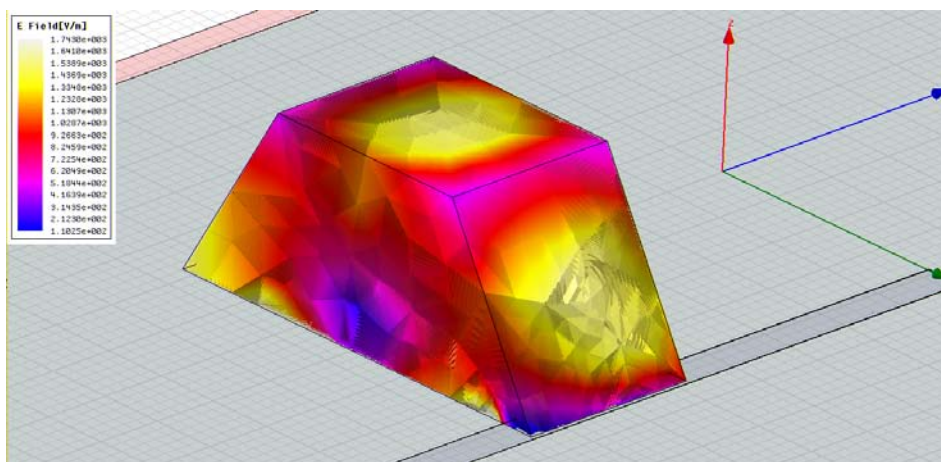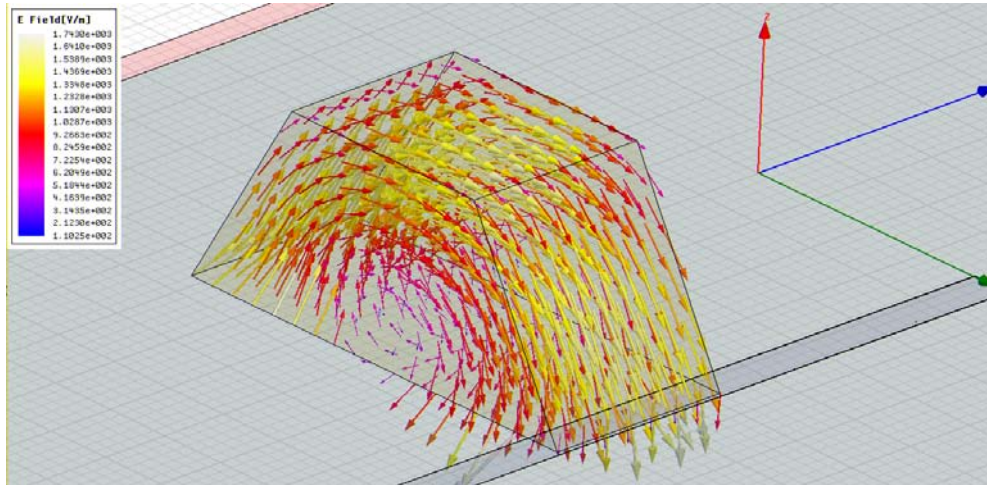
(b)

Figure 4.1.3.3.9: (a) E field and **(b)** E field vector distribution within DRA

Number of half wave variations along each dimensions b2, h and h1 of the DR as shown in figure 4.1.3.3.9 (a) implies that the mode of resonance is TE^{Y}_{110}.

4.2. HIGHER BAND OPERATION

4.2.1. DESIGN 2-1 （TE^{x}_{211} Mode）

In this design, ITDRA operating at the higher order TE^{x}_{211} is presented and the characteristics are studied. The ITDR is placed in the orientation as shown in figure 4.2.1.1.1 and fed at its smaller rectangular base area. The distance of displacement of the DR along y and x direction are optimized as L = 18mm as shown in figure.

4.2.1.1. ANTENNA CONFIGURATION
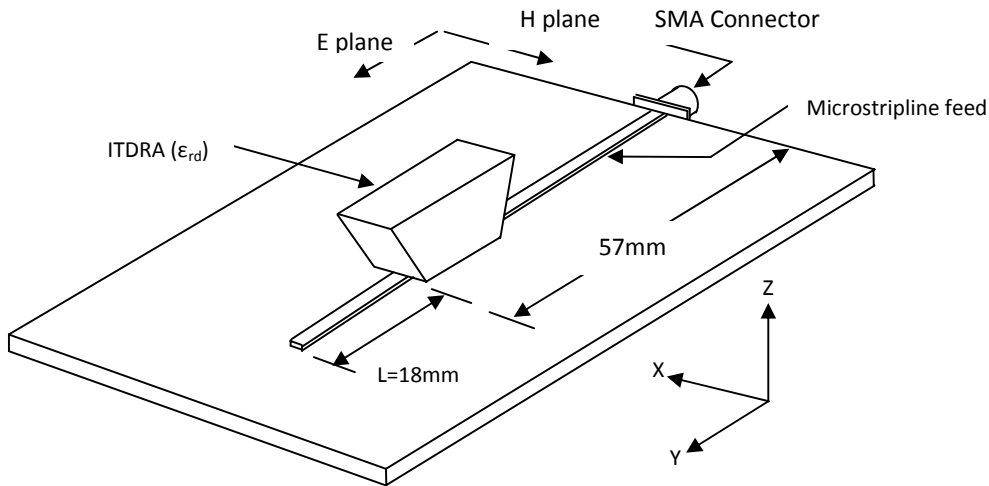
Figure 4.2.1.1.1: Excitation of ITDRA in Design 2.1

An isosceles trapezoidal DRA of permittivity ε_{r1} = 24, bases b1 = 16.5 mm, b2 = 33 mm, height h = 14.3 mm and thickness h1 = 13.8 mm is fed by a 50Ω transmission line of 77 mm (length) Χ 3mm (width) fabricated on a microwave substrate of permittivity ε_{r2}= 4.2 with size 115mm (length) Χ 115mm (breadth) Χ 1.6mm (thickness). The condition that ε_{r1} ›› ε_{r2} for efficient coupling between the strip-line and the DR is satisfied here. Offset Length (L) of the feed is optimized as 18 mm for getting the desired response as the maximum energy is coupled magnetically when the DR is located at the point of maximum electric field on the feed. The reflection (S11), impedance (Z), far field radiation characteristics and gain of the DRA are measured and discussed in the following section.

4.2.1.2. RESULTS AND DISCUSSIONS

(i) Reflection Characteristics
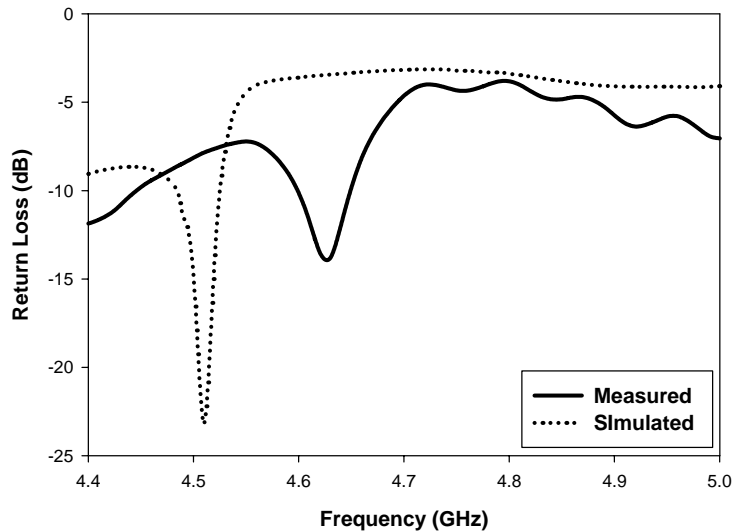
Figure 4.2.1.2.1: Measured and Simulated Return loss of the antenna

The reflection and transmission characteristics of the antenna are studied. Measured and simulated plot of return loss (|S11|), of the DRA are compared in figure 4.2.1.2.1 and shown that they are in good agreement. The antenna has a 2:1 SWR bandwidth ranging from 4.60 GHz to 4.64 GHz with a percentage bandwidth of 0.86 % .

(i) Gain of the antenna

The gain of the antenna measured at the useful band of frequencies is plotted and shown in figure 4.2.1.2.2. A maximum of 9.36 dB is obtained at 4.04 GHz and a minimum of 6.26 dB at 4.45 GHz with an average value of 7.81 dB. At the resonance

frequency 4.62 GHz, the gain obtained is 10.5 dB. The reflection characteristics and Gain are tabulated in the table 4.2.1.2.1.
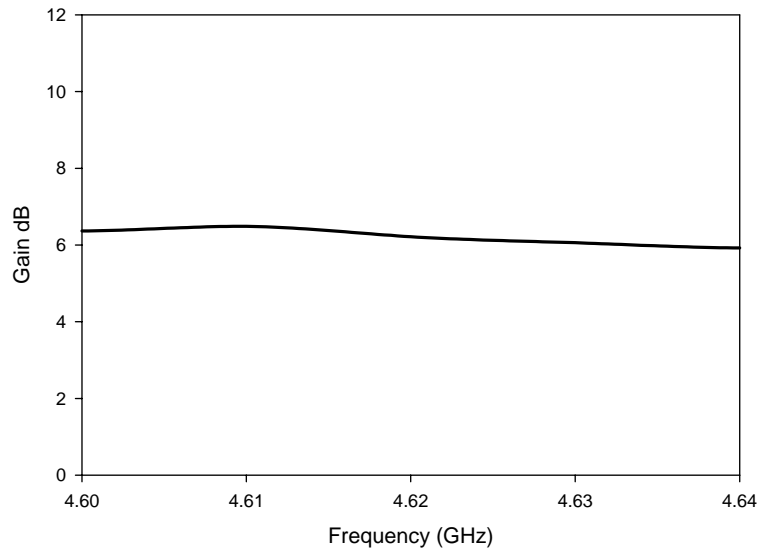
Figure 4.2.1.2.2: Gain of the antenna within the resonance band

Range of Frequencies (GHz)	Centre frequency(f_0) (GHz)	Percentage Impedance Band width	Gain in the band (dBi)			
			Maximum	Minimum	Average	At f_0
4.60 – 4.64	4.62	0.86%	6.48 (at 4.6 GHz)	5.94 (at 4.63 GHz)	6.21	6.22

Table 4.2.1.2.1: Reflection characteristics and Gain of the antenna

(ii) Radiation Pattern

The 2 D radiation patterns of the antenna in XZ and YZ plane are given in figure 4.2.1.2.3. It shows that a half power beam width of 86.0° and 55.4° are obtained in the XZ and YZ plane respectively. The polarization levels are sufficiently low for a linearly polarized

126

antenna. Peak radiation directions are 0° and 9.9° respectively in the XZ and YZ planes. Cross

polarization levels in the peak radiation directions are also given as **-**25.4 and -22.1 respectively

in two planes. A front to back ratio of 24.2 and 24.0 is also obtained. The radiation characteristics

of the antenna are tabulated in the table 4.2.1.2.2.
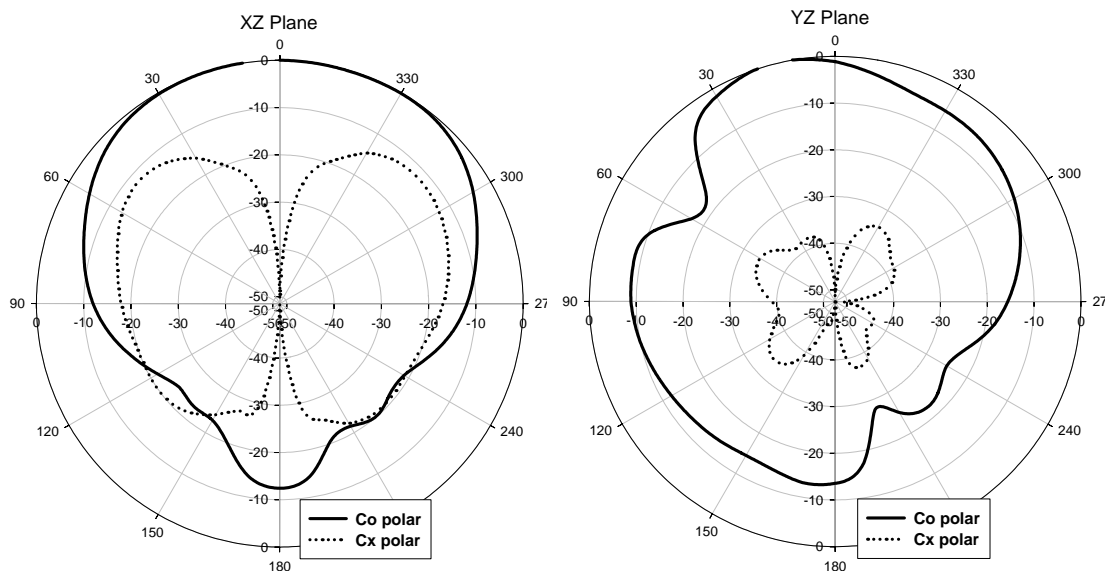
Figure 4.2.1.2.3: Measured 2 D Radiation pattern at 4.62 GHz

Polarization	Half Power Beam width		Boresight Cx-polar level (dB)		Peak radiation direction (θ_p, Deg.)		Cx-polar level in θ_p direction (dB)		Front to Back Ratio (dB)	
	(XZ plane)	(YZ plane)	(XZ plane)	(YZ plane)	(XZ plane)	(YZ plane)	(XZ plane)	(YZ plane)	(XZ plane)	(YZ plane)
Linear	**86.0°**	**55.4°**	**-25.36**	**-20**	**0°**	**9.9°**	**-25.4**	**-22.1**	**24.2**	**24**

Table 4.2.1.2.2:   : Radiation characteristics of the antenna at 4.62 GHz

(iii) **Simulated Results**
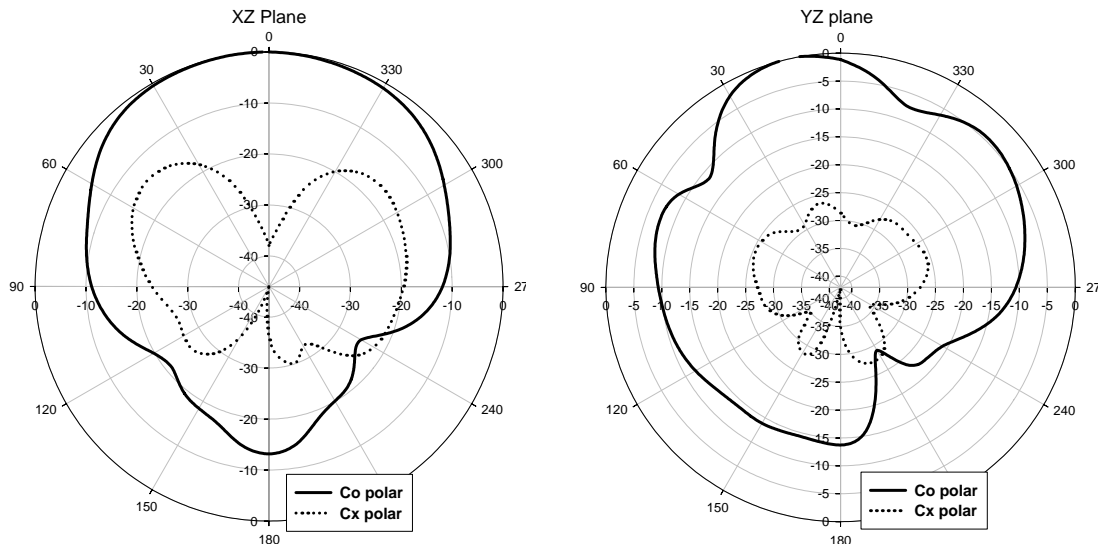
Figure 4.2.1.2.4: 2D Radiation pattern of the antenna at 4.62 GHz
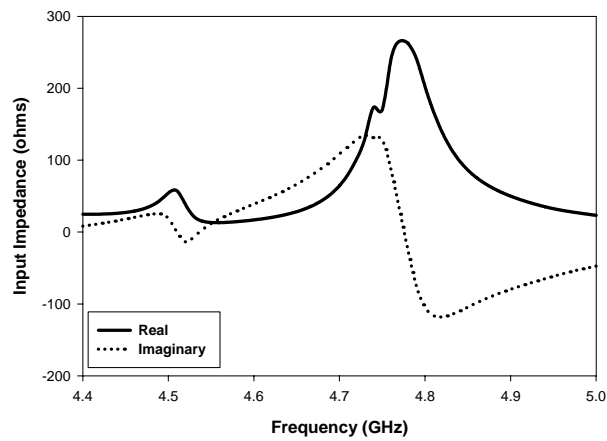
Figure 4.2.1.2.5: Input Impedance of the antenna

In put impedance of the antenna plotted against the frequency is shown in figure 4.2.1.2.5 which verifies that the resonance occurs only corresponding to the frequency where real and imaginary part of the impedance are 50 Ω and 0 Ω respectively.
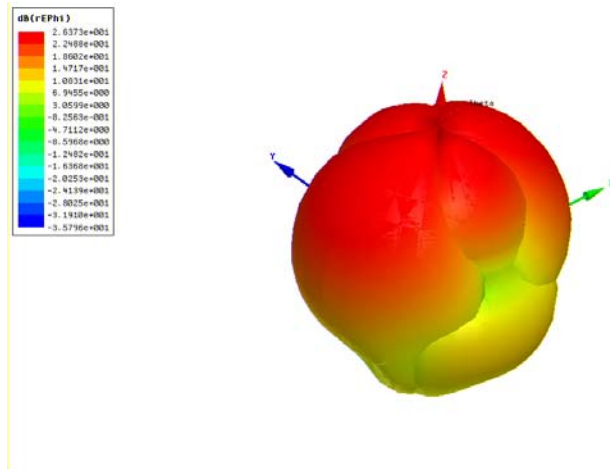
Figure 4.2.1.2.6: 3D Radiation Pattern at 4.51 GHz

The 3D radiation pattern simulated by HFSS^{TM} (figure 4.2.1.2.6) shows that the antenna gives a broad side radiation pattern with sufficient beam width.
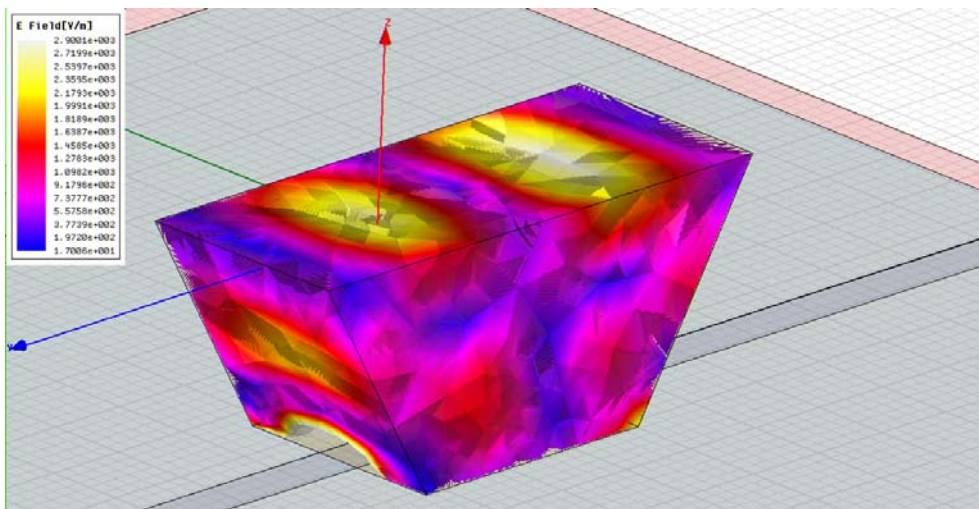
Figure 4.2.1.2.7: E field distribution within DRA identifies the mode as TE^x_{211}

The E field vector distribution within DR shows that the electric field is transverse to the *Y* axis and hence the mode is TE^x.
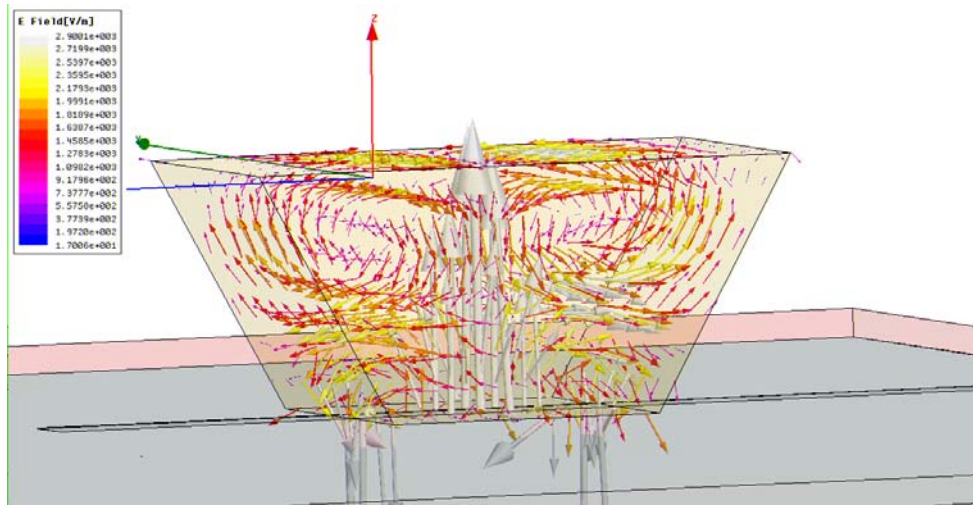
Figure 4.2.1.2.8: E vector distribution within DRA at 4.51 GHz

Number of half wave variations along each dimensions b2, h and h1 of the DR as

shown in figure 4.2.1.2.7 implies that the mode of resonance is TE^x_{211}.

4.2.1.3. COMPARISON OF PERFORMANCE OF ANTENNAS IN DESIGN 1-1 TO 2-1

Design	Mode	Range of Frequencies (GHz)	Centre frequency (f_0) (GHz)	Percentage Impedance Band width	Gain in the band (dBi)			
					Maximum	Minimum	Average	At f_0
Design 1-1	$TE^x_{1\delta0}$	2.38 - 2.54	2.46	11.6%	7.22 (at 2.48 GHz)	3.54 (at 2.36 GHz)	5.38	6.56
Design 1-2	$TE^y_{1\delta1}$	2.50 - 2.76	2.64	9.89%	10.66 (at 2.59 GHz)	9.67 (at 2.76 GHz)	10.16	10.51
Design 1-3	TE^y_{110}	2.12 - 2.28	2.20	7.27%	8.23 (at all frequencies in the band)	8.23	8.23	8.23
Design 2-1	TE^x_{211}	4.04 – 4.45 and 4.6 – 4.64	4.25 and 4.62	9.64% and 0.86%	11.6 (at 4.04 GHz)	7.8 (at 4.45 GHz)	9.7	10.5

Table 4.2.1.3.1: (a) Comparison of reflection characteristics, mode and gain of the designs.

Design	Polariz-ation	Half Power Beam width		Boresight Cx-polar level (dB)		Peak radiation direction (θ_p, Deg.)		Cx-polar level in θ_p direction (dB)		Front to Back Ratio (dB)	
		XZ plane	YZ plane	XZ plane	YZ plane	XZ plane	YZ plane	XZ plane	YZ plane	XZ plane	YZ plane
Design 1-1	**Linear**	**92°**	**106°**	**-25**	**-35**	**-4°**	**30°**	**-25**	**-19**	**20**	**26**
Design 1-2	**Linear**	**78.5°**	**95.3°**	**-14.6**	**-22.6**	**13.8°**	**15.2°**	**-18.4**	**-25.0**	**32.5**	**29.25**
Design 1-3	**Linear**	**72.1°**	**86.9°**	**-21.3**	**-22.4**	**-14.8°**	**-6.0°**	**-26.5**	**-26.7**	**22.9**	**-20.7**
Design 2-1	**Linear**	**86.0°**	**55.4°**	**-25.3**	**-20**	**0°**	**9.9°**	**-25.4**	**-22.1**	**24.2**	**24**

Table 4.2.1.3.1: Comparison of radiation characteristics of different designs

4.3.   MULTI BAND OPERATION

4.3.1. DESIGN 3-1 （MODES : $TE^x_{1\delta1}$ and TE^x_{100}）

With the development of wireless communication systems, the compact, high frequency and dual or multi-frequency antennas are highly desirable. But in compact systems, microstrip antennas are widely used, and have been extensively investigated with reference to dual-frequency applications [1]. Recently, many investigations have been reported on dielectric resonator antennas (DRAs) with dual-frequency or wideband operation using various approaches, such as exciting two modes, or stacking two DRAs [2]-[3]. However, dual-mode excitation is hardly designed because the different modes in

a DRA are sensitive to the antenna configuration. And stacking two DRAs increases the size and the weight of DRA and can lead to a complex fabrication process.

In this design, a simple microstrip line fed ITDRA operating at the resonance mode $TE^x_{1\delta1}$ and TE^x_{100} is presented and the characteristics are studied. At optimum position in this orientation, the antenna radiates at two different frequency bands with good radiation properties. Excitation of two frequency bands simultaneously with a single antenna facilitates the replacement of two individual antennas thereby miniaturization of the whole system is possible. The ITDRA is placed in the orientation as shown in figure 4.3.1.1.1 and fed at its larger rectangular base. The displacement of the DR along y direction are optimized as L = 23.5 mm as shown in figure.

4.3.1.1. ANTENNA CONFIGURATION
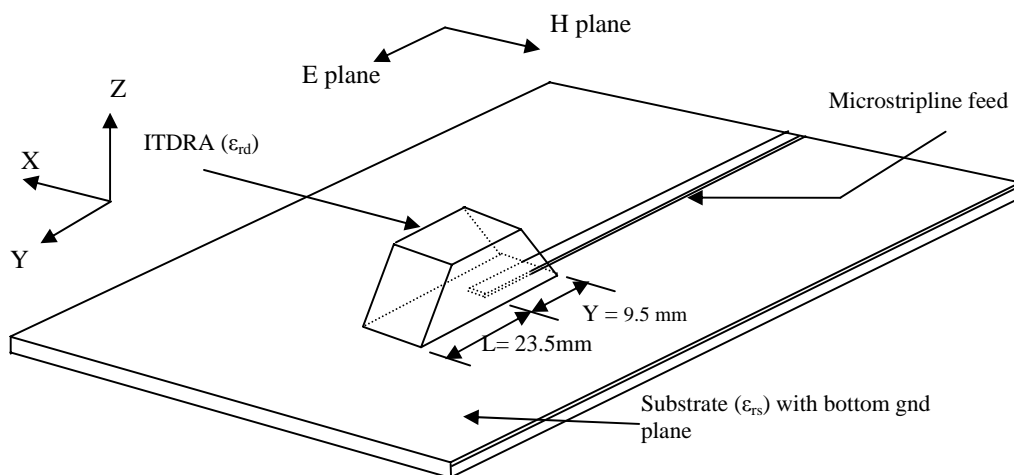
Figure 4.3.1.1.1: Excitation of the antenna

An isosceles trapezoidal DRA of permittivity $\varepsilon_{r1} = 24$, bases b1 = 16.5 mm, b2 = 33 mm, height h = 14.3 mm and thickness h1 = 13.8 mm is fed by a 50Ω transmission line of 77 mm (length) Χ 3mm (width) fabricated on a microwave substrate of permittivity $\varepsilon_{r2} = 4.2$ with size 115mm (length) Χ 115mm (breadth) Χ 1.6mm (thickness). The condition that $\varepsilon_{r1} \gg \varepsilon_{r2}$ for efficient coupling between the strip-line and the DR is satisfied here. Offset Length (L) of the feed is optimized as 23.5 mm (y = 9.5 mm) for getting the desired response as the maximum energy is coupled magnetically when the DR is located at the point of maximum electric field on the feed. The reflection (S11), impedance (Z), far field radiation characteristics and gain of the DRA are measured and discussed in the following section.

4.3.1.2. EFFECT OF MICROSTRIP FEED POSITION OF ITDRA

For optimizing the feed the DRA position is varied along x and y direction, where x and y are defined respectively as the distances from the strip line end to the centre of DR in x and y directions as shown in figure 4.3.1.1.1. DRA is placed symmetrical to the microstrip feed line in x direction in order to get a symmetrical radiation pattern. Reflection characteristics corresponding to the displacement of the DR along 'y' direction is shown in figure 4.3.1.2.1.

Figure 4.3.1.2.1 shows the effect of displacement of the ITDRA along the y-direction, on the return loss of the antenna for x = 0 mm. As 'y' increases, the resonant frequency of the DR as well as the band width, is also seen to be slightly increasing. It can be seen that a distance y = 9.5 mm is optimum in the sense that it gives a minimum return loss in the resonant band with a maximum band width.

133
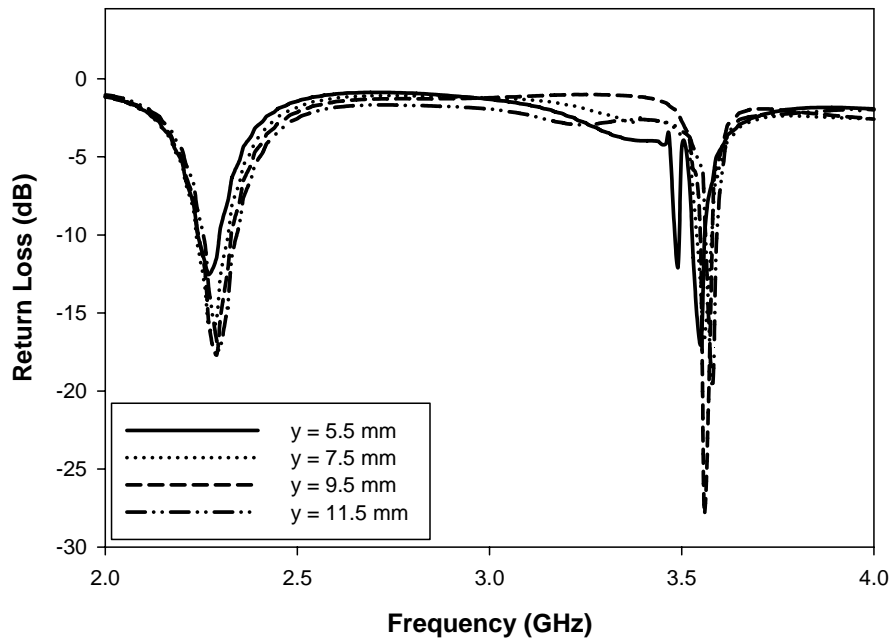
Figure 4.3.1.2.1: Return Loss of the antenna when 'y' varied

4.3.1.3. Results and Discussions

(i) Reflection Characteristics

The reflection and transmission characteristics of the antenna are studied. Measured and simulated plot of return loss ($|S11|$), of the DRA are compared in figure 4.3.1.3.1 and shown that they are in good agreement. The two resonances occurred at 2.24 GHz and 3.50 GHz. The antenna has a 2:1 SWR bandwidth ranging from 2.18 GHz to 2.32 GHz with a percentage bandwidth of 6.22 % for the band 1 and another range of frequencies starting from 3.48 to 3.51 GHz with a percentage bandwidth of 0.86%.

134
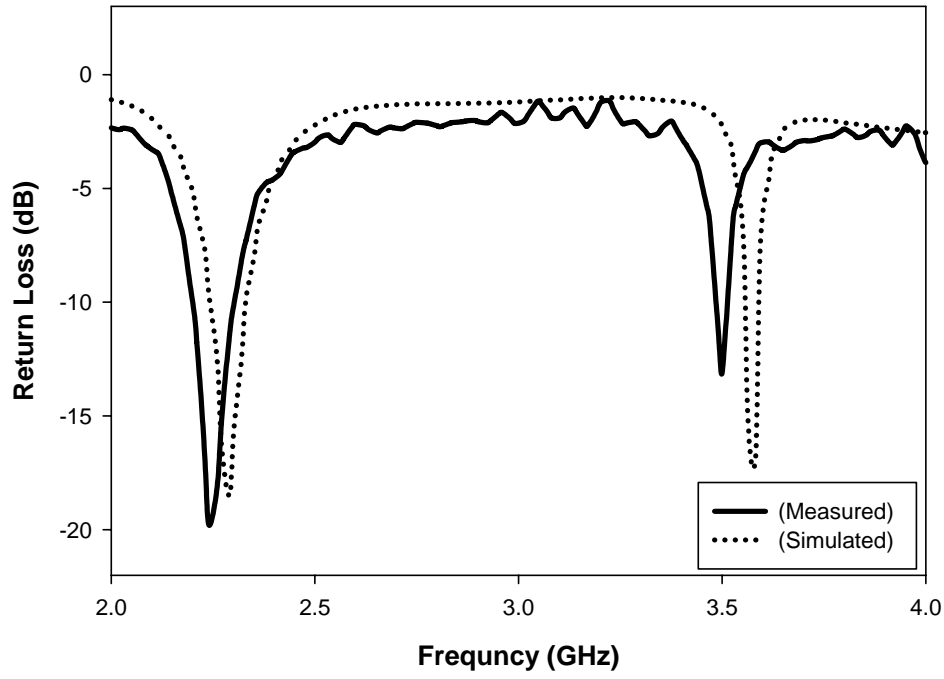
Figure 4.3.1.3.1 : Measured and Simulated Return loss of the Antenna

(ii) Gain of the Antenna
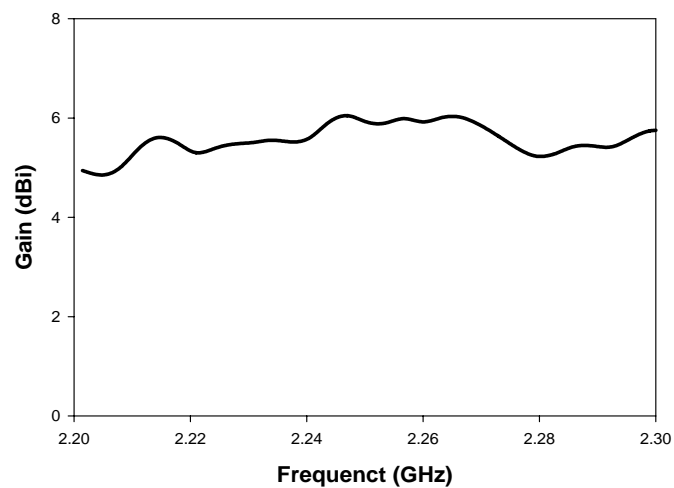
Figure 4.3.1.3.2: (a) Gain of the antenna for the resonance band 1
centered at 2.24 GHz

135

The gain of the antenna measured at the resonant bands of frequencies is plotted and shown in figure 4.3.1.3.2 (a) and (b). For the band 1, a maximum of 6.07 dB obtained at 2.25 GHz and a minimum of 4.88 dB at 2.20 GHz with an average value of 5.47 dB. At the resonance frequency 2.24 GHz, the gain obtained is 5.93 dB.
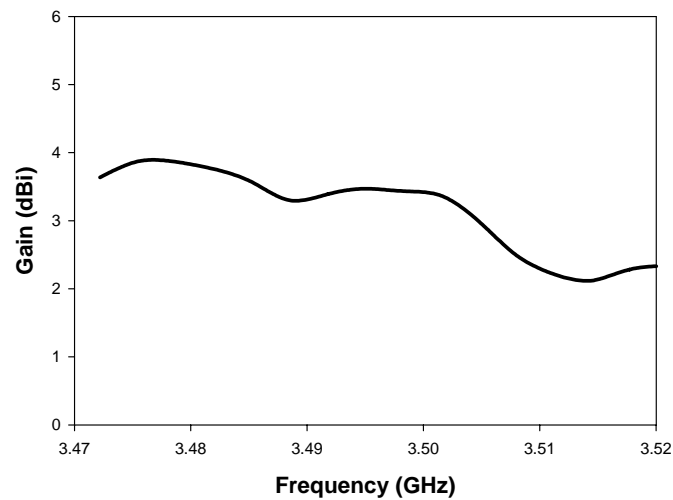
Figure 4.3.1.3.2 : **(b)** Gain of the antenna for resonance band 2 centered at 3.5 GHz

Desired Band	Range of Frequencies (GHz)	Centre frequency(f_0) (GHz)	Percentage Impedance Band width	Gain in the band (dBi)			
				Maximum	Minimum	Average	At f_0
Band 1	**2.18 - 2.32**	**2.25**	**6.22%**	**6.07 (At 2.25 GHz)**	**4.88 (At 2.20 GHz)**	**5.47**	**5.93**
Band 2	**3.48 – 3.51**	**3.495**	**0.86%**	**4.88 (At 3.477 GHz)**	**3.14 (At 3.51 GHz)**	**4.01**	**4.52**

Table 4.3.1.3.1: Reflection characteristics and Gain of the antenna

For the band 2, a maximum of 4.88 dB obtained at 3.47 GHz and a minimum of 3.14 dB at 3.51 GHz with an average value of 4.01 dB. At the resonance frequency 3.50 GHz, the

gain obtained is 4.52 dB. The reflection characteristics and Gain of the antenna is tabulated in table 4.3.1.3.1.

(iii)   Radiation Pattern

The 2 D radiation patterns of the antenna for band1 in XZ and YZ plane are given in figure 4.3.1.3.3. It shows that a half power beam width of $95.0^{°}$ and $183.1^{°}$ are obtained in the XZ and YZ plane respectively. The polarization levels are sufficiently low for a linearly polarized antenna. Peak radiation directions are $0^{°}$ and $27.2^{°}$ respectively in the XZ and YZ planes. Cross polarization levels in the peak radiation directions are also given as -31.8 and -29.5 dB respectively in two planes. A front to back ratio of 25.7 and 22.6 dB are also obtained. The radiation characteristics of the antenna are tabulated in the table 4.3.1.3.2.

At 2.24 GHz

(a)

137

At 3.50 GHz

(b)
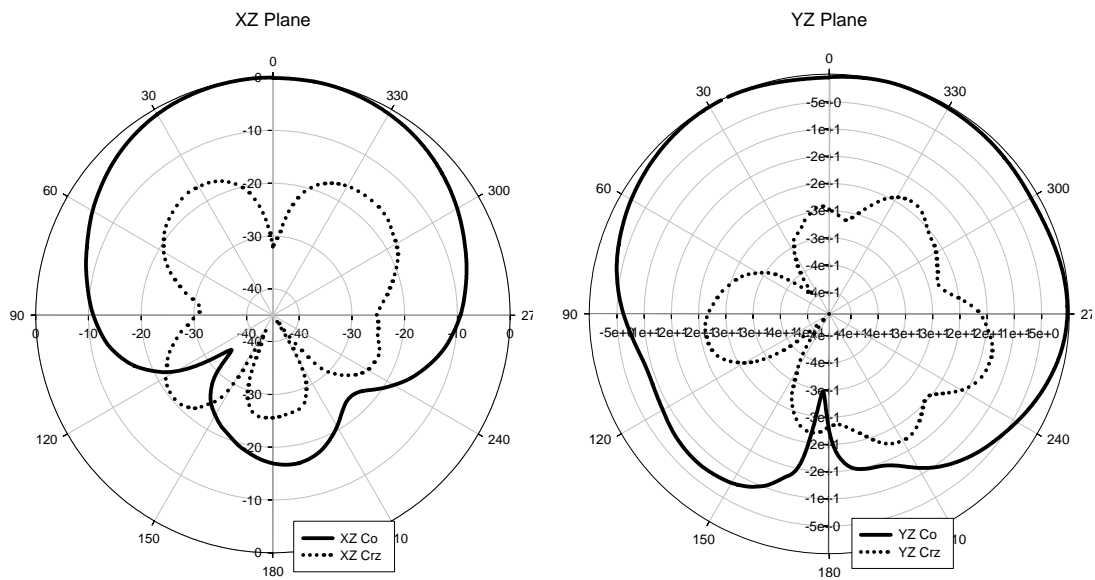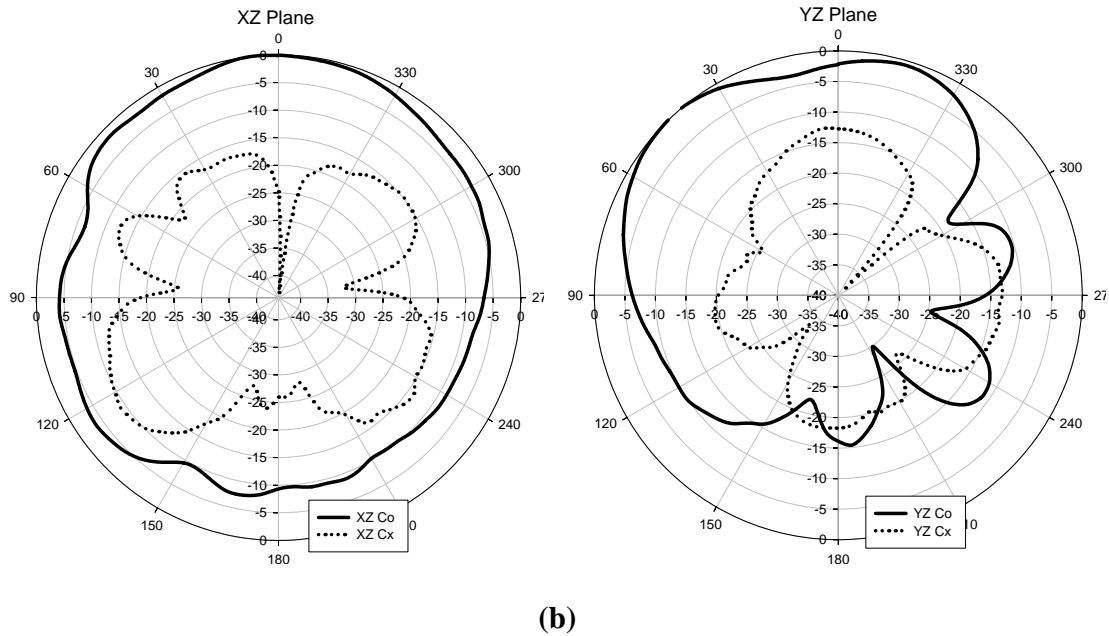
Figure 4.3.1.3.3: 2D Radiation pattern of the antenna (a) at 2.25 GHz and (b) at 3.49 GHz

Desired Band	Polariz ation	Half Power Beam width		Boresight Cx-polar level (dB)		Peak radiation direction (θ_p, Deg.)		Cx-polar level in θ_p direction (dB)		Front to Back Ratio (dB)	
		(XZ plane)	(YZ plane)	(XZ plane)	(YZ plane)	(XZ plane)	(YZ plane)	(XZ plane)	(YZ plane)	(XZ plane)	(YZ plane)
Band 1	**Linear**	**95.0°**	**183.1°**	**-31.8**	**-24.5**	**0°**	**27.2**	**-31.8**	**-29.5**	**25.7**	**22.6**
Band 2	**Linear**	**103.4°**	**106.2°**	**-24.8**	**-12.5**	**0°**	**44°**	**-24.8**	**-19.2**	**9.45**	**18**

Table 4.3.1.3.2: Radiation Characteristics of the Antenna

For the band 2, a half power beam width of $103.4°$ and $106.2°$ are obtained in the XZ and YZ plane respectively. The polarization levels are sufficiently low for a linearly polarized

antenna. Peak radiation directions are 0° and 44.0° respectively in the XZ and YZ planes. Cross polarization levels in the peak radiation directions are also given as **-**24.8 and -19.2 dB respectively in two planes. A front to back ratio of 9.45 and 18.0 dB are also obtained.
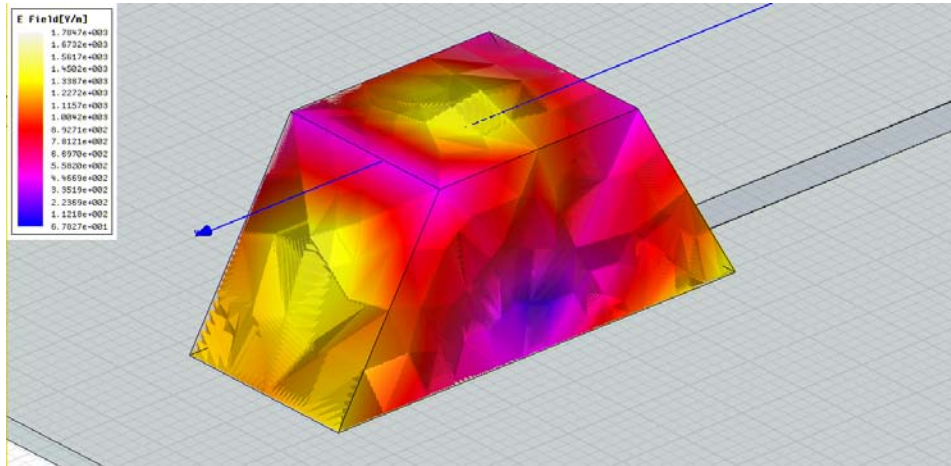
(a)
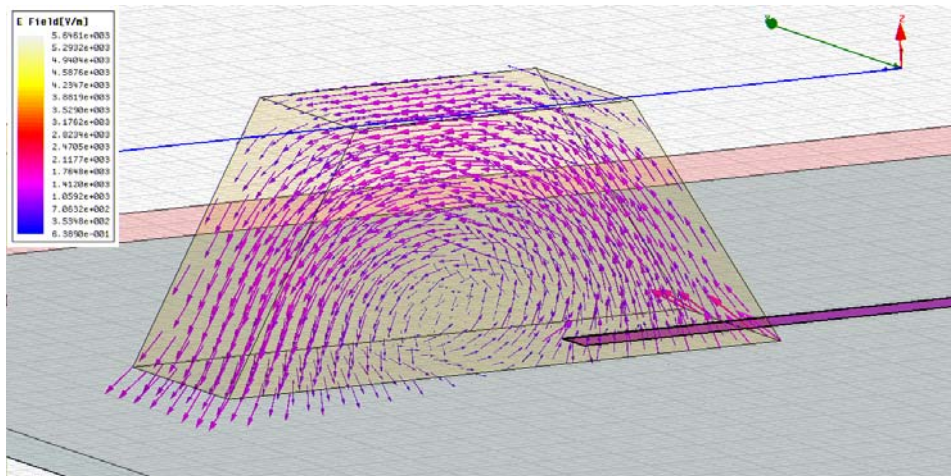
(b)

Figure 4.3.1.3.4: Simulated (a) E field and (b) E Vector distribution within DRA at 2.29 GHz identifies the mode of operation as $TE^x_{1\delta1}$

The E field vector distribution within DR shows that the electric field is transverse to the *X* axis and hence the mode is TE^x. Number of half wave variations along each dimensions b2, h and h1 of the DR as shown in figure 4.3.1.3.4 (a) implies that the mode of resonance is $TE^x_{1\delta 1}$.
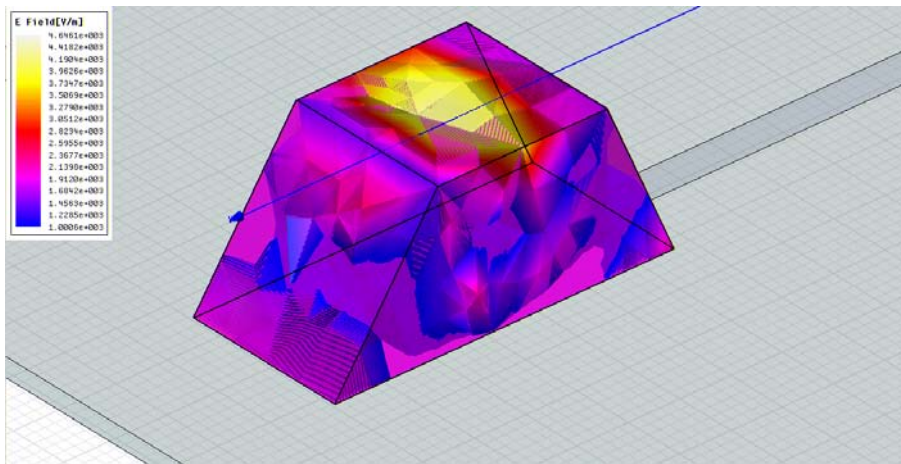
(a)
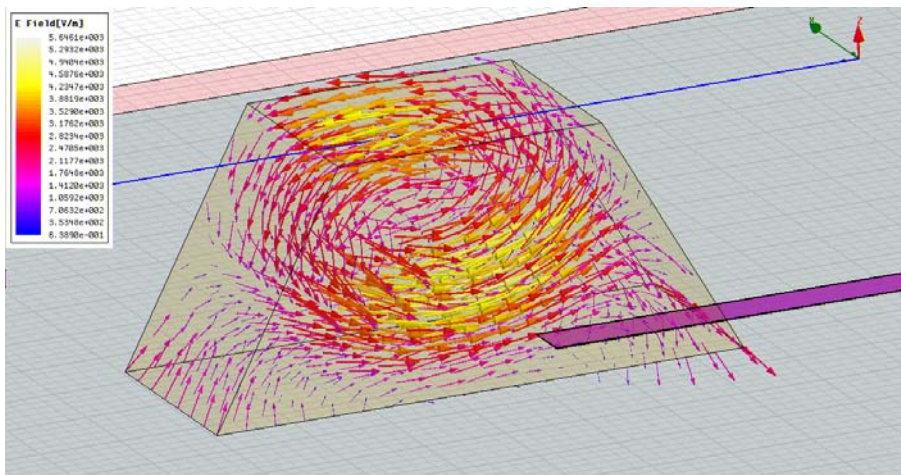
(b)

Figure 4.3.1.3.5: **(a)** E field and **(b)** E Vector distribution within DRA at 3.56 GHz identifies the mode of operation as TE^x_{100}

For the band 2, the E field vector distribution within DR shows that the electric field is transverse to the X axis and hence the mode is TE^x. Number of half wave variations along each dimensions b2, h and h1 of the DR as shown in figure 4.3.1.3.5 (a) implies that the mode of resonance is TE^x_{100}.

(a)

(b)
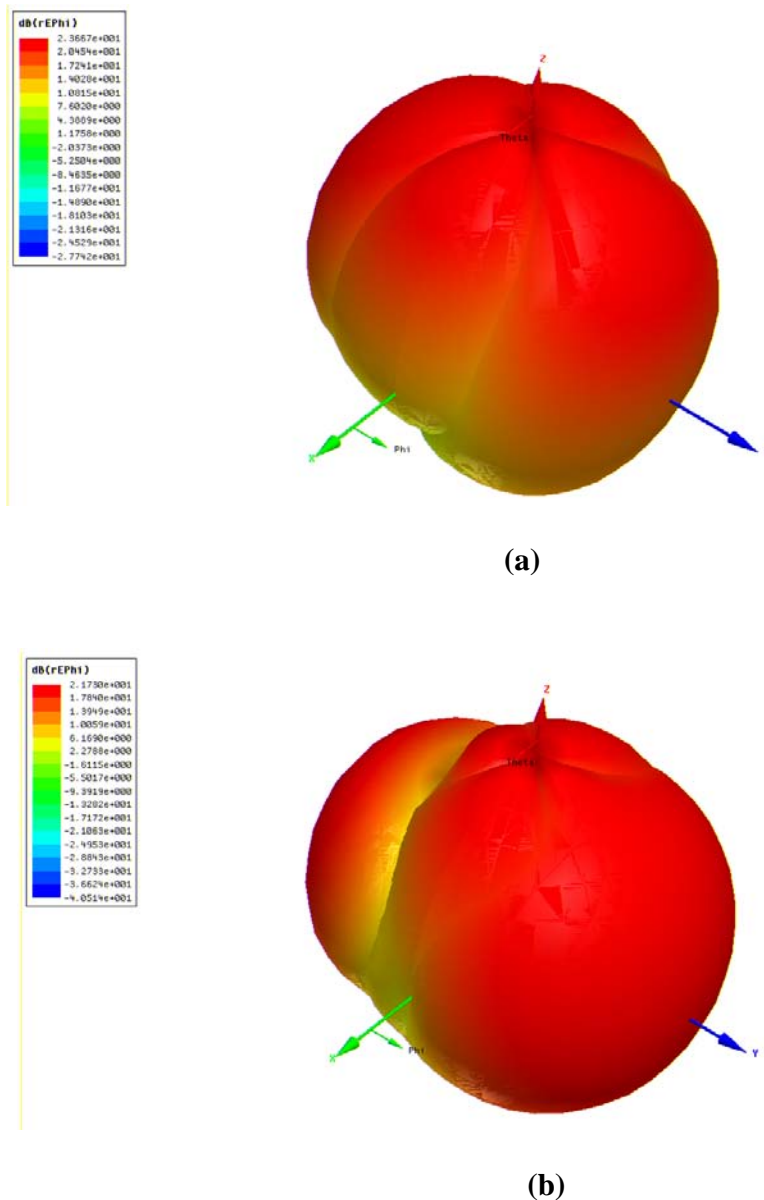
Figure 4.3.1.3.6: 3D radiation pattern of the anntenna **(a)** at 2.29 GHz and **(b)** at 3.56 GHz

The 3D radiation pattern simulated by HFSS[TM] shown in figure 4.3.1.3.6 (a) and (b) which shows that the antenna gives a wide beam broadside pattern.

4.4. DUAL BAND DUAL POLARIZATION OPERATION

4.4.1. DESIGN 4-1   (MODE: $TE^x_{11\delta}$)

This design presents a compact dual band dual polarized Isosceles Trapezoidal Dielectric Resonator Antenna with simple microstrip line feed. The two bands with linear polarizations have broadside radiation patterns. The presented design is characterized by reasonably good front-to-back ratios with average gains of 3.50 dBi and 4.08 dBi over the 2.35 GHz and 2.88 GHz bands respectively. The antenna's dual polarizations are orthogonal to each other and at 45° tilts in either direction of microstrip feed. This design makes it works as equivalent to two independent antennas in multipath environments. The proposed antenna offers a 2:1 VSWR bandwidth of 12.76% and 6.94% at frequency bands 1 & 2 respectively.

4.4.1.1.   Introduction

Antennas with dual polarization operation have been in demand for many applications, particularly for wireless communication. Polarization-diversity antennas are needed because they can better handle information than singly polarized antennas in certain situations; for example, they can reduce multi-path effects. The recent growth in the modern wireless communication has increased the demand for multi-band antennas with

polarization diversity, which can be achieved by making use of dual-polarized arrays similar to those shown in [2]. A fair amount of research has been done to develop suitable antenna elements with the capacity to support orthogonal polarizations with dual-frequency bands. Dual-frequency elements such as stacked-, notched- and dichroic patches have also been considered to be modified to facilitate dual-polarized operation. The size of the elements, the high cross polarization levels associated with dichroic- and stacked patches and the complex routing of feeding networks needed to implement some of the antenna patch designs [3] disqualifies these options in general to be used in dual-polarized arrays. The printed bow-tie design presented in [2] makes use of four dipoles and four ports to realize a very wide bandwidth dual-polarized design for C- and X-band applications. Most of the antennas adopt microstrip structures to realize the dual band and dual polarization function. Microstrip antenna has good performances in lower frequency, however in higher frequency, the radiation efficiency deteriorates apparently.

This paper presents a dual band dual polarized (DBDP) antenna design with a simple compact DRA of a novel, isosceles trapezoidal (IT) shape. The ITDRA is fed by a microstrip line and is operated in $TE^x_{11\delta}$ mode. The DRA is fed at its trapezoidal face and is placed asymmetrically to the microstrip line as shown in figure 1(b) and (c). This design makes it works as equivalent to two independent antennas in multipath environments. If the dimensions and permittivity of the DRA is varied along with the use of suitable impedance matching mechanisms the proposed antenna can be tuned for using in the useful application bands such as the bands of 2.4/5 GHz WLAN, dual band base station antenna for cellular radio communication etc.

4.4.1.2. ANTENNA CONFIGURATION

An ITDRA of permittivity $\varepsilon_{r1} = 24$, bases $b_1 = 16.5$mm, $b_2 = 33$mm, height h = 14.3 mm and thickness $h_1 = 13.8$ mm is fed by a 50 Ω transmission line of 77mm (length) ✗ 3 mm (width) fabricated on a microwave substrate of permittivity $\varepsilon_{r2} = 4.2$ with size 115mm (length) ✗ 115mm (breadth) ✗ 1.6mm (thickness) as shown in figure 4.4.1.2.1. The condition that $\varepsilon_{r1} \gg \varepsilon_{r2}$ for efficient coupling between the strip-line and the DR is satisfied here.
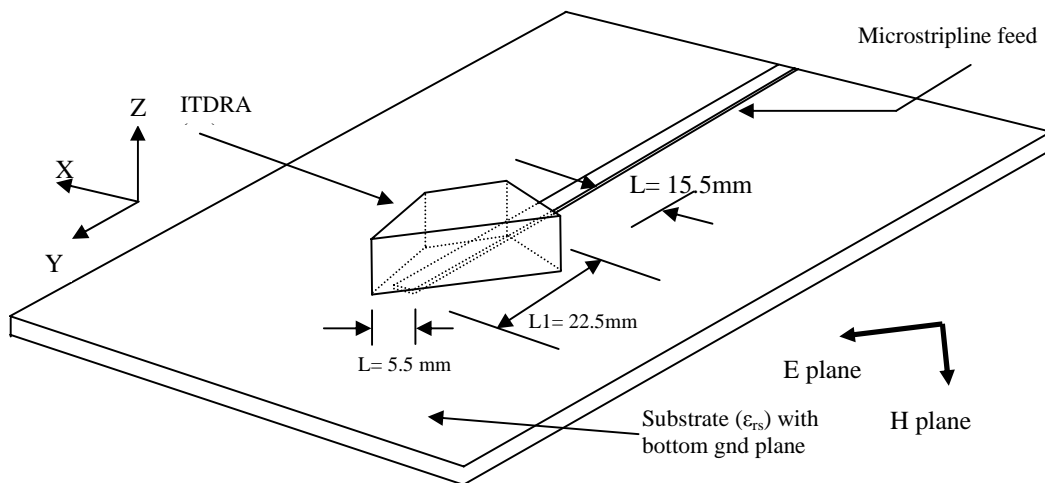
Figure 4.4.1.2.1. Excitation of ITDRA

The ITDRA is placed on the substrate with the orientation as shown in figure 4.4.1.2.1 and 4.4.1.2.2.
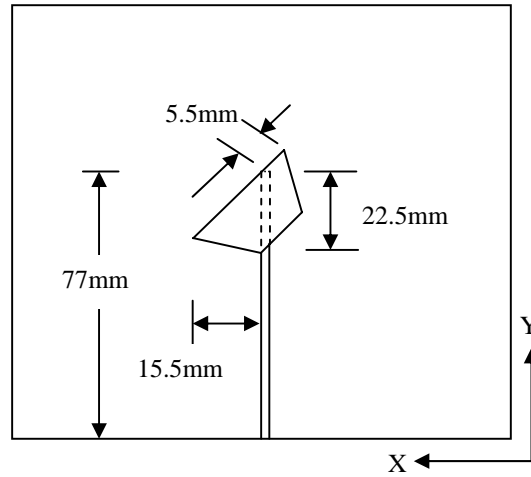
Figure 4.4.1.2.2: Top view of the antenna configuration.

4.4.1.3. RESULTS AND DISCUSSIONS

(i) Reflection Characteristics
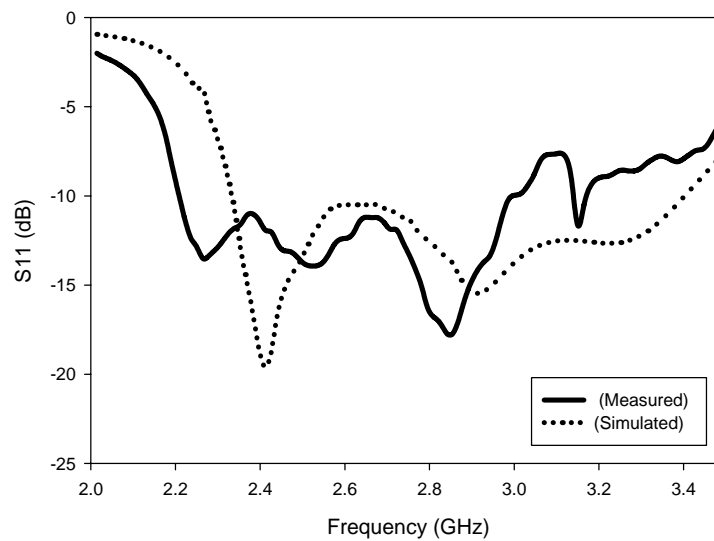
Figure 4.4.1.3.1: Measured and Simulated Return Loss of the antenna.

145

S21
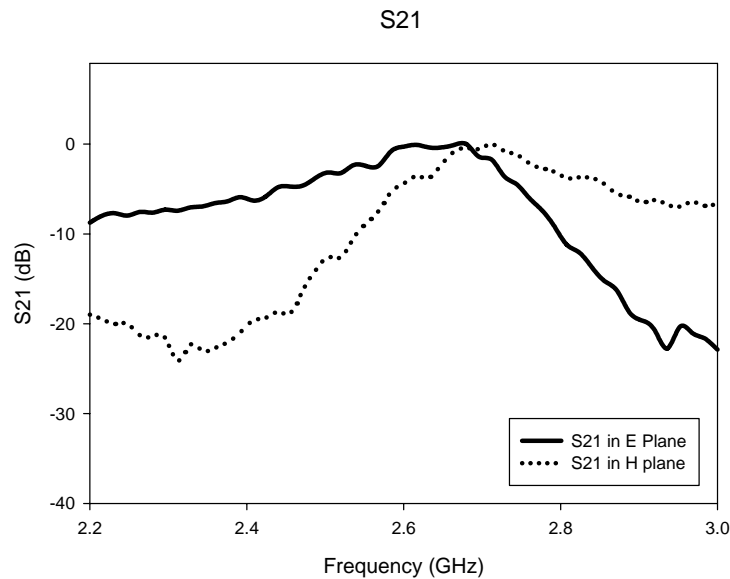
Figure 4.4.1.3.2: S21 of the antenna at E plane and H plane (45° tilted from the boresight direction) shows antenna has orthogonal polarizations

The reflection and transmission characteristics of the antenna are studied. Measured and simulated plot of return loss (|S11|), of the DRA are compared in figure 4.4.1.3.1. The antenna has a 2:1 SWR bandwidth ranging from 2.20 GHz to 2.50 GHz (12.76 %) in the band 1 and 2.78 GHz to 2.98 GHz (6.94%) in band 2.

S21 of the antenna at E and H plane are plotted in figure 4.4.1.3.2. It shows that in E plane, S21 dominates in band 1 while in H plane, it dominates in band 2. It implies that the antenna support orthogonal polarizations in different frequency bands. Also it is verified that the polarization of the antenna is linear in the entire frequency range in each band but is orthogonal to each other.

146

(ii) **Radiation Patterns**

At 2.26 GHz

(a)

At 2.52 GHz

(b)

147
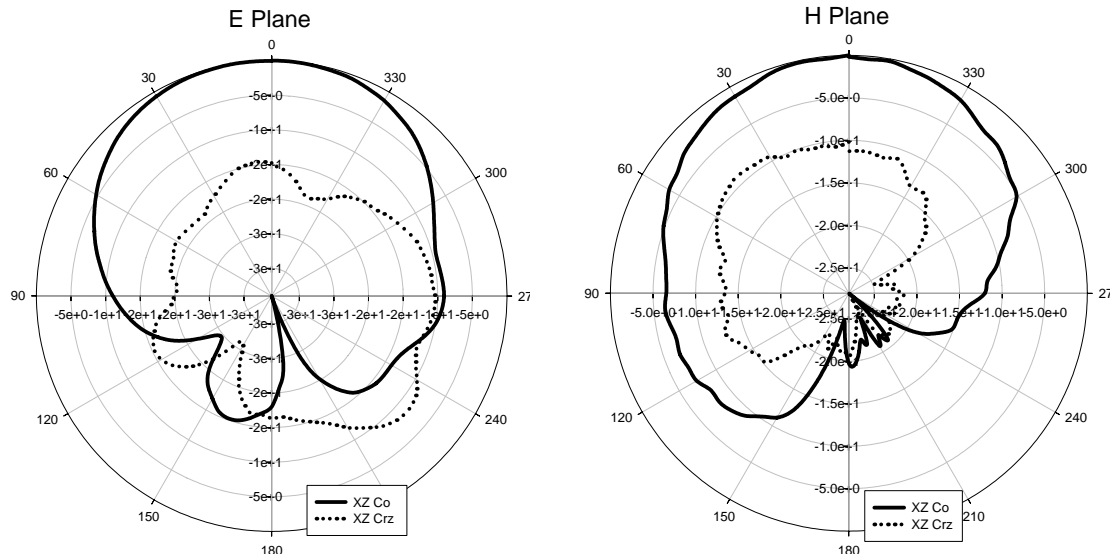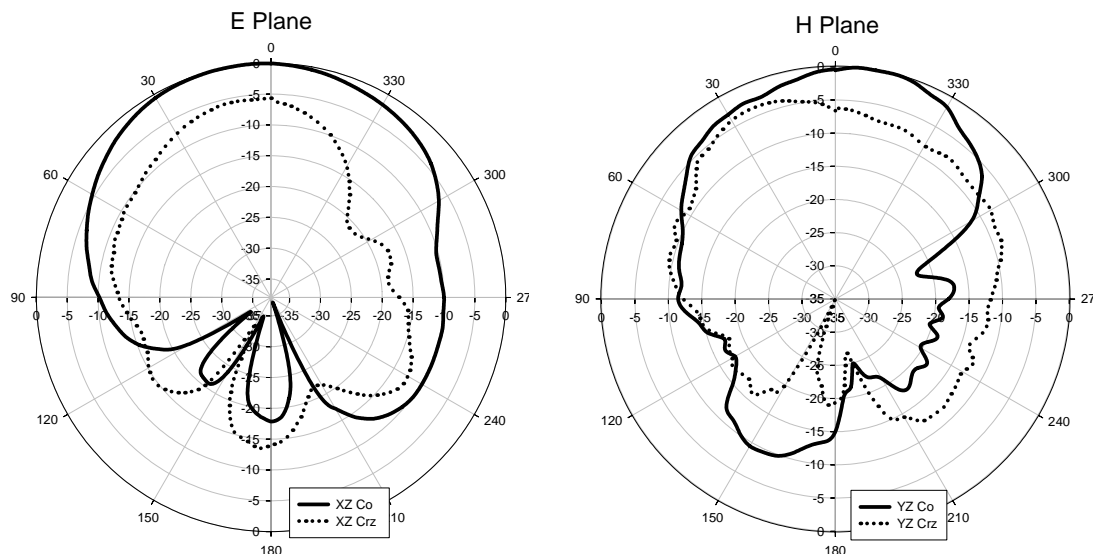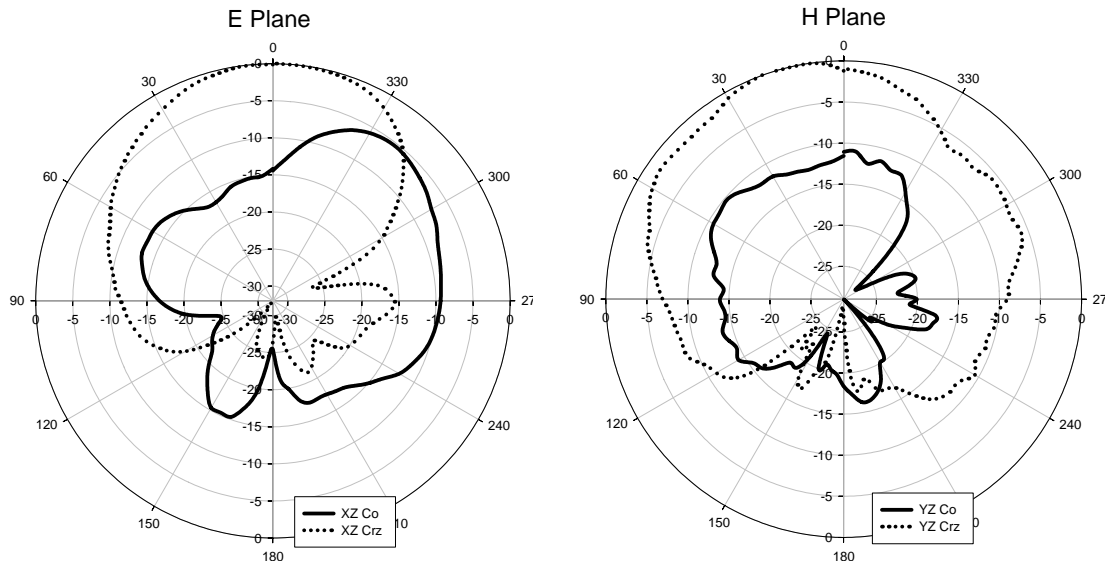
At 2.85 GHz

(c)

Figure 4.4.1.3.3: 2D Radiation patterns at (a) 2.26 GHz, (b) 2.52GHz and (c) 2.85 GHz

At 2.26 GHz (Band 1)

Polariza-tion	Half Power Beam width		Boresight Cx-polar level (dB)		Peak radiation direction (θ_p, Deg.)		Cx-polar level in θ_p direction (dB)		Front to Back Ratio (dB)	
	(XZ plane)	(YZ plane)	(XZ plane)	(YZ plane)	(XZ plane)	(YZ plane)	(XZ plane)	(YZ plane)	(XZ plane)	(YZ plane)
Linear	91.8°	91.38°	-14.8	-6.25	5.3°	2.0°	-14.4	-6.35	18.0	19.5

Table 4.4.1.3.1: Radiation characteristics of the antenna at 2.26 GHz

148

At 2.52 GHz

Polariza-tion	Half Power Beam width		Boresight Cx-polar level (dB)		Peak radiation direction (θ_p, Deg.)		Cx-polar level in θ_p direction (dB)		Front to Back Ratio (dB)	
	(XZ plane)	(YZ plane)	(XZ plane)	(YZ plane)	(XZ plane)	(YZ plane)	(XZ plane)	(YZ plane)	(XZ plane)	(YZ plane)
Linear	93.3°	67.53°	-5.7	-6.55	11.4°	-11.3°	-5.7	-7.16	-18.0	14.6

Table 4.4.1.3.2: Radiation characteristics of the antenna at 2.52 GHz

At 2.85 GHz (Band 2)

Polarization	Half Power Beam width (Cx-polar)		Boresight Co-polar level (dB)		Peak radiation direction (θ_p, Deg.) (Cx-polar)		Co-polar level in θ_p direction (dB)		Front to Back Ratio (dB) (Cx-to Co-)	
	(XZ plane)	(YZ plane)	(XZ plane)	(YZ plane)	(XZ plane)	(YZ plane)	(XZ plane)	(YZ plane)	(XZ plane)	(YZ plane)
Linear but Cx-polar level dominates Co-polar level	70.8°	86.52°	-14.3	-8.21	0.0°	14.2°	-14.3	-9.55	26.5	24.68

Table 4.4.1.3.3: Radiation characteristics of the antenna at 2.85GHz

Radiation patterns are shown in figure 4.4.1.3.3 for frequencies 2.26 GHz, 2.56 GHz and 2.85 GHz respectively. The beam widths of E and H plane patterns at 2.52 GHz in the band 1 is 91.8° and 91.38° respectively. The front to back ratios are 18 and 19.5 dB respectively for the above two patterns. Similarly 70.8° and 86.52° are the corresponding beam widths of the bands 2 at 2.85 GHz and 26.5 and 24.68dB are the front to back ratios. Cross-polarization levels are sufficiently less than co-polaristion levels in the patterns at 2.26 GHz (band 1) but cross polar levels greatly exceed co-polar level in patterns at 2.85 GHz (band 2). This means that the antenna gives orthogonal polarization in two different bands.
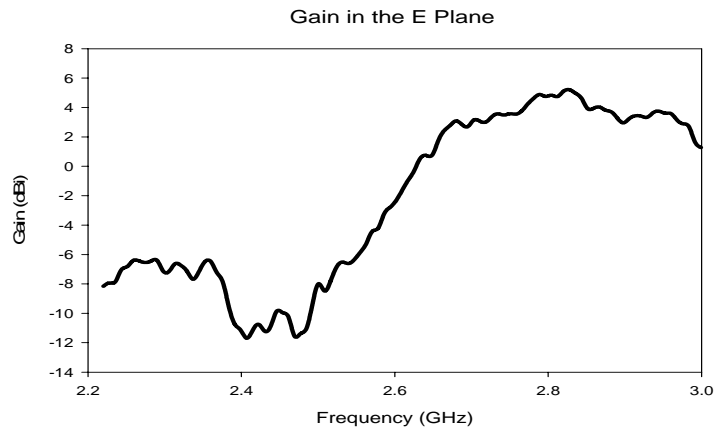
(a)
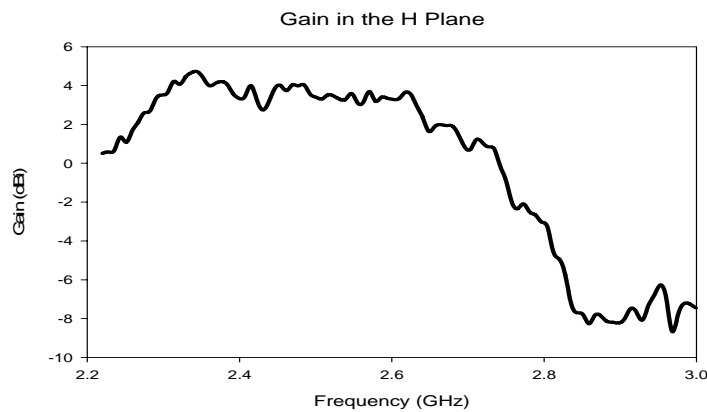
(b)

Figure 4.4.1.3.4: Gain of the antenna taken in **(a)** E plane and **(b)** H plane

Gain in dBi of the antenna measured at two orthogonal planes (E and H planes) are shown in figure 4.4.1.3.4. It reveals that the gain is moderately high only in upper band when measured in E plane and the reverse is getting in H plane as well. The antenna has a peak gain of 4.76 dBi at 2.35GHz with an average value of 3.5 dBi in the band 1. Similarly the maximum and average gains for the band 2 are 5.32 (at 2.84 GHz) and 4.08 dBi respectively.

150

Desired Bands	Range of Frequencies (GHz)	Centre frequency (f_0) (GHz)	Percentage Impedance Band width	Gain in the band (dBi)			
				Maximum	Minimum	Average	At f_0
Band 1	2.20 – 2.50	2.35	12.76%	4.76 at 2.35 GHz	2.24	3.5	4.67
Band 2	2.78 – 2.98	2.88	6.94%	5.32 at 2.84 GHz	2.84	4.08	3.74

Table 4.4.1.3.4: Reflection characteristics and Gain of the antenna
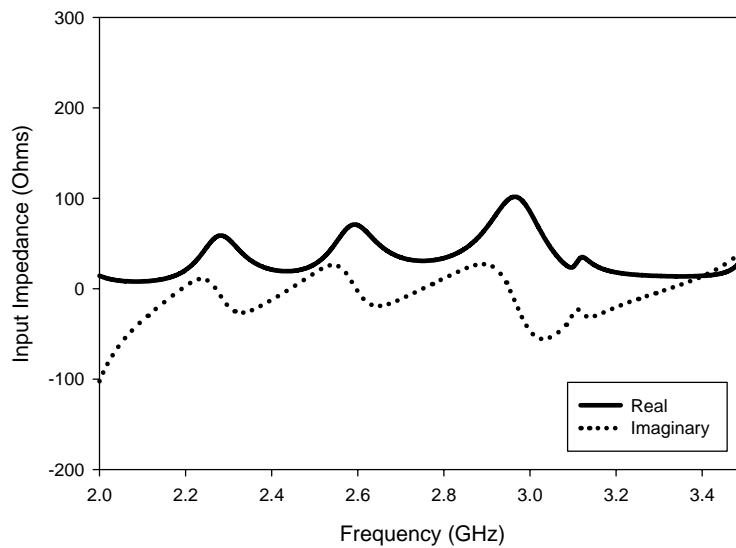
Figure 4.4.1.3.5: Input Impedance of the antenna.

Plot of input impedance against frequency which is shown in figure 4.4.1.3.5 confirms that the impedance matching between the feed and the antenna is occurred at frequency corresponding to the resonant modes.

151

(iii)   Simulated Results
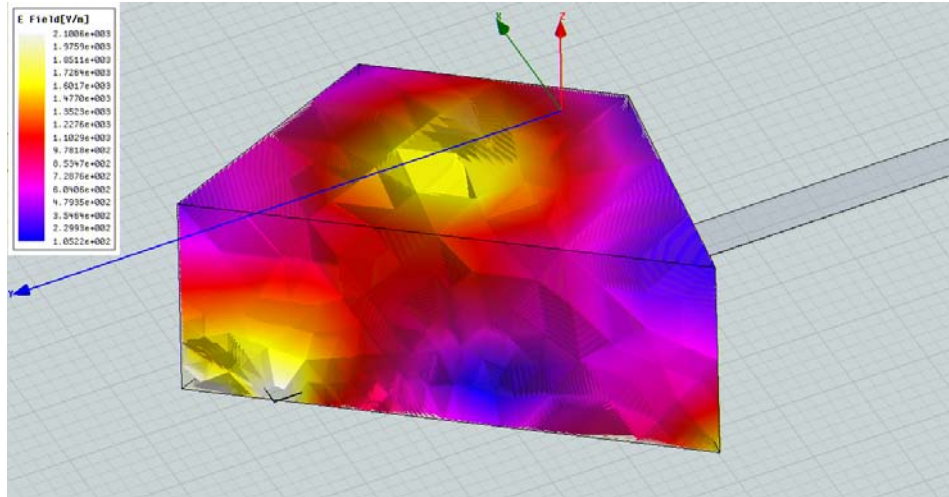
(a)
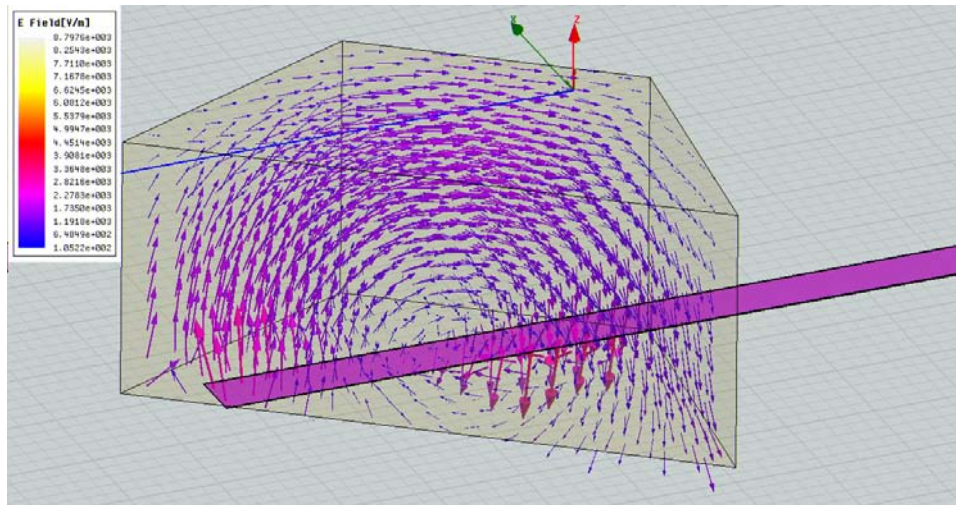
(b)
Figure 4.4.1.3.6: (a) E field and (b) E vector distribution within DRA at 2.26 GHz
identifies the mode of operation as $TE_{11\delta}$
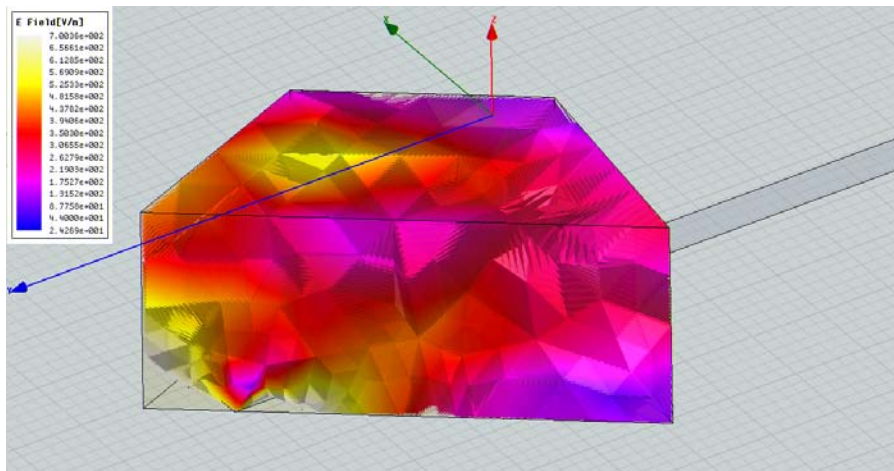
(a)
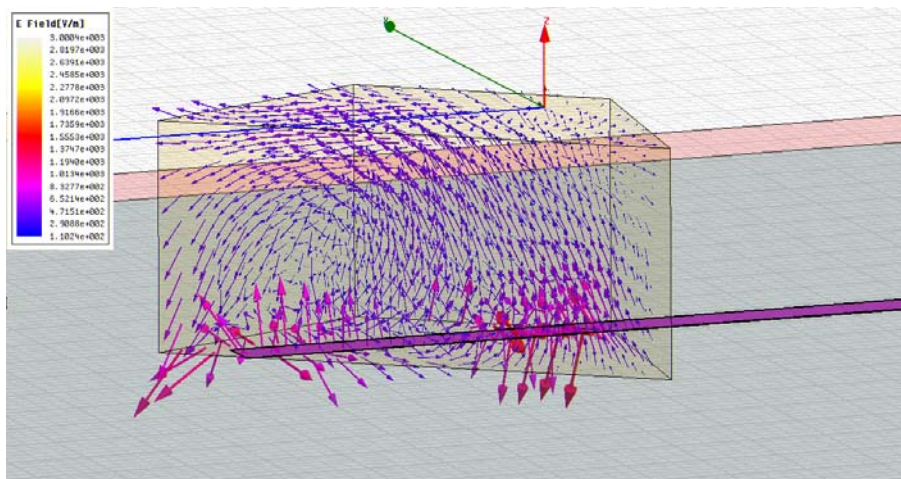
(b)

Figure 4.4.1.3.7: (a) E field and (b) E Vector distribution within DRA at 2.85 GHz identifies the mode of operation as $TE^{x}_{11\delta}$

Electric field vector distribution in figure 4.4.1.3.6 (b) shows that it is purely transverse to the H plane. The mode is identified as $TE_{11\delta}$ when the half wave variations of the E field are counted along the 3 dimensions of the ITDR. Figure 4.4.1.3.7 (b) exhibits strong electric field vectors transverse to E plane and hence it is realized that the

polarization is orthogonal to that at 2.26 GHz shown above. The exact mode of the DR is not exactly clear at 2.85 GHz since another loop of Electric vector is about to form within DRA as it is seen in the figure 4.4.1.3.7 (b). But electric field distribution within DRA (figure 4.4.1.3.7 (a)) shows the number of half wave variations of the field along all the 3 dimensions of the ITDRA corresponding to a mode of resonance $TE_{11\delta}$ like.
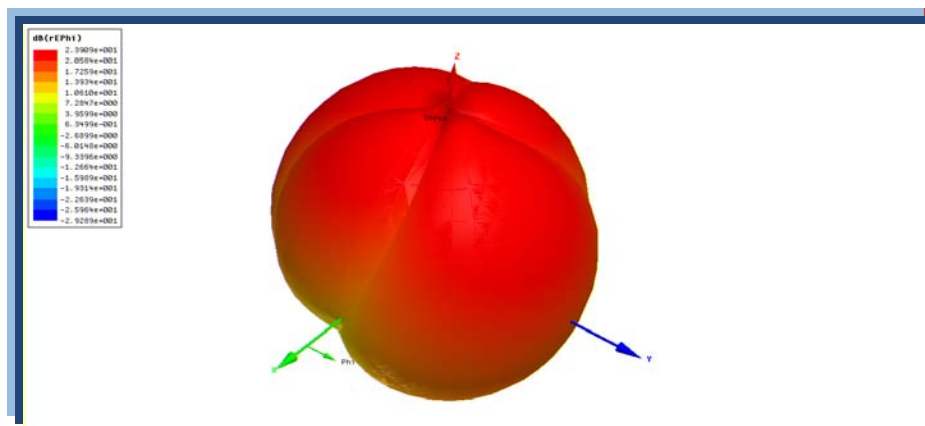
(a)
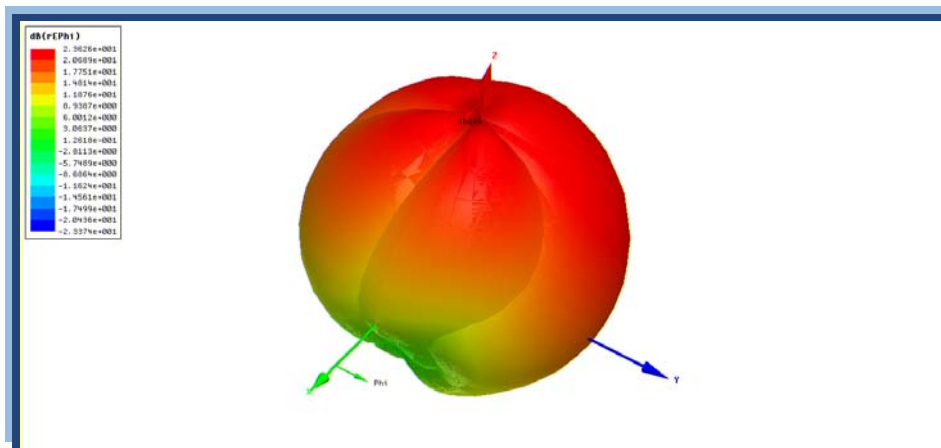
(b)

Figure 4.4.1.3.8: 3D radiation pattern of the anntenna (a) at 2.26 GHz and
(b) at 2.85 GHz

3D radiation patterns shows that the antenna gives abroad side radiation with sufficieny wibe beam width.

4.4.1.4. COMPARISON OF PERFORMANCE OF ANTENNA IN DESIGN 3-1 AND 4-1

Designs	Desired Band	Mode	Range of Frequencies (GHz)	Centre frequency (f_0) (GHz)	Percentage Impedance Band width	Gain in the band (dBi)			
						Maximum	Minimum	Average	At f_0
Design 3-1	Band 1	$TE^x_{1\delta1}$	2.18 - 2.32	2.25	6.22%	6.07 (At 2.25 GHz)	4.88 (At 2.20 GHz)	5.47	5.93
	Band 2	TE^x_{100}	3.48 – 3.51	3.495	0.86%	4.88 (At 3.477 GHz)	3.14 (At 3.51 GHz)	4.01	4.52
Design 4-1	Band 1	$TE^x_{11\delta}$	2.20 – 2.50	2.35	12.76%	4.76	2.24	3.5	4.67
	Band 2	$TE^x_{11\delta}$	2.78 – 2.98	2.88	6.94%	5.32	2.84	4.08	3.74

Table 4.4.1.4.1: Comparison of reflection characteristics, mode and gain of the designs 3-1 and 4-1.

| Design	Desired Band	Polarization	Half Power Beam width		Boresight Cx-polar level (dB)		Peak radiation direction (θ_p, Deg.)		Cx-polar level in θ_p direction (dB)		Front to Back Ratio (dB)	
			XZ plane	YZ plane	XZ plane	YZ plane	XZ plane	YZ plane	XZ plane	YZ plane	XZ plane	YZ plane
Design 3-1	Band 1	Linear	95.0°	183°	-31.8	-24.5	0.0°	27.2	-31.8	-29.5	25.7	22.6
	Band 2	Linear	103°	106°	-24.8	-12.5	0.0°	44°	-24.8	-19.2	9.45	18
Design 4-1	Band 1	Linear	91.8°	91.3°	-14.8	-6.25	5.3°	2.0°	-14.4	-6.35	18.0	19.5
	Band 2	Linear but Cx-polar level dominates Co-polar level	70.8°	86.5°	-14.2	-8.21	0.0°	14.2°	-14.2	-9.55	26.5	24.68

Table 4.4.1.4.2: Comparison of radiation characteristics of designs 3-1 and 4-1.

4.5.   BROAD BAND DESIGN
4.5.1. DESIGN 5-1

In this design the antenna (ITDRA) with a slotted ground plane is introduced. It is proved by simulation and experiment that the antenna's resonant frequency can be lowered and the bandwidth can be increased considerably by introducing slots and optimizing their position and dimensions in the ground plane. The proposed antenna is a wide band antenna with a 2:1 VSWR bandwidth of 21.3% centered at 2.43GHz and exhibits good radiation characteristics and moderate gain in the entire operating band. The antenna covers important application bands viz. ISM: Bluetooth/ WLAN 2.4/ Wibree (802.11 b/g/n)/ ZigBee, WiBro and DMB. Lowering of the antenna's fundamental resonant frequency can be easily attained by varying the length of either the slots or strip line. Reduced antenna size (≈28% less) at a fixed frequency can thus be achieved for the proposed design.

4.5.1.1.   Introduction

DRA size can be made smaller, through the use of high permittivity materials, since the guided wavelength is inversely proportional to the permittivity of the dielectric material $\left(\lambda_d = \lambda_0 / \sqrt{\varepsilon_d} \right)$. But high permittivity material results in increased Q factor at a rate of $\varepsilon_r^{3/2}$ and leads to a narrow bandwidth.

There has been a growing interest for slotted ground-plane (SGP) structures, exploiting the ground plane not only for filtering and slow-wave effects, but also to

obtain novel types of compact or broadband devices [4],[5]. In this design, a compact Isosceles Trapezoidal DRA with slotted ground plane is proposed.
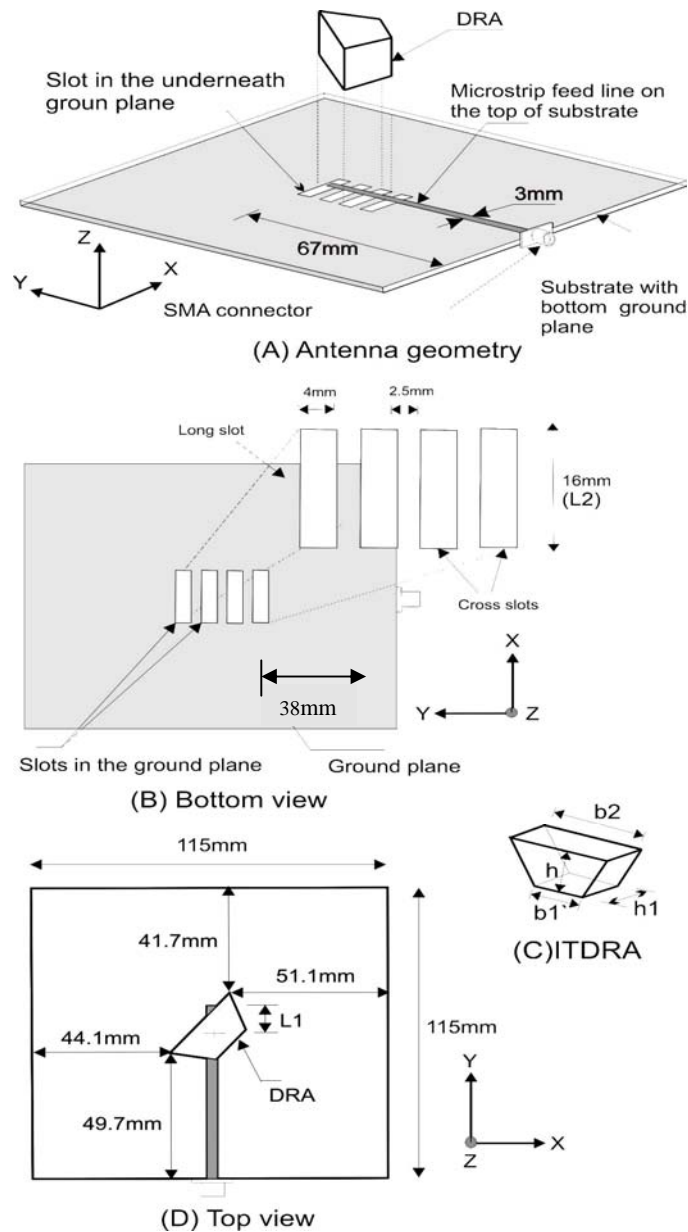
Figure 4.5.1.1.1: configuration of the proposed antenna

It is found that by properly embedding two pairs of narrow slots in the ground plane of an Isosceles Trapezoidal DRA, lowering of the antenna's fundamental resonant

frequency can be obtained along with a broad band response. Reduced antenna size at a fixed frequency can thus be achieved for the proposed design.

4.5.1.2. ANTENNA CONFIGURATION

Antenna structure is shown in Figure 4.5.1.1.1(C). An Isosceles Trapezoidal DR of permittivity $\varepsilon_{r1} = 20.8$, bases $b_1 = 15.4$mm, $b_2 = 30.8$mm, height $h = 13.3$mm and thickness $h_1 = 13$mm is fed by a 50 Ω transmission line of 66.5mm (length) X 3mm (width) fabricated on a microwave substrate of permittivity $\varepsilon_{r2} = 4.4$, loss tangent (tan δ) 0.02 with size 115mm (length) X 115mm (breadth) X 1.6mm (thickness). The condition that $\varepsilon_{r1} \gg \varepsilon_{r2}$ for efficient coupling between the strip-line and the DR is satisfied here. The DR is placed on the microstrip feed line and its position and orientation about the feed line are so adjusted as to get good reflection and transmission characteristics. The optimized position is shown in Figure 4.5.1.1.1(A) and (D) in which the DRA is oriented at angle of 50^0 with respect to the strip line. Two pairs of narrow rectangular slots each with dimension optimized as L2 = 16mm (length) X 4mm (breadth) with a separation of 2.5mm have been etched in the ground plane perpendicularly to the direction of the strip line as shown in Figure 4.5.1.1.1(B). All slots are kept symmetrical with respect to the position of the strip line for getting symmetrical radiation pattern.

4.5.1.3. EFFECT OF SLOTS IN LOWERING RESONANT FREQUENCY

In reference [6] it was concluded that the coupling between a microstrip line and a perpendicular slot in a ground plane is due to a magnetic field. So, we can represent the coupling phenomenon in terms of a mutual inductance in a circuit model. Since the strip

line and the slot are perpendicular to each other, i.e., the magnetic field direction of the microstrip line is the same as that of the slot, we choose the coupling ratio between the strip line and slot as N = 1, and expressing it as an ideal transformer [7]. The turns-ratio of this transformer can be easily varied by varying the length of the slot or feeding strip line and thereby the impedance can be matched. The impedance of the slot line is strongly dispersive, so that turns-ratio 'n' computed by expression (3) in [8] varies with frequency. This is the factor which helps in varying the resonant frequency of the antenna when the strip or slot-length is varied, as this coupling transformer acts as the impedance matching device. This indirectly results in reducing DR antenna size for a given material.

4.5.1.4. RESULTS AND DISCUSSIONS

(i) Return Loss and Gain

Measured and simulated plot of return loss (|S11|), of the DRA are compared in figure 4.5.1.4.1 and shown that they are in good agreement.
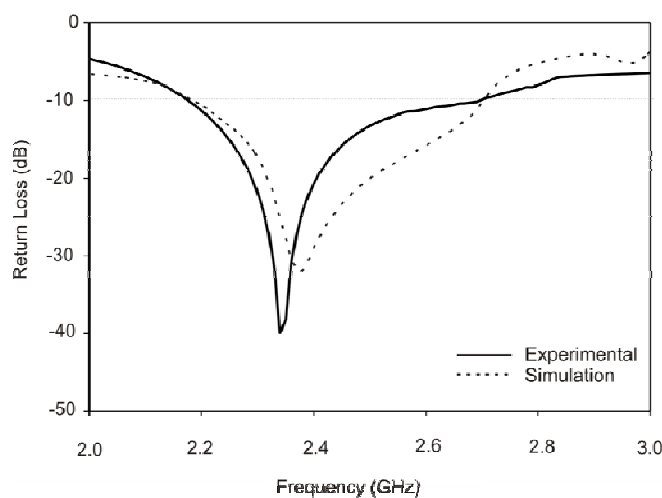
Figure 4.5.1.4.1: Measured and Simulated Return loss of the antenna

As can be seen in figure 4.5.1.4.1 a strong resonance occurred at 2.33 GHz. A range of frequencies from 2.17 GHz to 2.70 GHz is covered with a percentage impedance band width of 21.80 %.
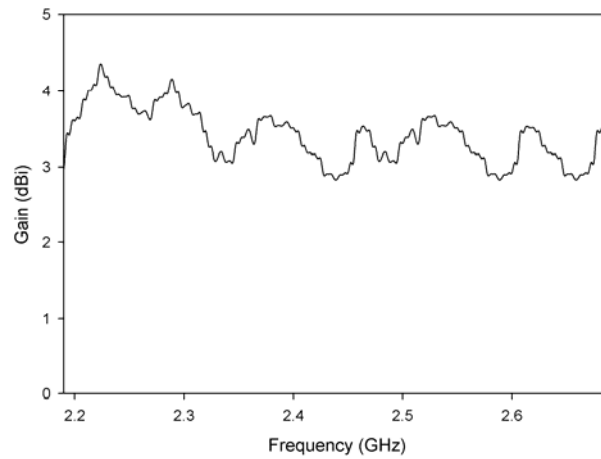
Figure 4.5.1.4.2: Measured Antenna Gain

The measured gain of the antenna is shown in figure 4.5.1.4.2. The antenna has a peak gain of 4.35 dBi at 2.22 GHz and a least of 2.84 dBi at 2.65 GHz with an average value of 3.6 dBi.

Range of Frequencies (GHz)	Centre frequency(f_0) (GHz)	Percentage Impedance Band width	Gain in the band (dBi)			
			Maximum	Minimum	Average	At f_0
2.17 – 2.70	2.43	21.80%	4.35 (at 2.22 GHz)	2.84 (at 2.65 GHz)	3.60	3.2

Table 4.5.1.4.1: Reflection characteristics and Gain of the antenna

Measurements were also done without the slots in ground plane but keeeping the DRA and shown in figure 4.5.1.4.3. Here the return loss of the antenna is compared with slots in ground plane, with regular ground plane and with feed and slots, but without the DR.
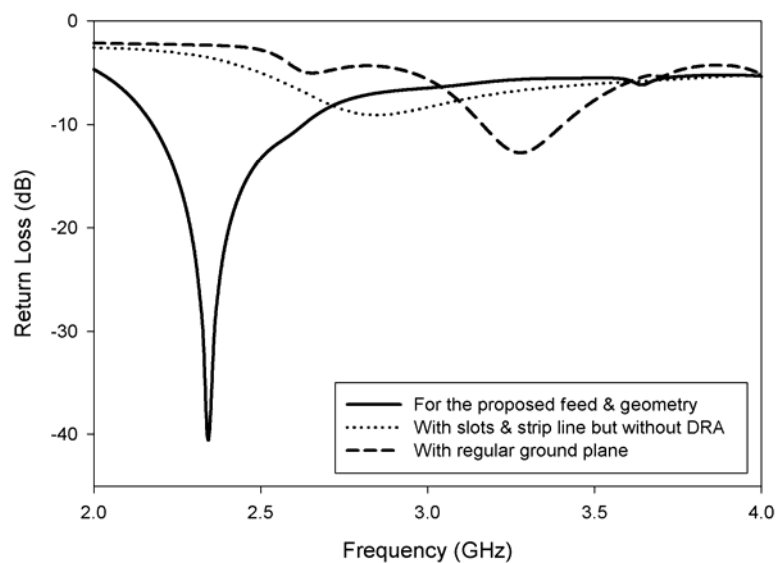
Figure 4.5.1.4.3: Return loss (with and without DRA and with regular gnd plane)

Reflection characteristics for different values of slot-lengths (L2) were measured and found (figure 4.5.1.4.4) that 16mm is optimum. Keeping this constant the strip-line-length extended out ward from the centre of the ITDRA (L1) was also varied and corresponding S11 were measured and plotted as shown in figure 4.5.1.4.5. It can be seen that the resonant frequency decreases as L2 increases. Similarly the resonant frequency decreases when L1 increases as well.
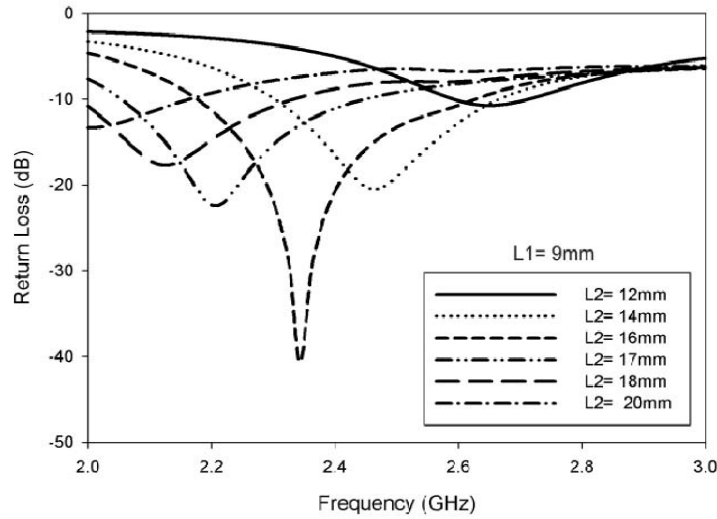
Figure 4.5.1.4.4: Return Loss (with L1 constant and L2 varied)
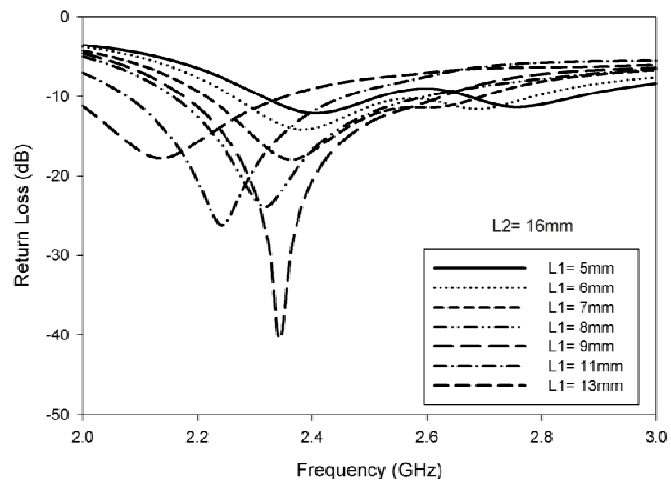
Figure 4.5.1.4.5: Return Loss (with L1 varied while keeping L2 constant)

It is seen that optimum values of strip-offset length (L1) and slot length (L2) for a resonance with useful application band are 9mm and 16mm respectively.

(ii) Radiation Patterns

Radiation patterns are found to be broad with wide beam width having more than

100° and 90° in H and E plane respectively over the entire bandwidth.

At 2.33 GHz

H Plane

E Plane

At 2.45 GHz

H Plane

E Plane
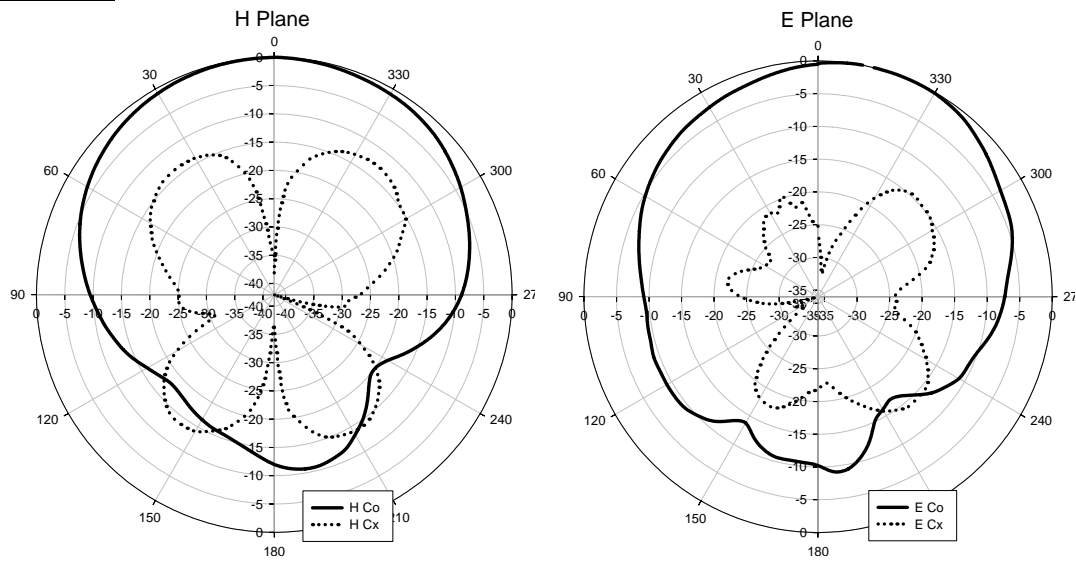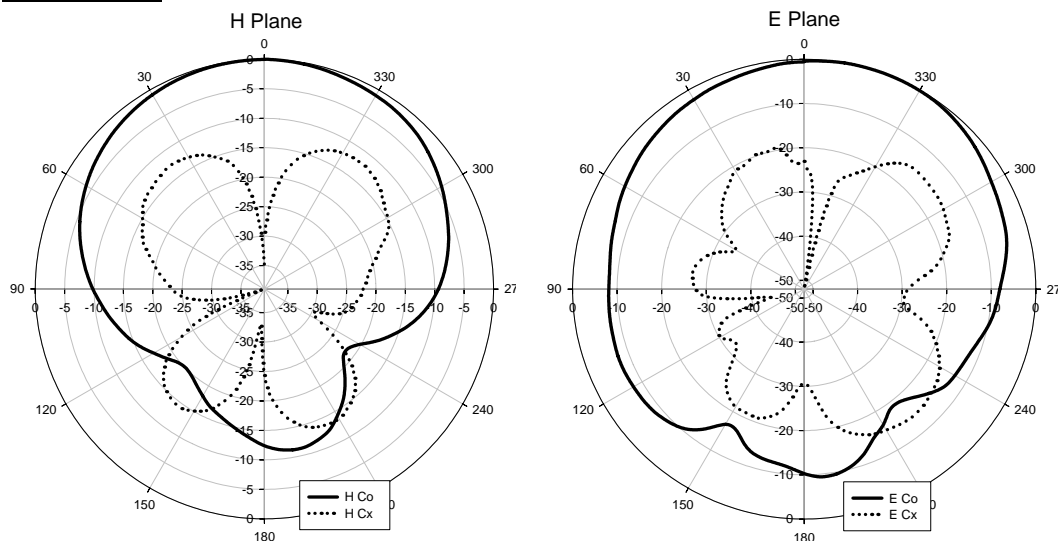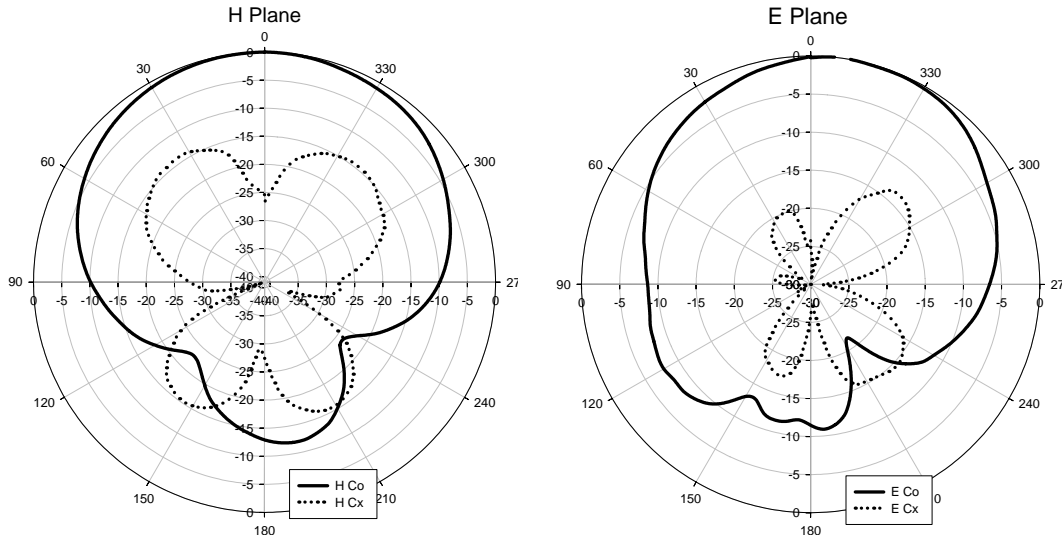
At 2.60 GHz

Figure 4.5.1.4.6: Measured 2-D Radiation patterns of the DRA at 2.33 GHz, 2.45 GHz and 2.60 GHz

The polarization of the antenna is also verified. The low cross-polarization levels confirm that the antenna is linearly polarized over the entire impedance band. The normalized H and E plane radiation patterns of the antenna for three different frequencies viz. 2.33GHz, 2.45GHz and 2.60 GHz in the resonance band are shown in Figure 4.5.1.4.6.

Desired frequency (GHz)	Polarization	Half Power Beam width		Boresight Cx-polar level (dB)		Peak radiation direction (θ_p, Deg.)		Cx-polar level in θ_p direction (dB)		Front to Back Ratio (dB)	
		(H plane)	(E plane)	(H plane)	(E plane)	(H plane)	(E plane)	(H plane)	(E plane)	(H plane)	(E plane)
2.33	Linear	107.8°	93.48°	-34.47	-25.20	0.00°	-15.7°	-34.47	-28.54	12.24	10.11
2.45	Linear	105.6°	97.28°	-30.38	-23.17	0.00°	-18.3°	-30.38	-25.74	12.68	10.32
2.60	Linear	104.6°	97.34°	-25.39	-24.11	0.00°	-14.0°	-25.39	-24.84	16.0	11.53

Table 4.5.1.4.2: Radiation characteristics and Gain of the antenna.

It can be seen from table 4.5.1.4.2 that, front to back ratio of the antenna is slightly less. Although, it should be noted that the SGP structure presented here exhibits relatively low radiation losses through the slots in the gaps, as observed in the radiation patterns.
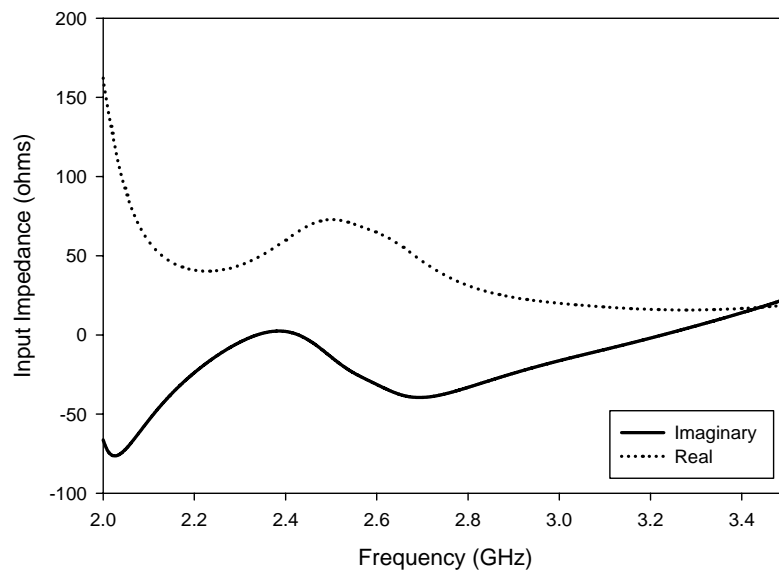
Figure 4.5.1.4.7: Input Impedance of the antenna

Input impedance vs frequency plot in figure 4.5.1.4.7 shows that the resonance occurred at matching impedance.

Plot of input impedance against frequency for various L2 values is shown in figure 4.5.1.4.8 which confirms the fact that the impedance matching between the feed and the antenna is occurred at frequencies corresponding to the resonant modes.
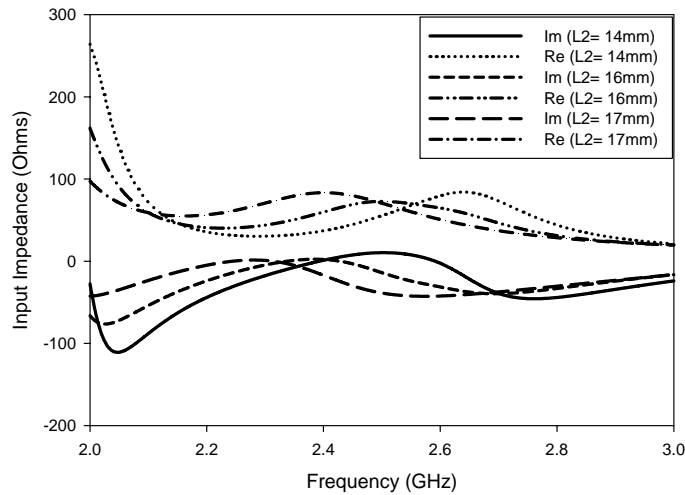
Figure 4.5.1.4.8: Input Impedance vs Freq. against varying L2.

Different orientations of the antenna with respect to the slot in ground plane and microstrip line feed is also tried out for studies and verified that the proposed one gives the best result. Studies were done by trying out different number of slots also, and found that the proposed one gives a wide and useful application band.

(iii)   Simulated Results
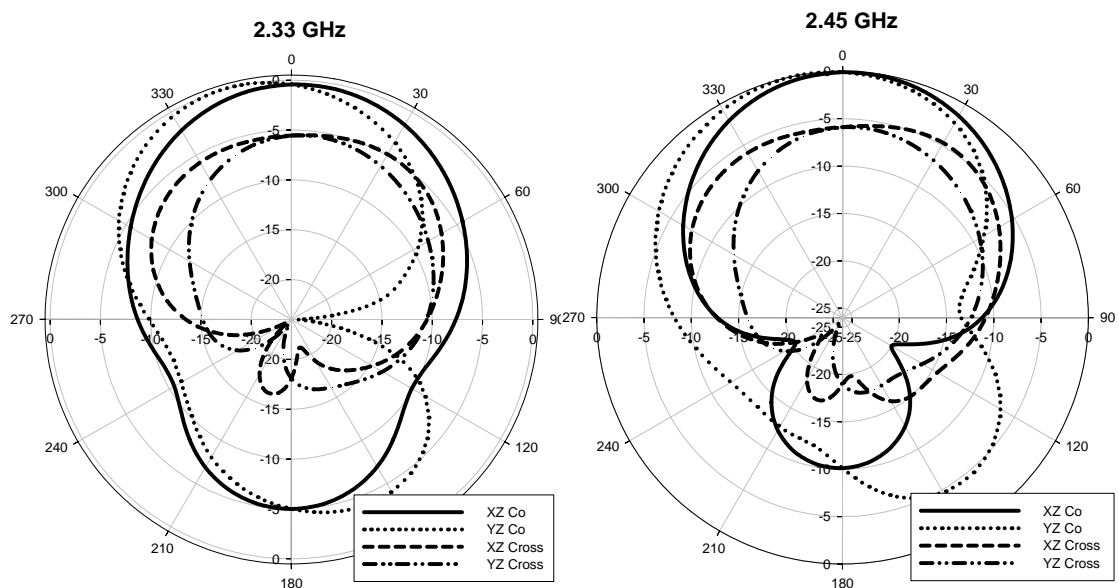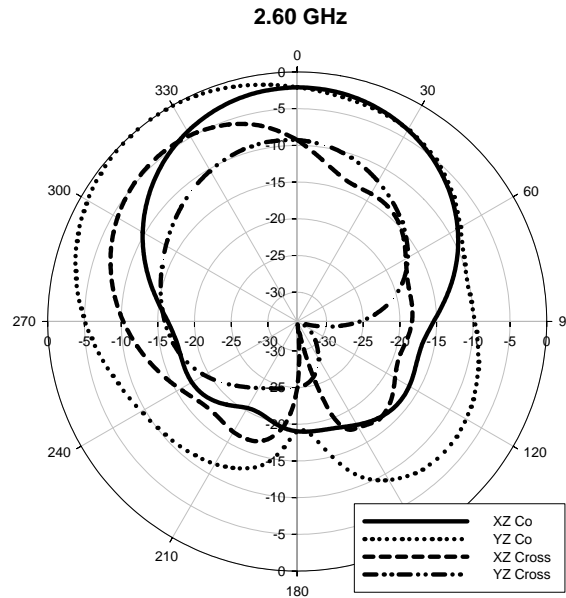
2.60 GHz

Figure 4.5.1.4.9: Simulated Radiation pattern for XZ and YZ plane at 2.33 GHz, 2.45 GHz and 2.60 GH

The simulated 2D radition patterns shown in fgure 4.5.1.4.9 agrees with the measured results.
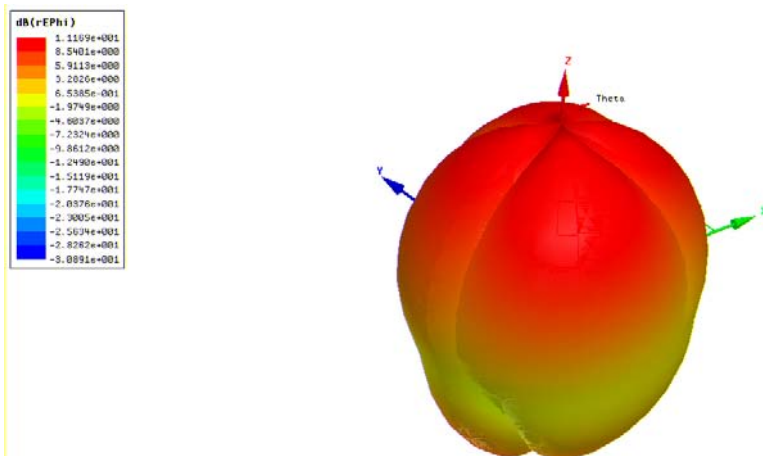
Figure 4.5.1.4.10: Simulated 3D radiation pattern of the antenna at 2.33 GHz

167
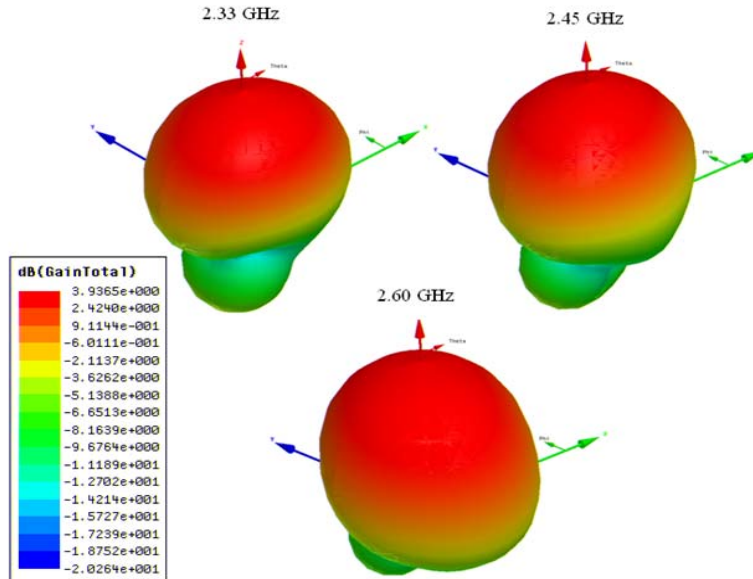
Figure 4.5.1.4.11: Simulated 3D Gain patterns of the antenna

The simulated 3D gain pattern shows that the antenna gives a broad side pattern with moderate gain.

Field Patterns
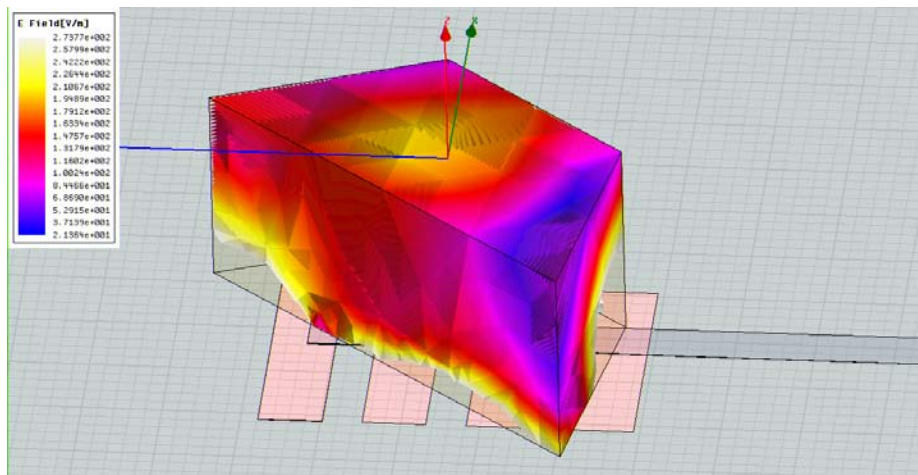
Figure 4.5.1.4.12 (a): E field distribution within DRA at 2.33 GHz

168
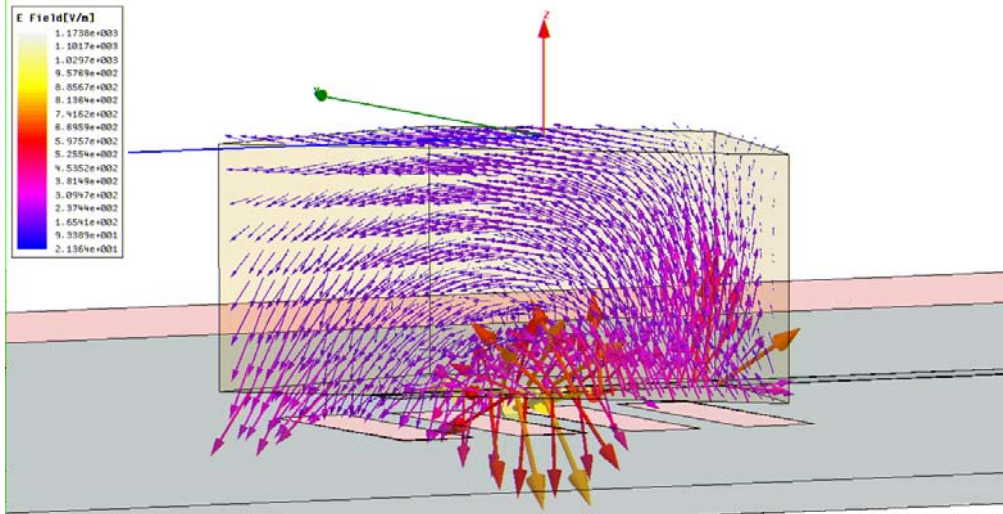
Figure 4.5.1.4.12 (b): E field Vector distribution within DRA at 2.33 GHz

The Electric field distribution within the ITDR is shown in figure 4.5.1.4.12 (a). The corresponding field vector distribution is shown in figure 4.5.1.4.12 (b) as well. The polarization of the antenna is seen at a direction $45°$ to the microstrip line. From the number of half wave variations along each of the 3 dimensions of the DR, we can assume the mode of resonance as $TE_{11\delta}$.

4.5.1.5. Wide band design result with DR1

Using the same feed with same slot dimensions and the same orientation, the performance of the antenna DR1 is investigated. The isosceles trapezoidal DR of permittivity $\varepsilon_{r1} = 24$, bases b1 = 16.5 mm, b2 = 33 mm, height h = 14.3 mm and thickness h1 = 13.8 mm is used here.
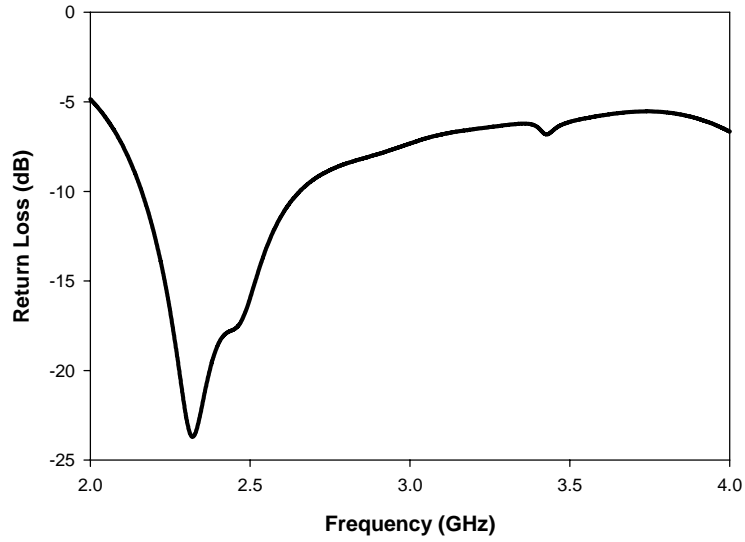
Figure 4.5.1.5.1: Return loss with DR1
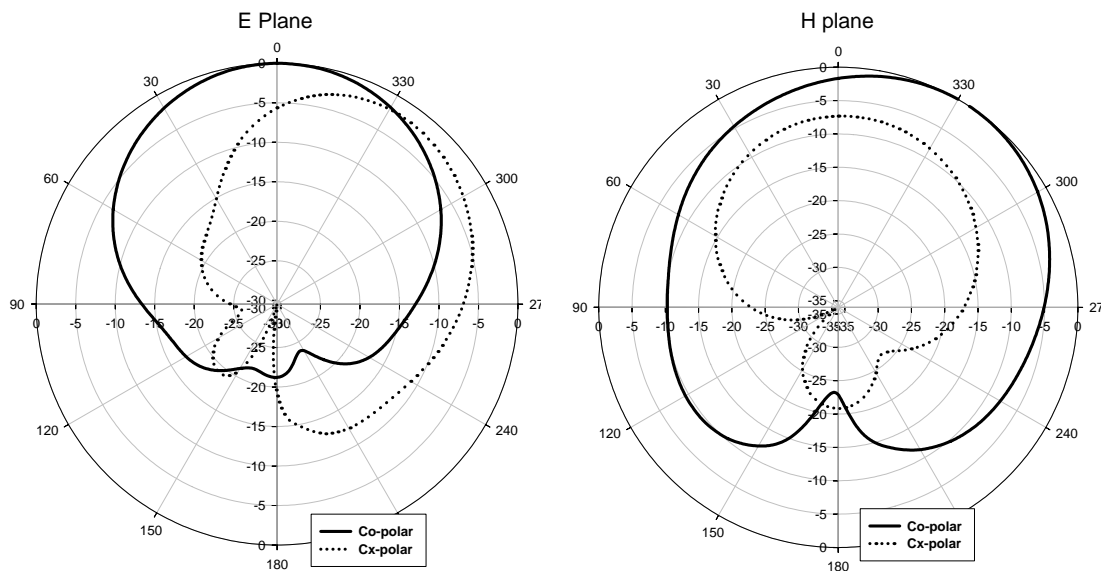
Figure 4.5.1.5.2: 2D Radiation Pattern of the antenna with DR1 at 2.31 GHz

170
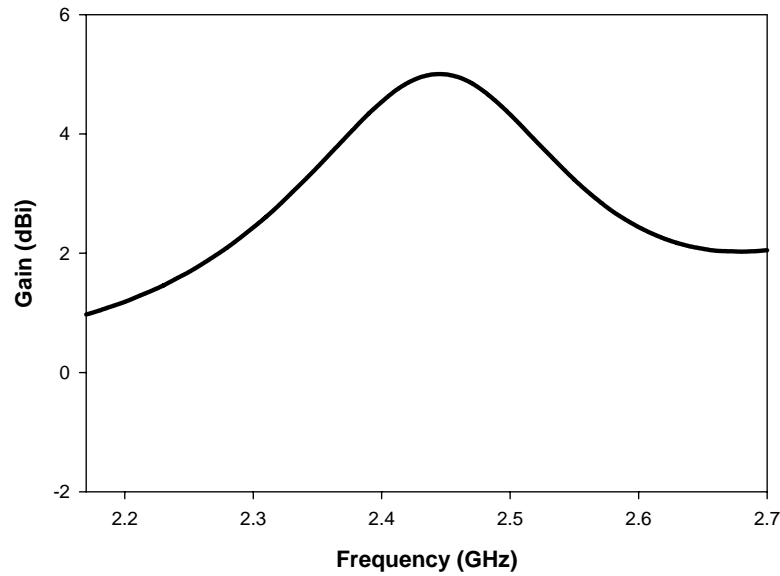
Figure 4.5.1.5.3 : Gain of the antenna.

4.5.1.6.**Comparison of Reflection characteristics and Gain of antenna with DR1 and DR2**

	Range of Frequencies (GHz)	Centre frequency (f_0) (GHz)	Percentage Impedance Band width	Gain in the band (dBi)			
				Maximum	Minimum	Average	At f_0
DR2	**2.17 – 2.70**	**2.43**	**21.80%**	**4.35 (at 2.22 GHz)**	**2.84 (at 2.65 GHz)**	**3.60**	**3.2**
DR1	**2.15 – 2.65**	**2.40**	**20.83%**	**5.02 (at 2.44 GHz)**	**1.00 (at 2.15 GHz)**	**3.00**	**2.69**

Table 4.5.1.5.1: Reflection characteristics and Gain of the antenna with DR1 and DR2.

171

As shown in table 4.5.1.5.1, Range of frequency, centre frequency and band width are almost same but the average gain is slightly greater for the antenna with DR2.

4.5.2. DESIGN 5-2 (TE$^x_{111}$ MODE)

It is a modified design of design 5-1 discussed above. In this a microstrip-line-fed ITDRA having a parasitic conducting strip on its larger base area and a slanted strip on its inclined surface along with one more rectangular slot in the ground plane is studied [9]. The parasitic strip, slanted strip and the new rectangular slot provides additional freedom for effectively tuning the impedance and reflection characteristics of the DRA.

Here the DR is placed in another orientation similar to that of the Design 1-1 discussed earlier in section 4.1.1 and the shape of the slot is optimized as in the form of a fish bone as shown in figure 4.5.2.1. The horizontal slot additionally introduced here has an effect on changing the reflection and radiation characteristics of the antenna. Increase in bandwidth is the result of merging multiple resonances originated in close neighborhood by the slot provided in the ground plane. Maximum bandwidth for the antenna is obtained in the useful range with cross slot length of 16mm.

DR position along the y- direction was initially optimized with respect to the feed. The slot structure in the ground plane was placed under the microstrip line and the DRA symmetrically along x direction to get a symmetrical radiation pattern in XZ plane. The long and cross slot dimensions are optimized by varying one parameter at a time while others kept constant. Initially study was carried out by using DR1 and then slightly more

compact DRA (DR2) was tried out and found that similar results are obtained with useful application band.

4.5.2.1 ANTENNA CONFIGURATION

Antenna structure is shown in figure 4.5.2.1. An isosceles trapezoidal DR (DR2) of permittivity $\varepsilon_{r1} = 20.8$, bases $b_1 = 15.4mm$, $b_2 = 30.8mm$, height $h = 13.3mm$ and thickness $h_1 = 13mm$ is fed by a 50 Ω transmission line of 66.5mm (length) X 3mm (width) fabricated on a microwave substrate of permittivity $\varepsilon_{r2} = 4.2$ with size 115mm (length) X 115mm (breadth) X 1.6mm (thickness). The condition that $\varepsilon_{r1} \gg \varepsilon_{r2}$ for efficient coupling between the strip-line and the DR is satisfied here. Length of the feed is optimized for getting desired response as the maximum energy is coupled capacitively [10] if the DR is located at the point of maximum electric field on the feed.

The DR position on the microstrip line was optimized as 1.5mm away from the microstrip terminal end in y direction as shown in figure 4.5.2.2. A metallic strip with a height and width optimized as 9.5mm and 3mm respectively is adhered to the slanting surface at the feed side of the TDRA and is connected electrically to the feed line at a length $L = 16.7mm$ from its open end as shown in Figure 1(a). Without the slanted strip the intensity of radiation pattern is seen to be dominated towards the feed side.

13mm

3mm

Slot in the underneath groun plane

vertical feed strip

3mm

3mm

67mm

Z

X

Y

b2

h

b1   h1

(b) ITDRA

Substrate with bottom ground plane

SMA connector

Microstrip feed above the substrate

(a) Feed of the Antenna

L=30.8mm

4mm   2.5mm   4mm

Long slot

3mm

16mm (L2)

Cross slots

X

Y   Z

Ground plane

Slot in ground plane

(c) Bottom view
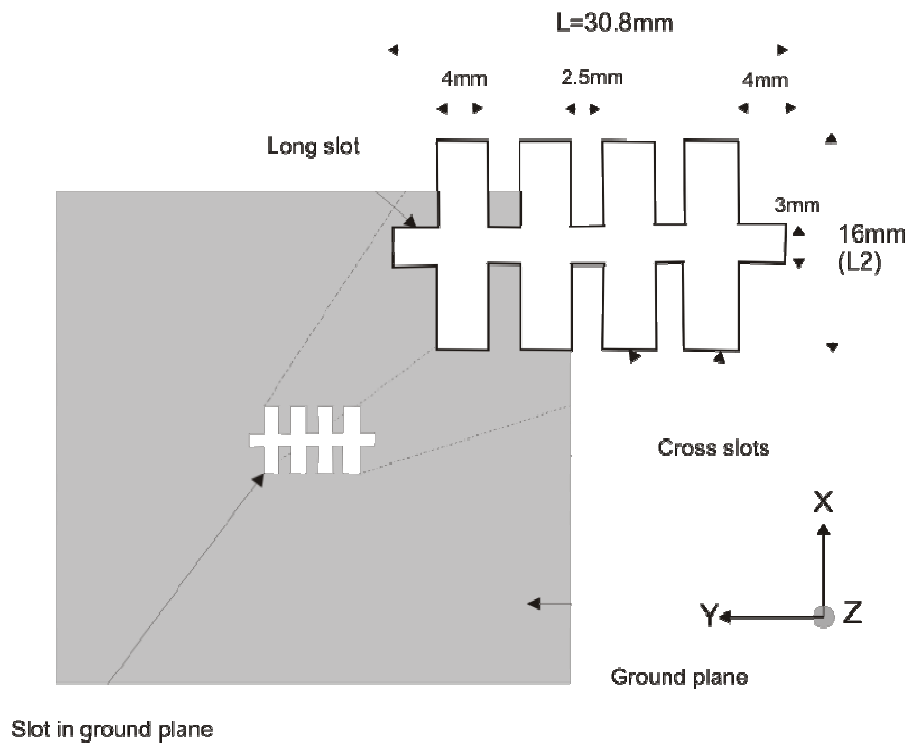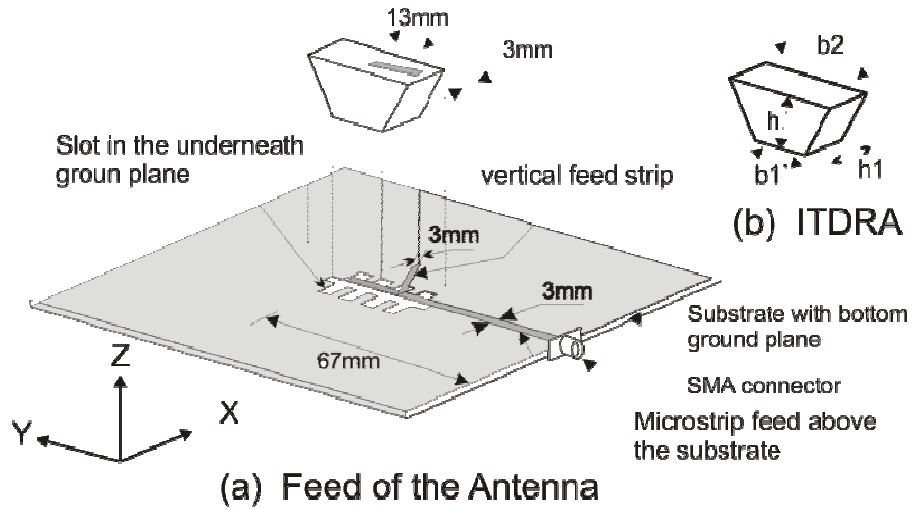
Figure 4.5.2.1: Feed and Geometry of the Antenna

174
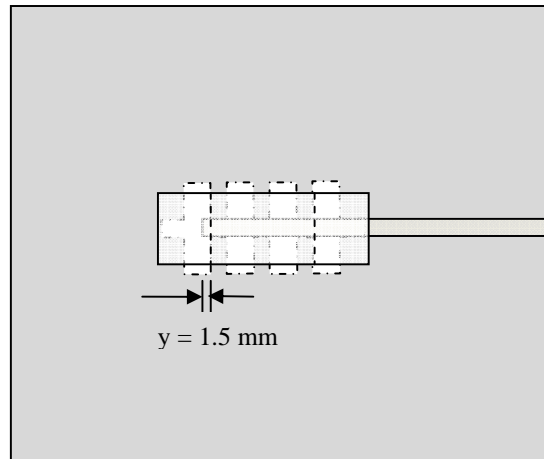
Figure 4.5.2.2: Top view of the ITDRA- 2 antenna configuration with y-distance -- optimised as 1.5 mm (top parasitic strip not shown for simplicity)

A parasitic strip on the top surface of the antenna with an offset of 5.9mm from the center of the surface with a length and width optimized as 13mm and 3mm respectively is adhered for obtaining maximum band width. The angle of inclination of this strip with reference to the micro-strip feed line is also optimized as 10^0. Loading effect of the top parasitic strip helps to reduce the Q of the antenna and thereby increasing its impedance band width to a certain extend.

The ground plane is modified as shown in figure 4.5.2.1 by making a slot in the form of a fish bone with a long and cross rectangular slots. The long slot is kept under and along the micro strip-line with a dimension of L1 = 30.8mm (length) X 3mm (breadth) and with an offset of 41.7mm from the feed position. The cross slots have the

dimensions of L2 = 16mm (length) X 4mm (breadth) and are separated among them by a distance of 2.5mm.

4.5.2.2. RESULTS AND DISCUSSIONS

Measured and simulated plot of return loss ($|S11|$), of the DRA are compared in Figure 4.5.2.2.1 and shown that they are in good agreement. Effect of ground plane modification on the return loss characteristics of the antenna is shown in figure 4.5.2.2.2. It is seen that the modification of ground plane changes the radiation characteristics of the antenna. It is apparent from the figure that long slot has the tendency to shift the resonances towards upper side of frequency whereas the cross slots shift them towards the lower side. When both long and cross slots are introduced together, two resonances occurred, one is at slightly lower side and the second is on far upper side of the original resonance that created when no modification on ground plane is made. So in the proposed antenna these two resonances are developed in the close neighborhood so as to merge together to form a wide band response of 540 MHz centered at 2.51 GHz giving 21.5% impedance bandwidth.

(i) Reflection Characteristics

Since there is a long slot in the ground plane underneath to the open end of microstrip feed, the feed itself acts as a monopole antenna and radiates at 4.8 GHz. The length of microstrip that extends to the slot in the ground plane decides the frequency of radiation of the monopole while the shape of the slot determines shape of the radiation pattern and hence the directions at which the maximum intensity of radiation occur.

176
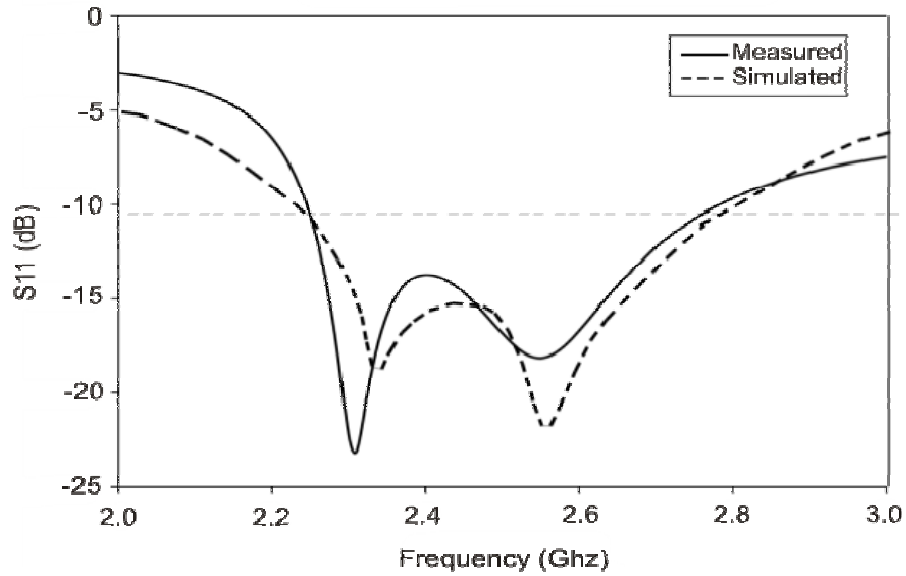
Figure 4.5.2.2.1: Measured and Simulated Return loss
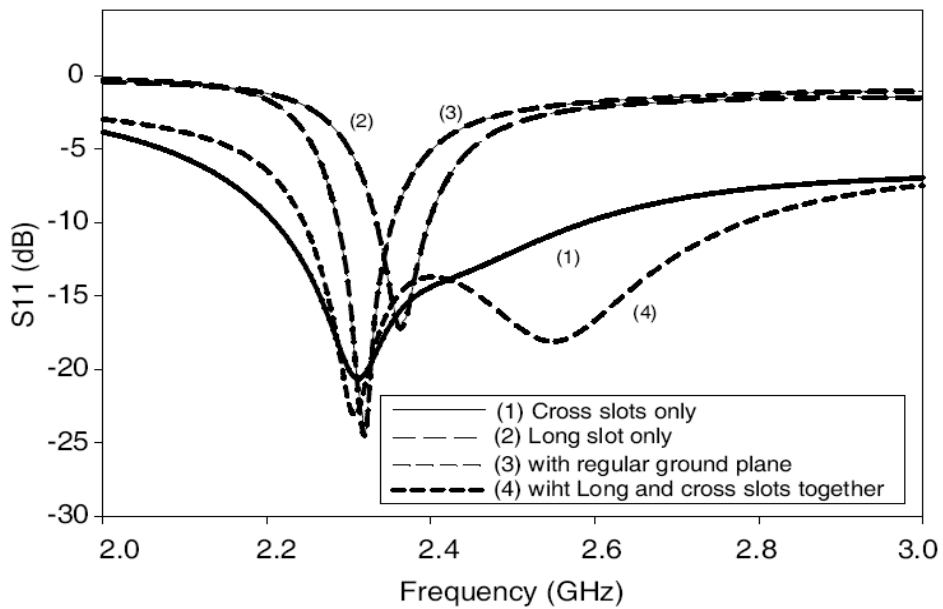
Figure 4.5.2.2.2: S11 with 1) Long slot only, 2) Cross slot only 3) with regular gnd

plane   and 4) Long and Cross slot together

177
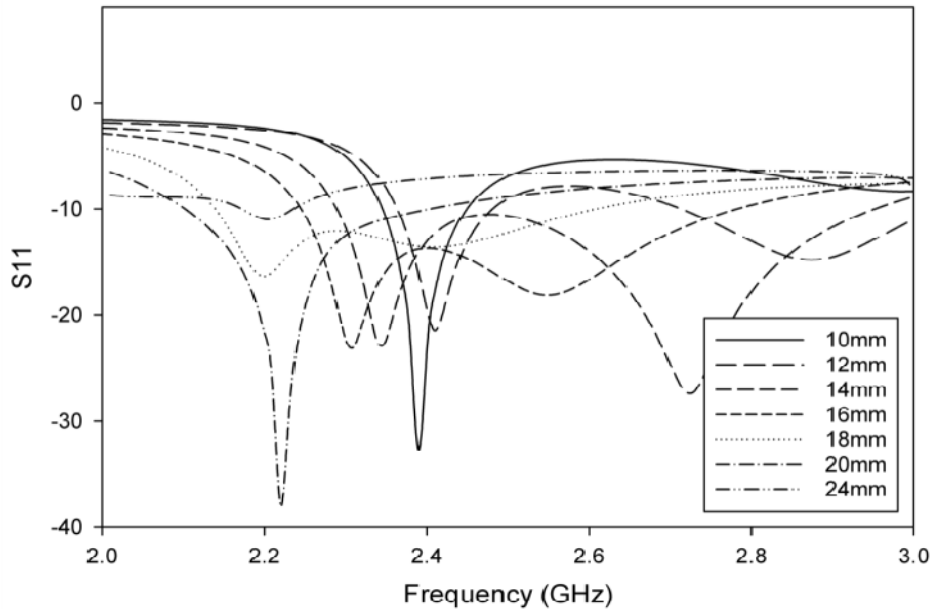
Figure 4.5.2.2.3: Return loss for different cross slot lengths L2 when B2 = 4mm and
L = 30.8 mm

The cross slot has an effect of reducing the resonance frequency of the antenna. This is because the coupling between a microstrip line and a perpendicular slot in a ground plane is due to a magnetic field [11] and thus can be expressed as an ideal transformer [12].

Figure 4.5.2.2.3 shows the effect of cross slot length L2 of the ground plane modification on the return loss characteristic of the antenna. Length of the long slot is having less effect compared to the cross slots. The cross slot length (L2) was gradually increased for verifying the corresponding S11. It was seen that the centre frequency is reduced for increasing length of cross slots. As the slot dimension L2 increases the first and second resonances shift towards the lower side up to L2 = 16mm and further the

second resonance disappears while the first resonance still shifts towards lower side. It is

noted that a strong matching resonance occurs for L2 = 20mm with a weak resonance on

either side of the dimension.
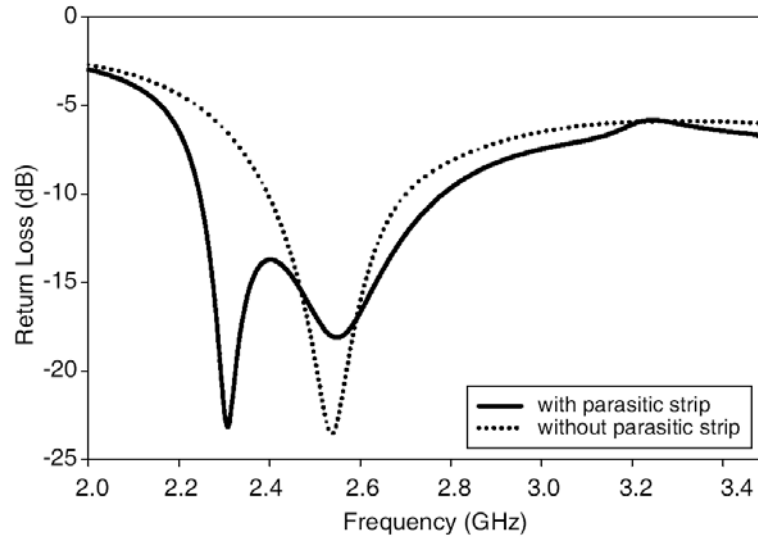
Figure 4.5.2.2.4: Effect of parasitic strip on the return loss characteristics of the DRA.
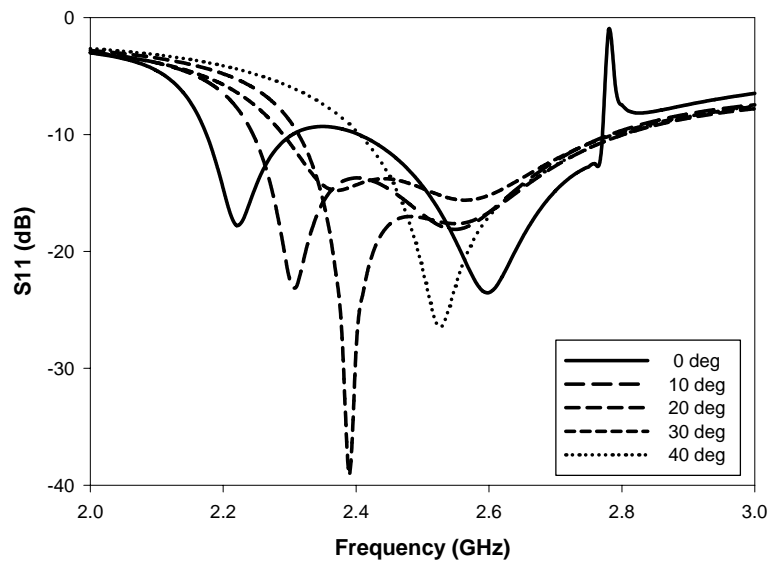
Figure 4.5.2.2.5: Effect of angle of inclination of parasitic strip on the Return loss
characteristics.

179

Effect of parasitic strip on the return loss of DRA is shown in figure 4.5.2.2.4. It reveals that the loading effect of the strip results in increase in band width by introducing another resonance in close neighborhood. Effect of tilt of parasitic strip with respect to the microstrip line on the return loss characteristics is also shown in Figure 4.5.2.2.5. It indicates that a tilt of 10° gives an optimum response for a strip-length and width of 13mm and 3mm respectively.

Different orientations of the antenna with respect to the slot in ground plane and microstrip line feed is also tried out for studies and verified that the proposed one gives the best result. Plot of input impedance against frequency which is shown in Figure 4.5.2.2.6 confirm that the impedance matching between the feed and the antenna is occurred at frequencies corresponding to the resonant modes.
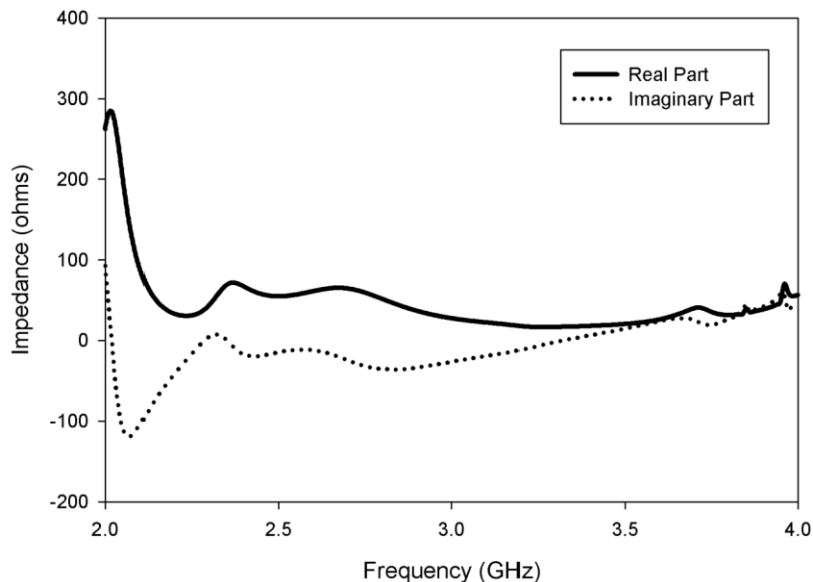
Figure 4.5.2.2.6: Input Impedance of the antenna

(ii) Radiation Patterns

At 2.3 GHz

XZ Plane

YZ Plane

(a)

At 2.45 GHz

XZ Plane

YZ Plane

(b)

181

At 2.60 GHz

(c)
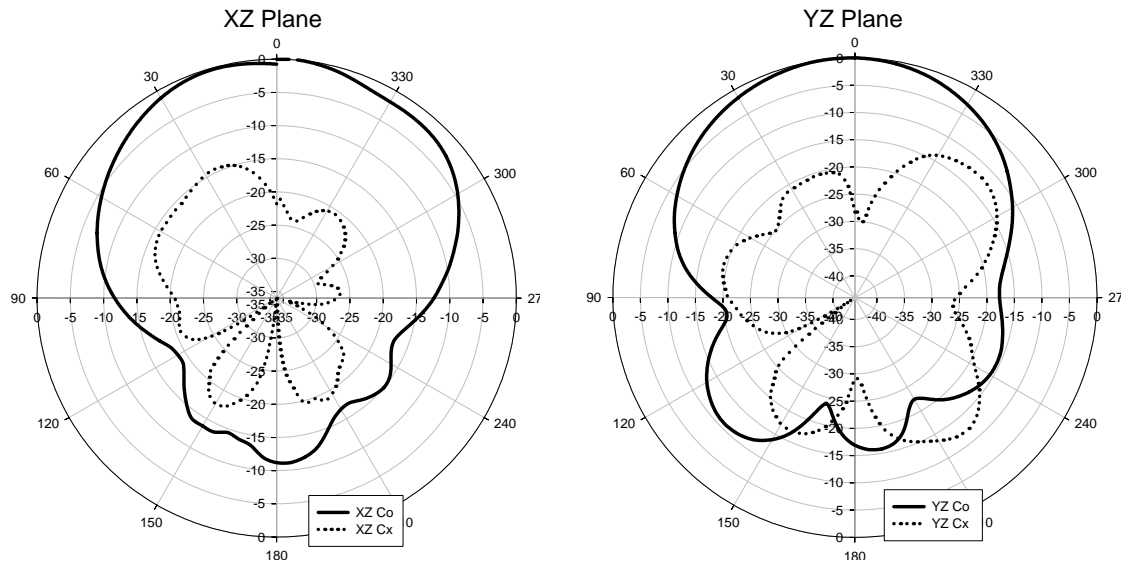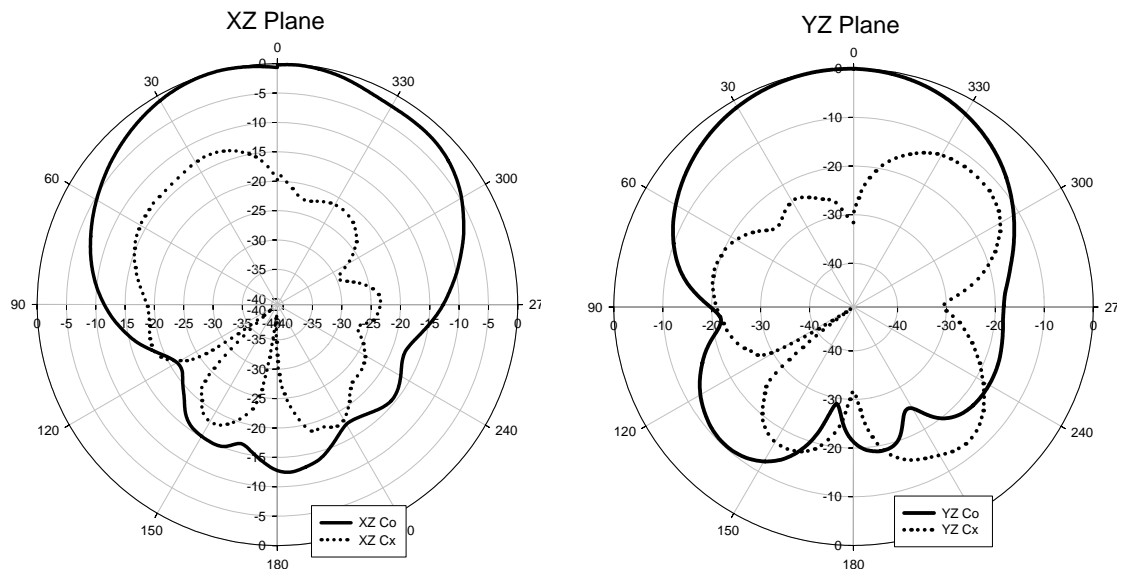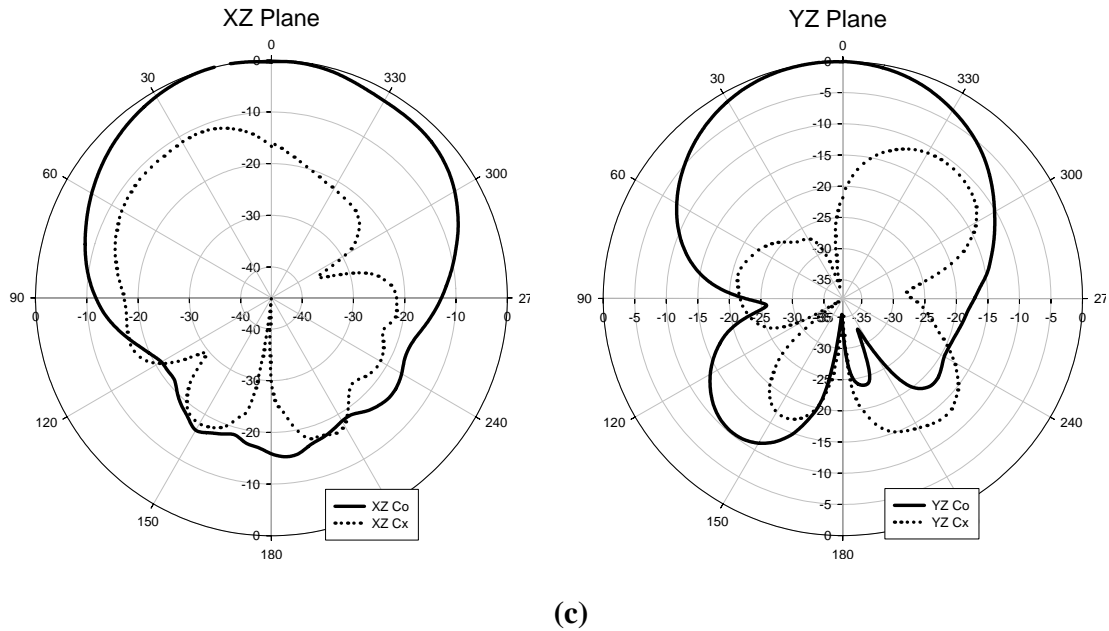
Figure 4.5.2.2.7: 2 D Radiation pattern of the antenna in XZ and YZ plane at different frequncies in the band

Desired frequency (GHz)	Polarization	Half Power Beam width		Boresight Cx-polar level (dB)		Peak radiation direction (θ_p, Deg.)		Cx-polar level in θ_p direction (dB)		Front to Back Ratio (dB)	
		(XZ plane)	(YZ plane)	(XZ plane)	(YZ plane)	(XZ plane)	(YZ plane)	(XZ plane)	(YZ plane)	(XZ plane)	(YZ plane)
2.30	**Linear**	**95.93°**	**71.78°**	**-21.68**	**-28.14**	**-5.70°**	**3.71°**	**-22.42**	**-23.34**	**11.31**	**17.0**
2.45	**Linear**	**96.64°**	**70.46°**	**-19.72**	**-31.46**	**8.16°**	**6.58°**	**-15.71**	**-28.46**	**12.89**	**21.42**
2.60	**Linear**	**96.25°**	**70.00°**	**-16.49**	**-21.78**	**7.68°**	**5.72°**	**-13.80**	**-26.12**	**16.0**	**32.29**

Table 4.5.2.2.1: Radiation characteristics of the antenna at different frequencies in the resonant band.

A broad side pattern with wide beam width is achieved. The polarization of the antenna is also verified. The low cross- polarization levels confirm that the antenna is

182

linearly polarized over the entire impedance band. The normalized *XZ* and *Y Z* plane radiation patterns of the antenna for three different frequencies viz. 2.3 GHz, 2.45 GHz and 2.6 GHz in the resonance band are shown in figure 4.5.2.2.7. Since the antenna structure is symmetrical with respect to the *XZ* and *YZ* plane separately, the radiation patterns in *Y Z* and *XZ* plane are symmetrical.
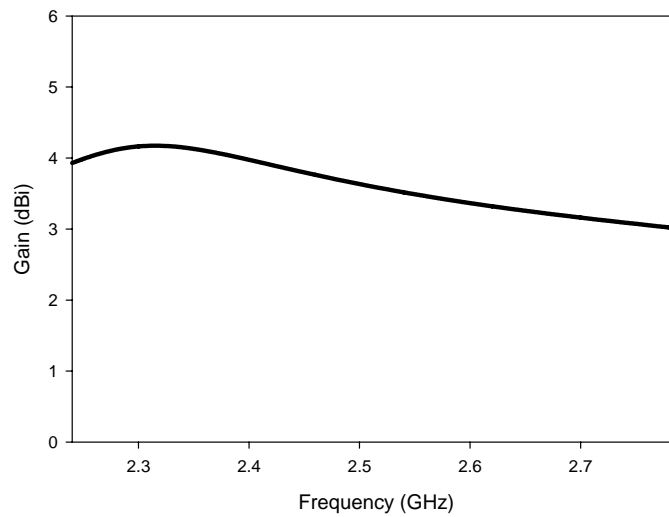
Figure 4.5.2.2.8: Gain of the antenna

The measured gain of the antenna is shown in Figure 4.5.2.2.8. The antenna has a peak gain of 4.17 dBi at 2.19 GHz and a least of 2.2 dBi at 2 GHz with an average value of 3.19 dBi.

Range of Frequencies (GHz)	Centre frequency(f_0) (GHz)	Percentage Impedance Band width	Gain in the band (dBi)			
			Maximum	Minimum	Average	At f_0
2.24 – 2.78	**2.517**	**21.45%**	**4.18 (at 2.31 GHz)**	**3.0 (at 2.79 GHz)**	**3.59**	**3.59**

Table 4.5.2.2.2: Reflection characteristics and Gain of the antenna

183

The reflection characteristics and Gain parameters of the antenna are tabulated in table 4.5.2.2.2. Resonant frequencies are $f_{01} = 2.31$ GHz and $f_{02} = 2.54$ GHz.
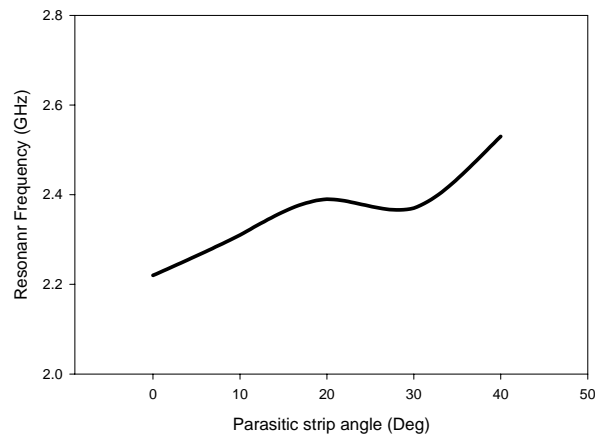
Figure 4.5.2.2.9: Resonant Frequency vs Parasitic Strip Angle

As shown in figure 4.5.2.2.9 it is seen that resonant frequency of the antenna is increased with increase in tilt of the parasitic strip. % Band width vs Parsitic Strip angle is also shown in figure 4.5.2.2.10 which shows that a maximum band width is obtained for a strip angle $= 10°$. For higher values of angle, resonant frequency increases while band width decreases.
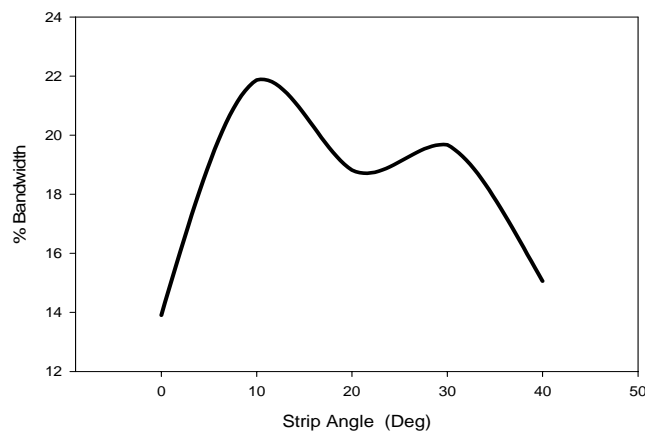
Figure 4.5.2.2.10: % BW vs Parasitic Strip Angle

184

(iii) **Simulated Results**

At 2.3 GHz

2.45 GHz

At 2.6 GHz
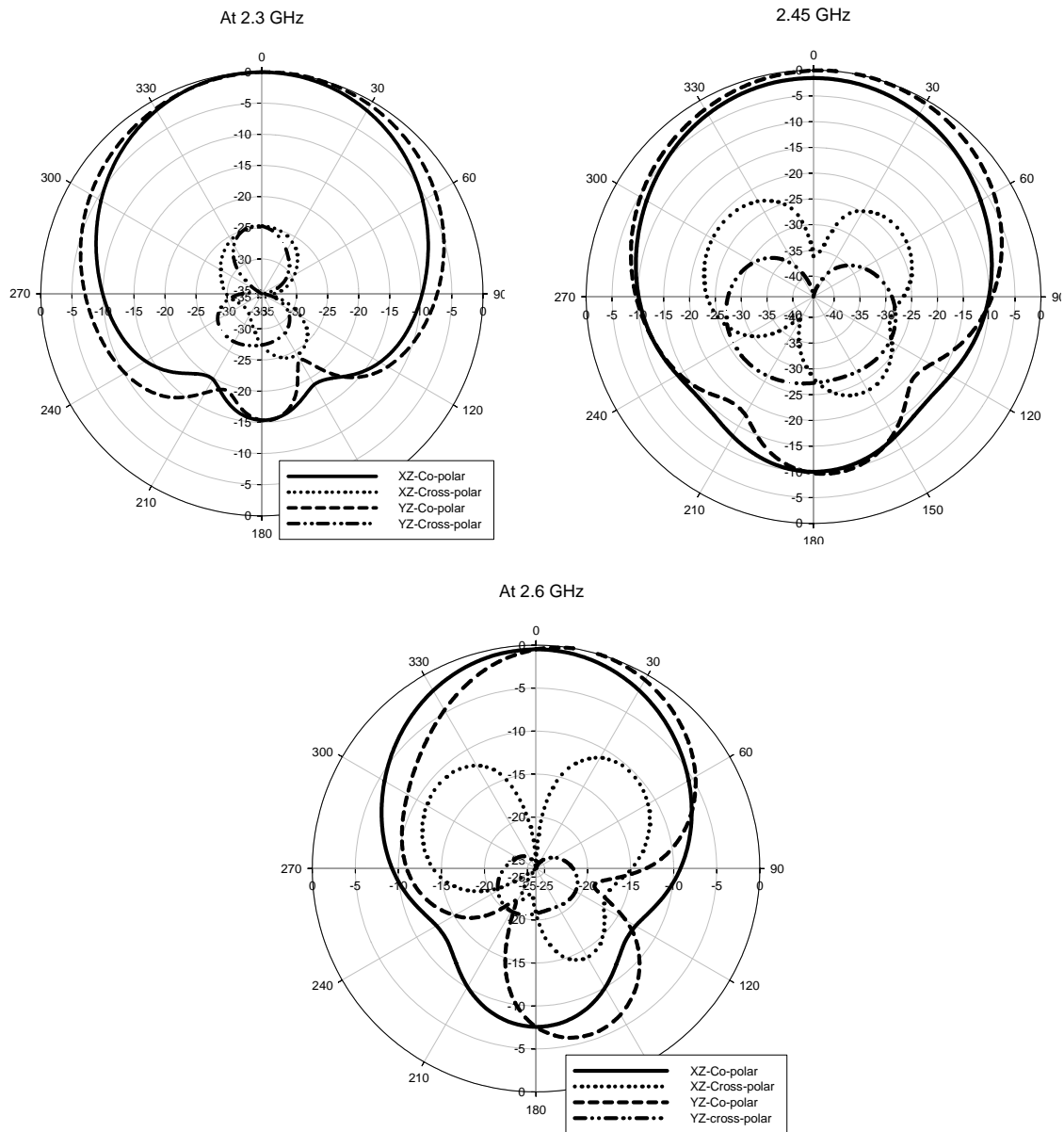
Figure 4.5.2.2.11: Radiation patterns at 2.3 GHz, 2.45 GHz and 2.60 GHz

The simulated 2D radition patterns shown in fgure 4.5.2.2.11 agrees with the measured results.
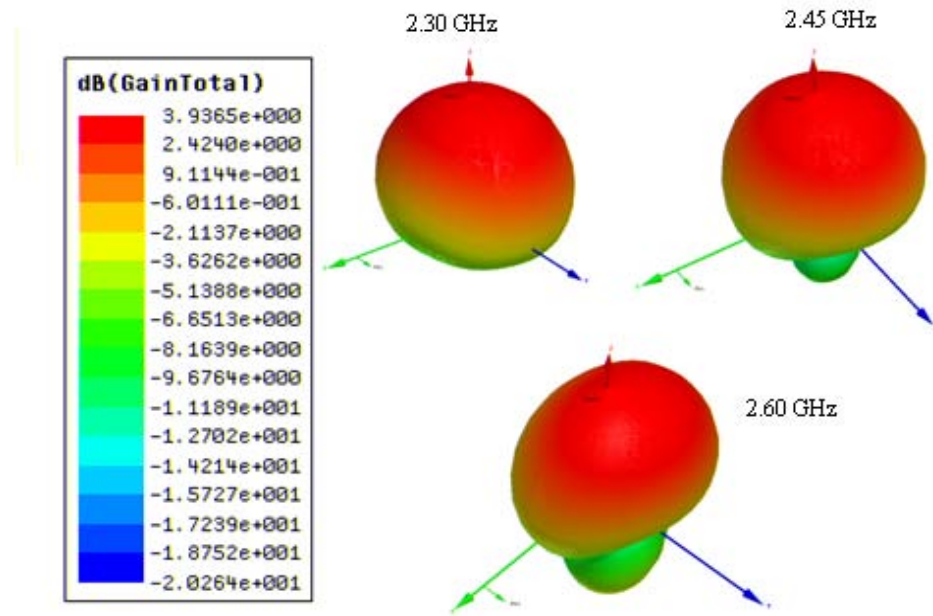
Figure 4.5.2.2.12: Simulated 3D gain patterns of the antenna.

The simulated 3D gain pattern shows that the antenna gives a broad side pattern with moderate gain.

(iv) Field Patterns
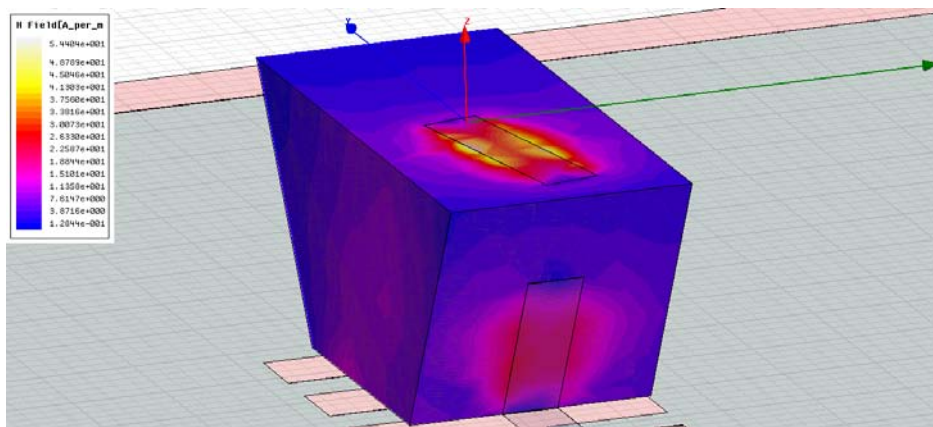
Figure 4.5.2.2.13: E field distribution within DRA at 2.54 GHz ($\mathbf{TE}^{\mathbf{x}}_{\mathbf{111}}$)

The input field is magnetically coupled to the DRA from the microstrip line at the bottom surface as well as from the tip of slanted strip. Without the parasitic strip, the simulated electric field distribution within the DRA indicates the fundamental TE^x_{111} modes (Figure 4.5.2.2.14 (a)). It is identified as TE^x from the E vector distributions as the field is transverse to the X- axis. But the presence of parasitic strip disturbs the field distribution as the boundary condition doesn't allow the tangential components of the electric field near to it. This causes the *E* field loop in the *YZ* plane to be broken at the top surface of DRA near to the parasitic strip. So the normal component of the field is concentrated at both sides of the parasitic strip as shown in Figure 4.5.2.2.14 (b). This makes the excited mode not a pure TE^x mode but instead a pseudo- TE^x mode. The plot of *S*11 for the antenna with and without parasitic strip is shown in Figure 4.5.2.2.4.
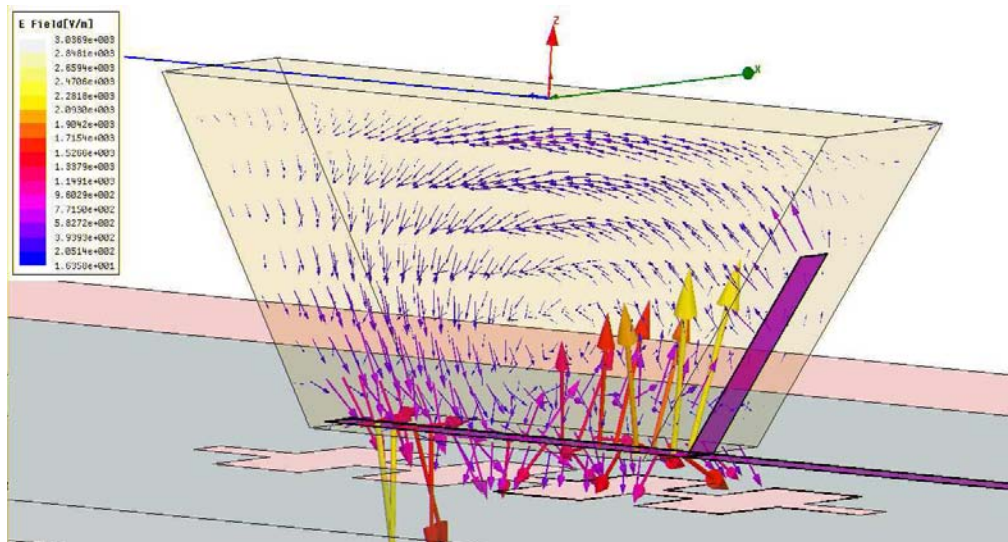
(a) Without parasitic strip at 2.54 GHz
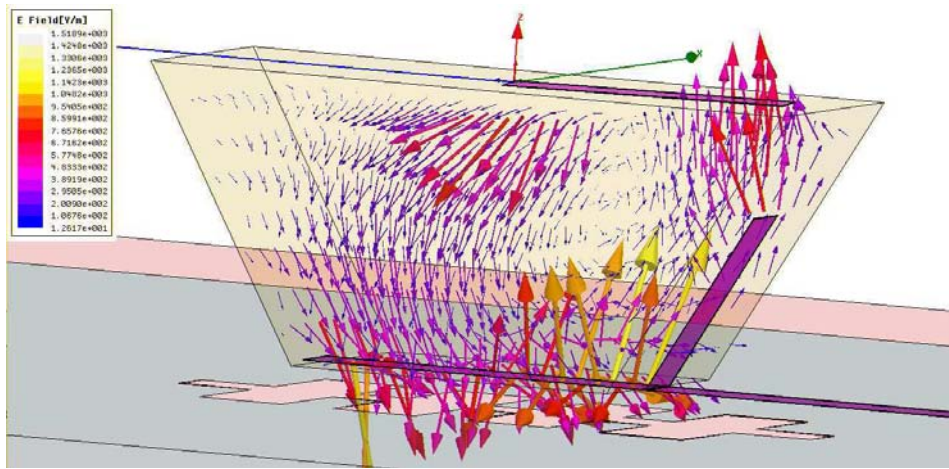
(b) with parasitic strip at 2.54 GHz

Figure 4.5.2.2.14: (a) and (b) Vector E distribution within the DRA

4.5.2.3. Wideband Design Results obtained with DR1
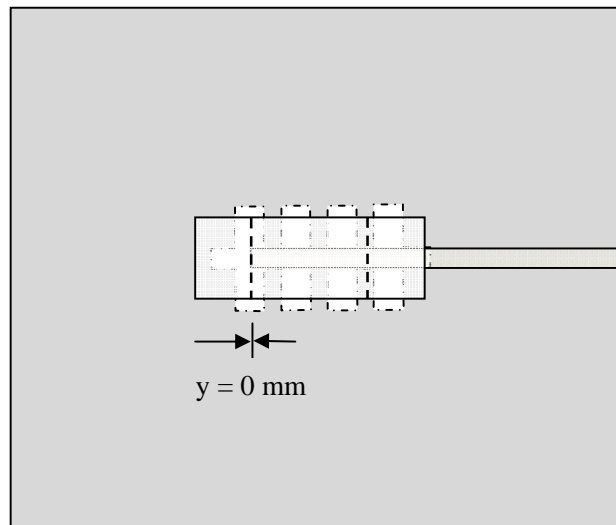
Figure 4.5.2.3.1: Top view of the ITDRA- 1 antenna with the similar configuration but y-distance optimised as 0 mm (top parasitic strip not shown for simplicity)

The return loss of the antenna is shown in figure 4.5.2.3.2. Resonant frequencies are 2.24 GHz and 2.47 Ghz. The range of frequencies in the band are 2.17 to 2.69 GHz.
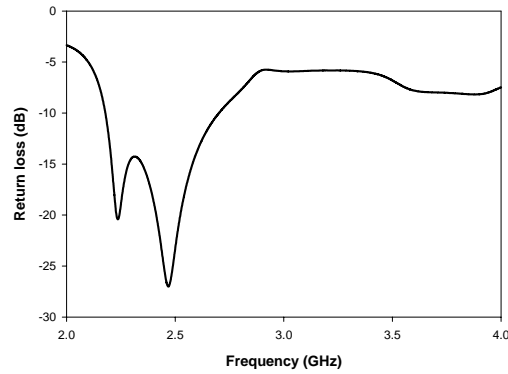
Figure 4.5.2.3.2: Return loss of the ITDRA 2 with similar configuration but with a

y- displacement 0 mm as shown in figure.
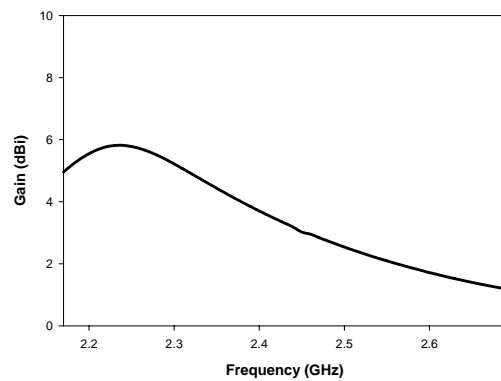
Figure 4.5.2.3.3: Gain of the configuration with DRA 2

Antenna has got a moderate gain with a maximum of 5.83 dBi at 2.23 GHz and a

minimum of 1.19 dBi at 2.69 GHz with an average of 3.51 dBi as shown in table

4.5.2.3.1.

As it is seen in the figure 4.5.2.3.4 (a) and (b), radiation patterns are broad

side and having a wide beam width. Cross polar levels show that the antenna is linearly

polarized.

189

Range of Frequencies (GHz)	Centre frequency(f_0) (GHz)	Percentage Impedance Band width	Gain in the band (dBi)			
			Maximum	Minimum	Average	At f_0
2.17 – 2.69	**2.43**	**21.5%**	**5.83 (at 2.23 GHz)**	**1.19 (at 2.69 GHz)**	**3.51**	**3.36**

Table 4.5.2.3.1: Reflection characteristics and Gain of the antenna
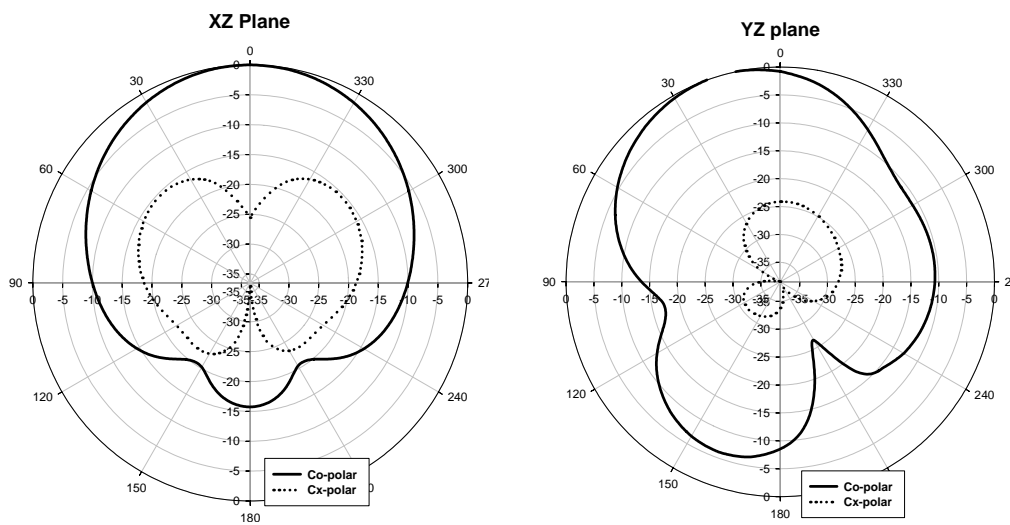
Figure 4.5.2.3.4: (a) 2D radiation patterns of configuration with DR2 at 2.23 GHz
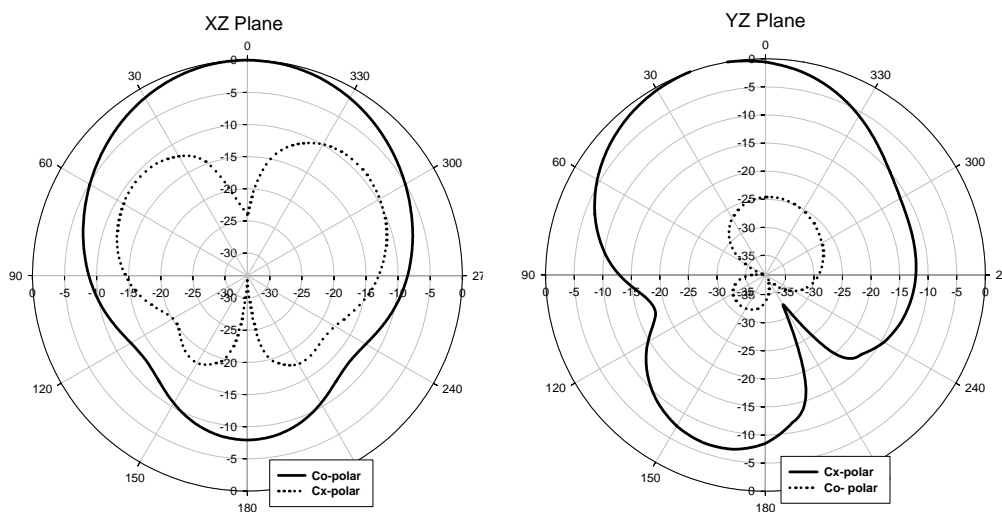
Figure 4.5.2.3.4: (b) 2D radiation patterns of configuration with DR2 at 2.46 GHz

	Range of Frequencies (GHz)	Centre frequency(f_0) (GHz)	Percentage Impedance Band width	Gain in the band (dBi)			
				Maximum	Minimum	Average	At f_0
DR1	2.17 – 2.69	2.43	21.5%	5.83 (at 2.23 GHz)	1.19 (at 2.69 GHz)	3.51	3.36
DR2	2.24 – 2.78	2.517	21.45%	4.18 (at 2.31 GHz)	3.0 (at 2.79 GHz)	3.59	3.59

Table 4.5.2.3.2: Comparison of performance of Design 5-2 with DR1 and DR2

4.5.2.4: RADIATION FROM THE ANTENNA FEED
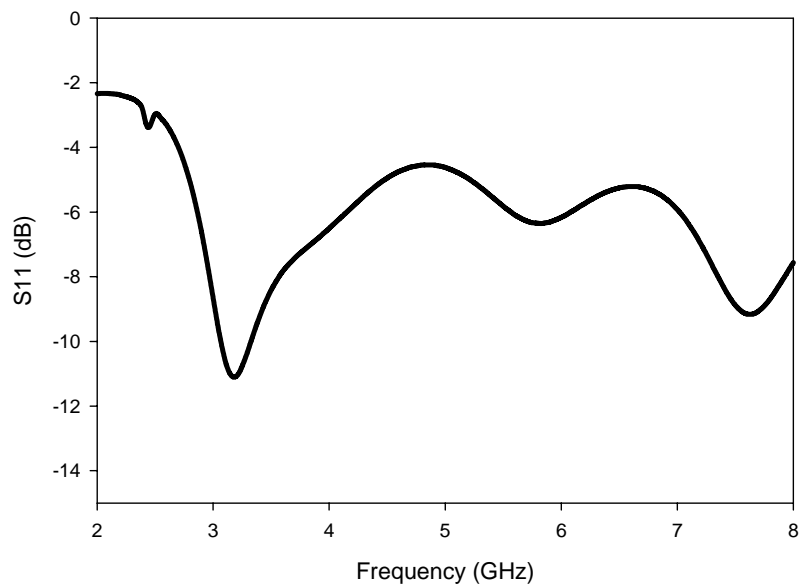
Figure 4.5.2.4.1: (a) Simulated Return loss of the feed alone without slanting strip
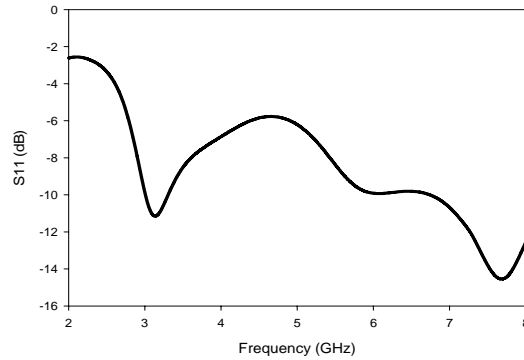
Figure 4.5.2.4.1: (b) Simulated Return loss of the feed alone along with slanting strip

As can be observed from the above plots, a resonance at 7.7 GHz along with a weak resonance at 3.2 GHz exists for the feed of this design. The higher frequency is equal to the resonant frequency of a $\lambda/4$ monopole of length 9.5 mm. Simulated radiation pattern at 7.7 GHz is given in Figure 4.5.2.4.2.
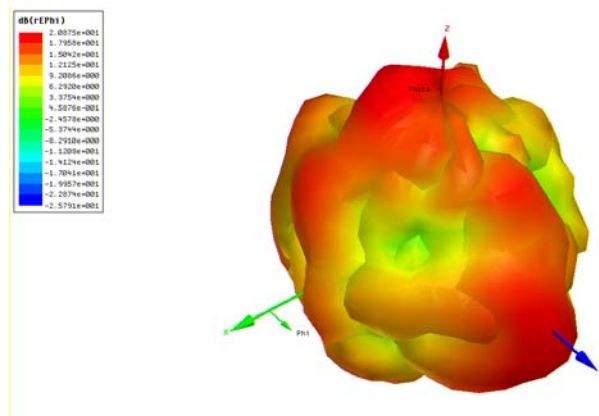
Figure 4.5.2.4.2: Simulated 3D radiation pattern of the feed at 7.7 GHz

Though the pattern shape is not well defined, it can disturb the radiation pattern of the DRA operating near the 7.7 GHz band. Since the operating band of

the DRA doesn't lie beyond 4 GHz, this monopole resonance is not at all a threat to the antenna performance.

The lower weak resonance that may be the result of the slots in the ground plane, is with very low gain and may not be able to make any disturbance in the nearby bands of any other communication systems.

4.5.3. COMPARISON OF RADIATION CHARACTERISTICS OF BROAD BAND DESIGNS

Comparison of the radiation parameters of the broad band designs in table 4.5.3.1 shows that design 5-1 is superior in the case of beam width.

Desired frequency (GHz)		Polariza-tion	Half Power Beam width		Boresight Cx-polar level (dB)		Peak radiation direction (θ_p, Deg.)		Cx-polar level in θ_p direction (dB)		Front to Back Ratio (dB)	
			H plane	E plane	H plane	E plane	H plane	E plane	H plane	E plane	H plane	E plane
Design 5-1	2.33	Linear	107°	93.4°	-34.4	-25.2	0.00°	-15°	-34.4	-28.5	12.24	10.11
	2.45	Linear	105°	97.2°	-30.3	-23.1	0.00°	-18°	-30.3	-25.7	12.68	10.32
	2.60	Linear	104°	97.3°	-25.3	-24.1	0.00°	-14°	-25.3	-24.8	16.0	11.53
Design 5-2	2.30	Linear	95.9°	71.7°	-21.6	-28.1	-5.70°	3.71°	-22.4	-23.3	11.31	17.0
	2.45	Linear	96.6°	70.4°	-19.7	-31.4	8.16°	6.58°	-15.7	-28.4	12.89	21.42
	2.60	Linear	96.2°	70.0°	-16.4	-21.7	7.68°	5.72°	-13.8	-26.1	16.0	32.29

Table 4.5.3.1: Comparison of radiation characteristics of broad band designs.

Cross polarization levels in boresight as well as in peak radiation direction are also comparatively greater in the case of design 5-1. Front to back ratio for Design 5-2 is

greater than that of Design 5-1. Also for design 5-1, the E and H planes are tilted by 45° with respect to the X and Y direction.

i) Radiation Efficiencies of the ITDRAs for different designs

Radiation efficiency of the DRAs was measured using the Wheeler cap method (Chapter 3). A cylindrical metallic cap of diameter = 15 cm and height = 7.5 mm was used to cover the DRA including the feed. Measured efficiencies are given in Table 4.

DRA 1	Design 1-1	Design 1-2	Design 1-3	Design 2-1	Design 3-1	Design 4-1	Design 5-1	Design 5-2
Radiation Efficiency (%)	93.31	94.24	93.07	92.85	91.65	92.08	91.62	90.71

Table 4.5.3.2: Measured radiation efficiencies of the ITDRAs for different Designs

4.6. CONCLUSION

The experimental and simulation studies on a novel dielectric resonator antenna with isosceles trapezoidal geometry are discussed. The characteristics of the antenna when excited with microstrip feed is described for different orientations by showing the reflection coefficient, 2D radiation pattern, half power beam width (HPBW), cross polar level, gain, input impedance, 3D gain pattern etc. High radiation efficiencies in excess of 90 % were obtained, due to the inherent low loss of the DR. The antenna performance is optimized for the feed location, offset length of the feed strip, dimensions of the slots in ground plane, dimensions of slanted and parasitic conducting strips etc.

REFERENCES

[1] High Frequency Structure Simulator (HFSS), Ansoft Corporation, Pittsburgh, PA

[2] Eldek A.A,; Elsherbeni A.Z., Smith C.E., 'Wide-band modified printed bow-tie antenna with single and dual polarization for C - and X-band applications," *IEEE Trans.on Antennas and Propagation.*, Vol. 53, No. 9, pp. 3067-3072, 2005.

[3] Targonski, S. D. and D. M. Pozar, "Dual-band and dual polarized printed antenna element," *Elect. Lett.*, Vol. 34, No. 23, pp. 2193-2194, 1998

[4] J. B. Knorr, "Slot-line transitions," *IEEE Trans. Microwave Theory Tech.*, Vol. 2, No. 5, pp. 548–554, May 1974.

[5] F.-R. Yang, K.-P. Ma, Y. Qian, and T. Itoh, "A uniplanar compact photonic bandgap (UC-PBG) structure and its applications for microwave circuits," *IEEE Trans. Microwave Theory Tech.*, vol. 47, pp. 1509–1514, Aug. 1999.

[6] F. Xiao, Y. Nakada, K. Murano, and Y. Kami, "Crosstalk Analysis Model for Traces Crossing Split Ground Plane and Its Reduction by Stitching Capacitor," *IEICE Trans. Electronics*, J89-C, 11, pp.885-893, 2006.

[7] Nagakubo Hitoshi, Murano Kimitoshi, Xiao Fengchao, Kami Yoshio, "Circuit Model for Two Parallel Microstrip Lines on Slotted Ground Plane," Electromagnetic Compatibility, 2007 (EMC 2007). International Symposium on, pp.130-133, 23-26 Oct. 2007.

[8] Caloz. C., Okabe. H., Iwai. T., Itoh. T., "A simple and accurate model for microstrip structures with slotted ground plane," Microwave and Wireless Components Letters, IEEE , vol.14, no.3, pp. 127- 129, March 2004.

[9] C. Gopakumar, K. T. Mathew, "A wideband microstrip-line-fed isosceles trapezoidal dielectric resonator antenna with modified ground plane," Progress In Electromagnetics Research C, Vol. 16, pp. 127-136, 2010.

[10] Leung K. W., K. Y. Chow, K. M. Luk and E. K. N. Yung, "Low profile circular disk DR antenna of very high permittivity excited by a microstripline," *Electronics Letters*, Vol. 33, No. 12, 1004-1005, 1997.

[11] Xiao, F., Y. Nakada, K. Murano and Y. Kami, "Crosstalk analysis model for traces crossing split ground plane and its reduction by stitching capacitor," *IEICE Trans. Electronics*, Vol. 11, pp. 885-893, 2006.

[12] Hitoshi N., M. Kimitoshi, F. Xiao and K. Yoshio, "Circuit model for two parallel microstrip lines on slotted ground plane," *International Symposium on Electromagnetic Compatibility, EMC 2007*, pp. 130-133, Oct. 23-26, 2007.

CHAPTER 5   **FINITE DFFERENCE TIME DOMAIN METHOD**

                          -A NUMERICAL ANALYSIS TECHNIQUE

An introduction to the fundamentals of Perfect Matched Layer (PML) based Finite Difference Time Domain (FDTD) computation technique is presented in this chapter. The PML based FDTD was found to be the best suited method to describe and analyse the radiation and resonance in the Antenna problem. The MATLAB based FDTD codes developed for this specific research topic is based on the PML based FDTD concept explained in this chapter. Using this, the wideband DRA in Design 5-2 measured in the previous chapter is modeled and analyzed. Finally the measured and computed results are compared.

5.1 FINITE DIFFERENCE TIME DOMAIN METHOD

As we have already discussed in section 1.4.2.3, the finite difference time domain (FDTD) method [1]–[6] is an electromagnetic computational technique in which Maxwell's partial differential equations are discretized using the Finite Difference approximation computed in the Time Domain. For this reason it is named the Finite Difference Time Domain method or FDTD. It is normally easy to understand and easy to implement in software. As it is a time-domain method, a wide frequency range is covered by the solution with a single simulation run.

It includes in the class of grid-based differential time-domain numerical modeling methods. In this method, using central-difference approximations, the time-dependent Maxwell's equations (in partial differential form) are discretized to the space and time

197

partial derivatives. Then the resulting finite-difference equations are solved in either hardware or software system in a leapfrog approach. That is the E field vector components in the given volume of space are solved at a given instant in time; then the magnetic field vector components in the same spatial volume are solved at the next instant in time. The process is repeated over and over again until the desired transient or steady-state electromagnetic field behavior is completely evolved.

The basic FDTD space grid and time-stepping algorithm trace back to a 1966 paper by Kane Yee in IEEE Transactions on Antennas and Propagation [7]. The descriptor "Finite-difference time-domain" and its corresponding "FDTD" acronym were originated by Allen Taflove in a 1980 paper [8].

Since two decades before, FDTD method have appeared as primary means to computationally model many scientific and engineering problems which are dealt with electromagnetic wave interactions with material structures. Current FDTD modeling applications range from near-DC (ultralow-frequency geophysics) through microwaves (antennas, radar signature technology, wireless communications devices, digital interconnects etc.) to visible light (photonic crystals, biophotonics, etc.) [9].

5.1.1 DETAILS OF THE FDTD METHOD

Maxwell's differential equations show that the change in the Electric field (E) in time (the time derivative) is dependent on change in the Magnetic field (H) across space (the curl of H). This results in the basic FDTD time-stepping relation. That is, at any point in space, the updated value of the E-field in time is dependent on the stored value of the E-field and the numerical curl of the local distribution of the H-field in space [7].

Similarly, the H-field is also in time-stepped mode. At any point in space, the updated value of the H-field in time is dependent on the stored value of the H-field and the numerical curl of the local distribution of the E-field in space. Iterating the E-field and H-field updates results in a marching-in-time process..
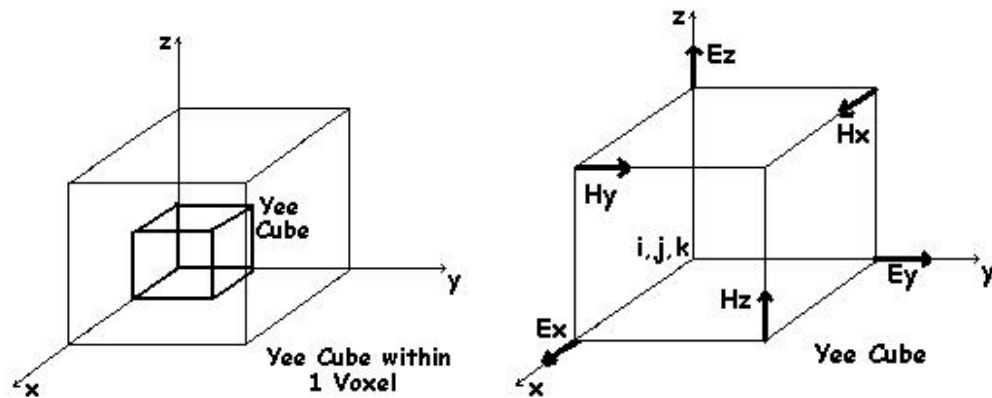
Figure 5.1.1.1: Standard Cartesian Yee Cube used for FDTD

This depiction is equally applicable for 1-D, 2-D, and 3-D FDTD techniques. Only thing is that, calculation of the numerical curl can become complicated when multiple dimensions are considered. Kane Yee's seminal 1966 paper proposed spatially staggering the vector components of the E-field and H-field about rectangular unit cells of a Cartesian computational grid so that each E-field vector component is located midway between a pair of H-field vector components, and conversely [7]. This scheme, named as Yee lattice, has proven to be very strong, and remains at the core of many current FDTD software constructs.

The Yee Cube used for FDTD is shown in figure 5.1.1.1. Visualized as a cubic voxel, the electric field components form the edges of the Yee cube, and the magnetic

field components form the normals to the faces of the cube. A three-dimensional space lattice consists of a multiplicity of such Yee cells.

Furthermore, Yee proposed a leapfrog method for walking in time wherein the electric (E) field and magnetic (H) field updates are staggered so that E-field updates are conducted midway during each time-step between successive H-field updates, and conversely [7]. As a benefit of this scheme, this explicit time-stepping scheme avoids the requirement of solving simultaneous equations, and furthermore yields dissipation-free numerical wave propagation. But as a disadvantage, this scheme mandates an upper bound on the time-step to make sure the numerical stability [10]. This results in, certain classes of simulations that may require many thousands of time-steps for completion.

5.1.2 APPLYING THE FDTD METHOD

For using FDTD, a computational domain must be established first. It is simply the physical region over which the simulation is to be performed. Within that computational domain, the E and H fields are determined at every point in space. Within the computational domain, the material of each cell has to be specified. Typically, the material is either free-space (air), dielectric or metal. Any material can be used as long as the permittivity, permeability and conductivity are specified.

As the computational domain and the grid materials are established, a source has to be specified now. The source can either be an impinging plane wave, an applied electric field or a current on a wire, depending on the required application.

Thus FDTD technique computes EM fields within a compact spatial region. To find the scattered fields or radiated far fields we can use near-to-far-field transformations [11].

5.1.3 EFFECTIVENESS OF FDTD MODELING

It is a versatile modeling technique used to solve Maxwell's equations. Users can easily understand how to use FDTD and know what to expect from a given model, as the method is much intuitive.

Normally a broadband pulse such as a Gaussian pulse is applied as the source in the FDTD technique, as it is a time domain method. So using this method, a wide range of frequencies can be obtained with a single simulation. In certain applications where resonant frequencies are not exactly known, or whenever a broad band result is required, this method is highly useful.

As FDTD calculates the E and H fields everywhere in the computational domain, it lends itself to providing animated displays of the EM field movement through the model. This type of display is useful in understanding what is going on in the model, and to check whether the model is working correctly.

The FDTD technique allows the user to specify the material at all points within the computational domain. A wide variety of linear and nonlinear dielectric and magnetic materials can be naturally and easily modeled.

5.1.4 LIMITATIONS OF FDTD MODELING

In FDTD it requires that the entire computational domain has to be discretized in the form of grids of Yee cells. But this grid spatial discretization must be sufficiently fine to resolve both the smallest electromagnetic wavelength and the smallest geometrical feature in the model. This leads to develop very large computation domains and results in very long solution time.

Since FDTD requires that the entire computational domain be gridded, and the grid spatial discretization must be sufficiently fine to resolve both the smallest electromagnetic wavelength and the smallest geometrical feature in the model, very large computational domains can be developed, which results in very long solution times. Models with long, thin features, (like wires etc.) are difficult to model in FDTD because it requires excessively large computational domain and solution time.

Usually far field computations are done only with the help of post-processing [9] methods such as transformation techniques. This is because, if the field values at some distance are desired, it is likely that this distance will force the computational domain to be excessively large and hence the solution time.

Since the computer memory is finite in size, the computational domain must also be finite. In many cases this is achieved by inserting artificial boundaries into the simulation space. But abrupt truncation of computational domain result in reflections of EM wave and causes errors. Care must be taken to minimize errors introduced by such boundaries. There are a number of available highly effective absorbing boundary conditions (ABCs) to simulate an infinite unbounded computational domain [9]. Most

modern FDTD implementations instead use a special absorbing "material", called a perfectly matched layer (PML) to implement absorbing boundaries.[12][13]

5.2 PRELIMINARY FACTS ON FDTD

The FDTD method has been developed in tandem with the progress of computer technology since K. S. Yee applied it to the analysis of an electromagnetic problem in 1966 [14]. As the effectiveness of this method is widely recognized, the FDTD method seems to have matured into a basic computational tool that every engineer engaged in electromagnetic analysis or related fields should know well, similar to the Method of Moments (MoM) [15], [16] and the Finite Element Method (FEM) [17].

Since FDTD is a time domain technique, the frequency characteristics of the structure under analysis will be obtained principally by the Fourier Transformation; however it is not always a simple process because computer resources are limited. Furthermore, it should be noted that the accuracy of the discrete Fourier Transform is not very high. As the accuracy of FDTD is proportional to the size of the cell, the number of spatial cells increases when higher accurate results are requested. Therefore, the accuracy of the final results depends, after all, on the power of the computer.

The modeling algorithm of the electromagnetic fields in the FDTD method is simple and straightforward because it is based on the finite difference approximation of Maxwell's equation, and a practical level of the accuracy can easily be obtained. For this reason, the FDTD method has been applied to various electromagnetic problems. The FDTD method in particular holds an unchallenged position as a method of dealing with the interaction problem between electromagnetic fields and the human body, because

realistic modeling of the human body is very simple in the FDTD framework. Without much difficulty, the FDTD method can be applied to nonlinear electromagnetic problems also. On the other hand, the Method of Moments and the Finite Element Modeling require some special treatments when they are applying to these problems. One of the merits of the FDTD technique is considered as its wide applicability.

5.2.1 FDTD METHOD IN COMPUTATIONAL ELECTROMAGNETICS

The progress in high-performance computers and the necessity for analyzing realistic models after the 1960s have resulted in the development of several numerical techniques for electromagnetic field analysis on the computer. This scientific discipline is collectively called computational electromagnetics. The most important techniques in computational electromagnetics are the MoM and the FEM in the frequency domain, and the Transmission Line Matrix (TLM) method [18, 19] and the FDTD method in the time domain. The basic ideas behind these methods are found in fluid mechanics or analytical mechanics. However, the application of these methods for analyzing electromagnetic problems began in earnest in the 1960s when the electronic computer came into of practical use in general. These methods appear to be distinct because specialized terms are often used in the different discipline. However the basic concepts are very similar. For example, the MoM in the field of electromagnetic and antennas is mainly applied to an integral equation for a current distribution. However, the MoM includes very wide-ranging concept and is applicable to a differential equation for the electric field or the magnetic field as well as to an eigenvalue problem. That is, the MoM is able to deal with the electromagnetic field itself or the electromagnetic mode as an unknown quantity, and

is based on the method of weighted residuals [18, 20]. On the other hand, the FEM calculates not the current distribution but the electric or magnetic field in space using a variation principle of a corresponding functional. However, the method of weighted residuals is used in general because a problem in which the corresponding functional is found in advance is unusual. Therefore, it is considered that both the MoM and the FEM are based on the same principle. Regarding the methods in the time domain, the TLM method models the electromagnetic fields by using the voltage and the current on the transmission line placed in a discretized calculation space. The field expressions equivalent to the FDTD method can be derived by an appropriate variable transformation [18, 21]. Therefore, the two methods are equivalent in principle. Thus, we can conclude that only two principles exist in computational electromagnetics, that is, the method of weighted residuals in the frequency domain and that of the finite difference in the time domain. Other computational methods have also been developed recently, such as the FEM in the time domain [18, 22], and the hybrid method of the FDTD method combined with the MoM [18, 23].

5.2.2 BASIC CONCEPTS

Formulation of the FDTD method begins by considering the differential form of Maxwell's two curl equations which govern the propagation of electric and magnetic fields in a medium. The medium is assumed to be uniform, isotropic, and homogeneous. Also the medium is assumed to be lossless i.e., absence of volume currents or finite conductivity. With these assumptions, Maxwell's curl equations may be written as

$$\frac{\partial \boldsymbol{E}}{\partial t} = -\frac{\sigma}{\varepsilon}\boldsymbol{E} + \frac{1}{\varepsilon}\nabla \times \boldsymbol{H} \qquad (1)$$

$$\frac{\partial \boldsymbol{H}}{\partial t} = -\frac{1}{\mu}\nabla \times \boldsymbol{E} \qquad (2)$$

A very robust formula that does not cause any unprecedented phenomenon even under unfavorable conditions should be chosen because one must solve a very complicated problem. A first-order finite difference scheme is used in the FDTD method for this reason. A discretization using a higher order finite difference scheme is certainly possible for the purpose of improving the accuracy, however it results in a complicated formula and becomes instable in general [18, 9].

There are three types of first-order finite difference scheme: a forward difference, a backward difference and a central difference. The central difference scheme is used in the FDTD method because it is the most accurate compared with the other two schemes. In this section, the Yee algorithm based on the central difference scheme, the method of modeling an object, the excitation of the electromagnetic waves and some points to note when using the FDTD method will be described. The computer resources required in the FDTD calculation will be roughly estimated at the end. Let one component of the electric or magnetic field be $F(x, y, z, t) = F(i\Delta x, j\Delta y, k\Delta z, n\Delta t)$. Then the central difference schemes for the x axis and time t are expressed as

$$\frac{\partial F}{\partial x} \simeq \frac{F\left(x + \frac{\Delta x}{2}, y, z, t\right) - F\left(x - \frac{\Delta x}{2}, y, z, t\right)}{\Delta x}$$

$$= \frac{F^n\left(i + \frac{1}{2}, j, k\right) - F^n\left(i - \frac{1}{2}, j, k\right)}{\Delta x} \tag{3}$$

$$\frac{\partial F}{\partial t} \simeq \frac{F\left(x, y, z, t + \frac{\Delta t}{2}\right) - F\left(x, y, z, t - \frac{\Delta t}{2}\right)}{\Delta t}$$

$$= \frac{F^{n+\frac{1}{2}}(i, j, k) - F^{n-\frac{1}{2}}(i, j, k)}{\Delta t}, \tag{4}$$

where the position in space is written in the parentheses of function F, and the time is written as the superscript. Other expressions are possible [18, 9], [18, 10], however Eqs. (3) and (4) are convenient for implementing the program in a computer. The electric or magnetic field is discretized in both space and time, as indicated by $F(x, y, z, t) = F(i\Delta x, j\Delta y, k\Delta z, n\Delta t)$, so that the calculation space is divided into small rectangles as shown in Figure 5.2.2.1. This small rectangle is referred to as a cell in the FDTD method. Its side is called a cell edge, and its length Δx, Δy or Δz is called a cell size.
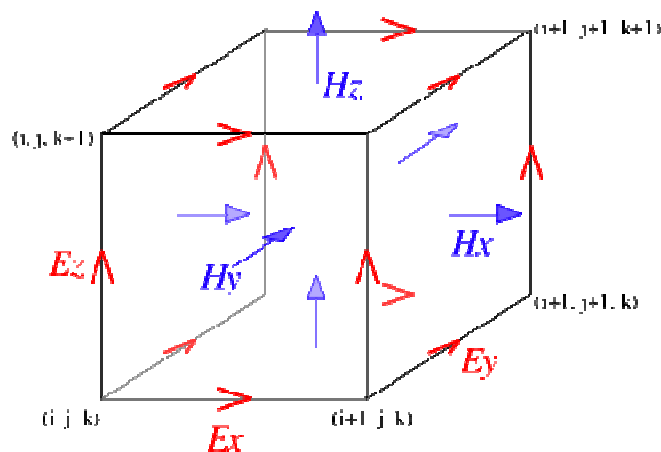
Figure 5.2.2.1: FDTD Cell

207

5.2.3 YEE ALGORITHM

The FDTD representations for electromagnetic fields in time are obtained by replacing the time derivative in Eqs. (1) and (2) with finite difference approximation. If we differentiate Ampere's law (1) and Faraday's law (2) at the same time, the time in the superscript of the electric field and the magnetic field are different from each other. To avoid this difficulty, Eq. (1) is differentiated at $t = \left(n - \dfrac{1}{2} \right)\Delta t$ whereas Eq. (2) is at $t = n\Delta t$. Then,

$$\left. \frac{\partial \boldsymbol{E}}{\partial t} \right|_{t=\left(n-\frac{1}{2}\right)\Delta t} = \frac{\boldsymbol{E}^n - \boldsymbol{E}^{n-1}}{\Delta t}$$

$$= -\frac{\sigma}{\varepsilon}\boldsymbol{E}^{n-\frac{1}{2}} + \frac{1}{\varepsilon}\nabla \times \boldsymbol{H}^{n-\frac{1}{2}} \tag{5}$$

$$\left. \frac{\partial \boldsymbol{H}}{\partial t} \right|_{t=n\Delta t} = \frac{\boldsymbol{H}^{n+\frac{1}{2}} - \boldsymbol{H}^{n-\frac{1}{2}}}{\Delta t}$$

$$= -\frac{1}{\mu}\nabla \times \boldsymbol{E}^n \tag{6}$$

are obtained. Furthermore, if we approximate the conduction current term which is the first term on the right-hand side in Eq. (5), as follows,

$$\sigma \boldsymbol{E}^{n-\frac{1}{2}} \simeq \sigma \frac{\boldsymbol{E}^{n-1} + \boldsymbol{E}^n}{2}, \tag{7}$$

the electric and magnetic field expressions

$$E^n = \frac{1 - \frac{\sigma \Delta t}{2\varepsilon}}{1 + \frac{\sigma \Delta t}{2\varepsilon}} E^{n-1} + \frac{\Delta t / \varepsilon}{1 + \frac{\sigma \Delta t}{2\varepsilon}} \nabla \times H^{n-\frac{1}{2}} \qquad (8)$$

$$H^{n+\frac{1}{2}} = H^{n-\frac{1}{2}} - \frac{\Delta t}{\mu} \nabla \times E^n \qquad (9)$$

are obtained. Thus in the FDTD method, the combination of the electric field E^{n-1} at $t = (n-1)\Delta t$ and the magnetic field $H^{n-\frac{1}{2}}$ at $t = \left(n - \frac{1}{2} \right) \Delta t$ yields the electric field E^n after

$\Delta t / 2$ increment, and this electric field E^n and the magnetic field $H^{n-\frac{1}{2}}$ produce the next

magnetic field $H^{n+\frac{1}{2}}$. Figure 5.3 illustrates a time chart for a one-dimensional wave propagation example in which **E** and **H** components are interleaved each other. That is, the electric fields are assigned at integer time steps $(n-1)\Delta t$, $n\Delta t$, $\cdots$. and the magnetic

fields are assigned at fractional time steps $\left(n - \frac{1}{2} \right) \Delta t$, $\left(n + \frac{1}{2} \right) \Delta t$, $\cdots$. This is referred to

as a leapfrog arrangement. Furthermore, the electric field is calculated before the magnetic field because antenna engineers and electromagnetic researchers focus their discussion on the phenomena of electric fields in most cases. The order of calculation
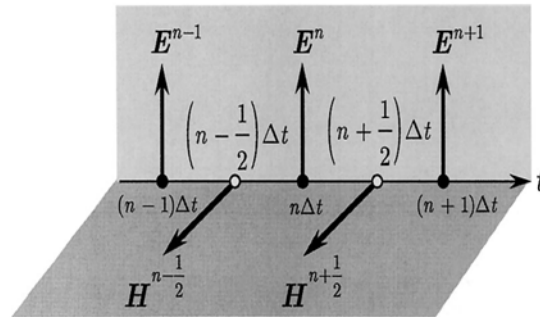
Figure 5.2.3.1: Leapfrog time integration of electromagnetic fields [18]

can certainly be reversed, for example, when analyzing magnetic materials [18, 8], [18, 24].

Next, let us decide the spatial arrangement of electromagnetic fields. There are two alternatives for assigning the electromagnetic fields on the cell edge shown in Figure 5.2.3.1, that is, to assign the electric field or the magnetic field; however the electric field is assigned in most cases because the discussion is focused on the electric field in the electromagnetic discipline.
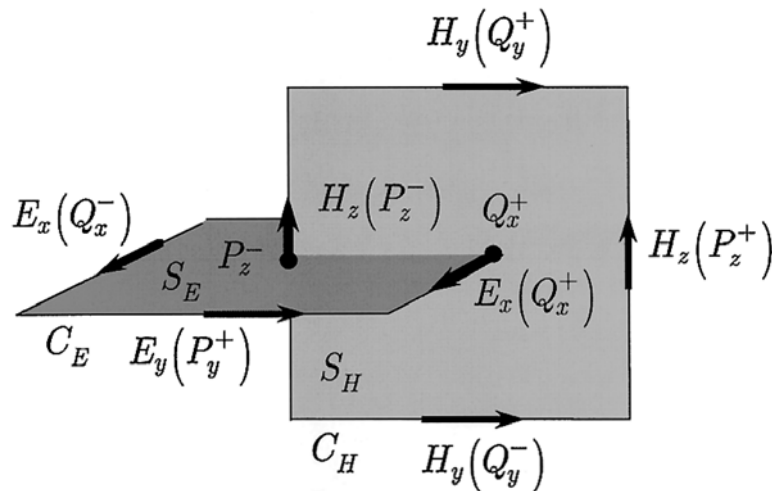
Figure 5.2.3.2: Electromagnetic fields on cell edges [18]

Figure 5.2.3.2. illustrates the electric field component on the cell edge C_E which is parallel to the $x - y$ plane. A surface made by C_E is referred to here as cell surface S_E. Another cell surface S_H perpendicular to S_E is also shown. The electric field $E_x\left(Q_x^+\right)$ at point Q_x^+ on the cell edge is given by using the mathematical definition of rotation $(\nabla\times)$ and Eq. (8) as follows:

210

$$E_x^n(Q_x^+) = \frac{1 - \dfrac{\sigma(Q_x^+)\Delta t}{2\varepsilon(Q_x^+)}}{1 + \dfrac{\sigma(Q_x^+)\Delta t}{2\varepsilon(Q_x^+)}} E_x^{n-1}(Q_x^+)$$

$$+ \frac{\Delta t/\varepsilon(Q_x^+)}{1 + \dfrac{\sigma(Q_x^+)\Delta t}{2\varepsilon(Q_x^+)}} \frac{1}{S_H} \oint_{C_H} \boldsymbol{H}^{n-\frac{1}{2}} ds$$

$$= \frac{1 - \dfrac{\sigma(Q_x^+)\Delta t}{2\varepsilon(Q_x^+)}}{1 + \dfrac{\sigma(Q_x^+)\Delta t}{2\varepsilon(Q_x^+)}} E_x^{n-1}(Q_x^+)$$

$$+ \frac{\Delta t/\varepsilon(Q_x^+)}{1 + \dfrac{\sigma(Q_x^+)\Delta t}{2\varepsilon(Q_x^+)}}$$

$$\left\{ -\frac{H_y^{n-\frac{1}{2}}(Q_y^+) - H_y^{n-\frac{1}{2}}(Q_y^-)}{\Delta z} \right.$$

$$\left. + \frac{H_z^{n-\frac{1}{2}}(P_z^+) - H_z^{n-\frac{1}{2}}(P_z^-)}{\Delta y} \right\}, \qquad (10)$$

where the magnetic field on contour *CH* was assumed to be constant.

Similarly the magnetic field component $H_z(P_z^-)$ at P_z^- is given, using Eq. (9), as follows.

$$H_z^{n+\frac{1}{2}}(P_z^-) = H_z^{n-\frac{1}{2}}(P_z^-)$$

$$- \frac{\Delta t}{\mu(P_z^-)} \frac{1}{S_E} \oint_{C_E} \boldsymbol{E}^n \cdot ds$$

$$= H_z^{n-\frac{1}{2}}(P_z^-) - \frac{\Delta t}{\mu(P_z^-)}$$

$$\left\{ -\frac{E_x^n(Q_x^+) - E_x^n(Q_x^-)}{\Delta y} \right.$$

$$\left. + \frac{E_y^n(P_y^+) - E_y^n(P_y^-)}{\Delta x} \right\} \qquad (11)$$

Update equations expressed by a discrete point in the cell for electric and magnetic fields

are obtained by setting $Q_x^+ = (i + 12, j, k)$, $P_z^- = (i + 12, j - 1/2, k)$, and so on in Eqs.

(10) and (11). The same update equations are derived by replacing the curl equations in

Eqs. (8) and (9) with corresponding spatial central differences.
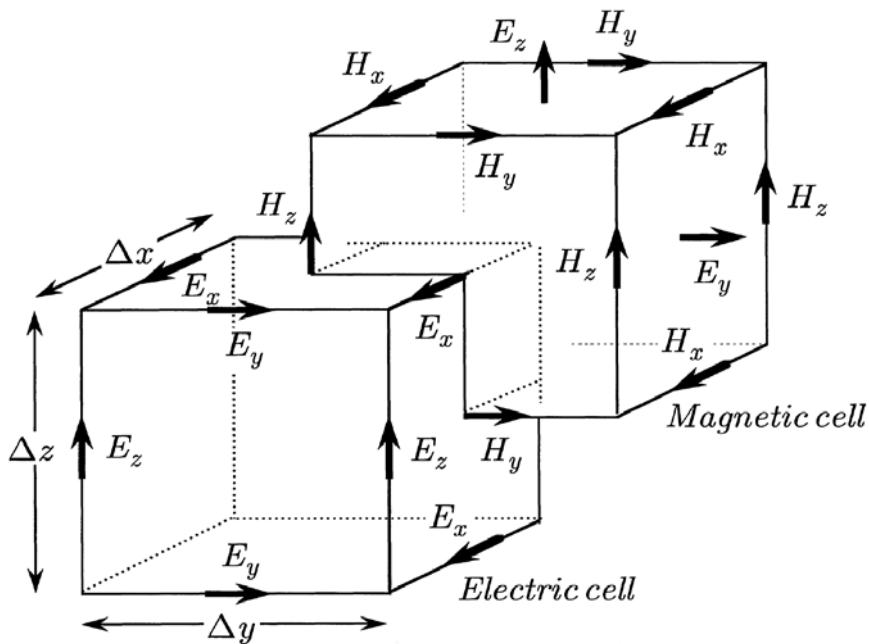
Figure 5.2.3.3: Electric cell and magnetic cell [18]

The update equations for other electromagnetic field components can be obtained in the

same way, and as a result, the electric and magnetic field components are placed as

illustrated in Figure 5.2.3.3. Thus every **E** component is surrounded by four circulating **H**

components, and every **H** component is surrounded by circulating **E** components. This

provides a three-dimensional space filled with interlinked rectangular contours of

Faraday's law and Ampere's law. For example, it is possible to understand that **E**

components associated with displacement current generate an **H** field around it. **H**

components associated with magnetic flux generates an **E** field as well. In effect, the FDTD algorithm, that is, Yee algorithm simultaneously simulates the Maxwell's equation. The above-mentioned cells formed by **E** components and **H** components are referred to as an electric unit cell or simply a unit cell, and a magnetic cell, respectively.

This natural arrangement of the field components is ideal for defining the central differences for the Maxwell's equations to yield the six field components as:

$$H^{n+0.5}_{x\ i,j,k} = H^{n-0.5}_{x\ i,j,k} + \frac{\Delta t}{\mu \Delta z}\left(E^n_{y\ i,j,k} - E^n_{y\ i,j,k-1}\right) - \frac{\Delta t}{\mu \Delta y}\left(E^n_{z\ i,j,k} - E^n_{z\ i,j-1,k}\right)$$

$$H^{n+0.5}_{y\ i,j,k} = H^{n-0.5}_{y\ i,j,k} + \frac{\Delta t}{\mu \Delta x}\left(E^n_{z\ i,j,k} - E^n_{z\ i-1,j,k}\right) - \frac{\Delta t}{\mu \Delta z}\left(E^n_{x\ i,j,k} - E^n_{x\ i,j,k-1}\right)$$

$$H^{n+0.5}_{z\ i,j,k} = H^{n-0.5}_{z\ i,j,k} + \frac{\Delta t}{\mu \Delta y}\left(E^n_{x\ i,j,k} - E^n_{x\ i,j-1,k}\right) - \frac{\Delta t}{\mu \Delta x}\left(E^n_{y\ i,j,k} - E^n_{y\ i-1,j,k}\right)$$

$$E^{n+1}_{x\ i,j,k} = E^n_{x\ i,j,k} + \frac{\Delta t}{\varepsilon \Delta z}\left(H^{n+0.5}_{z\ i,j+1,k} - H^{n+0.5}_{z\ i,j,k}\right) - \frac{\Delta t}{\varepsilon \Delta y}\left(H^{n+0.5}_{y\ i,j,k+1} - H^{n+0.5}_{y\ i,j,k}\right)$$

$$E^{n+1}_{y\ i,j,k} = E^n_{y\ i,j,k} + \frac{\Delta t}{\varepsilon \Delta x}\left(H^{n+0.5}_{x\ i,j,k+1} - H^{n+0.5}_{x\ i,j,k}\right) - \frac{\Delta t}{\varepsilon \Delta z}\left(H^{n+0.5}_{z\ i+1,j,k} - H^{n+0.5}_{z\ i,j,k}\right)$$

$$E^{n+1}_{z\ i,j,k} = E^n_{z\ i,j,k} + \frac{\Delta t}{\varepsilon \Delta y}\left(H^{n+0.5}_{y\ i+1,j,k} - H^{n+0.5}_{y\ i,j,k}\right) - \frac{\Delta t}{\varepsilon \Delta x}\left(H^{n+0.5}_{x\ i,j+1,k} - H^{n+0.5}_{x\ i,j,k}\right)$$

---------------------------- (12)

Here, not only the placement of the *E* and *H* nodes are off in space by half a space step, but the time instants when the *E* or *H* fields are calculated are also off by half a time step. That is, if the components of *E* are calculated at nΔt, where Δt is the discretization

unit in time and n is any non-negative integer, the components of *H* are calculated at (n + 0.5) Δt. For this reason, the Yee algorithm is also called the leapfrog algorithm.

5.2.4. CELL SIZE AND TIME STEP

While cell dimensions are assigning it is better to choose finer cells, since the field value is assumed to be a constant over a cell for computational accuracy. Often the side of each cell is set as λ/10 or less at the highest frequency of interest because the grid dispersion error is proportional to the cell sides [18] as follows

$$E \;\propto\; \left(\sqrt{\left(\Delta x^2 + \Delta y^2 + \Delta z^2 \right)} \Big/ \lambda \right)^2 \tag{13}$$

However, in some situations, such as accurate calculation of antenna impedances or radar cross sections, λ/20 or smaller size may be necessary. Here the wavelength in the material should be used to determine the minimum cell size if some portion of the computational space is filled with a dielectric material. For the problem involving high-permittivity dielectrics in a free space, it is better to use non-uniform cells, that is, smaller cells in the dielectrics, and larger cells outside.

Once the cell size is determined, the maximum size of the time step Δt immediately follows from the Courant–Friedrich–Lewy stability condition [18, 25], given by Eq. (14), which ensures that the numerical error generated in one step of the calculation does not accumulate and grow as the time-marching progresses.

$$\Delta t \le \frac{1}{v_{\max}} \sqrt{\left(\frac{1}{\Delta x^2} + \frac{1}{\Delta y^2} + \frac{1}{\Delta z^2} \right)} \tag{14}$$

where ν_{max} is the maximum phase velocity of the wave in the computational volume. The grid dispersion error is minimized by the equality in Eq. (14). This however, leads to instability in some cases because of a round-error in the computer. One method of avoiding this is to select 99.5 % of Δt as given by (14).

In the present work, a cubical cell with $\Delta x = \Delta y = \Delta z = 0.5$ mm is chosen to meet the aforesaid criteria, and also to fit an integral number of cells in the computational space. In addition, cubical cell is recommended for minimum grid dispersion error [18]. This yields the time step as $\Delta t = 0.95744$ picoseconds.

5.2.5. ANTENNA ANALYSIS

An antenna, generally comprises of structures of different shape, dimensions and properties. It simply consists of a set of conductors and dielectrics surrounded by free space. Perfect conductor approximation is used for antenna feeds, patches, ground planes, stubs etc. and perfect dielectric approximation is used for substrates, dielectric resonators, etc.

In the present context, the DRA studied is of design 5-2 whose parameters as explained in section 4.5.2, in the previous chapter. An Isosceles Trapezoidal DR of dielectric constant $\varepsilon_{rd} = 20.8$, base1 (b1) = 15.4 mm, base2 (b2) = 30.8 mm, height (h) = 13.3mm and thickness (h1) = 13 mm is used. A 50 Ω microstrip transmission line, having a width 3 mm and length 67 mm fabricated on a 1.6 mm thick microwave substrate of dielectric constant $\varepsilon_{rs} = 4.4$ and size 115 mm x 115 mm or 0.97 λ_o x 0.97 λ_o, (λ_o is the wavelength corresponding to the centre frequency of the operating band) feeds the DR. The antenna geometry analyzed using FDTD is shown in Figure 5.2.5.1.
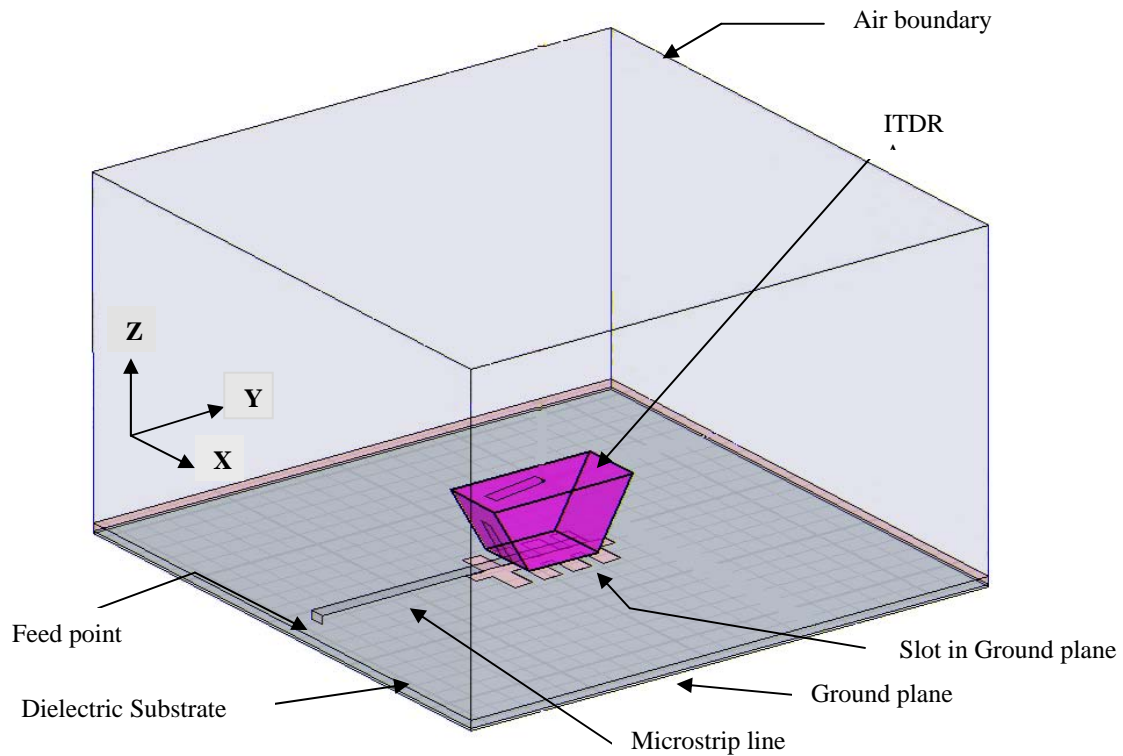
Figure 5.2.5.1: DRA geometries analyzed using FDTD (Design 5-2)

5.2.5.1. MODELING OBLECTS

It is obvious from Eqs. (10) and (11) that the electromagnetic fields can be calculated by setting the values of permittivity ε and conductivity σ to whole electric cell edges, and by setting the value of the permeability μ in whole magnetic cell edges. However, the problem in which constitutive parameters vary at every cell edge is extraordinarily unusual.
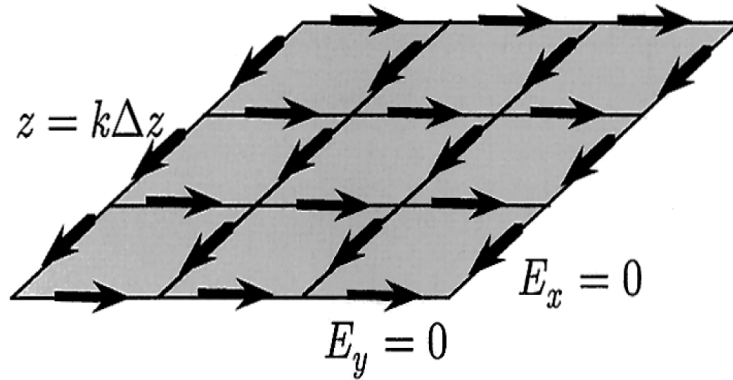
Figure 5.2.5.1.1: Electric field on perfectly conducting surface [18]

In most cases, the object for analysis consists of few kinds of media and the size is finite.

Furthermore, the space around the object is a free space whose constitutive parameters

are all constant. Therefore, usually only a few kinds of such parameters are needed. As

mentioned above, while the permittivity and the conductivity are set at the electric cell

edges, the permeability is set at the magnetic cell edges where the electric and magnetic

fields are located as shown in Figure 5.2.5.1.1, so that the object is modeled by spatially

alternating electric and magnetic cell edges. By this reason, an object whose permittivity

and permeability are different from those of the surrounding space cannot be modeled

perfectly even if the object is a rectangle. Moreover, a smooth surface is modeled by a

staircase approximation. In all cases, the objects are modeled by setting those constitutive

parameters at the corresponding point in the calculation space. In this section, the

modeling techniques for a perfect conductor and an interface between two or more media

are explained. It should be noted here that an efficient method for modeling the objects in

which the computer memories are effectively saved are introduced in Refs. [18, 8] and

[18, 12].

217

Since the tangential electric field component must be zero on the surface of a perfect conductor, for example, all electric field vectors tangential to a conducting plane at $z = k\Delta z$ are forced to set zero, as shown in Figure 5.2.5.1.1. A rectangular parallelepiped conductor can be set up by combining the above-mentioned conducting plane.

In FDTD, objects are modeled by assigning the constitutive parameters like permittivity, permeability and conductivity to the corresponding cells in the computational space.

Microstrip and ground plane are assumed to be perfect 2-D conductors. The tangential electric field component must be zero on the surface of a perfect conductor; hence are modeled by enforcing this condition on to the plane (s) of the appropriate cells. The cells those fill the air, substrate and DR are assigned the corresponding dielectric constants of 1, 4 and 20.8 respectively. The interface between two or more kinds of dielectrics is defined by enforcing the average value of permittivity to the intersecting cells [18, 26]. The above is implemented in the FDTD code by incorporating additional parameters *mulx*, *muly* and *mulz* in the *E* field components in Eqn. (5.3) as shown below.

ex(i,j,k) = ex(i,j,k)+***mulx***(i,j,k).*(ray*(hz(i,j,k)-hz(i,j-1,k))- raz*(hy(i,j,k)-hy(i,j,k-1)))/eps0;

ey(i,j,k) = ey(i,j,k)+***muly***(i,j,k).*(raz*(hx(i,j,k)-hx(i,j,k-1))-rax*(hz(i,j,k)-hz(i-1,j,k)))/eps0;

ez(i,j,k) = ez(i,j,k)+***mulz***(i,j,k).*(rax*(hy(i,j,k)-hy(i-1,j,k))-ray*(hx(i,j,k)-hx(i,j-1,k)))/eps0;

-------------------------------(15)

where, rax=Δt/Δx; ray=Δt/Δy; raz=Δt/Δz;

- For conductors, $mulx = muly = mulz = 0$

- For dielectrics, $mulx = muly = mulz = 1/\varepsilon_r$; $\varepsilon_r = 1, 4$ and 20.8 for air, substrate and DR respectively

- For interfaces between dielectrics (air-substrate, air-DR and DR-substrate), $mulx = muly = mulz = 2/(\varepsilon_{r1} + \varepsilon_{r2})$ for the cells on both sides of the interface; ε_{r1} and ε_{r2} are the parameters of the interfacing dielectrics.

Since the DR used is cylindrical in shape, its curved surface needs to be modeled properly since the cells lying at the curved edge will cover the DR only partially. By incorporating a staircase or conformal approach in the Yee algorithm, this can be achieved. The staircasing procedure, though simple, introduces significant errors in the computation, even with a fine cubical grid (side ~ $\lambda/25$) [18, 27]. Several enhanced FDTD methods for modeling curved dielectric surfaces have been proposed [18, 28–30]. These are implemented by a calculation procedure based on weighted volume effective dielectric constant [28, 29] or a linear weighted average dielectric constant [30]. The weighted volume approaches require computation of the area and volume of the partially filled cells. Also these deal with the average dielectric constant; hence, their use yields the same effective value for dielectric distributions, even when the geometry of the fillings is different. Also they require complicated mesh generation. On the other hand, in [29] the information on the edges of a cell is utilized to modify the Yee algorithm, thereby avoiding the need for the area and/or volume calculations.
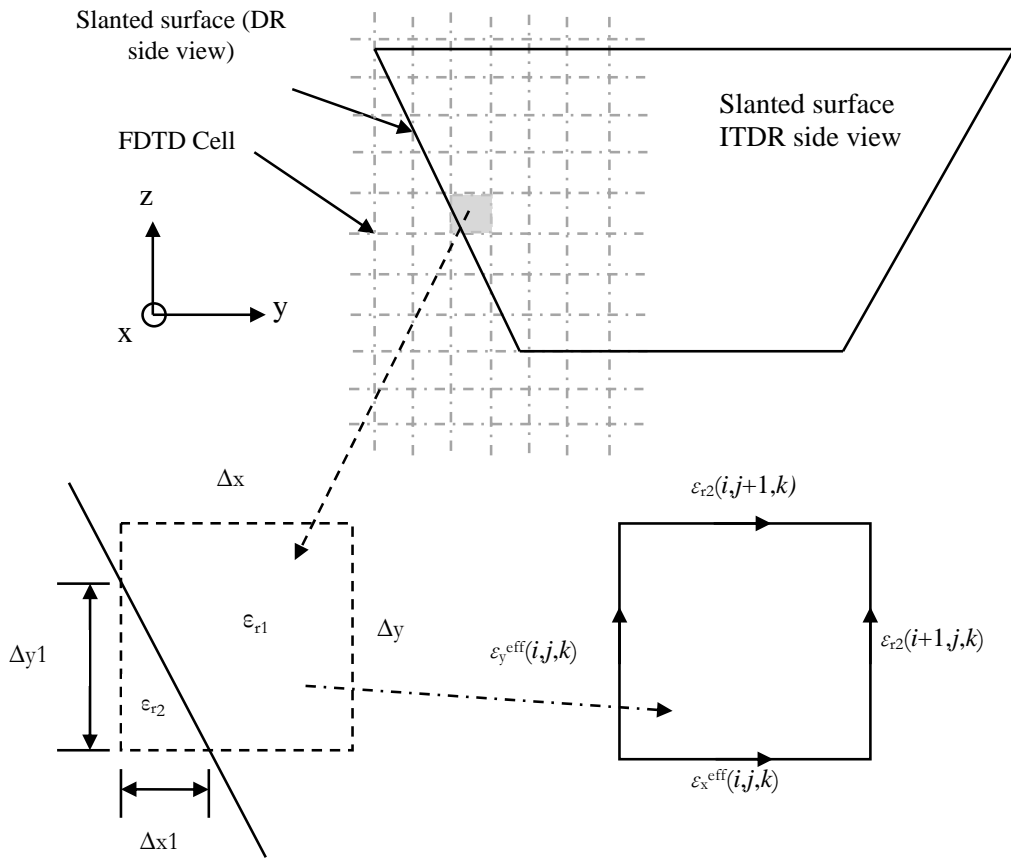
Figure 5.2.5.1.2: Conformal FDTD modeling (a) FDTD cells over the slanted surface (b) Enlarged view of a cell filled with two dielectrics (c) Modeled cell

If it is assumed that the s surface lies in the YZ-plane, in the present conformal method, a cell at the interface is modeled by a linear weighted average dielectric constant as shown in Figure 5.2.5.1.2. Effective dielectric constants for the particular cell are defined as:

$$\varepsilon_x^{\text{eff}}(i, j, k) = [\varepsilon_{r2}. \Delta x1\ (i, j, k) + \varepsilon_{r1}. (\Delta x - \Delta x1\ (i, j, k))]\ /\ (\Delta x) \qquad \text{---------(16)}$$

$$\varepsilon_y^{\text{eff}}(i, j, k) = [\varepsilon_{r2}. \Delta y1\ (i, j, k) + \varepsilon_{r1}. (\Delta y - \Delta y1\ (i, j, k))]\ /\ (\Delta y) \qquad \text{---------(17)}$$

However, the edges (i, $j+1$, k) and ($i+1$, j, k) of the cell, which indicate the immediate neighbouring cells are not penetrating the DR, so that the dielectric constant ε_{r1} is used for those cells. Now the parameters, $mulx = 1/\varepsilon_x^{\text{eff}}(i, j, k)$ $muly = 1/\varepsilon_y^{\text{eff}}(i, j, k)$ and $mulz = 1/\varepsilon_{r2}$ are used the FDTD computations, to model the cells of interest.

5.2.5.2. SOURCE SIGNAL

Normally a wide variety of excitation waveforms such as plane wave, pulse, modulated pulse etc. are used for exciting the structure under analysis. However, a Gaussian pulse is the most preferred one in frequency-dependent applications since it is having a smooth waveform in time, and its frequency spectrum is also Gaussian in shape centered at zero [31].

The Gaussian pulse is defined as, $\qquad p(t) = e^{-\left[\frac{(t-t_0)}{T_s}\right]^2}$ $\quad 0 \leq t \leq 2t_0$

$$= 0 \qquad \text{otherwise}$$

------(18)

For $T_s = 15$ ps and $t_0 = 3T_s$, the pulse is plotted in Figure 5.2.5.2.1. The frequency spectrum of the above pulse can be obtained by using the following relation.

$$\text{Amp (dB)} = 10.log \text{ [abs \{FFT (}p(t)\text{) \}]} \qquad\qquad \text{---------(19)}$$

where FFT is the fast Fourier transform an operator which finds the spectrun of the Gaussian pulse and the spectrum is shown in Figure 5.2.5.2.2.

221
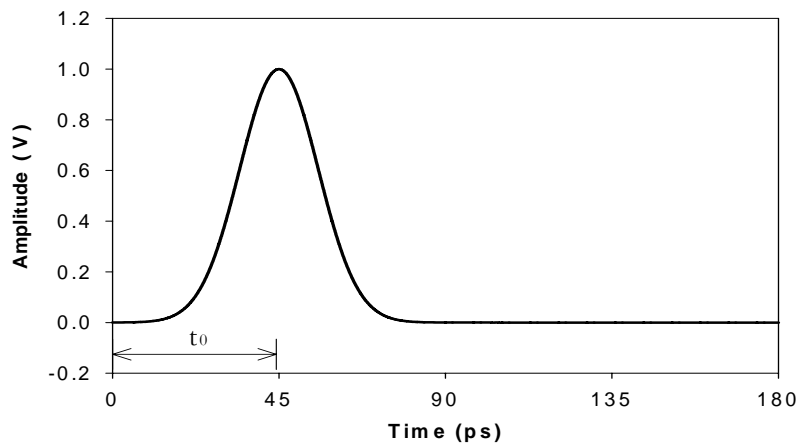
Figure 5.2.5.2.1: Gaussian pulse
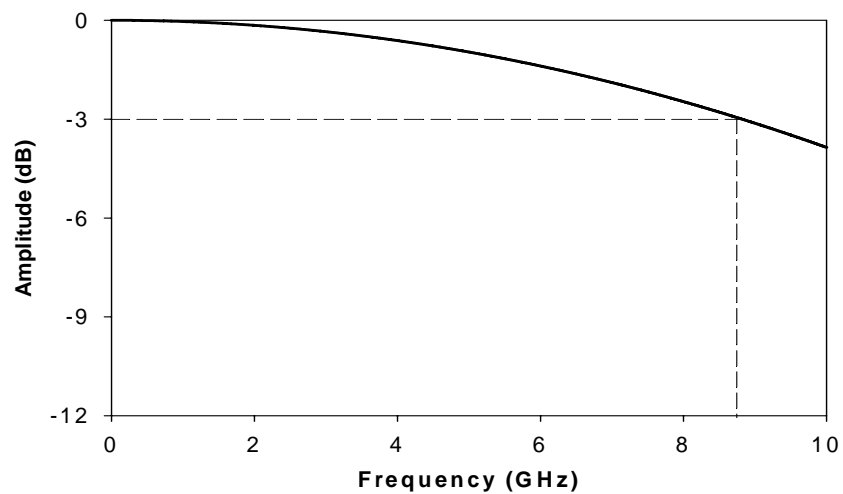
Figure 5.2.5.2.2: Spectrum of the Gaussian pulse

Though the highest frequency content of the pulse is $1/(2*\Delta t) = 522.23$ GHz, it is clear that the Fourier amplitude is within 3 dB only below 8.75 GHz, as determined by the pulse parameter *T*s. This frequency range is sufficient for the present analysis.

5.2.5.3. FEED MODELING

In practice, microwave energy is fed to the microstrip transmission line through an SMA connector soldered between the edges of the strip and the ground plane. This can be easily modeled in FDTD by assigning several electric field cells within the area coming under the strip. As seen in the above section, the amplitude of the exciting pulse is above zero for only a very short fraction of the total computational time, especially for resonant geometries such as antennas. Once the pulse amplitude drops, the source voltage becomes essentially zero and the source effectively becomes a short circuit. Any reflections from the antenna which return to the source are totally reflected to the computational space and a large number of time steps are required to stabilize the source signal. A dissipation mechanism can be added by modeling the Gaussian source Vs with a series internal resistance *Rs* [32] as shown in Figure 5.2.5.3.1.
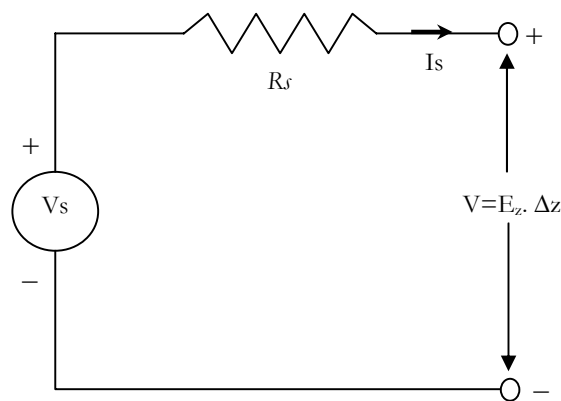
Figure 5.2.5.3.1: Source with series resistance

The value of the internal resistance does not appear to be critical. A reasonable choice for *Rs* is to use the value of the characteristic impedance of the transmission line i.e. $Z_0 = 50$ ohms. Usually, a voltage source that corresponds to an electric field *E* in the z

223

direction at a certain source location ($i_s\Delta$x, $j_s\Delta$y, $k_s\Delta$z) is used. If the source resistance Rs is set zero then the usual delta gap electric field at the source location at the nth time step is simply given by

$$E_s^n(i, j, k) = V_s(n\Delta t) / \Delta z \qquad \text{---------(20)}$$

When Rs is   included,

$$E_s^n(i, j, k) = (V_s(n\Delta t) + I_s^{n-1}R_s) / \Delta z \qquad \text{---------(21)}$$

By applying Ampere's circuital law by taking the line integral of the magnetic field around the feed point shown in Figure 5.2.5.3.2., the source current can be obtained as,

$$I_s^{n-1/2} = (H_x^{n-0.5}(is, js-1, ks) - H_x^{n-0.5}(is, js, ks))\Delta x$$
$$+ (H_y^{n-0.5}(is, js, ks) - H_y^{n-0.5}(is-1, js, ks))\Delta y \qquad \text{---------(22)}$$
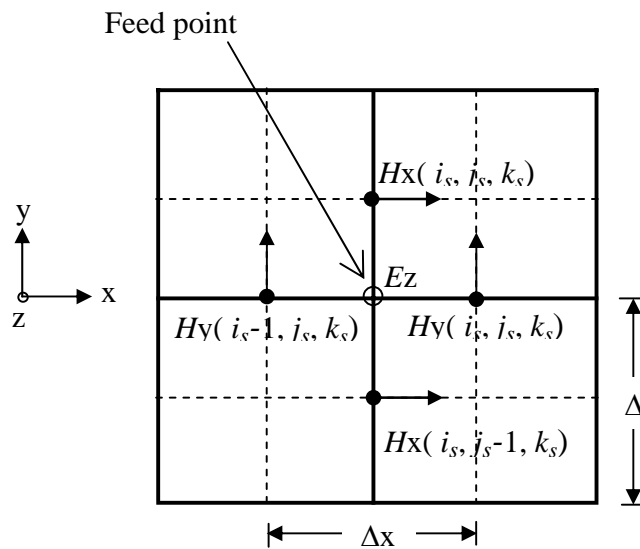
Figure 5.2.5.3.2: Magnetic field components around the feed point

Thus an electric field located at the z-edge of the cell just above the ground plane and directly below the end of the strip line is used as the feed. A stair-stepped perfect conductor transition from the feed cell to the microstrip edge is formed to provide a relatively smooth connection from the single electric feed location to the microstrip. This is illustrated in Figure 5.2.5.3.3.
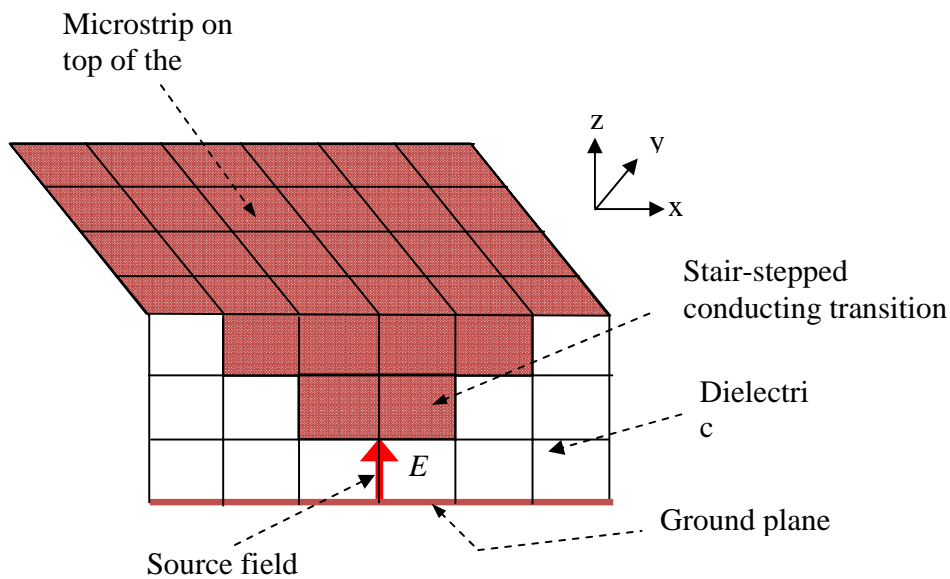
Figure 5.2.5.3.3: Source modeling in FDTD

Once the pulse is launched, the fields in the structure are computed for successive time steps until all the field intensities in the domain decay to a negligible steady-state value. At this instant, the input impedance of the antenna can be calculated as follows

$$Z_{in}(f) = \frac{V_s(f)}{I_s(f)} \qquad \text{-------- (5.23)}$$

Where $V_s(f)$ and $I_s(f)$ are the FFTs of the time domain voltage and current respectively. The antenna return loss can be calculated form Z_{in} as follows,

$$RL_{dB}(f) = 20.\log\left(\frac{Z_{in}(f) - Z_0}{Z_{in}(f) + Z_0}\right) \qquad \text{---------(5.24)}$$

where $Z_0 = 50\ \Omega$, the characteristic impedance

5.2.5.4 ABSORBING BOUNDARY CONDITION

A large number of electromagnetic problems have associated open space regions, where the spatial domain is unbounded in one or more directions. The solution of such a problem in this form will require an unlimited amount of computer resources. Therefore, the domain must be truncated such that the error involved is minimal. For this, the domain can be divided into two regions: the interior region and the exterior region as shown in Figure 5.2.5.4.1.
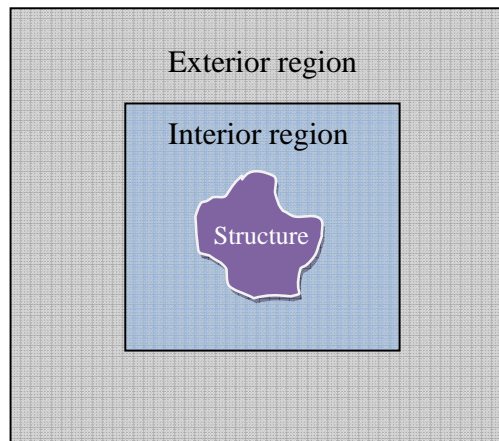
Figure 5.2.5.4.1: Truncation of the domain by the exterior region in FDTD algorithm

When the electromagnetic fields arrived at the truncation or boundary, they will reflect back into the computational space and cause erroneous computation unless the boundary perfectly absorbs the incident field. This can be made possible by forcing the incident fields to obey some conditions at the boundary which are termed as the absorbing boundary conditions (ABCs). The farther from the scatterers or the antennas

the absorbing boundary is located, the better is the absorption. This is because these waves become more like plane waves as they travel farther from the radiating structure, and also because the absorbing boundary is usually effective for a plane wave at normal incidence. However, the dimensions of the absorbing boundary are limited by the available computer memory.

ABCs can be classified roughly into two- (1) those derived from an approximate differential equation that expresses a traveling plane wave at the boundary, and (2) those in which the incident wave is absorbed by a virtual electromagnetic absorber. The Mur's absorbing boundary condition [33] and Berenger's Perfectly Matched Layer (PML) [34] are examples of the former and the latter classes respectively. In terms of accuracy, PML is the best available ABC, but its physical interpretation is very difficult to understand and the storage required for implementation is much larger than the Mur's ABC. As far as the limited computer resources are concerned, Mur's ABC is used for analyzing the DRA.

A plane wave having an z-component of electric field E_z propagating in the y direction should satisfy the following differential equation

$$\left(\frac{\partial}{\partial y} - \frac{1}{v}\frac{\partial}{\partial t} \right) E_z = 0$$

---------(25)

Discretizing (5.15) using the central difference method, we get the Mur's first order ABC equation. For example, the ABC at the y = 0 plane, that is the FDTD layer (*i*, 1, *k*), is given by

$$E_z^n(i,1,k) = E_z^{n-0.5}(i,2,k) + \frac{v\Delta t - \Delta z}{v\Delta t + \Delta z}\left[E_z^n(i,2,k) - E_z^{n-0.5}(i,1,k) \right] \qquad (26)$$

Similar expressions can be obtained for the other 5 layers constituting the boundaries of the cubical computational volume. However, the amount of reflection from the boundary becomes worse when the angle of incidence of the field increases. This limits the reflection coefficient of Mur's ABC to some – 30 to – 40 dB.

5.2.5.5. PARAMETERS CHOSEN FOR THE FDTD ANALYSIS

FDTD parameters used in the analysis of the DRA are given below:

❖ Cell dimensions, $\Delta x = \Delta y = \Delta z = 0.5$ mm $<< \lambda_0/20$, λ_0 being the lowest wavelength expected to exist in the structure

❖ Time step = 0.95744 ps

❖ Gaussian pulse parameters, $Ts = 15$ ps and $t_0 = 3Ts$

❖ Side of the computational volume

$$= \text{side of substrate} = 115 \text{ mm} = 230 \text{ cells}$$

❖ Width of the microstrip = width of the vertical strip = 3 mm =6 cells

❖ Length of the microstrip line = 67 mm = 134 cells

❖ Thickness of the substrate = 1.6 mm ≈ 3 cells

❖ Thickness of the DR = 13 mm = 26 cells

❖ Height of the DR = 13.3 mm ≈ 27 cells

❖ Height of the computational volume = 40 cells, i.e., 10 cells above the DR

5.2.5.6. ALGORITHM USED IN THE ANALYSIS

The following flow chart explains the algorithm used for analyzing the antenna using FDTD method.

$$\boxed{\text{START}}$$

Define cell size as 0.5mm $<< \lambda/20$

Give dimensions of the ITDRA, Substrate,
Ground plane, Microstrip line, Slanted strip
and Parasitic strip

Compute the number of cells required for the
geometrical structures viz. DRA, substrate,
strip line, slanted and parasitic strip.

Define the computational
domain by array of cells

Define Dielectric and Magnetic constants
c0,eps0,mu0,eps_sub and eps_dr

Calculate epseff1 = (1+eps_sub)/2 and
epseff2 = 1+eps_dr)/2

Calculate the sampling time step dt

Initialize E_x, E_y, E_z and H_x, H_y, H_z
arrays to zero

Initialize Mur's ABC arrays buffx, buffy
and buffz to zero

A

229

A

Define the entire computational volume as air by setting variables → $mulx = muly = mulz = 1$

Call the DR modeling routine

a) Define the dielectric substrate → $mulx = muly = mulz = 1/eps\_sub$;
b) Define air-substrate boundary → $mulx = muly = 1/epseff1$;
c) Define the microstrip and the ground plane → $mulx = muly = 0$;
d) Define the vertical feed → $mulx = mulz = 0$

Define the stair step transition for the feed

Define Gaussian pulse parameters, $Ts = 15ps$, $t_0 = 3Ts$

Set up counter $T = 0$ and Total step = 5000

if T >= Total-

C

Yes

No

Increment time step $T = T+1$ and calculate $t = (T-1)*dt$

a) Calculate input impedance as, $Z_{in}(f) = fft(s\_volt)/fft(s\_curr)$
b) Calculate return loss as, $RL(f) = (Z_{in}(f)-50)/(Z_{in}(f)+50)$
c) Save the results in the computer memory

Calculate Gaussian pulse value

$$p(t) = e^{-((t-t0)/Ts)^2}$$

END

B
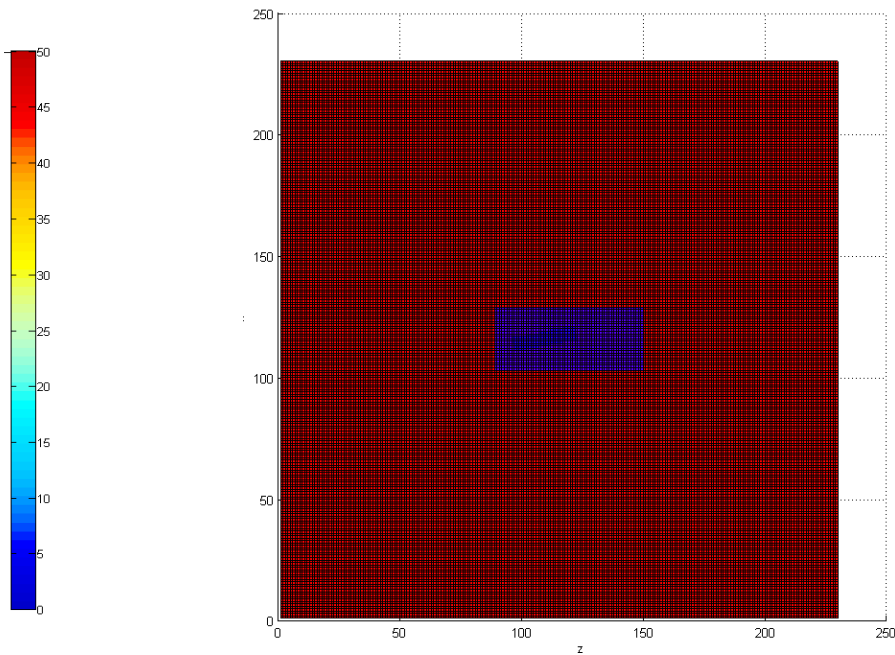
Figure 5.2.5.6.1: Flow chart of FDTD algorithm

5.2.5.7 RESULTS

Figure 5.15 (a) and (b) shows the FDTD model of the ITDRA in Design 5-2 on the *XY* plane and *YZ*-plane respectively. It is obtained by plotting the parameter *mulx*, which is the inverse of the dielectric constant. The contrast of dielectric constant among various materials in the structure is evident from the model.

Figure 5.2.5.7.1 (a): FDTD Model of ITDRA in Design 5-2 (Top view)
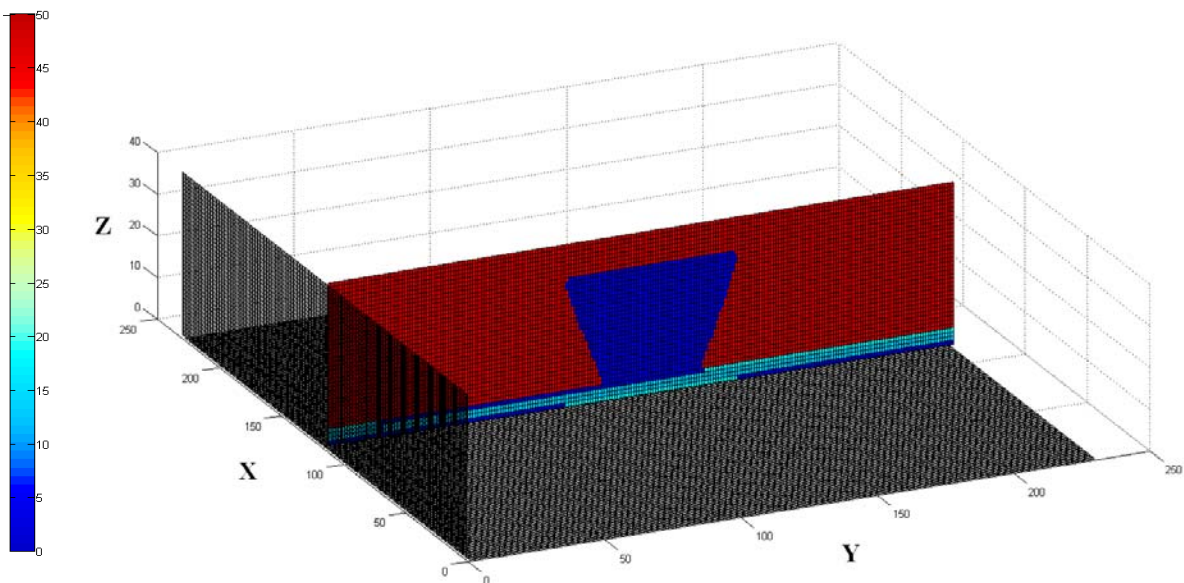
Figure 5.2.5.7.1 (b): FDTD Model of ITDRA in Design 5-2 (Side view)

Computed return loss and Input Impedance are plotted and compared with corresponding measured values as shown in figure 5.16 (a) and (b) respectively for the

232

optimum design with parasitic strip of 3mm width and 13mm length and having a tilt of

10°. The strip is modeled as adhered to the top face at an offset of 5.9mm from the centre**.**

The slanted strip is also optimized with a height and width of 9.5mm and 3mm

respectively. The model of microstrip line is realized with an offset length of 16.7 mm.

Cross and long slots are modeled within the ground plane with lengths of 30.8mm and

16mm respectively having a width of 3mm each. Computed matching band of -10 dB is

from 2.32 GHz to 2.75 GHz with a band width of 17.0%. The measured return loss has a

matching band of 2.17 to 2.7 GHz with a band width of 21.8%. Similarly the computed

resonant frequencies are 2.38 and 2.55 GHz and that of the measured are 2.30 and 2.54

GHz as shown in table 5.1. The corresponding errors in resonant frequencies are 3.36 %

and 0.4%. Percentage error in band width is 22.02%. Errors are tabulated in table 5.1.

(a)

233

(b)
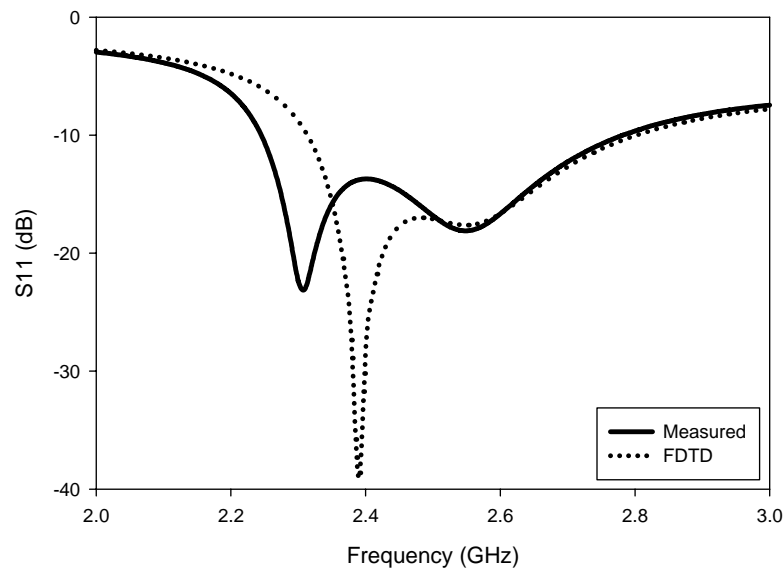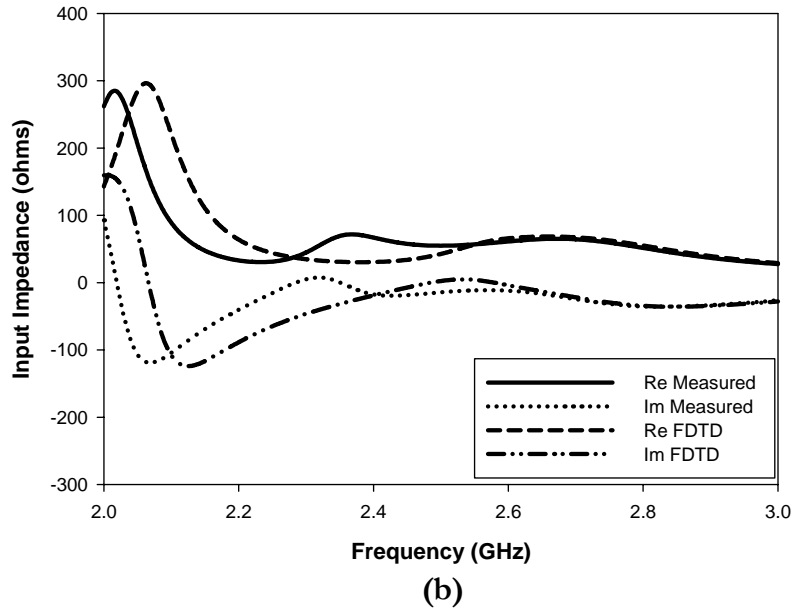
Figure 5.2.5.7.2: Measured and computed (FDTD) **(a)** Input Impedance and
(b) Return loss of the Design 5-2.

FDTD method Frequency (GHz)		Measured Frequency (GHz)		% Error FDTD & Experiment	
f_1	f_2	f_1	f_2	f_1	f_2
2.38	2.55	2.30	2.54	3.36	0.40

Table 5.2.5.7.1: Comparison of resonant frequencies with theory and
experimental results of broad band design of ITDRA (Design 5-2)

The measured and computed results show a slight disparity as shown in table
5.2.5.7.1. This may be because of the following reasons. The surface irregularities if any
are not accounted for in the simulation. The thin air line between the feed line and the

DRA due to these surface irregularities alters the effective dielectric constant of the DRA slightly, shifting the resonant frequency. The grid size in the computational domain also plays a crucial role in deciding the accuracy of prediction.

Figure 5.17 (a) shows the Gaussian pulse which is used to excite the DRA, figure 5.17 (b) and (c) are voltage and current waveforms respectively taken at the source point as a function of the FDTD time steps, for design 5-2. It is clear that the applied Gaussian pulse is propagated all over the computational space, converging to almost zero amplitude at about 5000 time steps. The input impedance and return loss of the antenna are computed from the source voltage and source current by Eq. **(5.23)** and **(5.24).**

(a) Gaussian Pulse

235
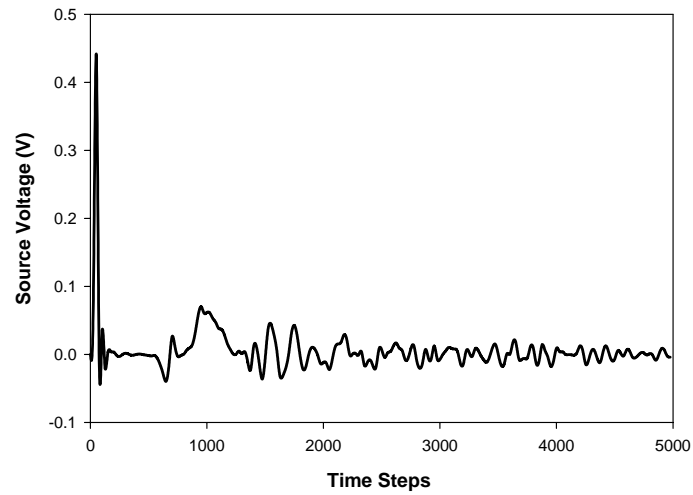
(b) Voltage waveform
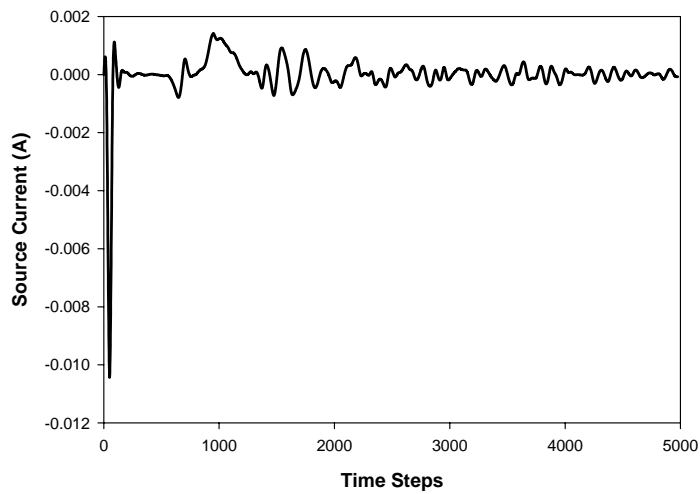
(b) Current waveform

Figure 5.2.5.7.3: (a) Gaussian pulse, **(b)** voltage and **(c)** current waveforms

at the feed point as a function of time steps

236

5.2.5.7.1 NEAR FIELD DISTRIBUTION

Distribution of the magnitude of electric field *magE* and its components *Ex*, *Ey* and *Hz* on the face 1 at *YZ*-plane and that on the top surface at the XY plane of the structure, at 2.38 GHz and 2.56 GHz (computed frequencies with minimum return loss) are shown below. Figures 5.2.5.7.1.1 (a)-(d) show *magE* and its field components and figures 5.2.5.7.1.1 (e)-(h) show *magH* and its field components at the face 1 and figures 5.2.5.7.1.1 (i)-(l) and 5.2.5.7.1.1 (m)-(p) are those which show corresponding field components of the top face of ITDRA at 2.38 GHz.   Similarly the corresponding figures in figure 5.2.5.7.1.2 are that of the E and H field distributions on the respective faces of ITDRA at 2.56 GHz. Figures of field distributions corresponding to components *Ex*, *Ey* and *Hz* are not shown as they are almost zero in the TE^x mode existing in the ITDRA. Face 1 is the surface of the ITDR in the YZ plane at the right side of the microstrip line when looking from the source side. Top face is the surface of the ITDR in the XY plane containing parasitic strip that lying opposite to the face by which the DR rests on the substrate. The boundary conditions applied for the metallic and dielectric bodies in the FDTD algorithm are very clear from the figure. On the vertical metallic strip on face 1, E_x and E_z which are the tangential components of electric field vanish and only E_y, the normal component exists. The magnitudes of E (*mag E*) on the faces are calculated from the field components by using the following relation,

$$mag\ E = \sqrt{E_x{}^2 + E_y{}^2 + E_z{}^2} \qquad \text{-------------(27)}$$

The magnetic field (*H*) distribution can also be obtained using a similar treatment.

At 2.38 GHz
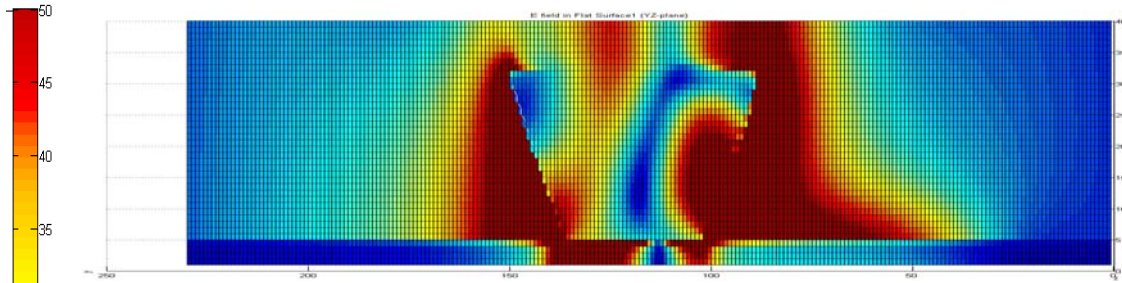
Figure 5.2.5.7.1.1 (a): E field distribution in the Face 1 (*YZ* plane)
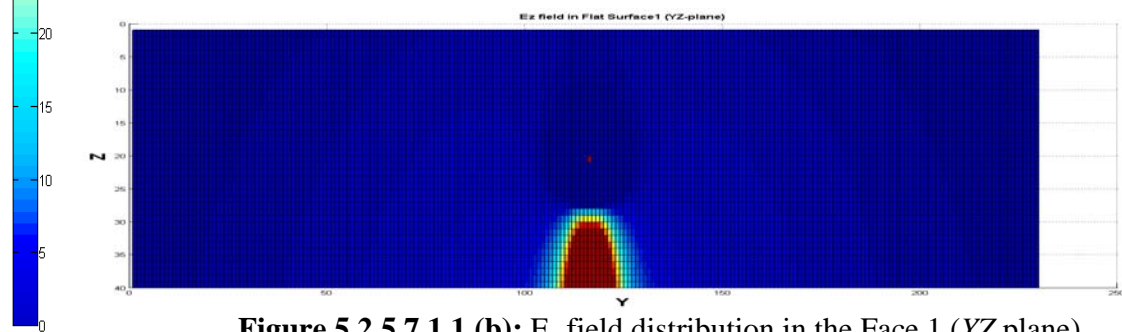
Figure 5.2.5.7.1.1 (b): E$_z$ field distribution in the Face 1 (*YZ* plane)
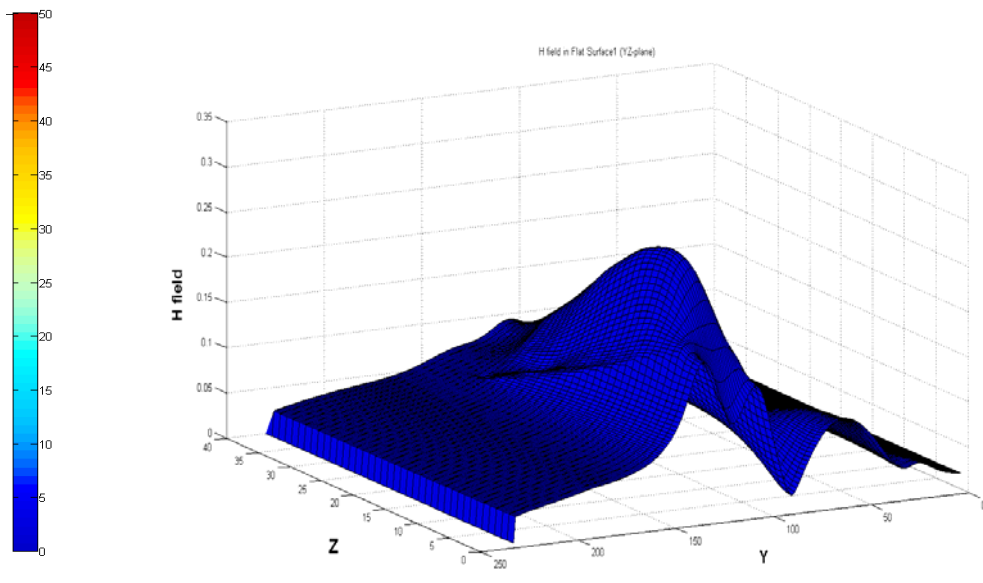
Figure 5.2.5.7.1.1 (e): H field distribution in the Face 1 (YZ plane)

238
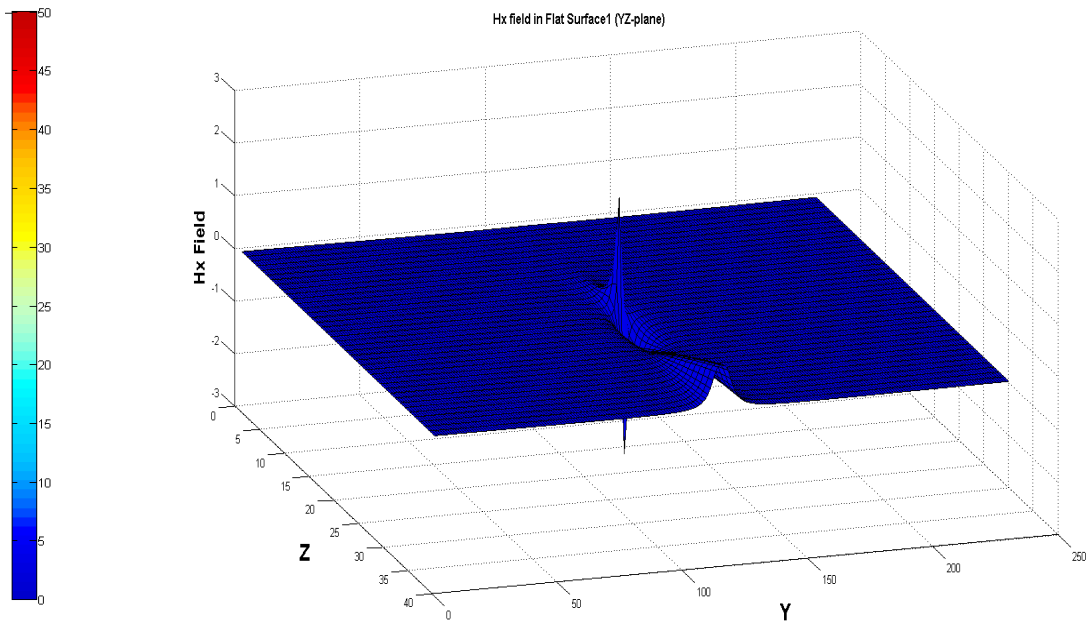
Figure 5.2.5.7.1.1 (f): H_x field distribution in the Face 1 (YZ plane)
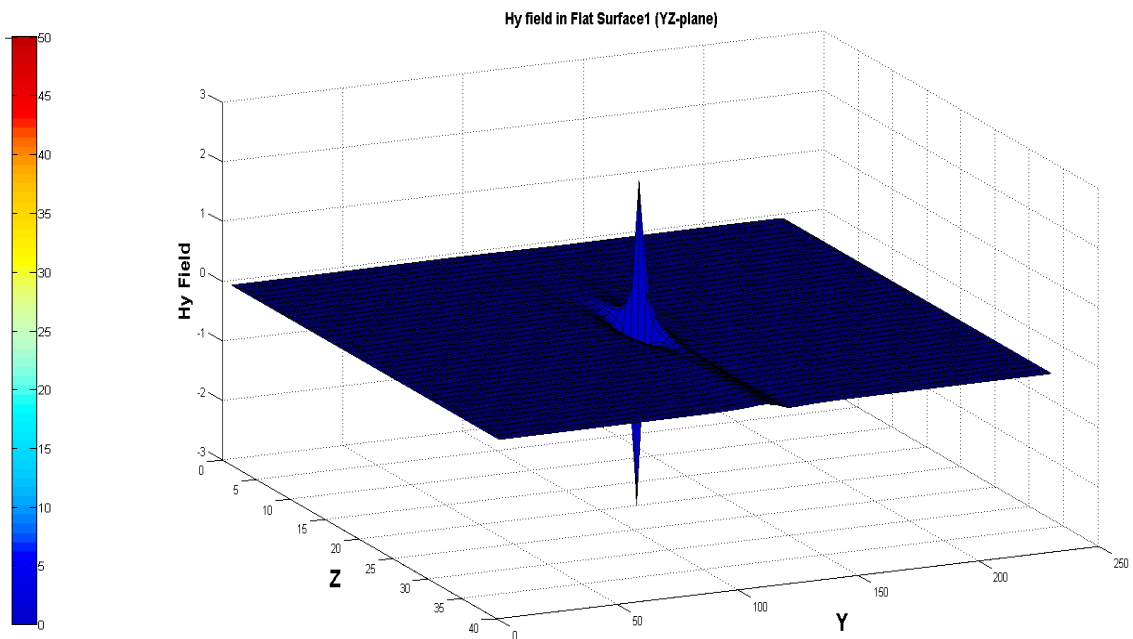
Figure 5.2.5.7.1.1 (g): H_y field distribution in the Face 1 (YZ plane)

239
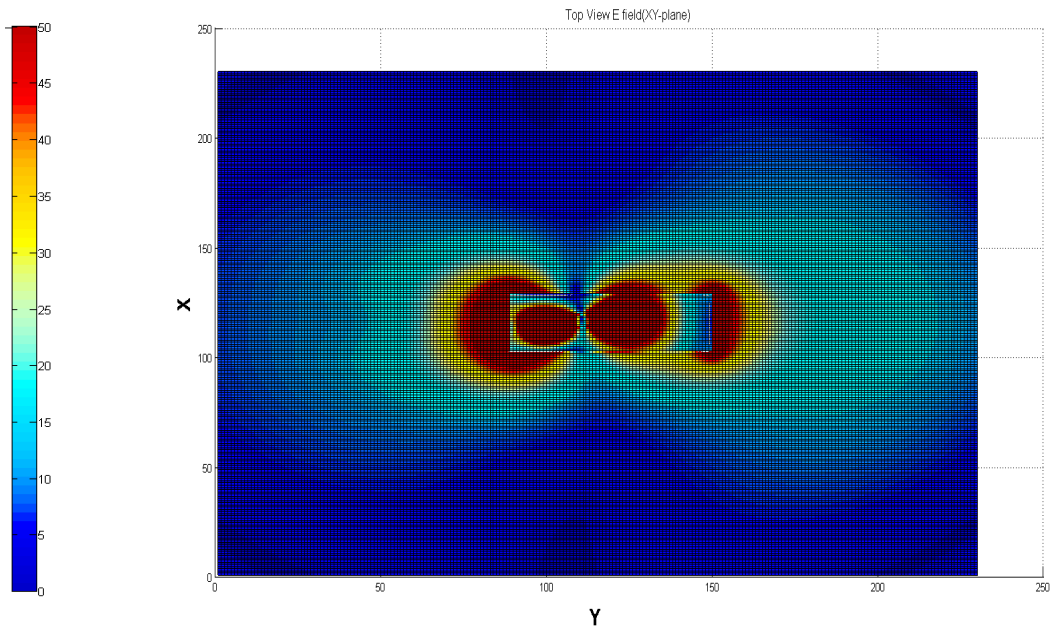
Figure 5.2.5.7.1.1 (i): E field distribution in the Top Face (XY plane)
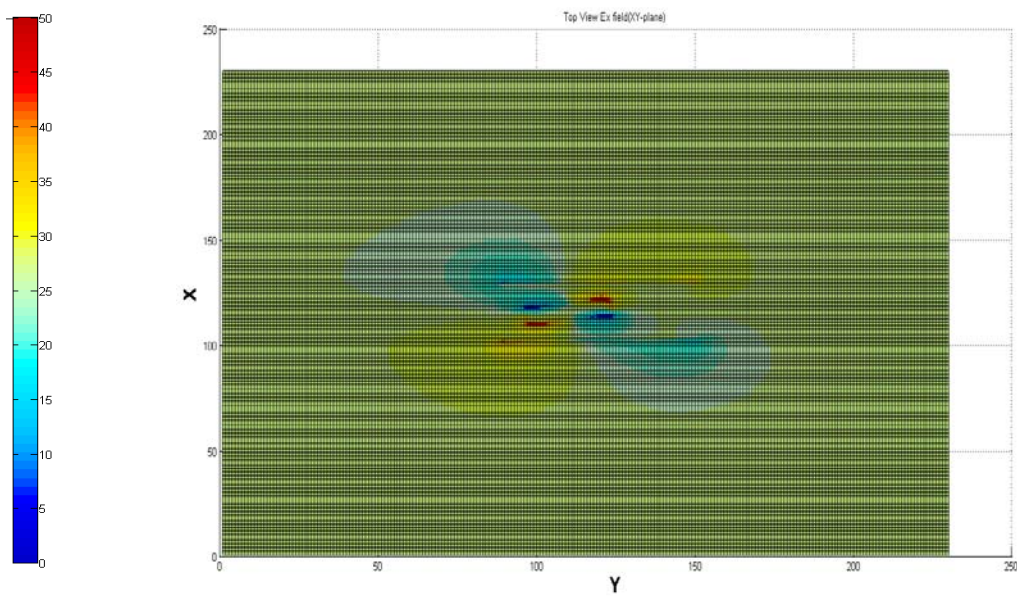
Figure 5.2.5.7.1.1 (j): E_x field distribution in the Top Face (XY plane)

240
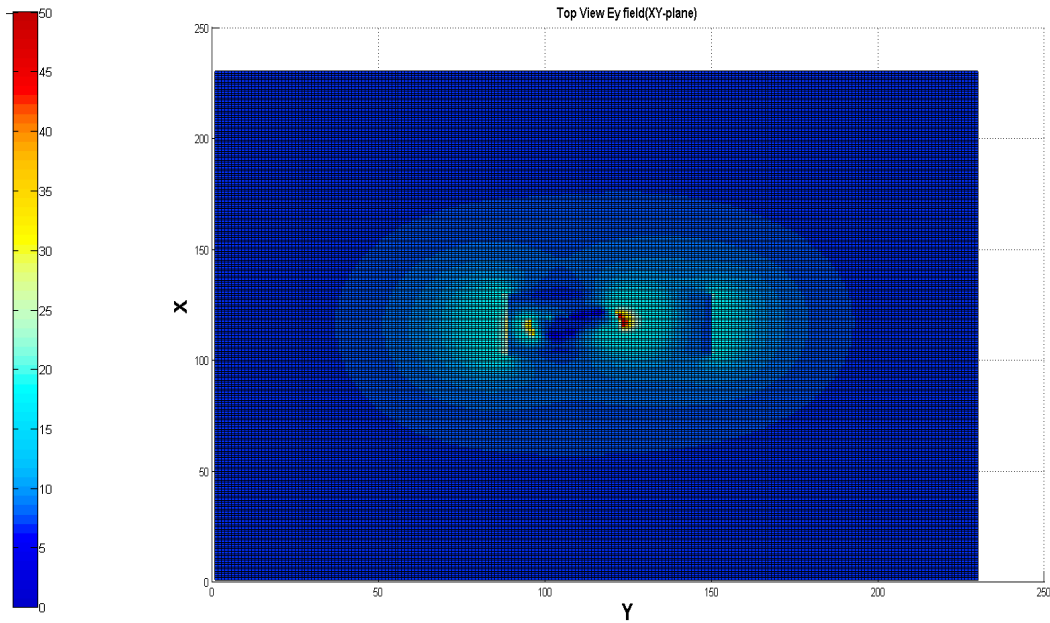
Figure 5.2.5.7.1.1 (k): E_y field distribution in the Top Face (XY plane)
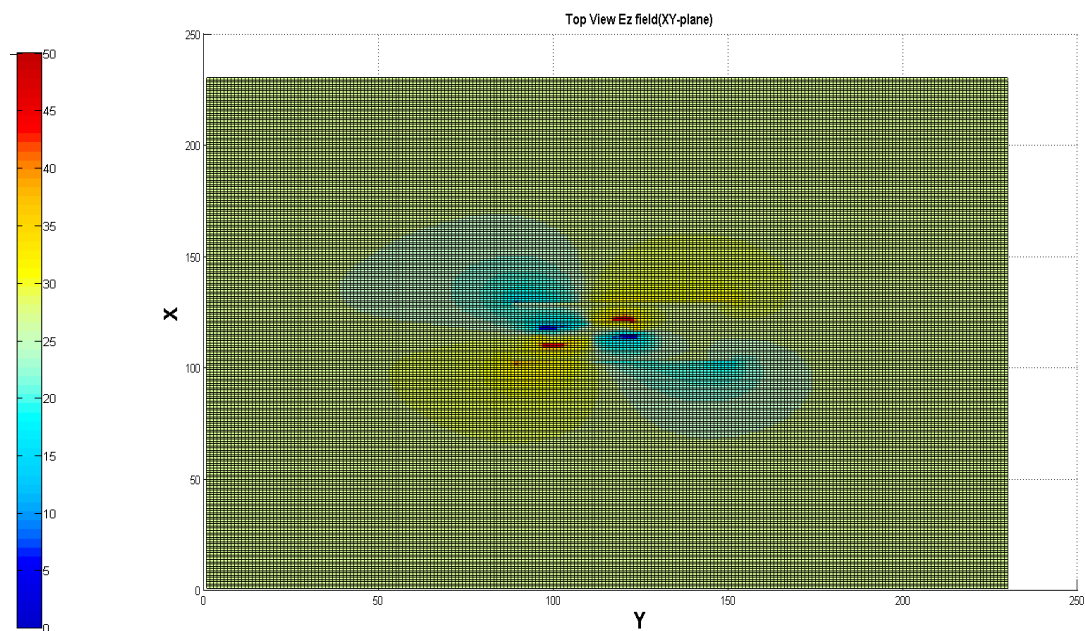
Figure 5.2.5.7.1.1 (l): E_z field distribution in the Top Face (XY plane)
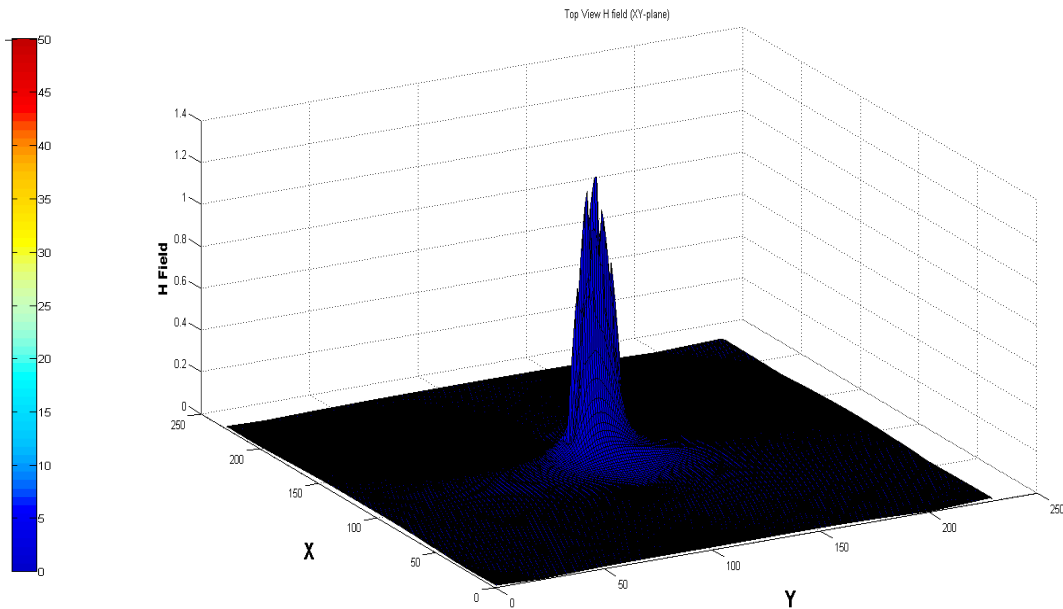
Figure 5.2.5.7.1.1 (m): H field distribution in the Top Face (XY plane)
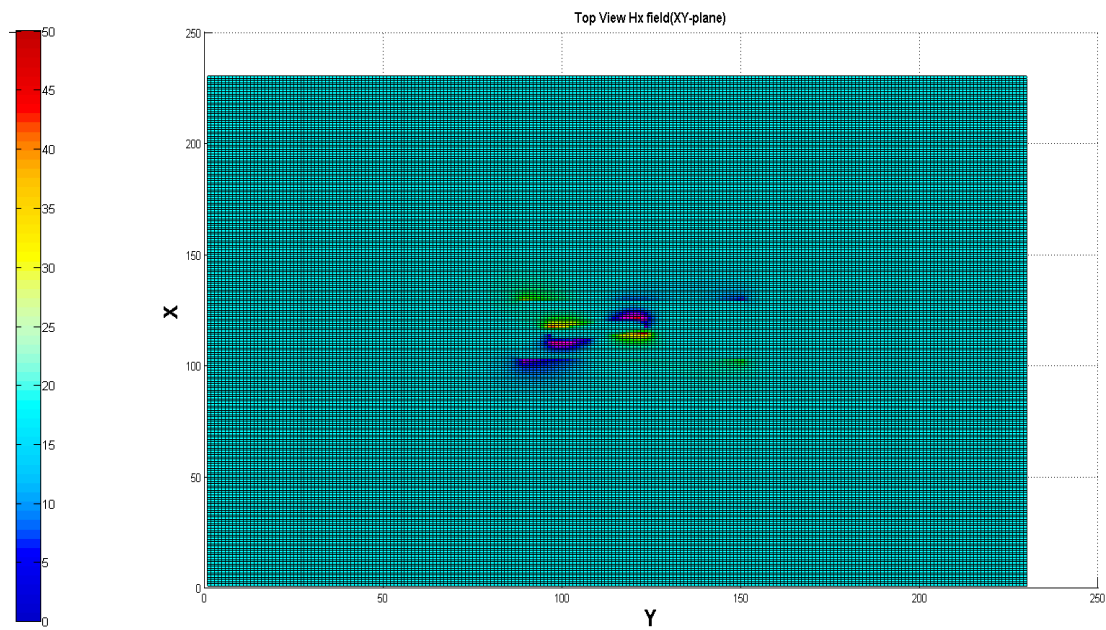
Figure 5.2.5.7.1.1 (n): H_x field distribution in the Top Face (XY plane)

242
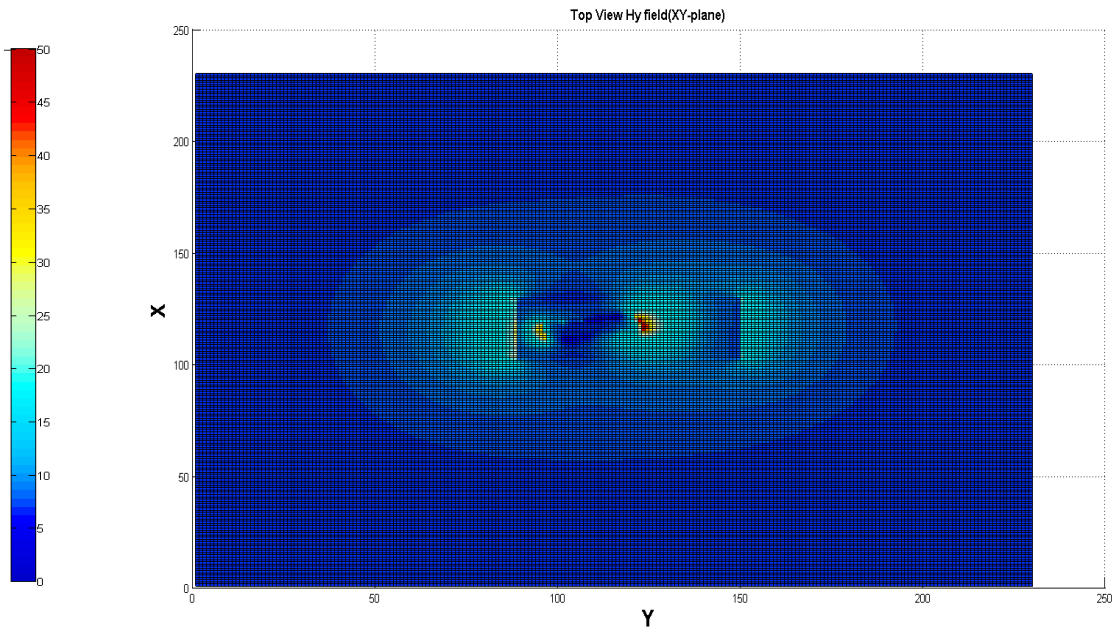
Figure 5.2.5.7.1.1 (o): H_y field distribution in the Top Face (XY plane)
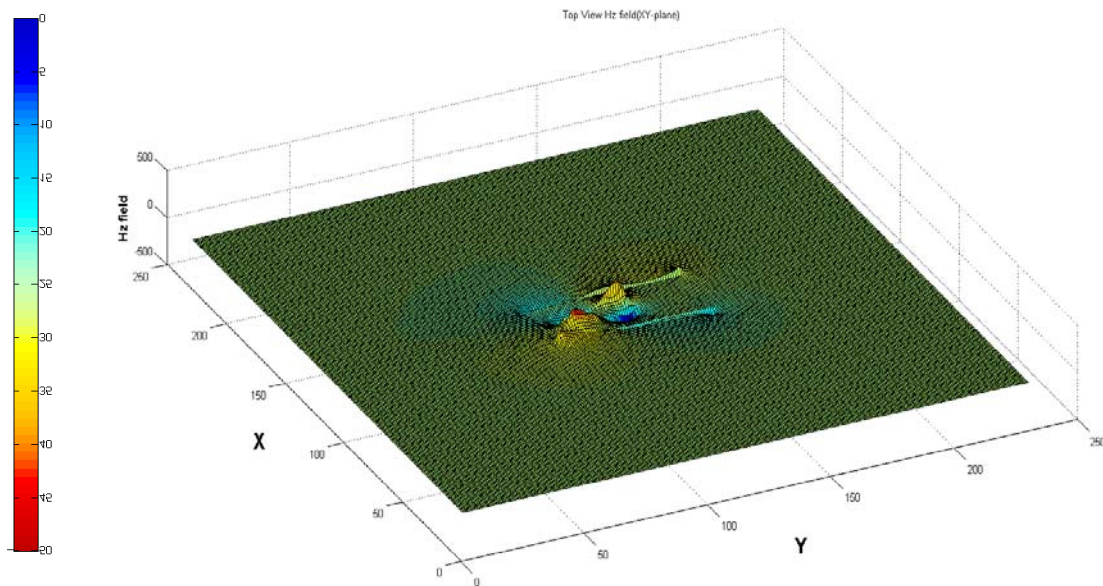
Figure 5.2.5.7.1.1 (p): H_z field distribution in the Top Face (XY plane)

243

AT 2.56 GHz
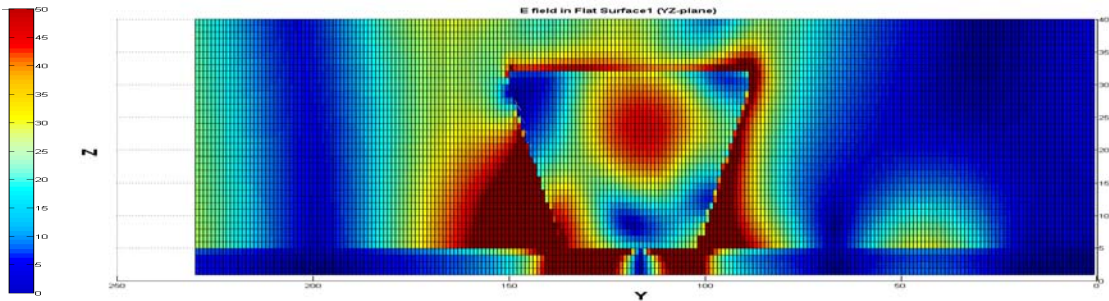
Figure 5.2.5.7.1.2 (a) : E field in face 1 of the DRA of Design 5-2 (*YZ* plane)
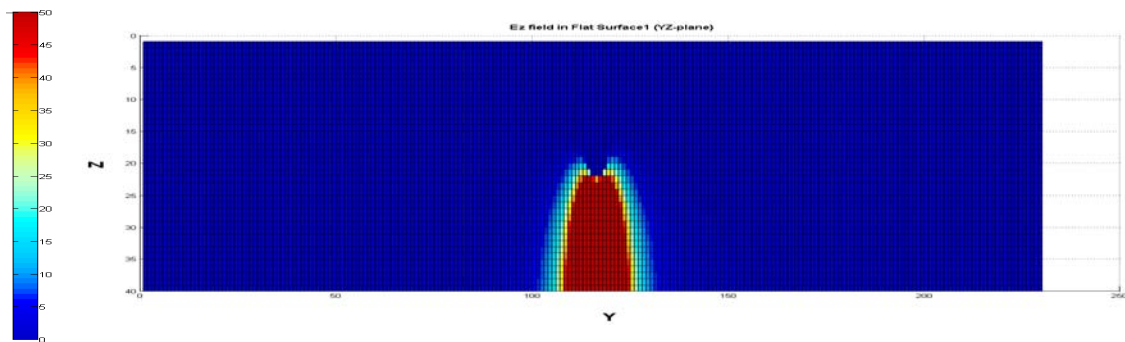
Figure 5.2.5.7.1.2 (d): E$_z$ field in face 1 of the DRA of Design 5-2 (*YZ* plane)
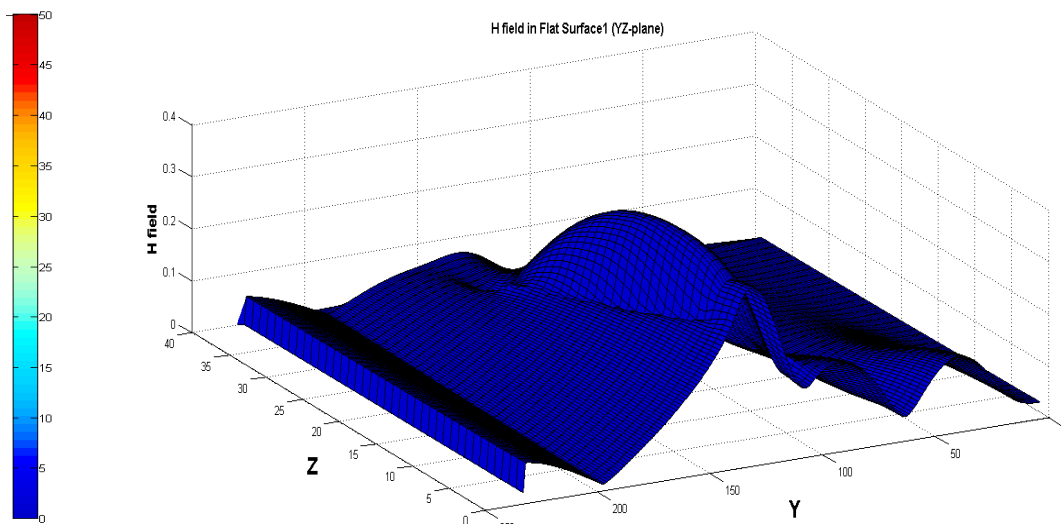
Figure 5.2.5.7.1.2 (e): H field in face 1 of the DRA of Design 5-2 (*YZ* plane)

244
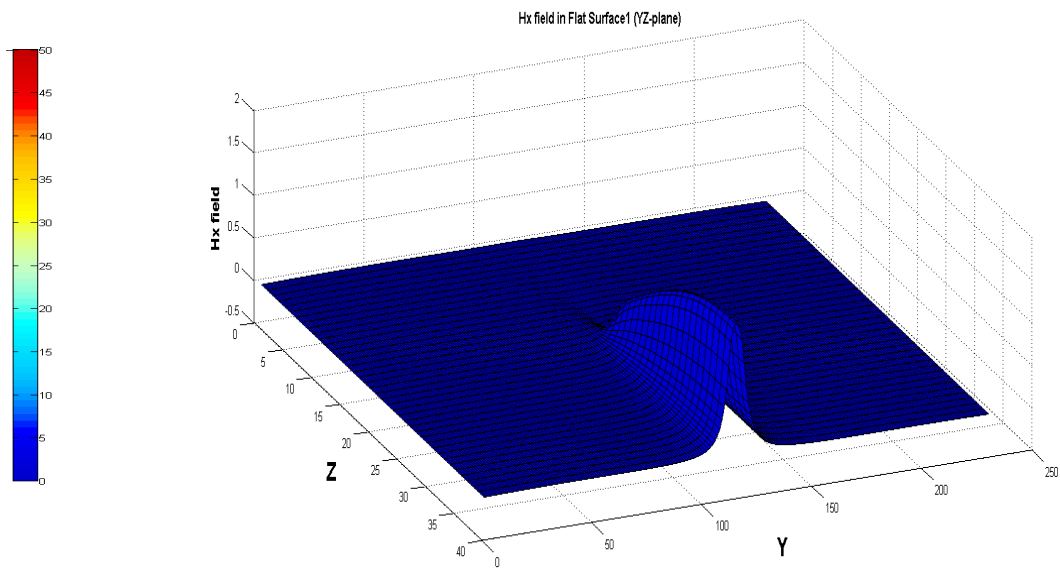
Figure 5.2.5.7.1.2 (f): H$_x$ field in face 1 of the DRA of Design 5-2 (*YZ* plane)
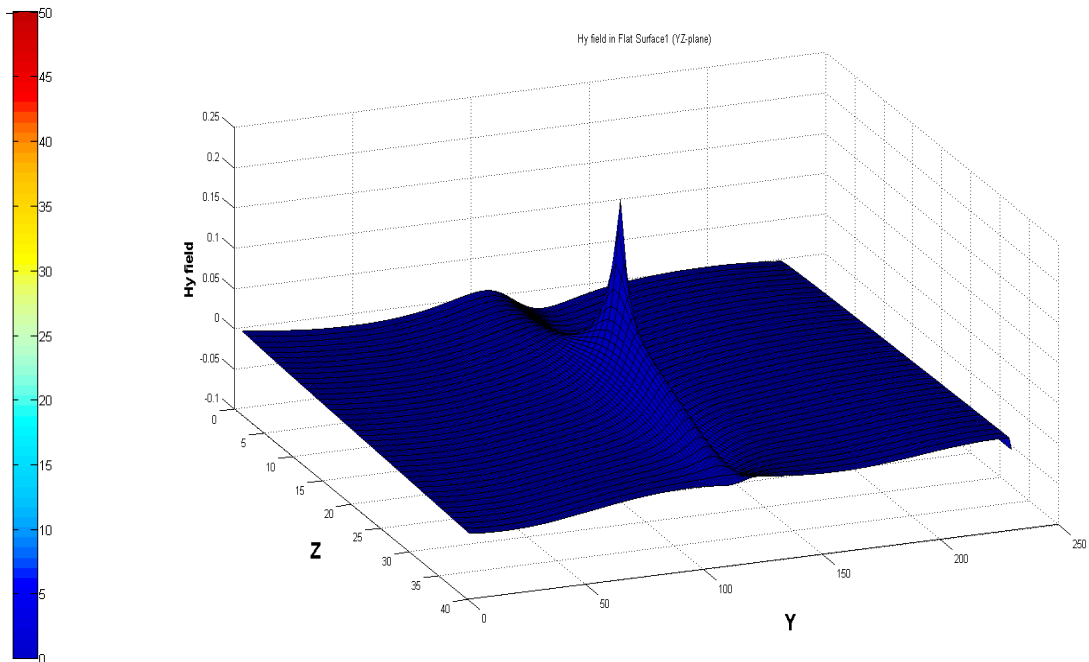
Figure 5.2.5.7.1.2 (g): H$_y$ field in face 1 of the DRA of Design 5-2 (*YZ* plane)
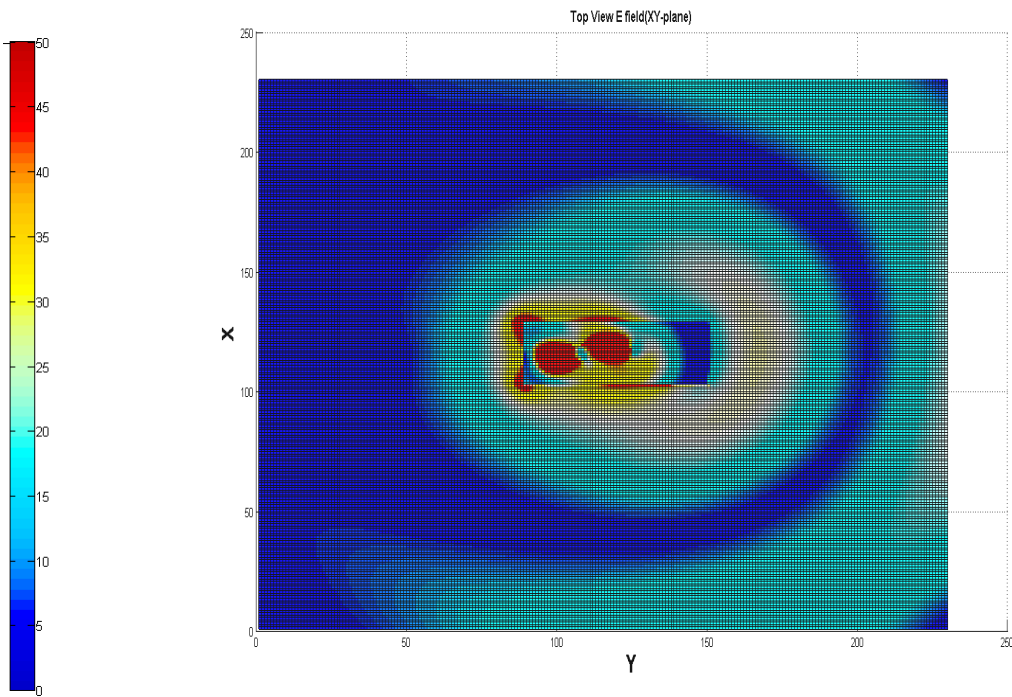
Figure 5.2.5.7.1.2 (i): E field in Top surface of the DRA of Design 5-2 (*XY* plane)
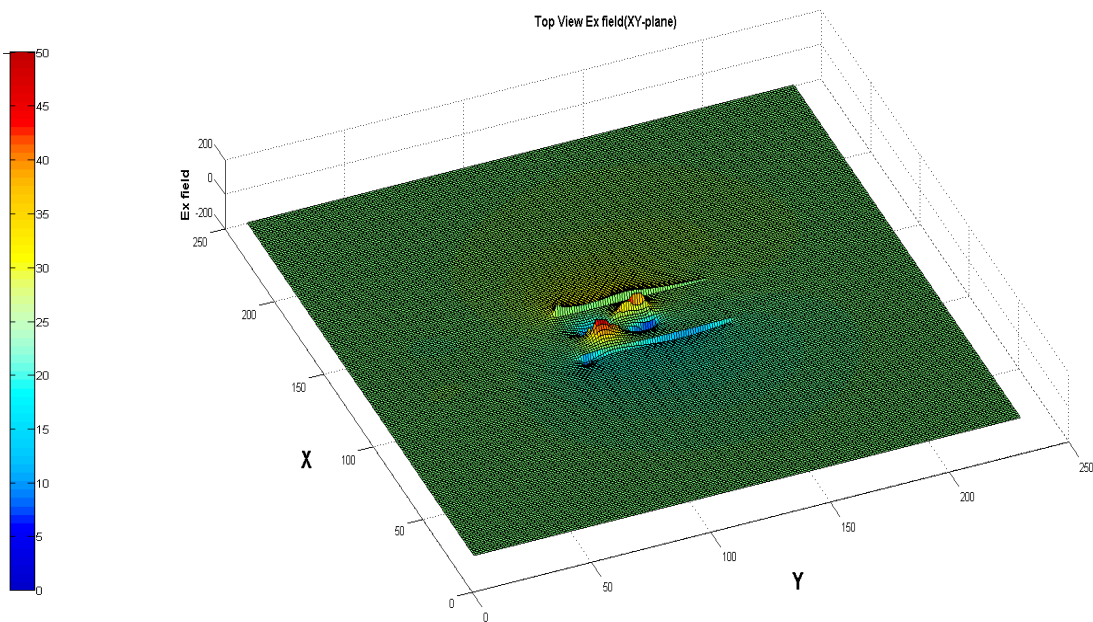
Figure 5.2.5.7.1.2 (j): E$_x$ field in Top surface of the DRA of Design 5-2 (*XY* plane)

246
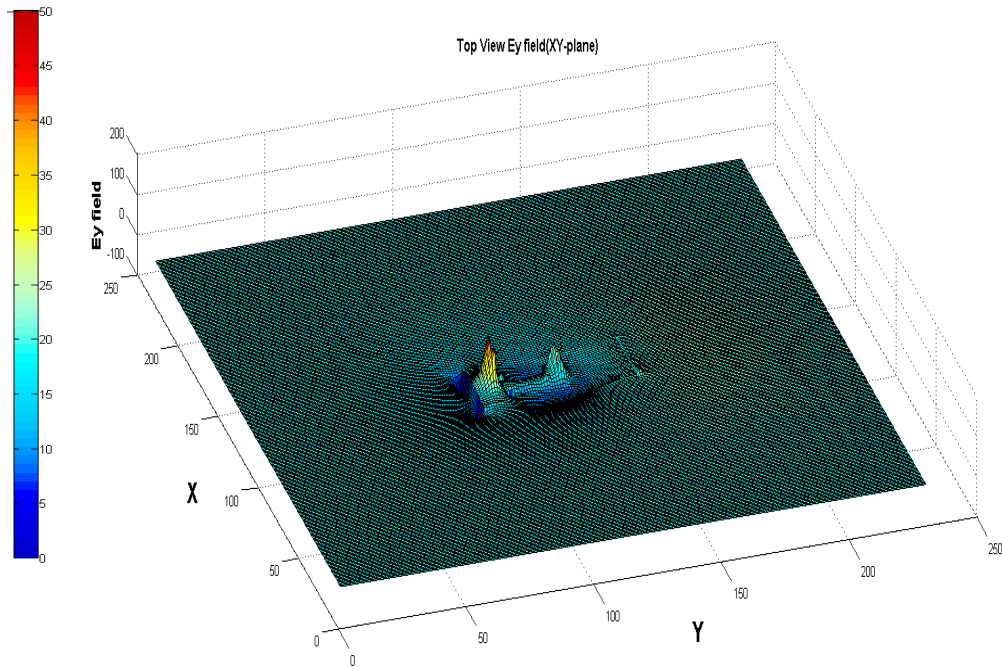
Figure 5.2.5.7.1.2 (k): E_y field in Top surface of the DRA of Design 5-2 (*XY* plane)
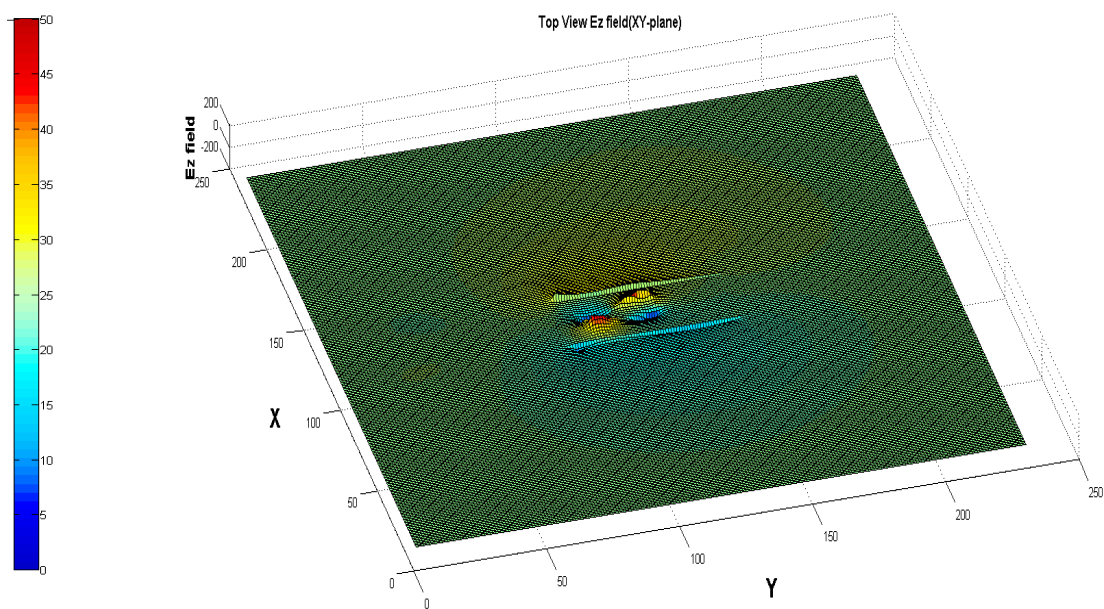
Figure 5.2.5.7.1.2 (l): E_z field in Top surface of the DRA of Design 5-2 (*XY* plane)

247
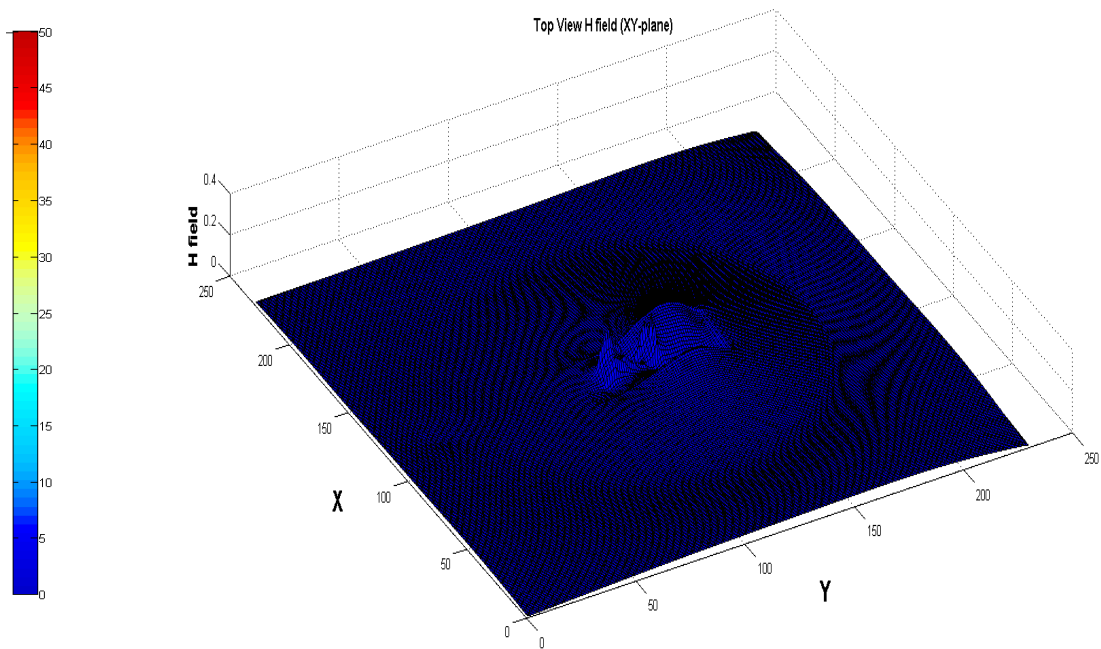
Figure 5.2.5.7.1.2 (m): H field in Top surface of the DRA of Design 5-2 (*XY* plane)
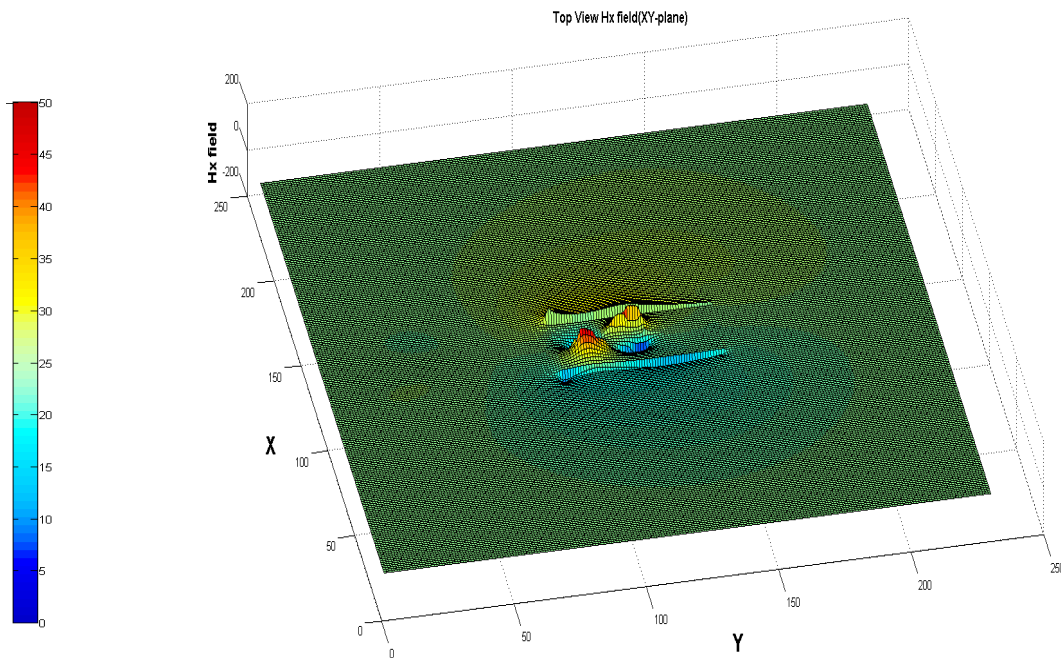
Figure 5.2.5.7.1.2 (n): H$_x$ field in Top surface of the DRA of Design 5-2 (*XY* plane)
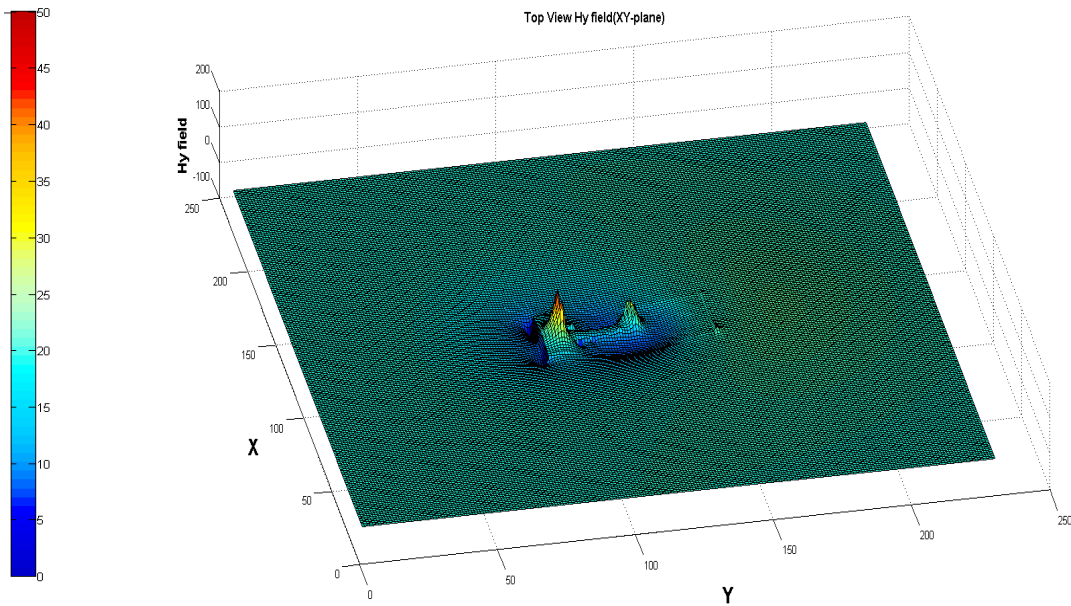
Figure 5.2.5.7.1.2 (o): H_y field in Top surface of the DRA of Design 5-2 (*XY* plane)
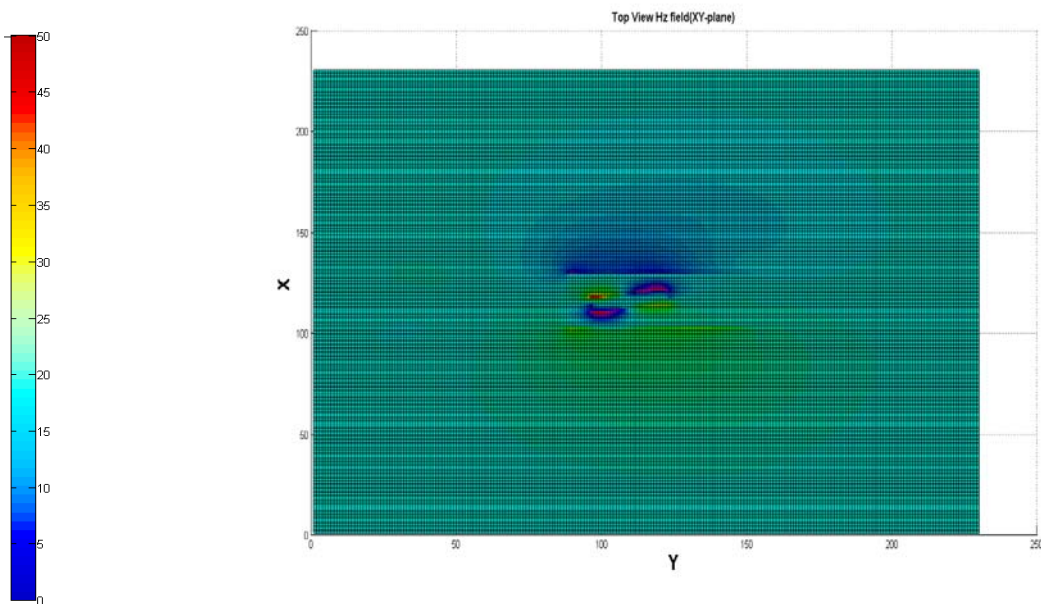
Figure 5.2.5.7.1.2 (p): H_z field in Top surface of the DRA of Design 5-2 (*XY* plane)

249

5.3. CONCLUSION

The numerical technique named FDTD was discussed in this chapter emphasizing its application in analyzing antenna problems. Starting with the basic Yee algorithm, the FDTD code for the broadband DRA was developed. Conformal method was used to model the ITDR. The input impedance, return loss and near-field patterns of the proposed DRA were computed.

REFERENCE

1. K.S. Kunz and R.J. Luebbers, "The Finite Difference Time Domain Method for Electromagnetics", *CRC Press*, 1993.

2. A. Taflove, "Computational Electrodynamics: The Finite-Difference Time-Domain Method", *Artech House*, 1995, 2-nd ed., 2000.

3. O. Hashimoto and T. Abe, "Introduction to the Finite Difference Time Domain Method", *Morikita Publ.*, 1996.

4. A. Taflove, ed., "Advances in Computational Electrodynamics: The Finite-Difference Time-Domain Method", *Artech House*, 1998.

5. T. Uno, "Finite Difference Time Domain Method for Electromagnetics and Antennas", Corona Publ., 1988.

6. D. Sullivan, "Electromagnetic Simulation Using the FDTD Method", *IEEE Press*, 2000.

7. Kane Yee "Numerical solution of initial boundary value problems involving Maxwell's equations in isotropic media" *IEEE Transactions on Antennas and Propagation,* Vol. 14, Issue:3, pg 302–307., May 1966.

8. A. Taflove "Application of the finite-difference time-domain method to sinusoidal steady state electromagnetic penetration problems". *IEEE Transactions on Electromagnetic Compatibility*, Vol. EMC-22, Issue: 3, pg 191–202., Aug. 1980.

9. Allen Taflove and Susan C. Hagness, "Computational Electrodynamics: The Finite-Difference Time-Domain Method", 3rd ed., *Artech House Publishers*., 2005. ISBN 1-58053-832-0.

10. A. Taflove and M. E. Brodwin "Numerical solution of steady-state electromagnetic scattering problems using the time-dependent Maxwell's equations", *IEEE Transactions on Microwave Theory and Techniques*, 23: Vol. 23, Issue: 8, pp. 623–630., Aug 1975.

11. K. R. Umashankar and A. Taflove, "A novel method to analyze electromagnetic scattering of complex objects". *IEEE Transactions on Electromagnetic Compatibility* : Vol. EMC-24, Issue:4, pp. 397–405., Nov. 1982.

12. J. Berenger (1994). "A perfectly matched layer for the absorption of electromagnetic waves", *Journal of Computational Physics* : Vol. 114, Issue 2, pp. 185–200., October 1994.

13. S. D. Gedney "An anisotropic perfectly matched layer absorbing media for the truncation of FDTD lattices", *IEEE Transactions on Antennas and Propagation,* Vol. 44, Issue: 12, 1630–1639, Dec 1996.

14. K.S. Yee, "Numerical solution of initial boundary value problems involving Maxwell's equations in isotropic media," *IEEE Trans. Antennas Propag*., vol.14, no.4, pp.302–307, April 1966.

15. R.F. Harrrington, "Field Computation by Moment Methods", *The Macmillian*, 1968.

16. H. Nakano, "Antenna analysis by integral equation", in Analysis Methods for Electromagnetic Wave Problems, ed. E. Yamashita, Chap3, Corona Publ., 1993.

17. M. Koshiba, "Fundamentals of Finite Element Method for Optics and Wave Motion", Morikita Publ., 1990.

18. Toru UNO, "Antenna Design Using The Finite Difference Time Domain Method", *IEICE Trans. Commun.*, Vol. E88–B, No. 5, May 2005.

19. Y. Kagawa, N. Yoshida, T. Tsuchiya, and M. Sato, "Introduction to the Spatial Equivalent Network Method", Morikita Publ., 2000.

20 A. Ishimaru, "Electromagnetic Wave Propagation, Radiation and Scattering", Chap.18, Prentice Hall, 1991.

21. M. Haneishi, K. Hirasawa, and Y. Suzuki, "Planar and Small Antennas", Chap.8, Corona Publ., 1996.

22. J.-F. Lee, R. Lee, and A. Cangellaris, "Time-domain finite-element methods," *IEEE Trans. Antennas Propag.*, vol.45, no.3, pp.430–442, March 1997.

23. G. Cerri, R. Russo, and A. Schiavoni, "Electromagnetic coupling between arbitrarily bent wires and scatterers analysed by a hybrid MoMTD/FDTD approach," *IEE Proc. Microwave Antennas Propag.*, vol.147, no.4, pp.261–266, Aug. 2000.

24. R. Luebbers, K. Kumagai, S. Adachi, and T. Uno, "FDTD calculation of transient pulse propagation through a nonlinear magnetic sheet," *IEEE Trans. Electromagn. Compat.*, vol.35, no.1, pp.90–94, Jan. 1993.

25. A. Taflove and M. E. Brodwin, "Numerical Solution of Steady-State Electromagnetic Scattering Problems Using the Time-Dependent Maxwell's Equations", *IEEE Microwave Theory Tech*, Vol. 23, pp 623–630, August 1979

26. A. Reineix and B. Jecko, "Analysis of Microstrip Patch Antennas Using Finite Difference Time Domain Method", *IEEE Trans. on Antennas Propag.*, Vol. 37, pp 1361–1369, November 1980

27. A. C. Cangellaris and D. B. Wright, "Analysis of the Numerical Error Caused by the Stair-Stepped Approximation of a Conducting Boundary in FDTD Simulations of Electromagnetic Phenomena", *IEEE Trans. Antennas Propagat.*, Vol. 39, pp. 1518–1525, October 1991

28. N. Kaneda, B. Houshm, and T. Itoh, "FDTD Analysis of Dielectric Resonators with Curved Surfaces", *IEEE Trans. Microwave Theory Tech.*, vol. 45, pp. 1645–1649, September 1997

29. S. Dey and R. Mittra, "A Conformal Finite-Difference Time-Domain Technique for Modeling Cylindrical Dielectric Resonators", *IEEE Microwave Theory Tech.*, Vol. 47, pp 1737-1739, September 1999.

30. W. Yu, and R. Mittra, "A Conformal Finite Difference Time Domain Technique for Modeling Curved Dielectric Surfaces", *IEEE Microwave Wireless Comp. Lett*, Vol. 11, pp 25-27, January 2001

31. X. Zhang and K. K. Mei, "Time Domain Finite Difference Approach to the calculation of the Frequency Dependent Characteristics of Microstrip

Discontinuities", *IEEE Trans. Microwave Theory Tech.*, Vol. 36, pp 1775-1787, December 1988

32. R. J. Luebbers and H. S. Langdon, "Simple Feed Model that Reduces Time Steps Needed for FDTD Antenna and Microstrip Calculations", *IEEE Trans. on Antennas Propag.*, Vol. 44, pp. 1000-1005 , July 1996.

33. G. Mur, "Absorbing Boundary Conditions for the Finite-Difference Approximation of the Time-Domain Electromagnetic Field Equations", *IEEE Trans. Electromag. Compatibility*, Vol. 23, pp 377–382, November 1981

34. J. P. Berenger, "A Perfectly Matched Layer for the Absorption of Electromagnetic Waves", *Jour. Comput. Phys.*, Vol. 114, pp185–200, October 1994

CHAPTER 6   **CONCLUSION AND FUTURE SCOPE**

The experimental and simulation studies on a novel dielectric resonator antenna with isosceles trapezoidal geometry are discussed. The characteristics of the antenna when excited with microstrip feed is described for different orientations by showing the reflection coefficient, 2D radiation pattern, half power beam width (HPBW), cross polar level, gain, input impedance, 3D gain pattern etc. The antenna performance is optimized for the feed location, offset length of the feed strip, dimensions of the slot in ground plane, slanted and parasitic strips etc. The radiation patterns for all the configurations are generally broadside, like a horizontal magnetic dipole.

Design 1-1 propose an antenna operating at a centre frequency of 2.46 GHz with a bandwidth of 11.6% and an average gain of 5.38. The antenna covers important application band of ISM: Bluetooth/ WLAN 2.4/ Wibree (802.11 b/g/n)/ ZigBee. As it is operating in the ISM band, it can as well be used in medical tomographic set up described in appendix-B.

In Design 3-1, the DR orientation is excited with microstrip feed and optimized for a position corresponds to dual frequency bands with good gain and polarization characteristics. In many cases dual frequencies are obtained by using either dual feed lines or a hybrid radiating structure, which may cause design complexity. But this antenna is unique in the sense that it is capable of producing dual frequencies with a single feed, without using any hybrid structure.

Most of the antennas adopt microstrip structures with two separate feeds excited by orthogonally polarized waves to realize the dual band and dual polarization function. Microstrip antenna has good performances in lower frequency, however in higher frequency, the radiation efficiency deteriorates apparently. Compared to the microstrip antenna, the radiation efficiency of the dielectric resonator antenna is as high as 95% even for frequencies up to 10 GHz, due to the absence of inherent conductor losses. Design 4-1 presents a dual band dual polarized (DBDP) antenna with a simple compact DRA with single feed alone. Here the single antenna substitutes the function of two separate antennae with different polarization and in that sense this is a compact and simple design. If the dimensions and permittivity of the DRA is varied along with the use of suitable impedance matching mechanisms, the proposed antenna can be tuned to use in the practical application bands such as the bands of 2.4/5 GHz WLAN etc.

In design 5-1, a new design of compact ITDRA with slotted ground plane is introduced. It is found that by properly embedding two pairs of narrow slots in the ground plane of an Isosceles Trapezoidal DRA, a wide band response is obtained. It also resulted in lowering of the antenna's fundamental resonant frequency. A reduced antenna size at a fixed frequency can thus be achieved for the proposed design.

Design 5-2 is a modified wideband design of Design 5-1, where the shape of the slot is optimized as in the form of a fish bone structure and the orientation of the DR is also changed. Increase in bandwidth is the result of merging multiple resonances originated in close neighborhood by the slot provided in the ground plane. The antenna offer an impedance band width of 21.5% centered at 2.51GHz and covers important application bands viz. ISM: Bluetooth/ WLAN 2.4/ Wibree (802.11 b/g/n)/ ZigBee,

WiBro and DMB similar to the above design. Although the radiation characteristics are almost similar, the reflection characteristics are better in the case of Design 5-2 when compared to Design 5-1.

All configurations shows broad side radiation patterns with moderately good gain and half power beam width (HPBW). Hence it is observed that ITDRA can act as a suitable candidate for wireless communication where a compact antenna is required with wide range of applications like multi band operation, dual band dual polarization operation and wideband operations. The radiation pattern is observed to be broad at different frequencies. A comparison with the simulated results using HFSS is also done and the results are discussed. Mode analysis is done by sketching the field distribution on ITDRA using HFSS.

Main features of the work are:

❖ **A new geometry, Isosceles Trapezoidal shaped DRA is introduced to the wireless communication system.**

❖ **The antenna can be used for designing dual band dual polarization operation with single feed.**

❖ **It can be used for Multi band operation.**

❖ **Can be used for Wide band application with slotted ground plane structure.**

❖ **Wide band operation covers important application bands viz. ISM: Bluetooth/ WLAN 2.4/ Wibree (802.11 b/g/n)/ ZigBee, WiBro and DMB.**

❖ **Slotted ground plane structure is resulted in reduced antenna size.**

❖ **Gain of ITDRA is high compared to other shapes.**

❖ **ITDRA excited by microstrip transmission line generally gives broadside radiation pattern as a horizontal magnetic dipole does.**

6.1 SCOPE OF FUTURE WORK

The effect of material properties on antenna performance such as antenna gain efficiency, radiation pattern, band width etc. can be studied. The validity of ITDRA for circular polarization can be tested by giving two feeds simultaneously. Investigations can be carried out with probe feed and proximity feed for the performance of the antenna. Possibility of incorporating components like microwave diodes, inductors, capacitors etc. in the antenna, in order to modify its properties for the purpose of band notching, beam scanning etc. can be tried. Other feeding techniques such as slot feed and coplanar waveguide feed can be attempted as a better alternative to the microstrip feed.

APPENDIX A   **AN INVESTIGATION OF WIDEBAND CIRCULAR CYLIDRICAL SECTOR DIELECTRIC RESONATOR ANTENNA WITH MICROSTRIPLINE FEED**

The letter proposes a compact microstrip line fed dielectric resonator antenna with half split circular cylindrical profile which is experimentally investigated. It shows that at optimum parameters, this low profile, small size antenna gives a wideband response similar to that of its full cylindrical counterpart with moderate gain but at different frequency. The return loss and radiation pattern of the proposed antenna are measured and studied. The simulated and measured results verify that the proposed antenna offers an impedance bandwidth of 36.7% (from 3.24GHz to 4.70 GHz) and shows a radiation pattern which is relatively conical in shape with linear polarization.

A1. INTRODUCTION

The dielectric resonators (DRs) were originally proposed as antennas in the early 1980s [1] and various configurations, geometrical shapes and feed mechanisms have been investigated in the following years. It provides an efficient radiating structure in the upper microwave and lower millimeter wave frequency bands, where its minimal ohmic loss gives it an inherent advantage over more conventional antennas. It has been shown that a dielectric resonator antenna (DRA) can be excited by either a coaxial probe or a microstrip transmission line [1, 2]. But the bandwidth of a common DRA is typically below 10%. Investigations of the DRA initially concentrated on low permittivity materials (dielectric constant $\varepsilon_r \sim$ 5-30) to enhance the radiation capability and antenna bandwidth. Simple and easy excitation arrangements had been reported for various

259

antenna configurations to provide wide bandwidth, flexible polarization adjustment and high radiation efficiency which make DRAs by far superior to conventional microstrip patch antennas [3]. In order to enhance the bandwidth, various techniques have been developed for DRAs, such as coplanar parasitic DRAs [4], stacked DRAs [5], [6] or various shaped DRAs [7].

It is shown here that by selecting optimum parameters like height and breadth of vertical feed-strip and its offset distance from the open end of the microstrip feed line, a wideband response with a moderate gain could be achieved for a half split dielectric resonator antenna which is comparable to the result obtained in its full cylindrical counterpart as reported in [8].

A2. PROPOSED GEOMETRY AND THEORY

The proposed antenna configuration used for the study is shown in Figure 1. A circular cylindrical sector dielectric resonator antenna of radius 2a = 24mm, and thickness d =7.3mm having a dielectric constant of ε_{rd} = 20.8 is used and is fed by a 3mm wide microstrip transmission line which is fabricated on a microwave substrate of ε_{rs}= 4 with a size of 115mm X 115mm X 1.6mm. DRA is mounted with its curved surface on the substrate symmetrically with the feed line which is directed along Y-axis. Surface area of the antenna from which radiation is emerged is increased due to this configuration. Besides, the newly raised rectangular flat surface area in the cut away section of the cylindrical sector DRA, contributes to increased total surface area compared to its cylindrical counterpart [8]. As it reduces the (volume/surface area) ratio and thereby the resonant Q-factor (Q_r) of the antenna, the bandwidth of the antenna increases.
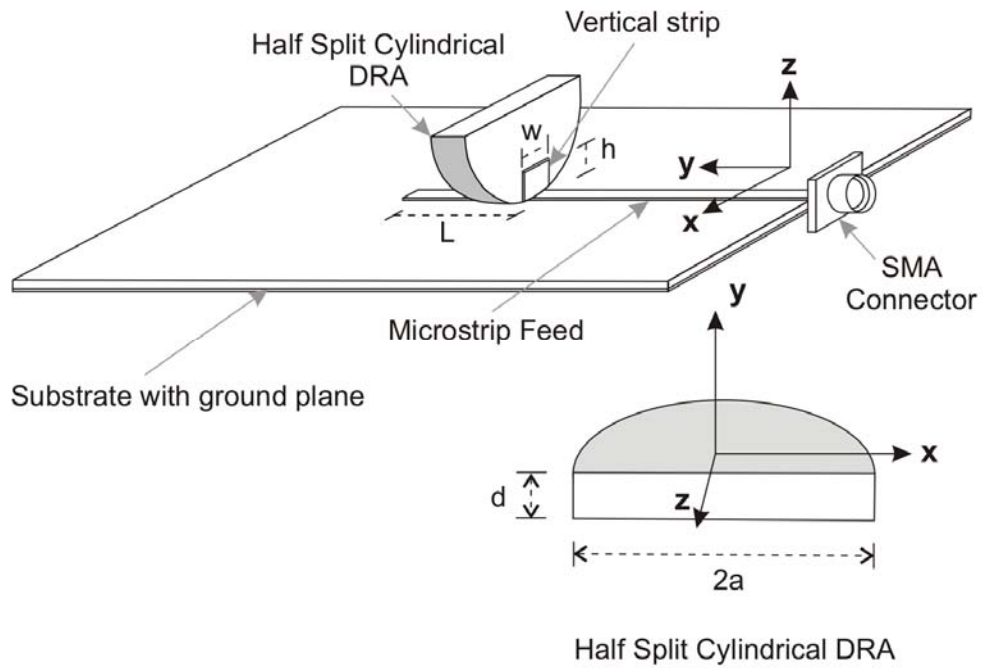
Figure A2.1: Geometry of the proposed antenna
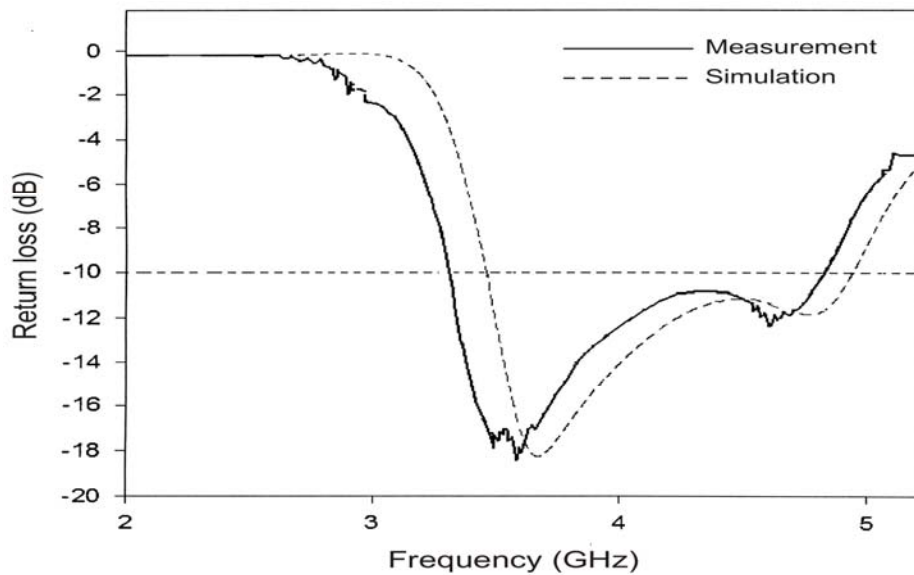
Figure A2.2: Return loss of the proposed antenna

A vertical metallic strip is adhered to one of the half circular flat surface of the DRA and is connected with the microstrip line at a length *L* from its open end. The width *w* and height *h* of the vertical strip line and the offset length *L* are the key factors that are varied for obtaining the optimum condition for a good result.

A3. RESULTS AND DISCUSSION

The antenna characteristics are measured using an HP 8510C vector network analyzer. Ansoft HFSS is used for computer simulation. $\left|S_{11}\right|$ is measured for different values of *L* for a particular width *w* and height *h* of vertical strip. It is found that for an offset length *L* =13mm, the maximum band width is obtained. Keeping this value unchanged, *h* is varied for a constant value of *w* and again the maximum BW is found out. Finally, for these optimum values of *L* and *h*, the best possible value of *w* is achieved. Thus it is established that for a combination of *L* = 13mm, *h* = 4mm and *w* = 8mm, a maximum impedance bandwidth of 36.7% is obtained from 3.24 to 4.70 GHz. The broadband response is due to multiple radiating modes having similar radiating properties like $TM_{21\delta}$ mode that are merged together when excited by this arrangement. Measured and simulated plot of return loss ($|S_{11}|$), of the DRA are compared in Figure 2 and shown that they are in good agreement. Different orientations of the antenna with respect to the microstrip line feed is also tried out for studies and verified that the proposed one gives the best result. Plot of input impedance against frequency which is shown in Figure 3 confirm that the impedance matching between the feed and the antenna is occurred at frequencies corresponding to the resonant modes.
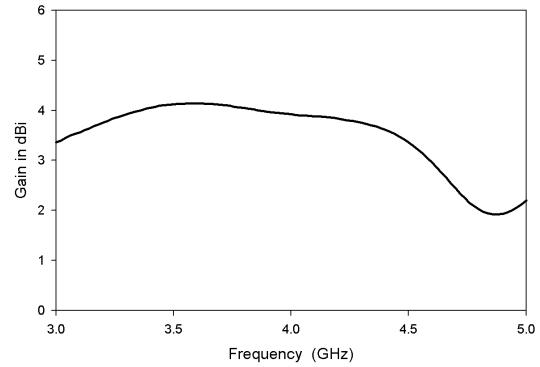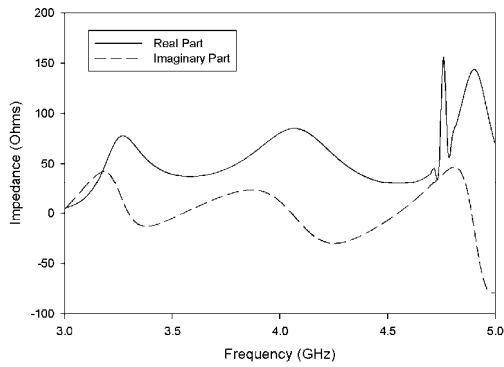
Figure A3.1: Input Impedance vs Frequency

Figure A3.2: Gain of the proposed antenna
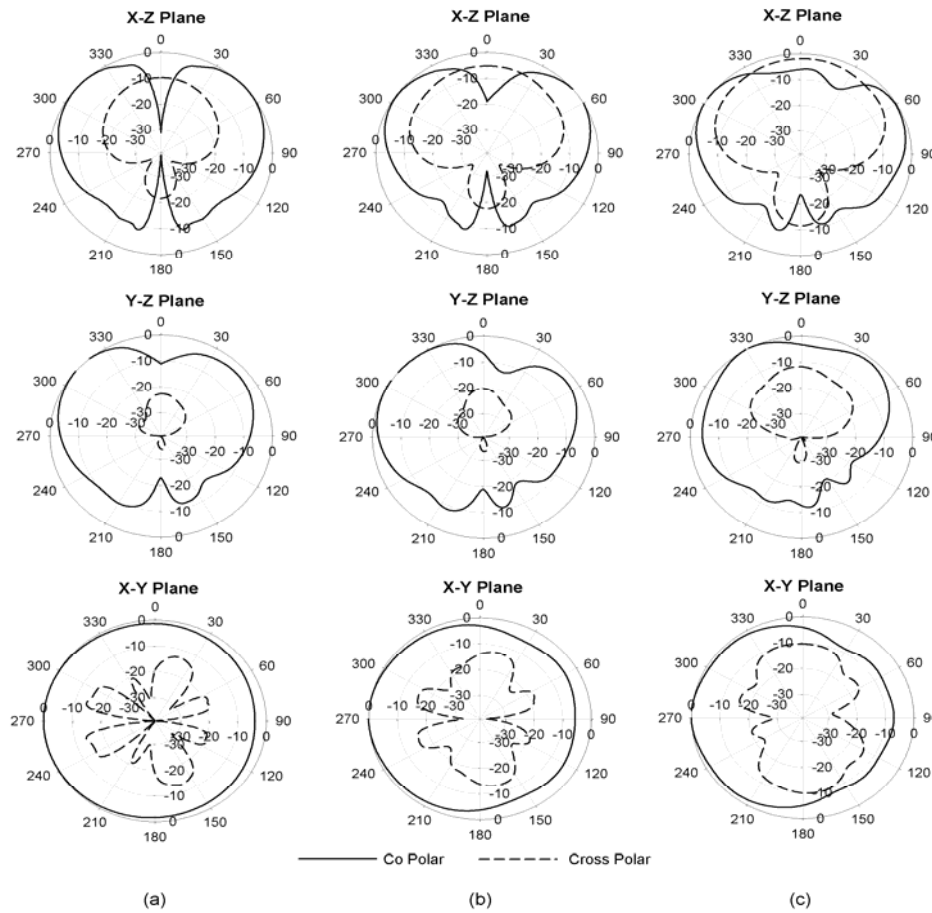
Figure A3.3: Radiation patterns at (a) 3.44 GHz, (b) 4 GHz and (c) 4.54 GHz

263
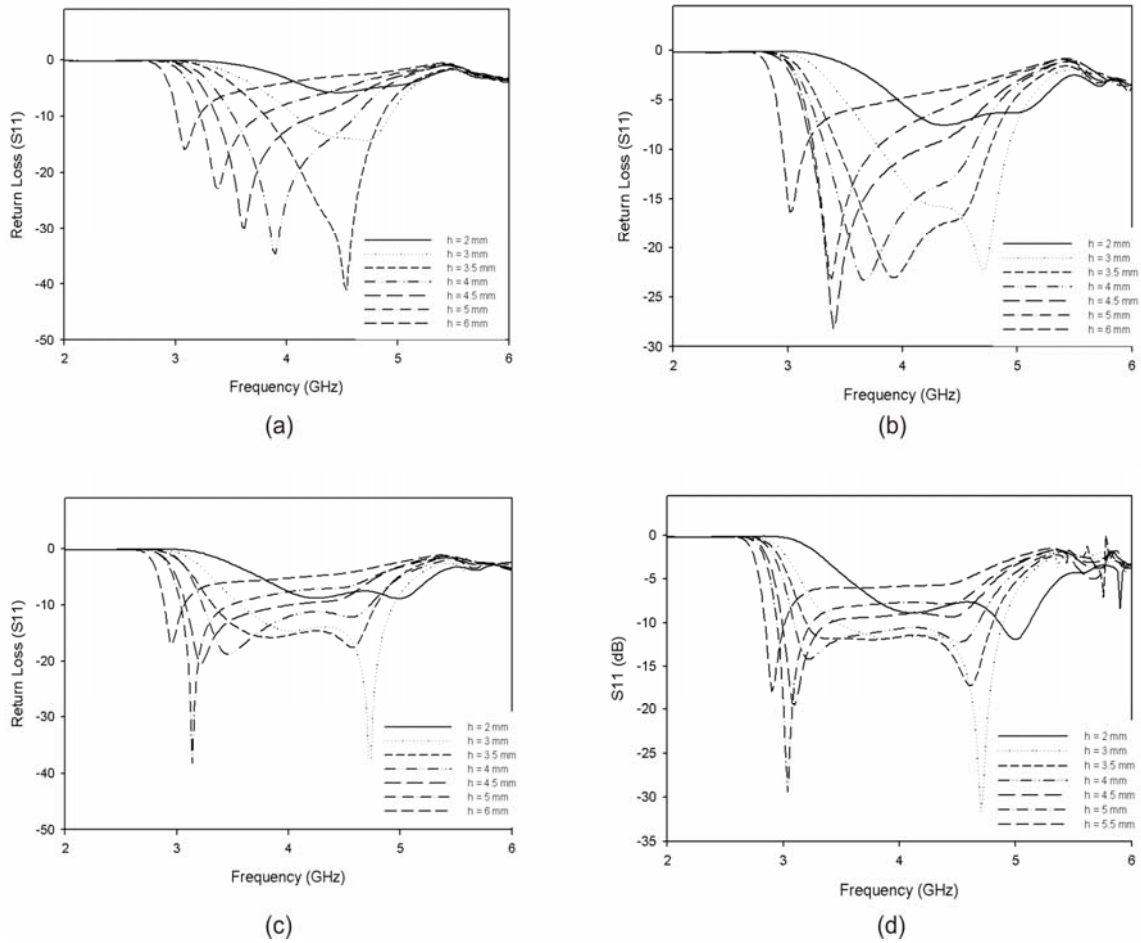
Figure A3.4: Effect of '*W*' and "*h*" on the return loss of the antenna (a) *W* = 4mm, (b) *W* = 6mm, (c) *W* = 8mm and (d) *W* = 10mm.

The antenna gain of this configuration is also studied. It is found that a maximum gain of 4.14 dBi with an average value of 3.03 dBi is obtained as shown in Figure 4. Far field radiation patterns are measured by setting a double ridged broadband horn antenna as the transmitter and the DRA as the receiver. Measured radiation patterns of the antenna at the three resonant frequencies are shown in Figure 5. It is apparent that the pattern is relatively conical in shape with low cross-polarization levels. The antenna is found to be linearly polarized. It is noted that the co-polar patterns in the elevation planes at all frequencies are acceptably similar with significant differences only in the cross-

polar levels. Hence this verifies that the antenna gives similar radiation characteristics for the entire useful band. The XZ plane pattern is symmetrical as the DRA is placed symmetrical to the feed. XY plane patterns of the antenna are omni-directional as in a monopole antenna.

Width W	Height h	Frequency Band (GHz)	% Bandwidth
4 mm (0.053λ)	4 mm (0.053λ)	3.50 - 4.60	27.16
6 mm (0.08λ)	4 mm (0.053λ)	3.20 - 4.60	35.89
8 mm (0.106λ)	**4 mm** (0.053λ)	**3.24 - 4.70**	**36.77**
10 mm (0.133λ)	4 mm (0.053λ)	3.18 - 4.60	36.50

Table A3.1: Reflection characteristics of the DRA for optimum *h* and *W*

Measured return loss ($|S_{11}|$) of the DRA for various heights (*h*) and widths *(w)* of vertical strip are shown in Figure 6g (a)-(d). The results indicate that for a given *W* an optimum value of *h* gives maximum impedance bandwidth. For lower values of *W,* the impedance bandwidth is proportional to it. However it is seen that as *h* is increased, the band is shifted to the lower frequency end. Hence h and *W* roughly are the parameters which can be used for tuning the impedance bandwidth of the DRA. It is also noted that the resonant characteristics are more influenced by the height *h* of the strip than by its width *w*. Table I summarizes the reflection characteristics for optimum combinations of *h* and *W*. A maximum bandwidth of 36.77 % from 3.24 to 4.70 GHz is obtained for *h* = 4 mm (0.053λ) and *W* = 8 mm (0.106λ). From the measured results in Table I, optimum

value of h can be expressed approximately as $h \approx \dfrac{\lambda_0}{4\sqrt{\varepsilon_{rd}}}$ where λ_0 is the free space

wavelength at the mid band frequency and ε_{rd} the dielectric constant of the DRA.

A4. CONCLUSION

A compact wideband DRA has been experimentally investigated. The results show that the proposed antenna offers more than 36% impedance bandwidth from 3.24 to 4.70 GHz, which covers several important application bands in WiMAX standard. By optimizing design, it can also be used for vehicular and indoor mobile communications. The antenna radiation is conical and stable within the operating band. Furthermore, this antenna configuration is very easy to construct and is suitable for integration with MIC's.

REFERENCES

1. S.A. Long, M.W. McAllister, and L.C. Shen, The resonant cylindrical dielectric cavity antenna, *IEEE Trans.,* Antennas *Propag.*, 31 (1983), pp. 406-4 12.

2. J.T.H. St. Martin, Y.M.M. Antar, A.A. Kishk, A. Ittipiboon and M. Cuhaci Dielectric resonator antenna using aperture coupling, *Electron. Lett.,*26 (1990), pp. 2015-2016.

3. R. K. Mongia, A. Ittipibon and M. Cuhaci, Measurement of radiation efficiency of dielectric resonator antennas, *IEEE Microwave Guided Wave Letters*, 4 (March 1994), no. 3, pp 80-82.

4. Z. Fan and Y. M. M. Antar, Slot-coupled DR antenna for dual-frequency operation, *IEEE Trans Antennas Propag.*, 45 (Feb. 1997), no. 2, pp. 306–308.

5. A. A. Kishk, X. Zhang, A.W. Glisson, and D. Kajfez, Numerical analysis of stacked dielectric resonator antenna excited by a coaxial probe for wideband applications, *IEEE Trans Antennas Propag.*, 51 (Aug. 2003), no. 8, pp. 1996–2005.

6. M. H. A Sharkawy, A. Z. Elsherbeni, and C. E. Smith, Stacked elliptical dielectric resonator antennas for wideband, *Proc. IEEE Antennas and Propagation Society Int. Symp.*, 2 (2004), pp. 1371–1374.

7. A. A. Kishk, Wide-band truncated tetrahedron dielectric resonator antenna excited by a coaxial probe, *IEEE Trans. Antennas Propag.*, 51 (Oct. 2003), no. 10, pp. 2913–2917.

8. A.V. Praveen Kumar, V. Hamsakkutty, Jaimon Yohannan and K.T. Mathew, A Wideband Conical Beam Cylindrical Dielectric Resonator Antenna*, IEEE Antennas and Propagation Letters*, 6 (2007).

APPENDIX B

A NOVEL TECHNIQUE FOR REDUCING THE IMAGING DOMAIN IN MICROWAVE IMAGING OF TWO DIMENSIONAL CIRCULARLY SYMMETRIC SCATTERERS

A novel technique for reducing the imaging domain in microwave imaging of two dimensional circularly symmetric scatterers is presented. The degree of symmetry vector of the measured scattered field is employed for the purpose of localizing the scatterer. The degree of symmetry for a transmitter position is computed as a function of the difference between the first half and the spatially reflected second half of the measured scattered field vector. The symmetry plots exhibit unique features for the direction and distance to the scatterer from the centre of the imaging domain, and thus the localization of the object in the imaging domain is possible. This reduces the degrees of freedom in the inversion for the unknown object, thereby aiding the global convergence of the solution. The computation time is considerably reduced and the convergence rate is improved. The technique has been tested on synthetic exact and noisy data and the results are promising.

B1. INTRODUCTION

Microwave imaging is of great interest in many applications, ranging from medical imaging to non destructive evaluation of buried pipelines. The measured scattered field and the contrast function of the unknown object whose dielectric profile is to be estimated are nonlinearly related because of multiple scattering [1].The inverse

problem of microwave imaging is ill posed in the Hadamard sense [2]. Both deterministic and stochastic methods have been developed to solve this inverse scattering problem. Some examples of the deterministic techniques are the Born iterative method [3], distorted Born iterative method [4], Newton Kantorovich method [5, 6] etc. Due to the nonlinearity of the inverse scattering problem, there is a risk of the solution from a deterministic method, getting trapped in a local minimum. One way to minimize the risk of local minima is to use a priori knowledge about the scatterer, so that the nonlinear problem is linearized about a different background. Such a priori knowledge includes, but is not limited to, the upper and lower bounds of the complex permittivity of the scatterer [5, 6] and knowledge of a part of the scatterer [7].

In this paper the imaging of a two dimensional dielectric cylinder is considered, with the assumption that the cross section of the unknown two dimensional object is circular and the complex permittivity distribution symmetric with respect to the centre of the cross section. By a 2-D dielectric cylinder, one refers to the fact that permittivity does not vary along the axis. A circular geometry is employed for the microwave scanner, which helps in generating the degrees of symmetry for the various transmitter positions. It is seen that the degree of symmetry plots exhibit unique features for the direction and distance to the scatterer, from the centre of the imaging domain and this makes it possible to localize the object in the imaging domain. This will reduce the number of degrees of freedom in the inversion for the unknown object, thereby aiding the global convergence of the solution. The computation time is considerably reduced and the convergence rate is improved. The Newton Kantorovich procedure is employed to image the roughly located

object. The details of the formulation of the problem are presented in section 2 and numerical simulations and discussions in section 3.

B2. FORMULATION

A 2-D dielectric scatterer of circular cross section and complex permittivity distribution symmetric with respect to the centre of the cross section is located in an imaging domain I, which is usually a square or a rectangle. The maximum diameter possible for the unknown circular object to be imaged is also assumed to be known. This a priori is valid for structures such as dielectric posts and pipe lines. However, since the location of the object to be imaged is not known, the imaging region has to be chosen sufficiently large. The background and the object are non magnetic. To simplify the implementation, TM polarization of the incident field is considered. A circular geometry for the imaging system is employed, with M line sources equispaced on a circle in the measurement domain. At a given time one of the antennas will be emitting and the others will be receiving. The scattered field is measured for different views. The measurement domain is outside the imaging domain. The circular geometry is selected for the following reasons:

a) Scattered information is collected all around the object for each incidence.

b) It helps in the computation of the degree of symmetry for the different transmitter positions, as will be shown in the following discussion.

The total field satisfies the scalar electric field integral equation for the view *v,*

$$e_v(r) = e_v^{inc}(r) + e_v^{scat}(r) \qquad\qquad\qquad \ldots\ldots\ldots\ldots 1,$$

where $e_v^{inc}(r)$ is the incident field and $e_v^{scat}(r)$ is the scattered field given by

$$e_v^{scat}(r) = \iint_I k_o^2 c(r^{'})e_v(r^{'})G(r,r^{'})dr^{'}, v = 1,2.....M \qquad ....2,$$

with G being the two dimensional Greens function, k_0 the free space propagation constant and c the object contrast. The integral equations are discretized with pulse basis functions and point matching. The imaging region is discretized into N cells. The degree of symmetry for a transmitter position v is defined as (assuming even number of receivers $M-1$ per view)

$$s_{real}(v) = \sum_{k=1}^{(M-1)/2} \left\| Re(e_v^{scat}(k) - e_v^{scat}(M-k)) \right\|^2$$

$$s_{imag}(v) = \sum_{k=1}^{(M-1)/2} \left\| Im(e_v^{scat}(k) - e_v^{scat}(M-k)) \right\|^2, v = 1,2,3,...M \qquad ....3$$

When circular geometry of measurement employed, if the dielectric cylinder is circularly symmetric and off centred, the measured scattered field vector e_v^{scat} exhibits symmetry with respect to its centre, only for the views v_1 and v_2 that are diametrically opposite as shown in figure 1. The symmetry plots also exhibit two maxima, a_1 and a_2 which correspond to the transmitter positions where the symmetry of the measured scattered field vector is minimum. The plots of s_{real} and s_{imag} with respect to v, exhibits two significant minima, at v_1 and v_2, and two significant maxima at a_1 and a_2 as shown in the example in figure 2. This means that the object centre is located in a line joining the views v_1 and v_2. It is clear that a_1 and a_2 will be symmetrically located with respect to both v_1 and v_2. When the centre of the circularly symmetric scatterer is much closer to v_2

than to v_1, a_1 and a_2 will be closer to v_2 than v_1. This is explained as follows: the scattered field at a measurement point depends on the distance to the scatterer via the Greens function, and the field inside the object which is a function of the object contrast and the incident field. When the transmitter is at position v_1 or v_2, the field inside the object is symmetric about the line joining v_1 and v_2. Since the receivers are symmetrically located with respect to the scatterer, the measured scattered field vector will be symmetric about its centre. However when the transmitter position is moved to either side of v_2 or v_1, the distances from the adjacent symmetrically located receivers on either side of the transmitter, to the circularly symmetric scatterer are different. This difference is more pronounced when the transmitter position is moved away from v_2, than when the transmitter position is moved away from v_1. Also the incident field at the position of the scatterer will exhibit a marked difference in symmetry about the line joining v_1 and v_2, the maximum symmetry direction, when the transmitter position is moved away from v_2 than v_1. This is because the field is inversely related to the distance. The distance from the transmitter to the position of the scatterer exhibits a larger variation when the transmitter is moved away from position v_2 than when moved away from position v_1 along the measurement domain. Therefore the asymmetric points in the symmetry plots will be closer to v_2 than v_1, when the scatterer is much closer to v_2 than v_1. The values of s_{real} and s_{imag} at a_1 and a_2 will be much larger when the scatterer is farther from the centre of the imaging domain than when it is closer. Also when the scatterer is close to the centre of the imaging domain, the maximum asymmetry positions a_1 and a_2 will be almost equidistant from the symmetry positions v_1 and v_2. However if the object centre and the centre of the imaging domain coincide, the measured scattered field vector for all the

views will be symmetric with respect to its centre and hence the degree of symmetry values for all the views will be very small. Since the maximum diameter possible for the unknown object is assumed to be known, a reduced image may be defined at the centre of the imaging domain in this case. Thus by measuring the maximum values of s_{real} and s_{imag} and the distance between the maxima, and also noting the direction of symmetry of the scattered field, it is possible to localize the 2-D circularly symmetric dielectric scatterer in the imaging domain. Thus a new reduced imaging domain $I_r \supset I$ may be defined. This is illustrated in the numerical example in the following section. Since a reduced imaging region is employed, the number of degrees of freedom is reduced and there is a larger data redundancy from which better reconstructions may be obtained. The computation time per iteration for the direct solution of the integral equations are reduced from $O(N^3)$ to $O(N_r^3)$ where N_r is the number of pixels in the reduced imaging domain.

B3. NUMERICAL SIMULATIONS AND DISCUSSIONS

The coupled equations 1 and 2 are employed to generate synthetic scattered field data in the measurement domain for the inversion, for known object profiles. For the simulations, 49 transceivers have been used, that is 48 receivers per view. The frequency employed is 3 GHz. The degree of symmetry for each transmitter position is computed as per equation 3, for various radii and distances of the cylinder centres from the origin. The variations in the symmetry parameters for varying distances from the centre, permittivities and radii are studied, which enable the localization of the cylinder in the imaging domain I, thereby allowing the reduction of the imaging domain to I_r. Some typical symmetry plots are considered in figure 3. Here the symmetry plots have been

generated from noisy measurement data with an SNR of 30 dB. The symmetry positions are 19 and 44. The distances between the asymmetry positions through 19 and through 44 along the measurement circle are not as different in figure 3.a, as in figure 3.b. The peak values at the asymmetry positions are much smaller in figure 3 a than in figure 3 b, indicating that the circularly symmetric scatterer is very close to the origin in the first example and farther away from the origin and closer to the transmitter position 44 in the second case . In the case of figure 3 c, the degree of symmetry values for all the transmitter positions are very small, indicating that the object centre and the centre of the imaging domain coincide. The reduced imaging domains in the three cases are chosen accordingly, as indicated in figure 4. The Newton Kantorovich procedure has been employed for the imaging of the approximately located scatterer. The figure 5 a shows the actual profile of a 2-D circularly symmetric dielectric scatterer. Its degree of symmetry values for the different transmitter positions are plotted in figure 5 b. The figure 5 c shows the reconstructed image after the 6th iteration of Newton Kantorovich procedure when the entire imaging region is employed. The reconstructed image when the reduced imaging region is employed is shown in figure 5 d. The result with the proposed technique is seen to be much better. There is also a considerable reduction in computation time compared to the case where the entire imaging domain is employed.
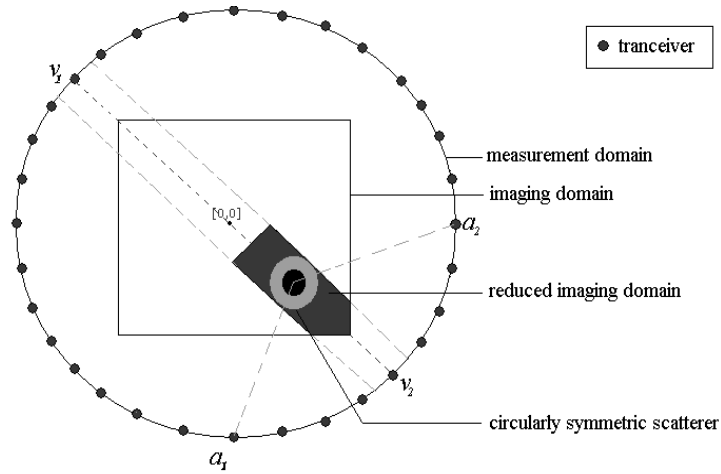
Figure B3.1:

Experimental setup. v_1 and v_2 are the maximum symmetric
views, while a_1 and a_2 are the maximum asymmetric views.
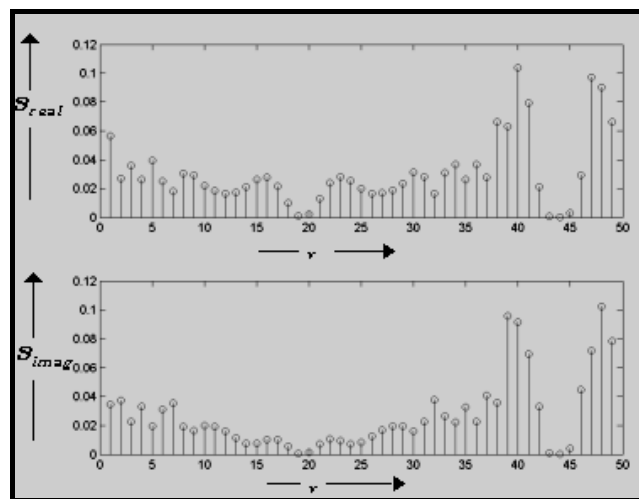
Figure B3.2:

The degree of symmetry values are plotted for various
transmitter positions. The minimum values indicate the
maximum symmetric positions and the maximum values

275

3 a

3 b

276

3 c
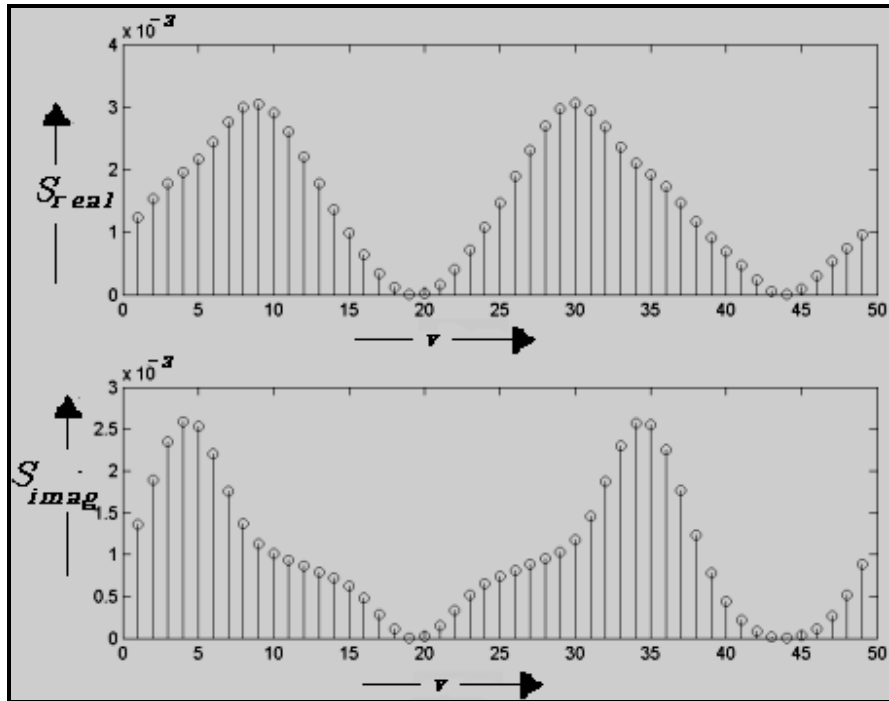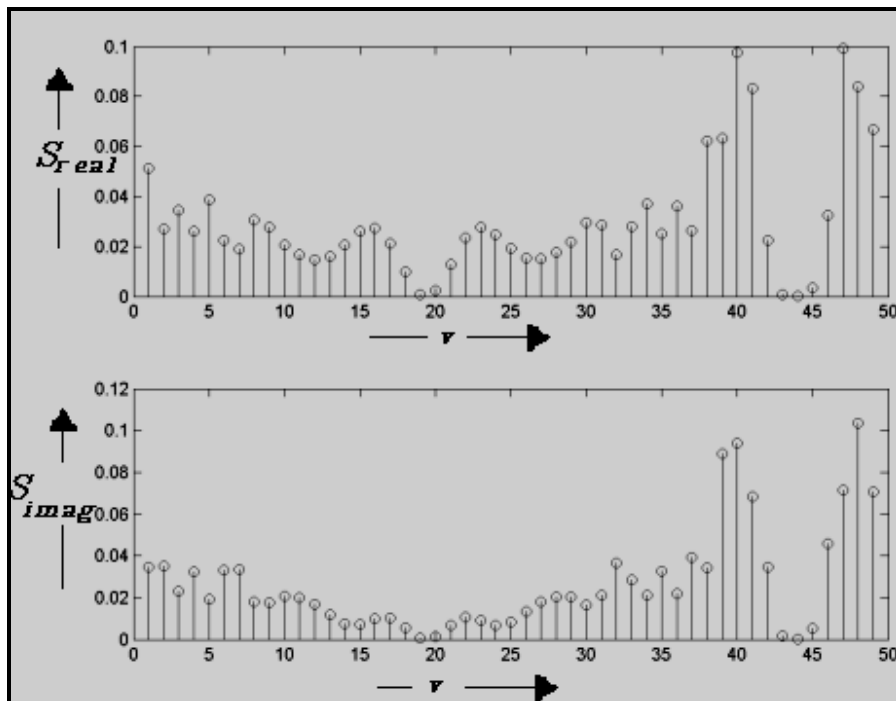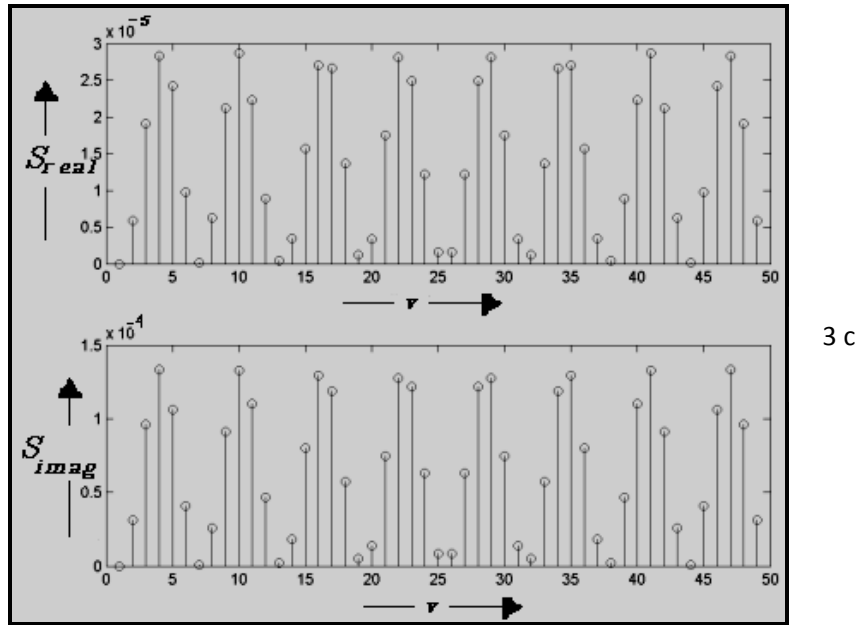
Figure B3.3:

a. degree of symmetry plot when the object centre is close to the centre of the imaging domain

b. degree of symmetry plot when the object is nearer to transmitter 44

c. degree of symmetry plot when the centre of the object and the centre of the imaging domain coincide.

4 a   4 b   4 c
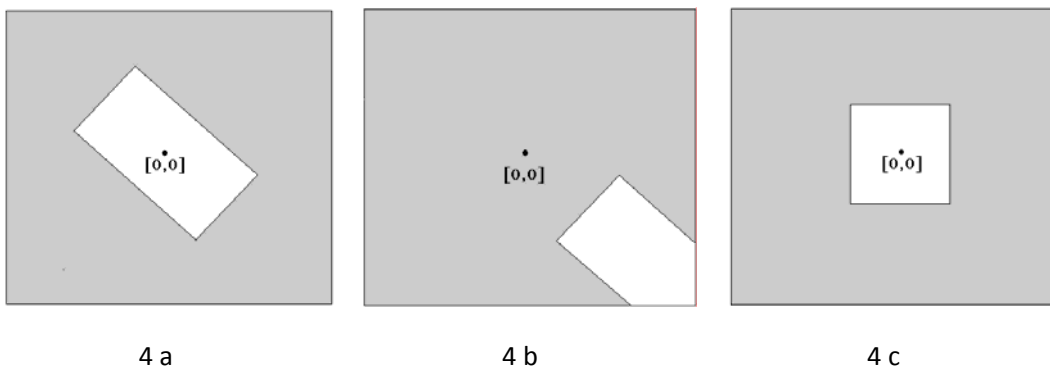
Figure B3.4:

a. reduced imaging region for the symmetry plots in figure 3.a

b. reduced imaging region for the symmetry plots in figure 3.b

c. reduced imaging region for the symmetry plots in figure 3.c

5 a

5 b

5 c

5 d
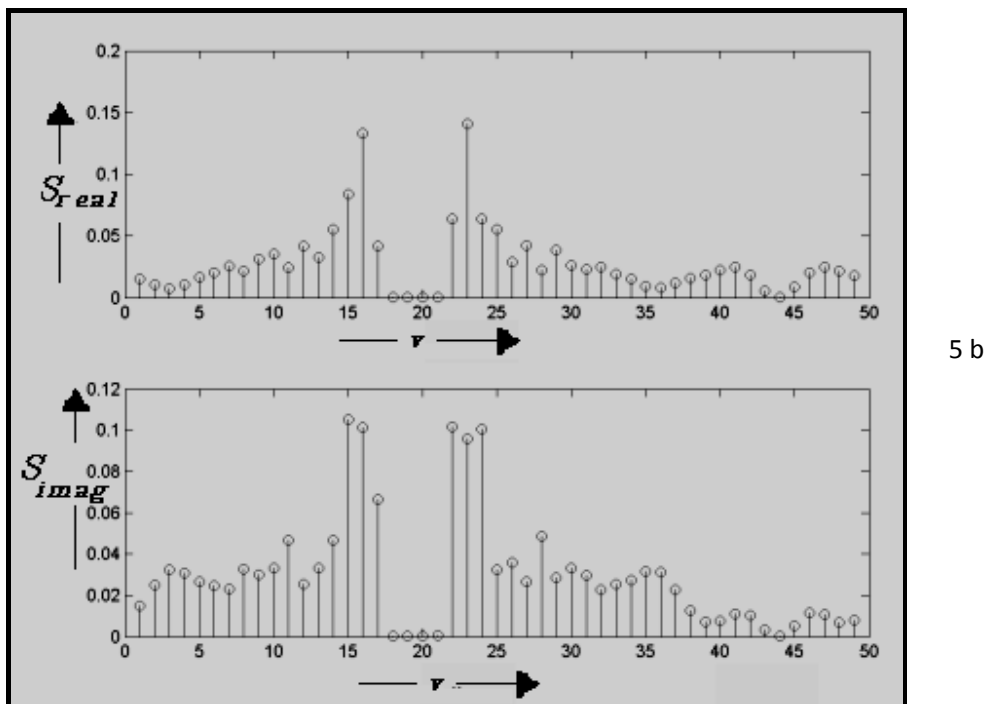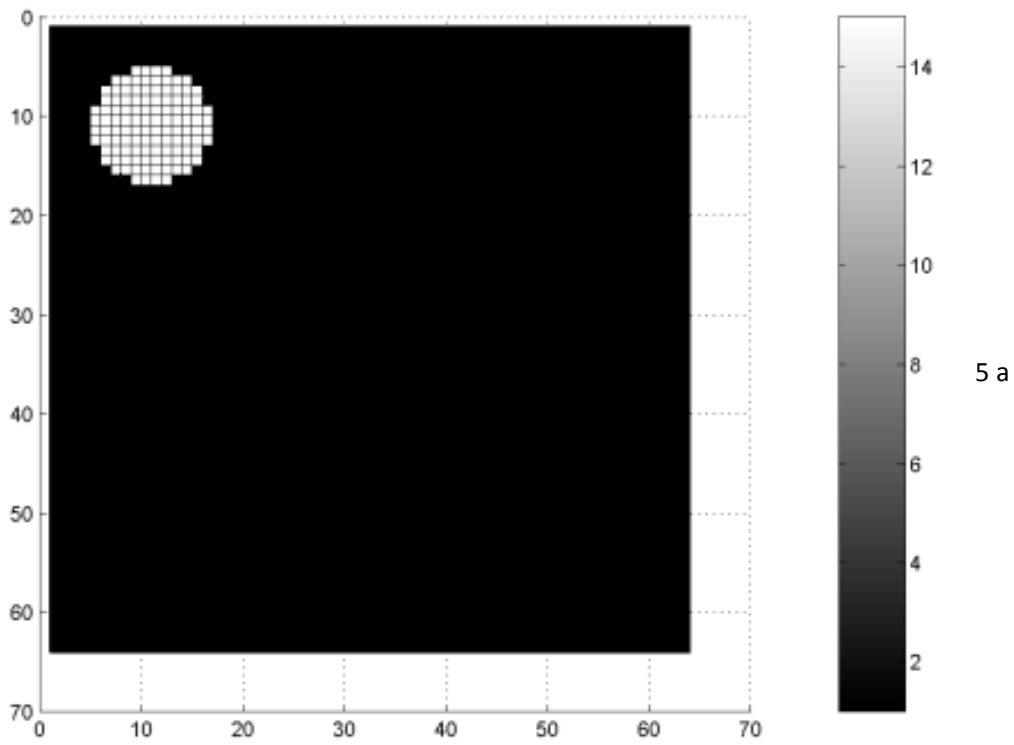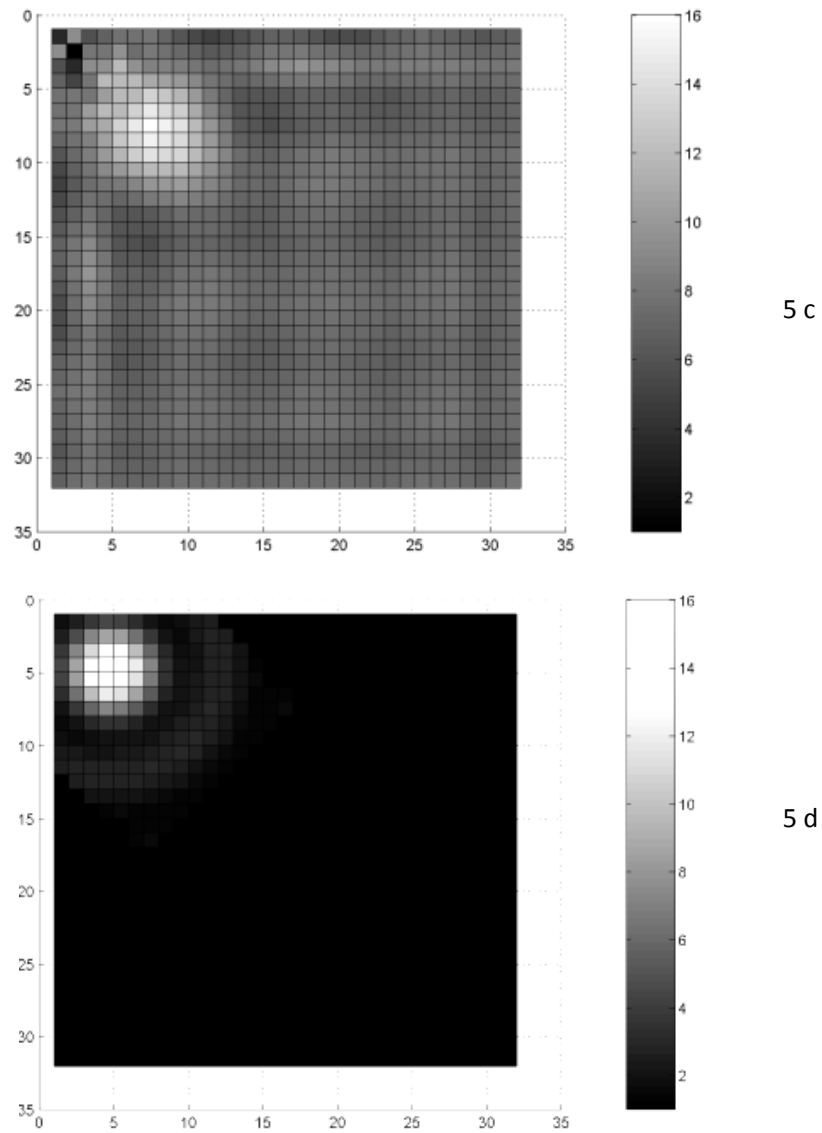
Figure B3.5:

a. The actual profile of a two dimensional circularly symmetric scatterer

b. The symmetry plot for the above object profile. The object lies in the line
   joining the views 19 and 44, and is close to the view 19.

c. The reconstructed image after the sixth iteration of the Newton Kantorovich
   method. The entire imaging domain is employed

d. The reconstructed image after the sixth iteration, considering the reduced
   imaging domain

B.4 CONCLUSION

A novel preconditioning technique for reducing the imaging domain in microwave imaging of two dimensional circularly symmetric scatterers has been presented. The proposed technique reduces the number of unknowns of the inverse scattering problem of microwave imaging, and also results in considerable reduction in the computation time and improvement in the convergence rate. Since a reduced imaging region is employed, the number of degrees of freedom is reduced and there is a larger data redundancy from which better reconstructions are obtained.

REFERENCES

1. W.C. Chew, Waves and Fields in Inhomogeneous Media, IEEE Press, New York, 1995

2. J. Hadamard, Lectures on Cauchy's problem in linear partial differential equations, New Haven, C.T, Yale University Press, 1923

3. Y.M. Wang and W.C. Chew, An iterative solution of two dimensional inverse scattering problem, Int J Imag Syst Tech 1 (1989), 100 – 108

4. W.C. Chew and Y.M. Wang, Reconstruction of two dimensional permittivity using Distorted Born Iterative Method, IEEE Trans Med Imag MI-9 (1990) ,218 - 225

5. N. Joachimowicz, C. Pichot and J. P. Hugonin, Inverse Scattering: An Iterative Numerical Method for Electromagnetic Imaging, IEEE Trans. Antennas Propagat., vol. 39, no. 12, pp 1742 – 1751, Dec. 1991

6. A. Franchois and C. Pichot, Microwave Imaging – Complex permittivity reconstruction with a Levenberg – Marquardt method, IEEE Trans. Antennas Propagat., vol. 45, no. 2, pp 203 – 215, Feb. 1997

7. C.C. Lu and X.G. Zhong, Image reconstruction of Two Dimensional objects inside Dielectric Walls, Microwave and Opt Tech Lett 36 no 2, pp 91 – 95, Jan 2003

List of Publications

International Journal Papers

1. **C. Gopakumar**, Jaimon Yohannan, Ullas G Kalappura, K.T. Mathew, "An Investigation of Wideband Circular Cylindrical Sector Dielectric Resonator Antenna with Microstripline Feed", Microwave and Optical Technology Letters (USA), Volume 51, Issue 12, Pages 2861 – 2865, Sep 2009.

2. **C. Gopakumar**, K. T. Mathew, "A wideband microstrip-line-fed isosceles trapezoidal dielectric resonator antenna with modified ground plane," Progress In Electromagnetics Research C, Vol. 16, pp. 127-136, 2010.

3. **C. Gopakumar**, K.T. Mathew, "A Microstrip-line-fed Isosceles-Trapezoidal Dielectric Resonator Antenna with Slotted Ground Plane for 2.4 GHz WLAN Operation", Microwave and Optical Technology Letters (USA). (Accepted for publication).

4. Vinu Thomas, **C. Gopakumar**, Anil Lonappan, G. Bindu, V. Hamsakutty, K.T. Mathew "Microwave Imaging of Two-dimensional Dielectric cylinders with a Multiscaled Frequency Hopping Approach", Microwave and Optical Technology Letters (USA) Vol. 43, No.4, pp. 353-355, 20th November 2004.

5. Vinu Thomas, **C. Gopakumar**, A.V. Praveen Kumar, V. Hamsakutty, Anil Lonappan, G. Bindu, K.T. Mathew "A novel technique for reducing the imaging domain in microwave imaging of two dimensional circularly symmetric scatterers", Microwave and Optical Technology Letters (USA) Vol.44, No.5 pp423-427, 5th March 2005.

6. Vinu Thomas, **C. Gopakumar**, Jaimon Yohannan, Anil Lonappan, G. bindu, A.V. Praveen Kumar, V. Hamsakutty, K.T. Mathew, "A novel Technology for Localizing the scatterer in Inverse Profiling of Two-Dimensional Circularly symmetric Dielectric Scatterers Using the Degree of Symmetry and Neural Networks", Journal of Electromagnetic Waves and Application (USA) Vol. 19, No. 15, pp 2113-2121, 2005

International Conference Papers

1. **C. Gopakumar**, K.T. Mathew, "Compact Isosceles Trapezoidal Dielectric Resonator Antenna for 2.4 GHz WLAN Application", International Conference on Communications and Signal Processing (ICCSP-2011), (Organizing in collaboration with IEEE) National Institute of Technology, Calicut, 10-12 February, 2011. **(Accepted for presentation).**

2. **C. Gopakumar**, K.T. Mathew, "Bandwidth Enhancement and Frequency Tuning of Trapezoidal Dielectric Resonator Antenna with Slotted Ground Plane", The International Conference on Recent Innovation in Technology (ICRIT-2011), Rajiv Gandhi Institute of Technology, Kottayam, Kerala, India, 10-12 February, 2011. (**Accepted for presentation on 06-01-2011**)

3. **C. Gopakumar**, K.T. Mathew, "Dual Band Dual Polarized Isosceles Trapezoidal Dielectric Resonator Antenna", The International Conference on Devices and Communications (ICDeCom - 11), (Organizing in association with IEEE) Birla Institute of Technology, Mesra, India 24-25 February, 2011. (**Accepted for presentation on 07-01-2011**)

4. Vinu Thomas, **C. Gopakumar**, Jaimon Yohannan, Anil Lonappan, G. bindu, A.V. Praveen Kumar, V. Hamsakutty, K.T. Mathew, "A novel Technology for Localizing the scatterer in Inverse Profiling of Two-Dimensional Circularly symmetric Dielectric Scatterers Using the Degree of Symmetry and Neural Networks", Electromagnetic Research Symposium, PIERS 2005, August 2-26, 2005, Hangzhou, China.

5. Vinu Thomas, **C. Gopakumar**, C. K. Ramachandran, Tessamma Thomas, "Detection of Micro-calsification in mammograms Using Wavelet Transforms" International Workshop on Linear Algebra, Numerical Analysis and Wavelet Analysis, August 6-15, 2001, Department of Mathematics, Cochin University of Science and Technology, Cochi, India.

6. Vinu Thomas, **C. Gopakumar**, A.V. Praveen Kumar, V. Hamsakutty, Jaimon Yohannan, K.T. Mathew, "Imaging Domain reduction in Micowave imaging of two dimensional circularly symmetric dielectric scatterers using degree of symmetry vector", Seventh International Conference on Photonics, Optoelectronics and Fiber-optics, SPIE, 2004 December 9-11, Cochin, India.

National Conference Papers

1. **C. Gopakumar**, Jaimon Yohannan, Ullas G Kalappura, K.T. Mathew, "An investigation of wide band Microstripline fed Half split Cylindrical Dielectric Resonator Antenna", Proceedings of APSYM 2008, National Symposium on Antennas and Propagation, Organized by Department of Electronics, CUSAT, Cochi, Kerala. India.

2. **C. Gopakumar**, K.T. Mathew, "An Experimental Investigation on a Trapezoidal Dielectric Resonator Antenna for 2.4 GHz WLAN Operation", Proceedings of APSYM 2010, National Symposium on Antennas and Propagation, Organized by Department of Electronics, CUSAT, Cochi, Kerala. India.

3. **C. Gopakumar**, Vinu Thomas and K.T. Mathew, "A Reduction Technique for Imaging Domain in Microwave Imaging of Two Dimensional circularly Symmetric Scatterers", Proceedings of National Seminar on Information, Communication & Intelligent Systems, Jointly organized by Model Engineering college, Thrikkakkara, Cochi, Kerala, India and IETE, Cochi, Kerala, India.

4. **C. Gopakumar**, Vinu Thomas and K.T. Mathew, "A multi-Scaled Frequency Hopping Approach in the Microwave Imaging of Two Dimensional Dielectric Cylinders", Proceedings of National Seminar on Information, Communication & Intelligent Systems, Jointly organized by Model Engineering college, Thrikkakkara, Cochi, Kerala, India and IETE, Cochi, Kerala, India.

5. Vinu Thomas, **C. Gopakumar**, C. K. Ramachandran, Tessamma Thomas, "Zero Crossings of Wavelet Transforms to Detect early Breast Cancer", Proceeding of National Conference on Advanced Computer Applications, Department of Computer Science, MGM College, Pollachi, Tamil Nadu.

Gopakumar C

Research Scholar,
Department of Electronics,
Cochin University of Science and Technology
Kochi-682 022, INDIA.
Phone: 91-484-2576418; Mob: +91-9497618731
E-mail: gopakumar@cusat.ac.in, gopan.c.menon@gmail.com

Gopakumar C
Chandralayam,
Ramankulangara,
Kavanadu PO,
Kollam, Kerala state, INDIA.

Objectives:

To pursue research activities and a challenging career in Academics.
To carry out my duties with integrity and dedication.

Academic Qualifications:

- **Ph.D in Microwave Engineering (2004–till date**, Synopsis submitted, Soon submitting thesis**)**, Microwave Tomography and Materials Research Laboratory, Department of Electronics, Cochin University of Science and Technology, Cochin, India.
- **M Tech in Electronics Engg.** (1999-2001) from Cochin University of Science and Technology, kerala, with **Distinction** and an aggregate of **78.79% (CGPA-3.20)**
  * Specialization in DSP and Image processing.
- **B Tech in Electronics Engg.** (1992-96) from Model Engg. College, Thrikkakkara, Cochin, affiliated to Cochin University of Science and Technology, kerala, India, with **Distinction** and an aggregate of **75.42%.**
- **Post Diploma in 'Electro-Medical Equipment Maintenance'** (1987-89) from Institute of Human Resources Development for electronics, Kerala, India, with **First class** and an aggregate of **70%.**
- **Diploma in Electrical Engg.** (1984-87) from Sree Narayana Polytechnic Kottiyam, Kerala, affiliated to State Board of Technical Education, Kerala, India, with **First class** and an aggregate of **71.50%.**

Work Experience:

- 10 years experience as Sr. Grade Lecturer in Electronics Engg. in Engineering Colleges under IHRD, Government of Kerala, Kerala state, India.
- 2 years experience as Lecturer in the Dept. of Electrical Engg., Debub University, Awassa, ETHIOPIA.
- Worked as Research Scientist/Engineer in the project entitled "*Development of Autonomous Buoy System for Radio – Acoustic Positioning and Tracking*" in the Department of Electronics, CUSAT, Kochi, Kerala, INDIA, for two months under Prof. P. R. S. Pillai, sponsored by department of Information Technology, Govt. of India.
- 10 years experience as Technician/Foreman Gr.I, under IHRD, Government of Kerala, India.
  Nature of job: *** Guidance and assistance in the experiments and mini project work for B-Tech level students.
  * Servicing Electro medical and Electronic equipments.

Publications

International Journals	:	6
International Conference papers	:	6
National Conferences	:	5

Subjects taught.

- Digital signal Processing.
- Signals and Systems Analysis
- Artificial Neural Networks.
- Network Analysis.
- Communication Theory.
- Electronic Circuits.
- Digital System Design
- Micro Processors.
- Applied Electronics.
- Communication Engg.
- Process Instrumentatior
- Control Systems
- Power Electronics
- E M Theory.

Short term training programs attended

➤ A 3 weaks training program in **"High Reliability interconnections"** at vicram Sarabhai Space centre, Trivandrum, Kerala, India.

➤ AICTE-ISTE sponsored Winter School on **INTERNET AND E-COMMERCE** organized by the College of Engg., Chengannur from 18th to 30th December, 2000. (2 weeks)

➤ UGC Sponsered refresher course on **VLSI DESIGN** organized by Ackadamic Staff college, JNT University, Hyderabad, Andhra Pradesh, India from 03/06/2002 to 22/06/2002. (3weeks)

➤ AICTE-ISTE Short term Training Program on **3G MOBILE NETWORKS** conducted by Kongu Engg. College, Perundurai, Erode from 17/10/2002 to 30/10/2002. (2 weeks)

➤ ISTE sponsored short-term course on **CRM STRATEGIES FOR TECHNICAL INSTITUTIONS** at College of Engg., Chengannur, Kerala, from 02/01/2003 to 15/01/2003. (2 weeks)

➤ AICTE-ISTE sponsored Short Term Training Programme on **WEB TECHNOLOGIES** conducted by the College of Engg.Cenganur, from 17th to 30th march 2004. (2 weeks)

Computer Proficiency

- **Languages** High Level : C, Pascal.
                 Assembly   : Intel 8085/86 MPU, 8051, PIC16XXX MCUs

- Tools   : MATLAB, VHDL, Or cad, MS Office.

- Electromagnetic Simulation tools : Ansoft HFSS, CST Microwave Studio

- Operating Systems   : MS-DOS , Windows 9x, XP, Windows 7.

Personal Profile:

Father's Name	:	C. K. Chandra Sekhara Menon.
Age and Date of Birth	:	41Years, 27- 03 - 1969
Sex	:	Male
Nationality	:	Indian
Marital Status	:	Married
Religion	:	Hindu
Languages Known	:	English, German, Hindi, Malayalam.
Hobbies	:	Singing, listening music, Chess, Cricket

Membership in Technical Organizations:

- Life time Member of " The Indian Society for Technical education" an organization for promoting the quality and standards in Technical Education.
  * Membership No: **LM 31979**

Reference:

- Dr. V. P. Devassia, Additional Director, Institute of Human Resources Development, Prajoe Towers, Thiruvananthapuram, Kerala, INDIA.
  Phone: 0091-479 –2456046.; Mob: +91- 9447 082280.

- Dr. P.R.S Pillai, Professor/Head of the Department, Department of Electronics, Cochin-University of Science and Technology, Cochin-22, Kerala, INDIA.
  Phone: 0091-484 –2576418. E-mail: ktm@cusat.ac.in

- Dr. Mohanan P. Professor, Department of Electronics, Cochin University of Science and Technology, Cochin-22, Kerala, INDIA.
  Phone: 0091-484 –2576418. E-mail: tt@cusat.ac.in

The above-mentioned facts are true and correct from the best of my knowledge and belief.

Gopakumar C.